Report
P-16-05
October 2017

SKB Task Forces EBS and GWFTS

Modelling the interaction between engineered and natural barriers

A compilation of Task 8 descriptions

Patrik Vidstrand
Martin Stigsson
Mattias Åkesson
Åsa Fransson

SVENSK KÄRNBRÄNSLEHANTERING AB

SWEDISH NUCLEAR FUEL
AND WASTE MANAGEMENT CO

Box 3091, SE-169 03 Solna
Phone +46 8 459 84 00
skb.se

SVENSK KÄRNBRÄNSLEHANTERING

ISSN 1651-4416
SKB P-16-05
ID 1593364
October 2017

Task Forces EBS and GWFTS

Modelling the interaction between engineered and natural barriers

A compilation of Task 8 descriptions

Patrik Vidstrand, Martin Stigsson
Svensk Kärnbränslehantering AB

Mattias Åkesson, Clay Technology AB

Åsa Fransson, Chalmers Tekniska Högskola

Preface

Task 8 was the first common task between the two Äspö Task Forces, and the Task, as such, was initialised by Gunnar Gustafson, Chairman of the Task Force on Groundwater Flow and Transport and Lennart Börgesson, Secretary of the Task Force on Engineered Barriers. During the Task Gunnar passed away and Lennart resigned as Secretary. But, the task was finalised in the spirit of these two men. Many are the modellers that have gained experience and become grown-ups under the leadership of Gunnar and Lennart.

The final results of the Task 8 will be presented in a series of reports; this report represents the compilation of the all the task definitions that has governed the work for all groups.

Summary

This report presents the task description for a modeling task, denoted Task 8, performed within the framework of the SKB Task Forces on Groundwater Flow and Transport of Solutes (GWFTS) and on Engineered Barrier Systems (EBS), focusing on the hydraulic interaction between the bentonite backfill material and near-field host rock. The objective of the task and the joint field experiment BRIE (Bentonite Rock Interaction Experiment) was that these would lead to: i) a scientific understanding of the exchange of water across the bentonite-rock interface; ii) better predictions of the wetting of the bentonite buffer; and iii) better characterization methods of the canister boreholes. The actual modeling task was divided and developed in several subtasks.

The experiment was performed in the TASO tunnel located at a depth of 420 m at Äspö Hard Rock Laboratory in Sweden, and was subdivided into two main parts: i) the selection and characterization of a test site and two central boreholes; and ii) the installation, hydration and dismantling of two bentonite parcels.

The first step for the preparation of the task description was to compile background information, especially regarding the hydraulic material properties, for both bentonite and rock materials. This also included some generic scoping calculations for bentonite hydration for some simple geometries: with bentonite only, and with a bentonite-filled borehole surrounded by cylinder of rock.

Task 8a was a generic hydraulic scoping calculation with a 2D axi-symmetric geometry with a bentonite-filled borehole and a tunnel cross section, both surrounded by rock which was either completely homogenous, or intersected by a horizontal fracture. All hydraulic material properties were specified. This task also included a sensitivity analysis with alternative sets of material properties.

Task 8b was a generic hydraulic scoping calculation for a 3D geometry within a $(40)^3$ m^3 cube incorporating the TASO tunnel, with defined boundary conditions but no other data from the test site, and one generic bentonite-filled borehole.

Task 8c was a prediction of the hydraulic evolution for the same 3D geometry as before, but with information on site-specific deformation zones and with defined sets of fracture statistics for the TASO tunnel. The modelers were asked to predict: i) the water inflow into an empty borehole; and ii) the bentonite hydration of a bentonite-filled borehole.

Task 8d was a prediction of the hydraulic evolution for the same 3D geometry and same data on deformation zones and fracture statistics as before, but with detailed information from the site characterization, e.g. inflows and fracture locations in two Ø300 mm bore holes, and from the installation of two bentonite parcels, including sensor positions. The modelers were asked to predict: i) the water inflow into empty boreholes; and ii) the bentonite hydration of two bentonite-filled borehole.

The next step of the task description to model the hydraulic evolution of two of the water uptake tests performed within the framework of the BRIE project. The objective of these tests was to provide data from an experiment with radial water-uptake, which would give a refined description of the hydraulic processes in the bentonite in the BRIE field experiment.

Task 8e addressed the Prototype Repository field experiment which is also carried out at Äspö HRL. This test was used as a separate modeling task for the EBS Task Force which was described separately.

Finally, Task 8f was a final evaluation of the BRIE field experiment in which all sensor data and all results from the dismantling of the bentonite parcels were available for the modelers.

Sammanfattning

Denna rapport redovisar en beskrivning av en modelleringsuppgift, benämnd Task 8, vilken har utförts inom ramen för SKB:s arbetsgrupper för grundvattenflöde och transport av lösta ämnen (GWFTS-TF) respektive ingenjörsbarriärer (EBS-TF), och som har varit inriktad på interaktionen mellan bentonitbaserade återfyllningsmaterial och angränsande berggrund. Syftet med modelleringsuppgiften och det tillhörande fältförsöket BRIE (Bentonite Rock Interaction Experiment) var att dessa skulle leda till: i) en vetenskaplig förståelse för utbytet av vatten över gränssnittet bentonit-berg; ii) bättre prediktioner av bentonitens bevätning; och iii) bättre karakteriseringsmetoder för deponeringshål. Modelleringsuppgiften definierades och utvecklades som successiva deluppgifter.

Experimentet utfördes i TASO tunneln på ett djup av 420 m vid Äspölaboratoriet utanför Oskarshamn, och var uppdelat i två faser: i) val och karakterisering av försöksplats och två centrala borrhål; och ii) installation, bevätning och upptag av två bentonitpaket.

Första steget med att definiera en uppgiftsbeskrivning var att sammanställa bakgrundsmaterial, i synnerhet beträffande hydrauliska egenskaper för bentonit och bergmaterial. Detta bakgrundsmaterial inkluderade även generiska vattenmättnadsberäkningar för några enkla geometrier: med enbart bentonit, eller med ett bentonitfyllt borrhål omgärdat av berg.

Task 8a var en generisk beräkning med en 2D axisymmetrisk geometri med ett bentonitfyllt borrhål samt med en tvärsektion av en tunnel, båda omgärdade av berg som antingen var fullständigt homogent, eller genomskuret av en horisontell spricka. Alla hydrauliska materialegenskaper specificerades. Denna uppgift inkluderade även en känslighetsanalys med alternativa parametervärdesuppsättningar.

Task 8b var en generisk beräkning för en 3D geometri inom en kub (40^3 m^3), inneslutande TASO tunneln, med ett generiskt bentonitfyllt borrhål och med definierade randvillkor, men utan någon ytterligare data från testområdet.

Task 8c var en prediktion av den hydrauliska utvecklingen för samma 3D geometri som tidigare, men med information om platsspecifika deformationszoner och med definierade uppsättningar med sprickstatistik för TASO tunneln. Med dessa förutsättningar skulle modellörerna prediktera: i) vatteninflödet till ett tomt borrhål, och ii) vattenupptaget i ett bentonitfyllt borrhål.

Task 8d var en prediktion av den hydrauliska utvecklingen för samma 3D geometri, och med samma information om platsspecifika deformationszoner och sprickstatistik som tidigare, men med detaljerad information från platskarakteriseringen, t ex inflöden och sprickpositioner i två Ø300 mm borrhål, och från installationen av två bentonitpaket, inklusive givarpositioner. Med dessa förutsättningar skulle modellörerna prediktera: i) vatteninflödet till de tomma borrhålen, och ii) vattenupptaget i två bentonitfyllda borrhål.

Nästa steg i uppdragsbeskrivningen var att modellera två av de vattenupptagsförsök som utfördes inom ramen för BRIE projektet. Syftet med dessa var att tillhandahålla data från ett försök med radiellt vattenupptag som renodlat beskriver de hydrauliska processerna i bentoniten i fältförsöket i BRIE.

Task 8e behandlade Prototypförvaret, ett fältförsök som också utförs vid Äspölaboratoriet. Detta experiment har används som en separat modelleringsuppgift inom EBS-TF och har beskrivits separat.

Task 8f var den slutliga utvärderingen av BRIE fältförsök. Detta innebar att all mätdata från givare, samt alla resultat från brytningen av bentonitpaketen var tillgängliga för modellörerna.

Contents

1 Introduction

This report presents the task description for a modeling task, denoted Task 8, focusing on the hydraulic interaction between the bentonite backfill material and near-field host rock. The objective of the task and the joint field experiment BRIE (Bentonite Rock Interaction Experiment) was that these would lead to: i) a scientific understanding of the exchange of water across the bentonite-rock interface; ii) better predictions of the wetting of the bentonite buffer; and iii) better characterization methods of the canister boreholes. The actual modeling task was divided and developed in several subtasks.

In order to carry out the task, the following project groups were involved or/and established:

- A joint Task Secretariat between the Task Forces – This coordinated the task, proposed task definitions and administrated data. The Task Secretariat also provided material for the task evaluation.
- An Experiment Group – The Experiment Group was tied to the Äspö HRL. The group carried out the field activities, i.e. characterization of the experimental area, drilling of boreholes, installation of equipment as well as monitoring and collection of testing data.
- The Task Force on Modelling of Groundwater Flow and Transport of Solutes (GWFTS) and its associated Modelling Teams.
- The Task Force on Engineered Barrier Systems (EBS) and its associated Modelling Teams.

Several persons have contributed to this task description:

- Patrik Vidstrand (SKB) has been the main coordinator and author of the task description. He has also contributed with background information on granitic rock, the model domain and the main deformation zones.
- Mattias Åkesson (Clay Technology) has contributed with background information on bentonite. He has also been responsible for the bentonite installations and the water uptake tests in the BRIE project.
- Åsa Fransson (Chalmers University) has been the project manager of the BRIE project and has been responsible for the site characterizations in the TASO tunnel.
- Martin Stigsson (SKB) has contributed with the DFN model and fracture statistics defined for the task.

The task description was revised each time a new subtask was added: 2010-04-14 (Task 8a and 8b); 2011-02-23 (Task 8a sensitivity analysis and 8c); 2011-07-14 (Task 8c updates); 2012-02-15 (Task 8c updates); 2012-10-10 (Task 8d), 2013-10-27 (Water uptake tests and Task 8e); and 2014-11-25 (Task 8f).

The outline of this report generally follows the same order as the modelling task has been developed. A brief overview of the BRIE project is given in Chapter 2. An overview of the hydraulic properties of MX-80 bentonite and granitic rock is presented together with some introductory scoping calculations in Chapter 3. Detailed task definitions of Task 8a to Task 8d is presented in Chapters 4 to 7. A hydraulic evaluation of two of the water uptake tests are presented in Chapter 8 together with a defined modeling task for this. A task definition addressing the Prototype repository, denoted Task 8e, is described in Chapter 9. Finally, the task definition for Task 8f is described in Chapter 10.

It should be noted that this task description has been a “living document” during a significant time period with several revisions. Some editing was therefore considered necessary during the final preparation of this report.

2 BRIE

The experiment at Äspö HRL that is conducted concurrently with Task 8 is referred to as the Bentonite Rock Interaction Experiment (BRIE). The experiment is subdivided into two main parts: Part I describes the selection and characterisation of a test site and one or two central boreholes; Part II handles the installation and extraction of the bentonite buffer.

The main objectives of Part I of the Bentonite Rock Interaction Experiment (BRIE) are to:

- Select a site: Choose an experimental area based on Äspö hydrogeological conditions and a few exploratory boreholes.
- Characterise the site using cored boreholes, borehole logging and hydraulic tests.
- Characterise one or two central boreholes for installation of bentonite buffer; drill and test the central borehole and surrounding boreholes; develop structural model of the experimental area.

The expected results from this part of the BRIE experiment are conclusions and recommendations concerning the hydraulic characteristics of the deposition holes. This includes suggestions of different methods (an overall characterisation method and the investigation methods included) and rules (criteria) for future work.

The experiment should focus on hydraulic investigations and address mechanical constraints only if deemed necessary. Conducting interference tests for estimates of transmissivity and storage coefficient, linking the results to those from previously conducted tests (Rhén et al. 2008) and developing a relation between storage coefficient and fracture normal stiffness (e.g. Fransson 2009) would give a useful link to the mechanical behaviour.

The selection of deposition hole positions is related to the fracture geometry and the hydraulic properties. Fracture size, water inflow and transmissivity are of importance.

2.1 The planned Swedish layout

Deposition holes are drilled vertically in the floor of a deposition tunnel. Based on current experiences, the maximum distributed inflow to the deposition tunnel is set to be less than or equal to 1.7 l/min per 100 m (based on 5 l/min in a 300 m long deposition tunnel), and the maximum point inflow less than or equal to 0.1 l/min (SKB 2010b).

Regarding *fracture geometry*, the following should be considered:

- Distance to deformation zones (with trace length longer than 3 km) should be larger than 100 m.
- Considering shearing of fractures, deposition positions should be selected so that they do not intersect with extensively long fractures. Currently, the *Extended Full Perimeter Intersection* criterion (EFPC) should be satisfied (Munier 2006).
- The deposition holes should be located in solid or sparsely fractured rock.

Regarding inflow and transmissivity, it is said that during the time from when the buffer is first exposed to inflowing water to full saturation no more than a given amount of the initially deposited buffer material should be lost (due to piping and erosion). In addition, the connected effective transmissivity along the full length of the deposition hole wall, and as averaged around the hole, must be less than 10^{-10} m^2/s.

Deposition holes are excavated with a full-phase down-hole drilling technique, and excavation of a bevel at the top of the hole is made using wire sawing. The diameter of the deposition hole should be 1.75 m and the depth approximately 8 meters. When drilling is finalised, the bottom of the hole should be levelled, and loose rock debris should be removed. Further, it is important to remove water, clean the deposition hole and inspect it for inflow points and the presence of fractures.

Before deposition of the bentonite buffer, a bottom plate of low-pH concrete combined with a copper plate is installed.

Also prior to the installation of the buffer, canister and backfill shall be verified in underground openings to confirm that the connected effective transmissivity in the excavation-induced damage zone is acceptably low. Further, the deposition hole should not be intersected by any discriminating fracture as described above. Before deposition, a protection sheet is placed in the deposition hole (attached to the border of the copper plate) and a drainage system (pipe, an ejection pump and an alarm system) is placed between the sheet and the wall of the deposition hole.

In all, the installed buffer consists of one bottom block, six ring shaped blocks and three solid blocks on top. The gap between the blocks and the rock surface will be filled with pellets with the specified density of loose filling (SKB 2010a). The total height of the buffer blocks is 6.68 m, whereas the height of the upper part of the deposition hole is 1.25 m (SKB 2010b).

The gap between rock and bentonite needs to be large enough to hold equipment required to keep the blocks dry and pump out water so the buffer does not start to swell until the deposition tunnel is backfilled (SKB 2010a).

The installation of the pellets commences when the backfilling of the deposition tunnel has reached the section of the deposition hole. The drainage system, the protections sheet and sensors are removed before doing so.

Tests and inspections of the installed buffer geometry and density should be made. Important inputs are deposition hole volume, deposition hole radii and cross-sectional area along its centre axis. Further, weight, dimensions and positions of installed blocks and weight and volume of installed pellets are used.

2.2 Suggested investigation stages for field experiment

The following stages are suggested for the Bentonite Rock Interaction Experiment (BRIE) (Figure 2-1):

a) Selection of site.

b) Site characterisation.

c) Drilling of central borehole(s) (and characterisation).

d) Draw-down and stabilisation.

e) Installation of bentonite buffer.

f) Recovery and saturation.

g) Over-coring after resaturation.

The damage to the rock induced by excavation should be taken into account as it is considered an important process that influences the system behaviour. There may also be disturbance to the rock as a result of grouting and rock support. In addition, the work will cause changes in chemical conditions.

Drilling of the central borehole may result in a disturbed zone and a change in the hydraulic properties (Autio 1997, Andersson and Martin 2009, Andersson et al. 2009). Further, the pressure draw-down may cause changes in hydraulic properties due to groundwater degassing and deformation (Jarsjö et al. 2001). Degassing results in unsaturated (or two-phase) flow. Following installation of the bentonite, fluid flow may change its properties due to e.g. piping and erosion. Further, extrusion of buffer material into the rock (fractures) following swelling may allow for fluid flow in the rock fractures to erode the material. The initial part (Part I) of the experiment covers steps a) to d) illustrated below. Possibly, the draw-down should be followed by a recovery period without deposition of bentonite buffer to obtain pressure recovery data.

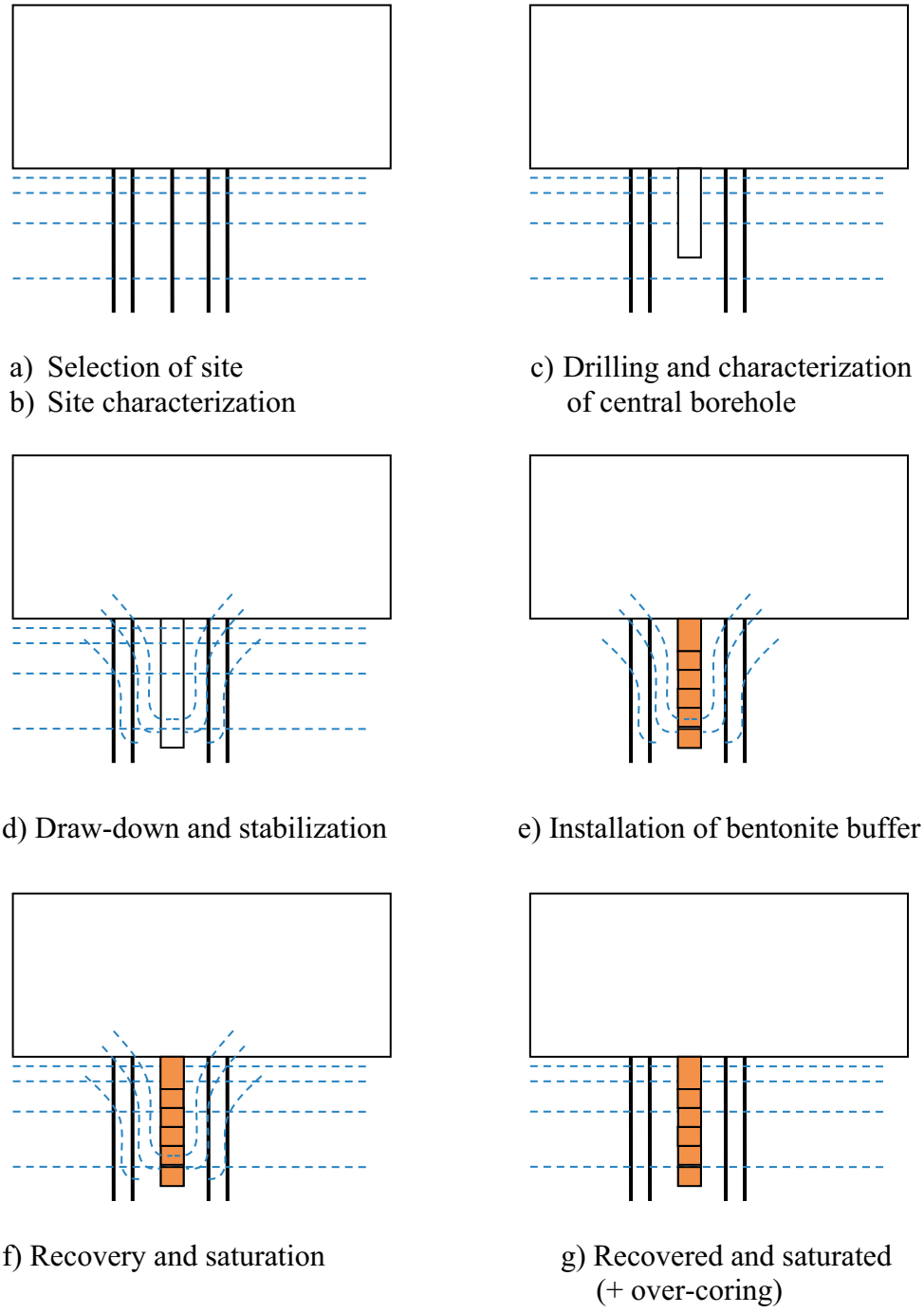

Figure 2-1. *Suggested investigation stages for the Bentonite Rock Interaction Experiment.*

3 Background

3.1 Hydraulic properties of MX-80

3.3.1 Definitions for description of bentonite

To be able to describe the conditions of a buffer material, several parameters and definitions are used in this report. The buffer materials consist of solid particles and voids which can be partly filled with water (see Figure 3-1). The volume of the material can be divided into the volume of the porous system ($V_p = V_w + V_g$) and the volume of the solid particles (V_s) and corresponding masses, m_w and m_s. From these definitions several other parameters describing the condition of the buffer can be defined. Some of the most common definitions are listed in Table 3-1 below.

Table 3-1. Definitions for some useful quantities

Water content (gravimetric)	$w = \frac{m_w}{m_s}$
Density of solid particles	$\rho_s = \frac{m_s}{V_s} \quad (= 2\,780\, kg/m^3)$
Dry density	$\rho_d = \frac{m_s}{V}$
Density at saturation	$\rho_m = \frac{(\rho_w \times V_p + m_s)}{V}$
Degree of saturation	$S_r = \frac{V_w}{V_p}$
Void ratio	$e = \frac{V_p}{V_s}$
Porosity	$n = \frac{V_p}{V}$
Volumetric water content	$\theta = \frac{V_w}{V}$

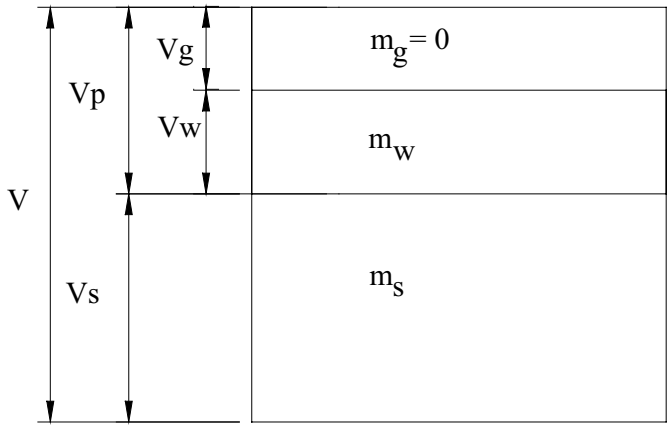

Figure 3-1. *Definition of masses and volumes for different phases.*

3.3.2 Bentonite – Initial state

The initial state of the bentonite is specified in the original Task 8 proposal. The following conditions have been specified: density at saturation: ~ 2 000 kg/m^3, initial water content: 10 %. These conditions correspond to the following quantities:

- Dry density: 1 560 kg/m^3.
- Void ratio: 0.78 (–).
- Porosity: 0.438 (–).
- Initial liquid saturation: 36 %.

The calculations of these quantities are shown in Figure 3-2.

3.3.3 Darcy's law for unsaturated conditions

The water transport in porous media is typically described by Darcy's law:

$$\bar{q} = -\frac{k \cdot k_r}{\mu} \cdot \left(\nabla P_l - \rho_w \cdot \bar{g}\right) \qquad (m/s) \tag{3-1}$$

where k is the intrinsic permeability, k_r is the relative permeability, μ is the viscosity, P_l is the liquid pressure, ρ_w is the density of water and $\bar{g}$ is the gravity vector. The relation between the intrinsic permeability (k) and the hydraulic conductivity is given by:

$$k = \frac{\mu}{\rho_w \cdot g} \cdot K \quad (m^2) \tag{3-2}$$

At room temperature, the intrinsic permeability is thus approximately seven orders of magnitude lower than the hydraulic conductivity.

$\rho_s \equiv 2780$	Particle density	
$\rho_w \equiv 1000$	Water density	
$\rho_m \equiv 2000$	Saturated density	
$\omega \equiv 0.10$	Initial water content	
$\rho_d := \frac{\rho_m - \rho_w}{1 - \frac{\rho_w}{\rho_s}}$	Dry density	$\rho_d = 1.562 \times 10^3$
$e1 := \frac{\rho_s}{\rho_d} - 1$	Void ratio	$e1 = 0.78$
$n := \frac{e1}{e1 + 1}$	Porosity	$n = 0.438$
$S_l := \frac{\omega \cdot \rho_s}{e1 \cdot \rho_w}$	Degree of saturation	$S_l = 0.356$

Figure 3-2. *Calculation of different quantities for description of the initial state (excerpt from MathCad document).*

The relative permeability is the ratio between the conductivity at unsaturated and saturated conditions, and therefore has values between zero and one, the latter value at saturated conditions. The relative permeability is generally defined as a function of the degree of saturation. Two forms are commonly used: either the power law:

$$k_r(S_l) = (S_l)^{\delta} \tag{3-3}$$

where δ is a parameter, or the van Genuchten expression:

$$k_r(S_l) = \sqrt{S_l}\left(1-\left(1-S_l^{1/\lambda}\right)^{\lambda}\right)^2 \tag{3-4}$$

where λ is a parameter which should correspond to the parameter values of the retention curve.

The retention curve describes a relation between the degree of saturation and the suction value, which in turn can be equated with the difference in gas and liquid pressure ($s = p_g - p_l$). The van Genuchten form of this curve is defined as:

$$S_l(P_l) = \left(1+\left(\frac{P_g - P_l}{P_0}\right)^{\frac{1}{1-\lambda}}\right)^{-\lambda} \quad (P_l < P_g) \tag{3-5}$$

where λ and P_0 are parameters.

The employment of a relative permeability function and a retention curve provides a means to describe both saturated and unsaturated flow with the liquid pressure as a common flow potential (see Figure 3-3), even though the transfer doesn't necessarily take place in liquid form.

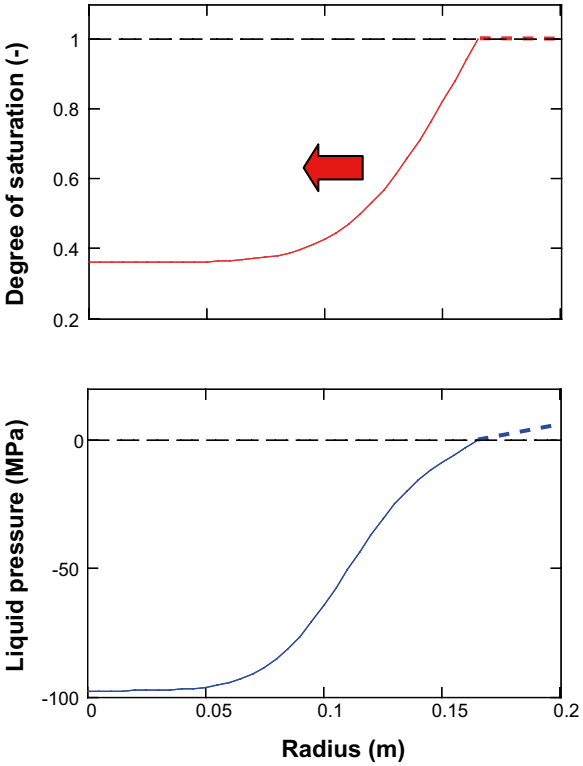

Figure 3-3. *Application of the liquid pressure as a potential for moisture transfer at unsaturated conditions.*

3.3.4 MX-80: Retention properties – free swelling conditions

Bentonite can exhibit quite significant hysteresis behaviour. It is therefore of importance to take the initial water content into consideration. Measurements are thus performed in two directions in order to obtain a complete description of the properties; both for increasing and decreasing relative humidity. Results from measurements with six such initial water contents are shown in Figure 3-4. One of these sets represents data for an initial water content of 9.8 %, which is relevant for the problem specification examined in Task 8 (see Figure 3-5).

The purest form of retention properties are measured at free swelling conditions. Two methods for such measurements are performed with jars and with sorption balance (see Dueck 2004). In general, in these measurement samples are equilibrated in a climate with a certain relative humidity (RH) after which the water content is measured.

The first step to adopt a van Genuchten retention curve is to convert the relative humidity values to suction values. The relation between these quantities is given by Kelvin's law:

$$s(RH,T) = \frac{-\ln(RH)\cdot\rho_w\cdot R\cdot(273.15+T)}{M_w} \quad (Pa) \qquad (3\text{-}6)$$

where T is the temperature (in °C), R is the universal gas constant and M_w is the molecular weight of water. The suction values for the 9.8 % measurements are also shown in Figure 3-5.

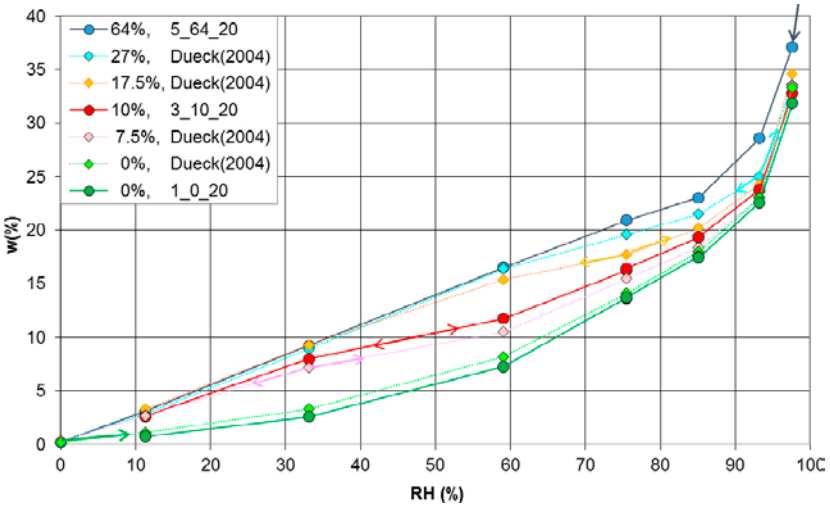

Figure 3-4. Retention data, determined with jars, for different initial conditions (Dueck and Nilsson 2010).

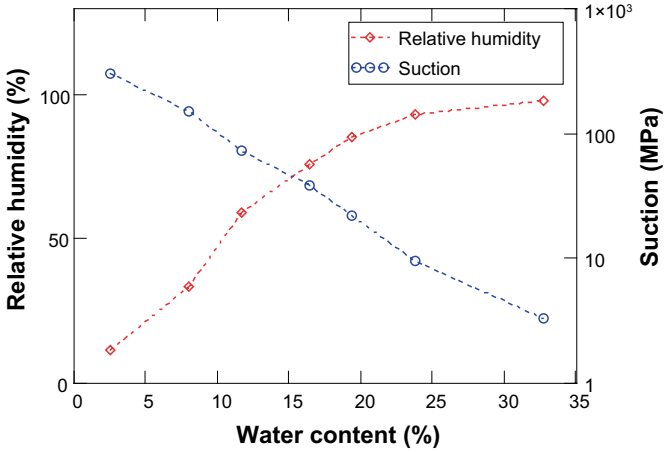

Figure 3-5. Retention data for 9.8 % initial water content. Relative humidity and corresponding suction values.

3.3.5 MX-80: Retention properties – confined conditions

The retention properties at confined conditions are influenced by mechanical interactions; a relation for this coupling has been proposed as:

$$s_{conf}(w, p) = s_{free}(w) - \alpha \cdot p \qquad (3\text{-}7)$$

where p is the mean stress, s_{conf} and s_{free} are the suction values for confined and free swelling conditions, respectively (see Dueck 2004). The value of the parameter α is usually assumed to be equal to unity, even though other values have been reported.

A complete curve for confined conditions is given by the unconfined data and the buildup of swelling pressure. This buildup has been proposed to be proportional to the increase in the degree of saturation (Börgesson 1985, Dueck 2004). At the initial point with zero swelling pressure the two curves coincide. At the final point, the swelling pressure is equal to the unconfined suction value, which yields a zero suction value.

The void ratio in the current problem with Task 8 is 0.78, which corresponds to a water content of 28.1 % at saturation (see Figure 3-6).

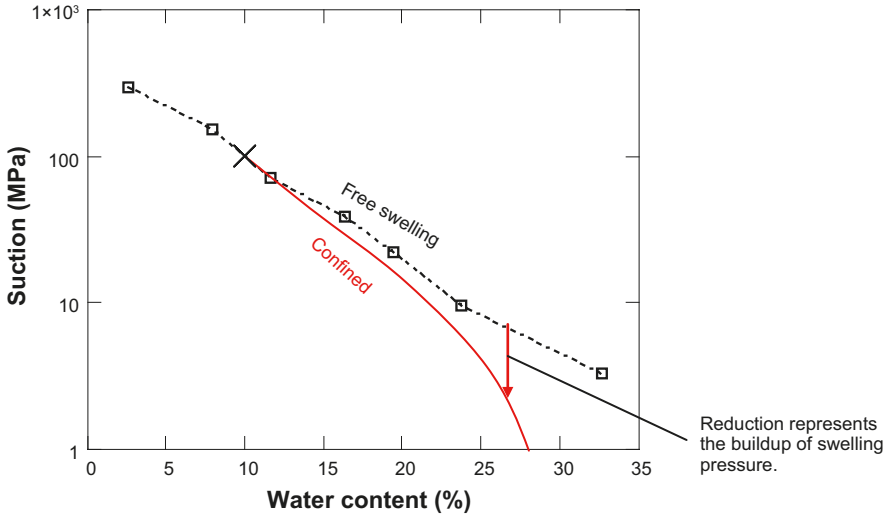

Figure 3-6. *Retention data for 9.8 % initial water content. Measured data at free swelling condition and principle for reduction due to confinement.*

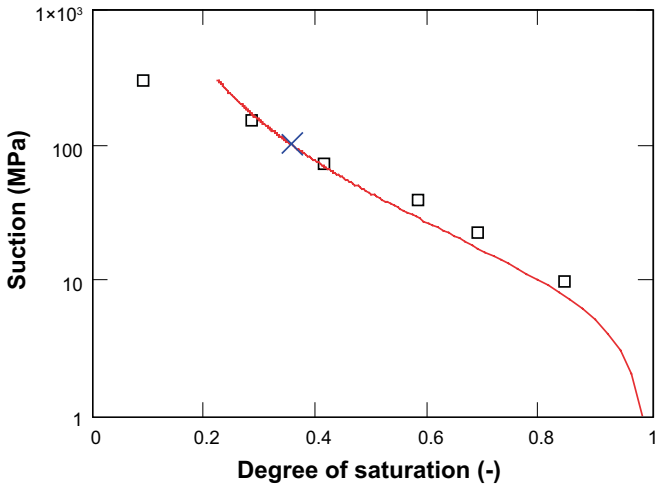

Figure 3-7. *Retention data for 9.8 % initial water content. Measured data at free swelling condition and adopted van Genuchten curve.*

The van Genuchten curve includes two parameters (λ and P_0). But only one of these is independent, since the initial point is specified (s: 100 MPa, and S_l: 0.36). There is therefore only one parameter to adjust, and different values yield different slopes. A fitted curve should follow the sketched curve in Figure 3-6 as closely as possible. An adopted set with P_0: 9.23 MPa and λ: 0.3 is shown in Figure 3-7.

3.3.6 MX-80: Hydraulic conductivity

A compilation of results from fairly recent measurements of the hydraulic conductivity of MX-80 is shown in Figure 3-8. It can be noticed that the dry density (or the void ratio) has a strong influence on the hydraulic conductivity. This dependence has been described on the following form by Börgesson et al. (1995):

$$K(e) = K_0 \cdot \left(\frac{e}{e_0} \right)^{\eta} \tag{3-8}$$

where K_0 and e_0 are reference values and η is a parameter.

A selection of the shown data has through least square regression yielded the following set of parameters: $K_0 = 2.4 \times 10^{-13}$ (m/s); $e_0 = 1.0$ (–); $\eta = 5.33$ (–) (Åkesson et al. 2010). This is illustrated as a solid black line in Figure 3-8. The void ratio in the current problem with Task 8 is 0.78, which corresponds to a hydraulic conductivity of 6.4×10^{-14} (m/s) according to this adopted line.

The data exhibit a significant scatter and it has therefore been recommended that this is taken into account through sensitivity analysis in which the conductivity is reduced by 40 % and increased by 100 %.

3.3.7 MX-80: Relative permeability

There is no practical way to measure the relative permeability directly. Instead it must be indirectly evaluated, through modeling of water uptake tests with assigned values of the hydraulic conductivity and the retention curve. An example of such an evaluation is shown in Figure 3-9. This shows experimental and model results for a water uptake test. The relative permeability law used in this model was a cubic power law, i.e. with δ = 3. This law is frequently used for modeling of highly compacted bentonite.

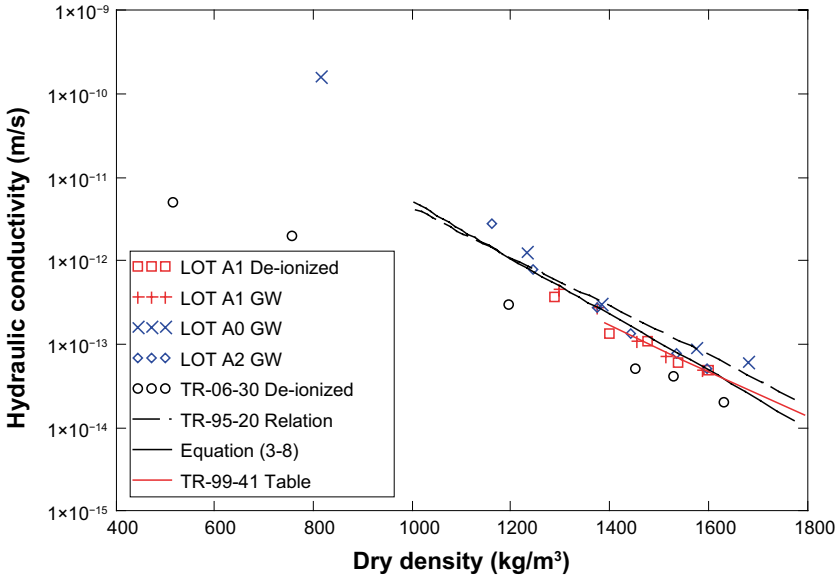

Figure 3-8. *Hydraulic conductivity versus dry density (from Åkesson et al. 2010). Experimental data (symbols) and adopted relations (lines).*

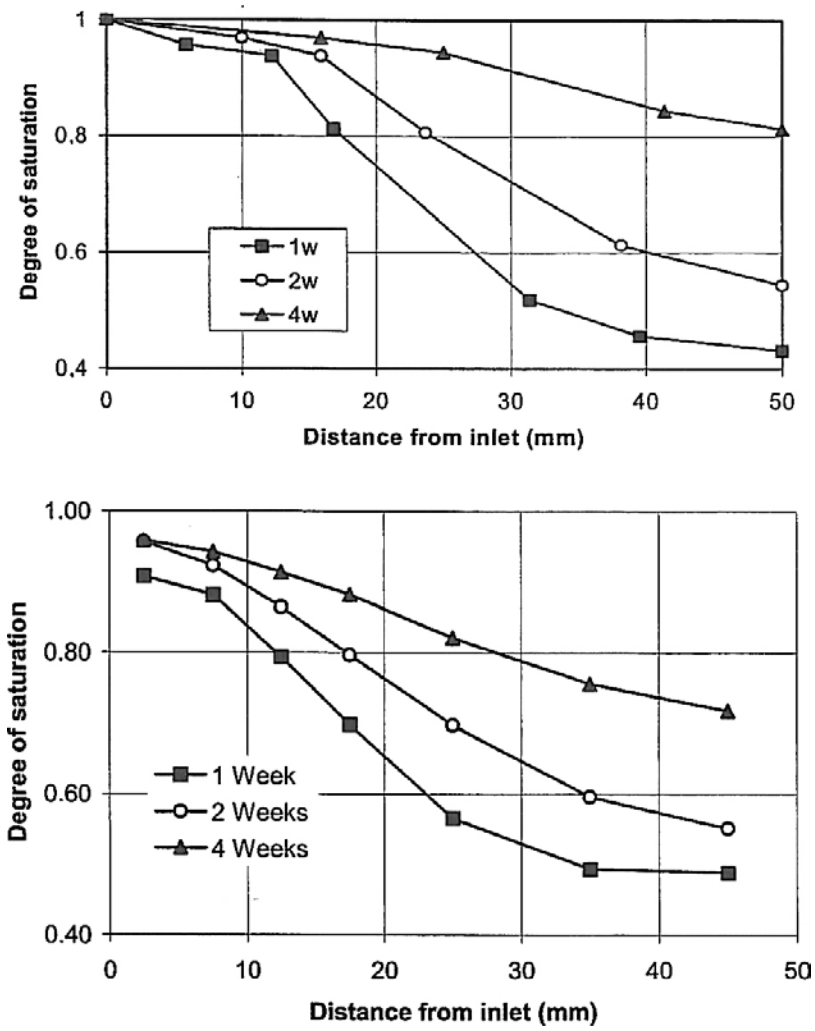

Figure 3-9. *Calculated degree of saturation as a function of the distance from the water inlet after 1, 2 and 4 weeks (upper) and corresponding measurements (lower) (from Börgesson and Hernelind 1999).*

3.3.8 Bentonite: Vapor transport

In the FEM code Code_Bright, the vapour diffusion is driven by a gradient in the vapour mass fraction of the gas phase (ω_g^w):

$$\vec{i} = -n \cdot \tau \cdot D \cdot (1 - S_l) \cdot \rho_g \cdot \nabla \omega_g^w \qquad (3\text{-}9)$$

where n is the porosity, S_l is the water saturation and ρ_g is the gas density. The diffusion coefficient of vapour in air is calculated as:

$$D = 5.9 \cdot 10^{-6} \frac{(273.15 + T)^{2.3}}{P_g} \qquad (m^2 / s) \qquad (3\text{-}10)$$

where T is the temperature (in °C) and P_g is the gas pressure (in Pa). The only remaining parameter to be quantified is the tortuosity factor (τ).

Since there is no plan to include any heater or canister in Task 8, this transport process can be neglected.

3.2 Hydraulic properties of granitic rock

In the following some main notations will be introduced:

- Rock matrix is the “fracture free” environment in between fractures.
- Fractures are, for the usage herein, mostly single fracture features but do in a broader sense include also conductive deformation zones of large scale.
- Bedrock is the combined material composed of rock matrix and fractures. Limited information exists on the rock matrix and most properties are extracted from small-scale hydraulic tests in bedrock.

3.2.1 Rock matrix properties

Hydraulic conductivity

Within the “Matrix fluid chemistry experiment” at Äspö HRL, the recommendation on hydraulic conductivity on Äspö diorite was to use a value of 3×10^{-13} m/s, based on hydraulic characterisation of the rock matrix, as core samples, with the He-gas method (Gustafsson 2001).

In-situ hydraulic injections tests most often report higher hydraulic conductivity values, typically in the range of 10^{-12} to 10^{-10} m/s; these results, however, are constrained by both measurement limitations and the tested scale. In the Äspö HRL environment it is not known that any hydraulic injection tests have been conducted in a fracture free borehole section. Reports from AECL’s Underground Research Laboratory (with a much lower fracture intensity) indicate a hydraulic conductivity as low as 1.5×10^{-14} m/s based on pressure pulse tests (Vilks and Miller 2007). In the Isothermal Buffer Test (Dixon et al. 2001) the hydraulic conductivity of the granite at URL was estimated to be between 10^{-14} and 10^{-12} m/s.

Porosity

Measured mean values of the total porosity for the major rock types in the Laxemar area have been obtained in the range of 0.26–0.36 vol-% (Byegård et al. 2006). In the granite at URL (Dixon et al. 2001) the total porosity (effective porosity) is estimated within the interval 0.32–0.67 vol-%.

Measured values from short cored holes from deposition hole walls indicate a narrow layer of increased porosity before stable values around the above given mean is reached only 1–2 centimeters into the rock matrix (Figure 3-10).

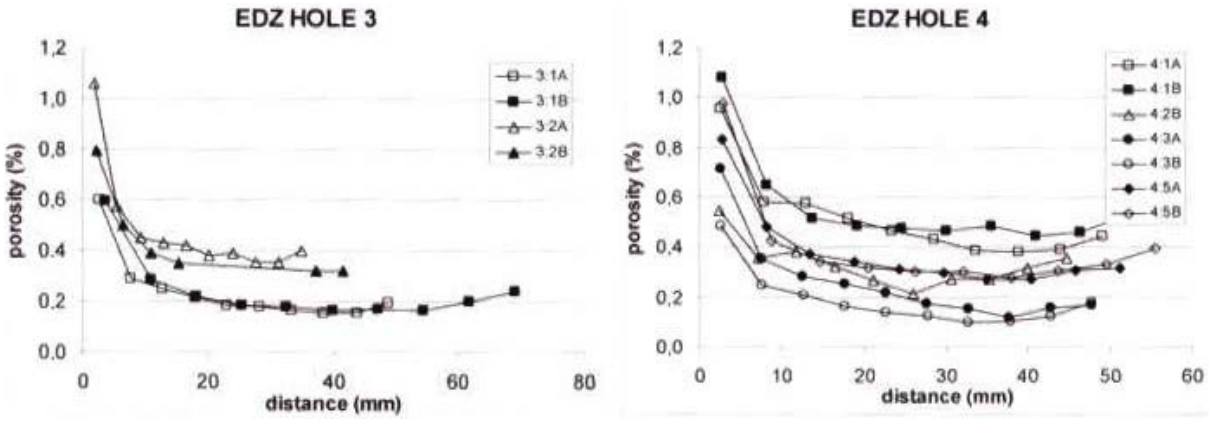

Figure 3-10. *Porosity data for granitic rock measured from deposition hole walls and inwards into the rock matrix. Samples from Äspö HRL (from Rhén and Forsmark 2001).*

3.2.2 Rock fracture properties

Fracture aperture

Rocks, deep down in the Earth's crust, are well confined and under a significant influence of a temperature field. Furthermore, the loads in nature are mainly from tectonic processes acting over a significant time scale. These are conditions mainly supporting ductile deformation and not in general conditions supporting the assumptions behind the theories of brittle failures; neither is the rock a homogeneous and isotropic material. However, if it is assumed that the rock mass behaves as a perfectly elastic, homogeneous, and isotropic body then linear elastic fracture mechanics can be successful in many rock mechanical problems (Olson 2003), including the analysis of joint spacing and clustering (e.g. Pollard and Segall 1987). A standard assumption in the reported works is that all fractures within a population opened up in response to one driving stress event. This assumption yields a nice theoretical relationship between fracture length (L) and maximum fracture opening, d_{max} (aperture):

$$d_{\max} = (u - \sigma_n)\left(\frac{2(1-\upsilon^2)}{E}\right)L \qquad (3\text{-}11)$$

where ν is Poisson's number and E stands for Young's modulus.

As it is realistic to assume that the change both in pore pressure, u, and the normal load on the fracture, σ_n, can be expressed through a constant and a volumetric change of the fracture, it is plausible that the maximal opening of a fracture can be expressed in the form:

$$d = a \cdot L^b \qquad (3\text{-}12)$$

That the width of fracture openings in relation to the fracture size follows a power-law is supported by different findings in nature. As one example, Vermilye and Scholz (1995) presented field data on the relation between vein length and vein thickness (aperture) from a couple of hard rock sites (Figure 3-11).

The relationship established by Vermilye and Scholz (1995) was in agreement with several published data on mafic dikes and faults. The proposed relationship for single segment features was later verified by the results presented by Gudmundsson (2000). Although, most data is indicative and large variations exists it is a generally accepted hypotheses that a dependency between aperture and fracture size similar to what is presented above exist.

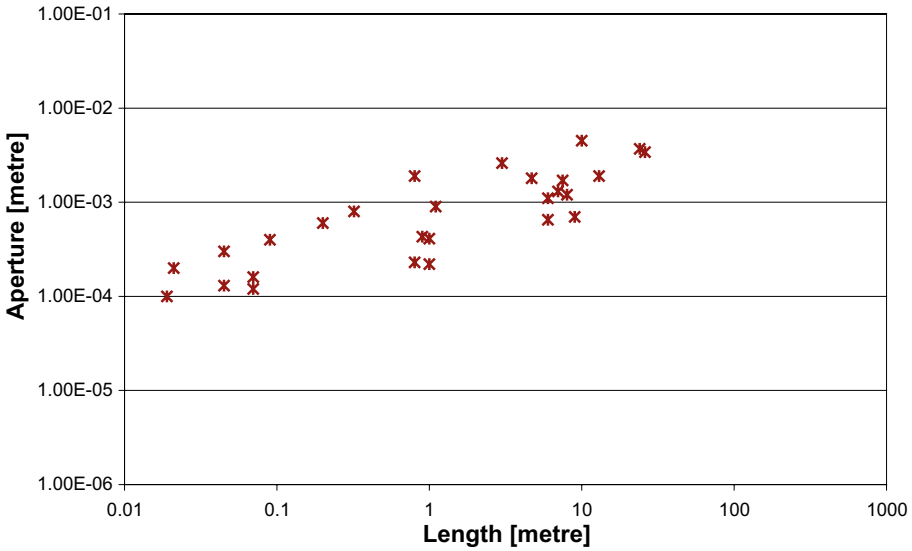

Figure 3-11. *Aperture (maximum width on veins) in relation with measured length (trace length). Reproduction of some of the compiled data presented in Vermilye and Scholz (1995).*

Fluxes of a Newtonian liquid (e.g. water) within a medium can theoretically be expressed by the Navier-Stokes equation, which for the case of flow between smooth and parallel plates results in a solution known as the cubic law (e.g. Zimmerman and Bodvarsson 1996):

$$Q_f = \frac{d^3 \rho g}{12 \mu} \frac{\partial h}{\partial x} \qquad (3\text{-}13)$$

Although, as concluded by Zimmerman and Bodvarsson (1996), variations in aperture within a natural fracture deviate the relationship by dependencies on the standard deviation and, not least, the area of contact between the two fracture surfaces, it is still a valid assumption that the transmissivity of a fracture is related to its size with some relationship and likely that the transmissivity to the fracture size relationship is close to a power of 3 larger than the aperture to fracture size relationship.

Fracture transmissivity

A compilation of data from Äspö HRL yields some estimated transmissivity values on single fractures or large-scale zones and from different bounds one could assign a typical size of these structures (Figure 3-12).

Applying a 1 to 3 order of magnitude relationship a trend line for the small-scale fractures could be specified. In a similar manner the large-scale structures could be fitted. For large-scale structures, however, it is important to recognise that the relationship not only describes transmissivity but also contains a strong factor related to connectivity. It is worth observing that in order to create the small-scale fracture trend as done below, one has to ignore the evaluated hydraulic conductivity based on matrix core samples. Omitting the matrix values is relevant since it is based on an alternative conceptual bases, that is porous media flow and not fracture flow.

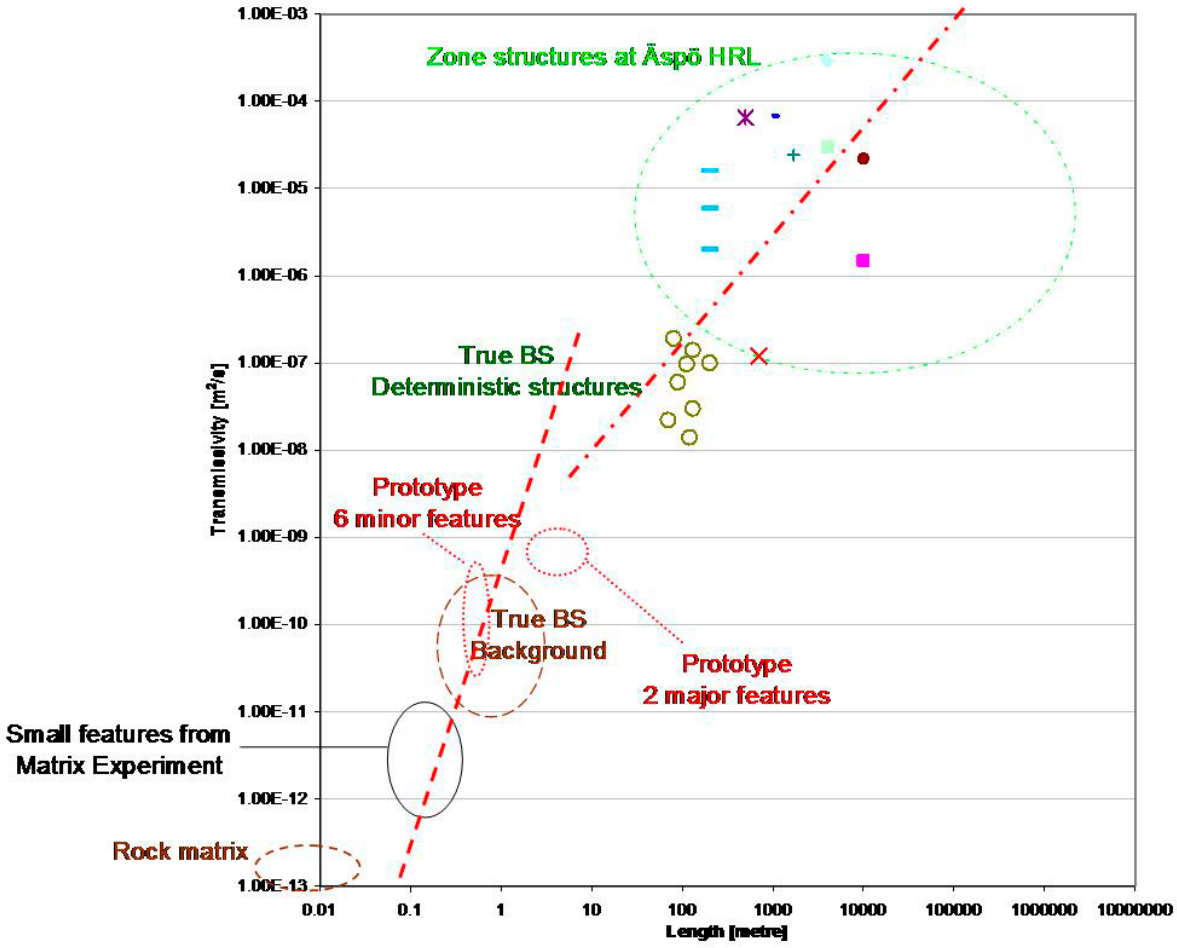

Figure 3-12. *Transmissivity to size data from Äspö HRL.*

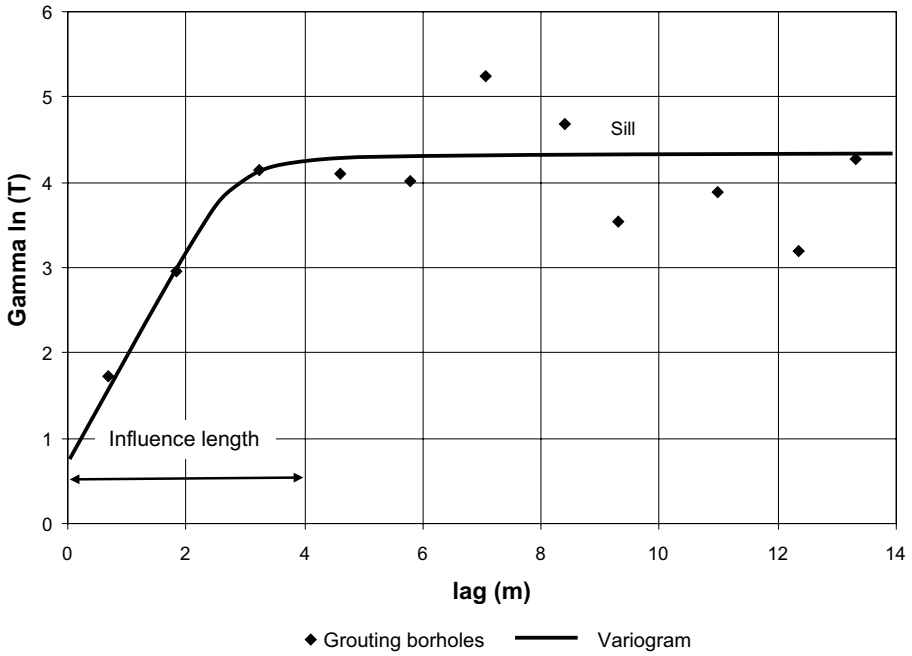

Figure 3-13. *Variogram of ln(T) for some grouting boreholes (from Gustafson et al. 2008).*

Recognising the existence of a connectivity dependence on the large-scale structures a similar dependence may exist also for the small-scale structures. Small-scale structures could be viewed as relatively short single fractures. If a single structure follows a transmissivity size trend as indicated above the large size of a fracture is somewhat restricted, and an approximate 100 metre large fracture could possibly be of a transmissivity around 10^{-3} m^2/s. Alternatively, small-scale structures could be bounded by spatial variability of apertures and hence some kind of correlation on transmissivity values and distance should be apparent. In Gustafson et al. (2008) a variance statistical analysis on evaluated transmissivity values from hydraulic tests performed in the same section yields a typical correlation distance of 3–4 metres (Figure 3-13). A similar distance was found for Äspö HRL data for section-to-section analyses from long boreholes at Äspö HRL. These works indicate that some correlation exists for transmissivity values.

3.2.3 Fracture storativity

In traditional hydrogeology, storativity or storage coefficient (S) is the volume of water released from storage per unit decline in hydraulic head in the aquifer, per unit area of the aquifer, i.e. storativity is the vertically integrated specific storage value for the aquifer. Storativity is a dimensionless quantity.

If the continuity equation over an aquifer is combined with equations of state one will find that the mass accumulation is dependent on among other factors the compressibility of both the fluid and the aquifer skeleton. The combination of these factors within an aquifer is defined as the storativity. The storativity is defined within a porous medium and therein expressed as:

$$S = b(\alpha\rho g + n\beta\rho g) \tag{3-14}$$

where b is the aquifer thickness (or the hydraulic aperture of a fracture), α is the compressibility of the water, n is the porosity, and β is the compressibility of the medium (pores and solid).

On a larger scale it is plausible that this concept of storativity is valid for a fracture aquifer; however, at the scale of individual fractures the concept of porosity is as earlier stated dubious and the release or accumulation of mass from a fracture is maybe best described by the hydro-mechanical responses depending on among other factors the fracture stiffness.

3.2.4 Bedrock properties

Hydraulic conductivity

The Zedex tunnel experiment investigated the near tunnel wall hydraulic conductivity on a relatively small scale. The majority of tests were conducted in test sections of length 1 metre or less. Based on the results presented in Figure 3-14 hydraulic conductivity values below approximately 5×10^{-12} m/s seem affected by measurement limitations and the convergence towards 1×10^{-12} m/s is most likely yielding too high values for the lower range of hydraulic conductivity. However, as the median value falls on a lognormal trend line it is a reasonable estimate that the bedrock, for the investigated volume, on a one metre scale has a reasonable median value somewhere between $5^{-10} \times 10^{-12}$ m/s.

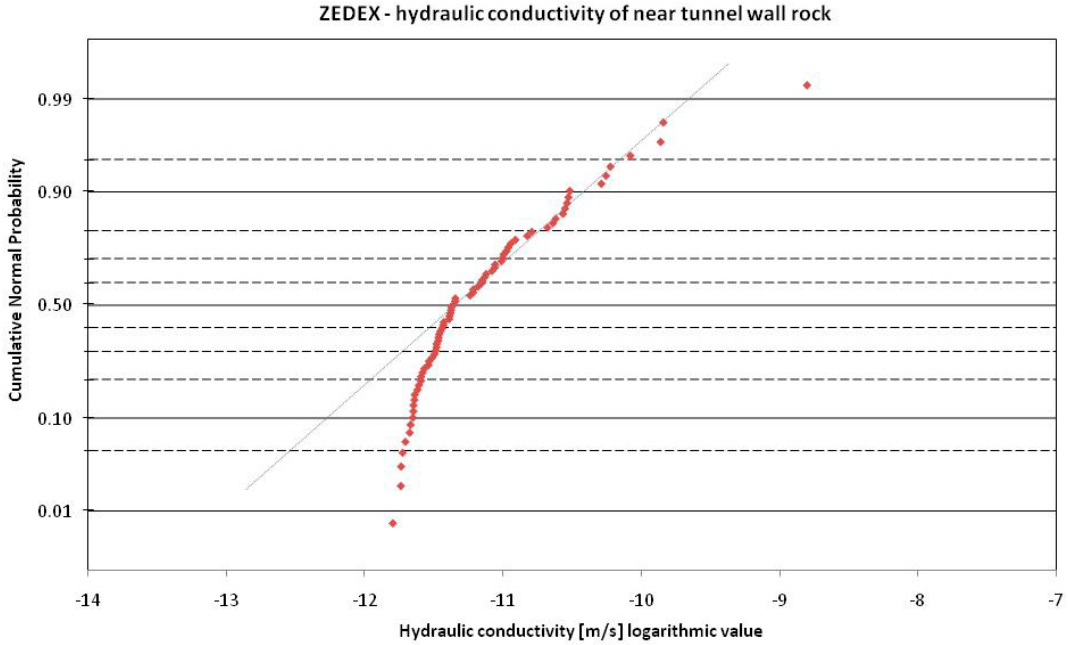

Figure 3-14. *Hydraulic conductivity data evaluated from pressure tests in the TBM part of Zedex tunnel experiment at Äspö HRL.*

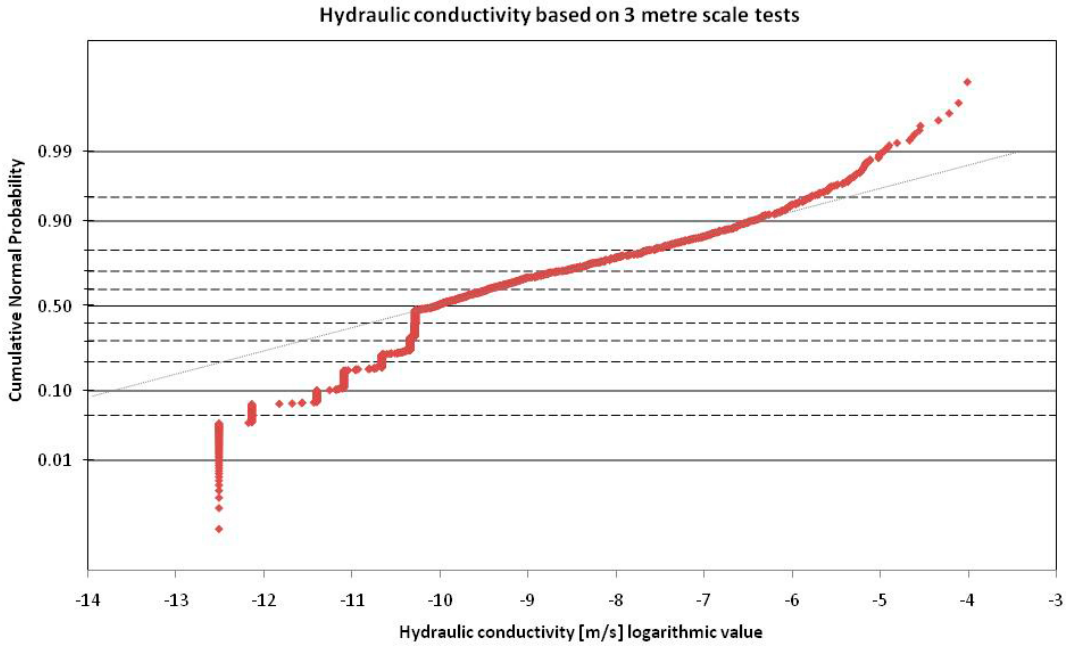

Figure 3-15. *Hydraulic conductivity data evaluated from pressure tests in the 3-metre test scale at Äspö HRL (updated to the GeoMOD project).*

The tests on this part are primarily established in horizontal boreholes and as such reflect the hydraulic conductivity of predominantly vertical or sub-vertical structures.

The most common test scale at Äspö HRL is the 3-metre scale; this scale is supported with more than 1 000 unique entries in the Äspö HRL data base (SICADA), see Figure 3-15.. The majority of these tests were conducted during the pre-investigation phase in vertical or sub-vertical boreholes. This results in hydraulic conductivity values representative primarily of horizontal or sub-horizontal structures.

In Vidstrand (1999) it was hypothesized that at Äspö HRL a scale threshold located somewhere below the 10-metre scale divided the available hydraulic conductivity measurements into two sub-sets. This hypothesis is supported by the results presented in Rhén and Forsmark (2001), where the average distances between tested sections with a transmissivity value above a certain value was analyzed on the 3-metre scale sections available, suggesting that one needs to assess a scale larger than approximate 10 metres in order to capture the overall bedrock properties.

Specific Storage

The Specific Storage (Ss) is the amount of water that a portion of an aquifer releases from storage, per unit mass or volume of aquifer, per unit change in hydraulic head, while remaining fully saturated.

Some interference tests on southern Äspö were used to provide an estimate of specific storage on the order of $2.0 \cdot 10^{-6}$ (m^{-1}). Based on these data and an estimate based on evaluated rock mechanical properties, Rhén et al. (1997) established a linear relationship between the logarithms of the hydraulic conductivity and the specific storage. This relationship is presented in Figure 3-16 and Figure 3-17 as comparison to compiled data.

Figure 3-16 and Figure 3-17 present the established specific storage values in relation to hydraulic conductivity from the La Scala and the Prototype Repository experiment, conducted at Äspö HRL during the 1990s, respectively.

The diagnostic results from the La Scala experiment indicate higher values for the specific storage than presented by Rhén et al. (1997); while estimates for the specific storage from the hydraulic tests performed in the Prototype Repository experiment indicate a lower limit for the specific storage than previously suggested by Rhén et al. (1997).

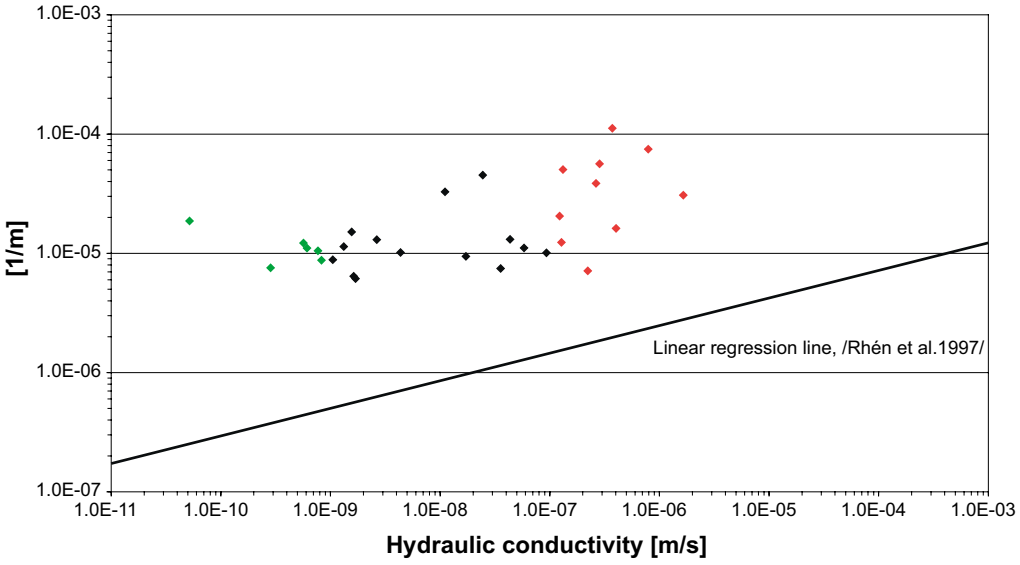

Figure 3-16. *Estimated specific storage from the La Scala experiment.*

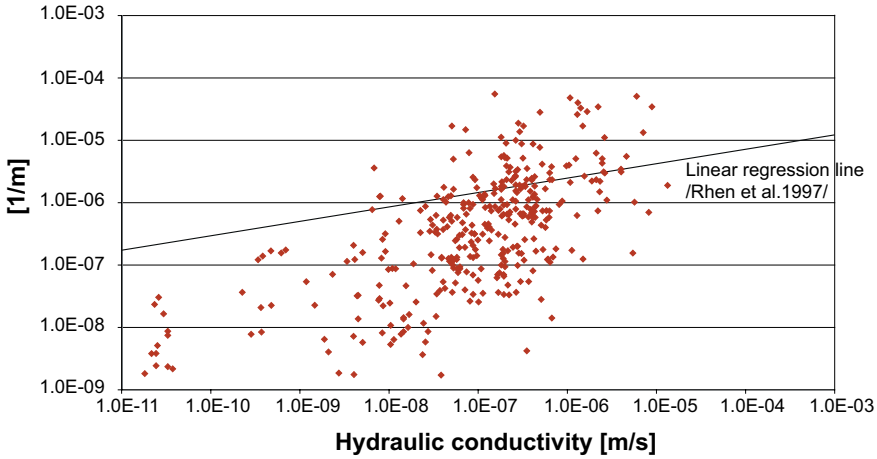

Figure 3-17. *Estimated specific storage from the Prototype Repository experiment (Rhén and Forsmark 2001).*

Storativity

The storativity is often difficult to determine from a hydraulic test. In Rhén and Forsmark (2001) a compilation of transmissivity and storativity, from test sections where both entities have been evaluated, is assessed yielding an empirical relationship:

$$Log_{10}S = 0.640 \cdot Log_{10}T - 1.570 \qquad (3\text{-}15)$$

The transmissivity values are between 10^{-7} and 10^{-6} m^2/s. Hence, the applicability of the regression results to tight single fractures is doubtful.

Porosity

Typically the total porosity is not considered in hydrogeology application and instead a kinematic porosity is assigned. Snow (1968) compiled data and suggested the porosity in fractured rock to be on the order of 10^{-4}, a value that coincides with data still used for Äspö HRL applications.

3.2.5 Retention and relative permeability

Reported retention curves and relative permeability parameters for granitic rock are shown in Table 3-2 and Figure 3-18. Among these, only the data given by Finsterle and Pruess (1995) appear to be based on actual measurements (in Grimsel). These data are therefore proposed for the modelling tasks.

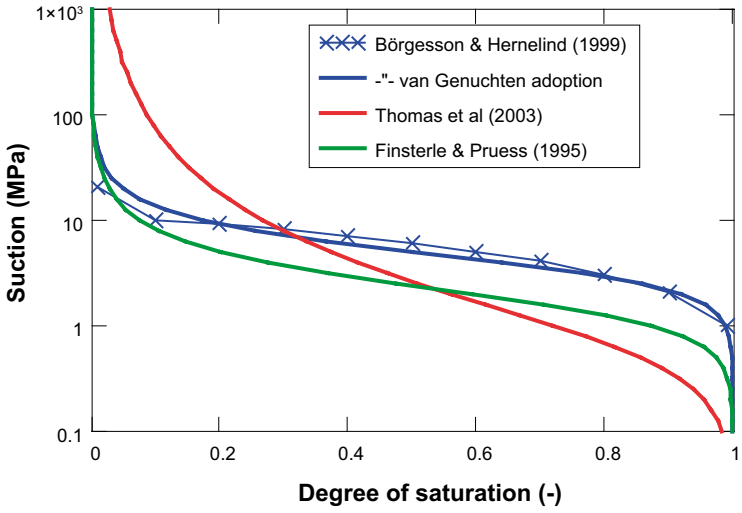

Figure 3-18. *Reported retention curves for granitic rock.*

Table 3-2. Reported retention curves.

Source	P_0 (MPa)	λ (–)	Relative permeability
Börgesson and Hernelind (1999)	4	0.65	Power law (δ = 3)
Thomas et al. (2003)	0.7	0.33	vG (λ = 0.33)
Finsterle and Pruess (1995)	1.74	0.60	vG (λ = 0.60)

3.3 Example as an introduction to scoping calculations of Task 8

Scoping calculations of idealized representations of the planned Task 8 test have been performed with a number of models. Two numerical models, using the FEM code Code_Bright v2.2 have been made: one 1D axi-symmetric and one 2D axi-symmetric. In addition, calculations have also been made using analytical solutions of diffusion in a cylinder and in a plane.

3.3.1 1D axi-symmetric Code_Bright model – only MX-80

The 1D model only includes the bentonite. The geometry, the mesh and the initial and the boundary conditions are shown in Figure 3-19. The properties of the bentonite were adopted in accordance to the descriptions in the sections above, with a porosity of 0.438, an intrinsic permeability of 6.4×10^{-21} m^2, a van Genuchten retention curve with a P_0 of 9.23 MPa and a λ of 0.3. Finally, a cubic power law was used for the relative permeability. Results are shown as radial distributions of saturation in Figure 3-20. It can be noticed that full saturation is reached after approximately one year.

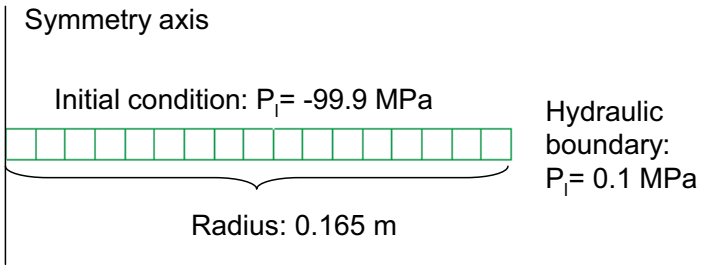

Figure 3-19. *Geometry, mesh, initial and boundary conditions of 1D axi-symmetric model.*

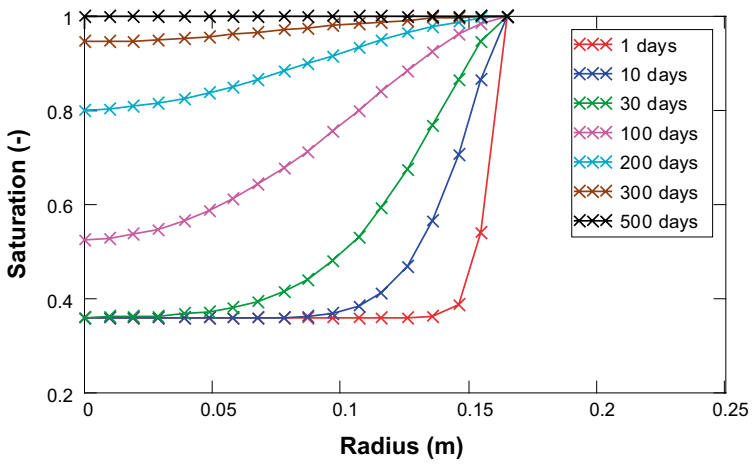

Figure 3-20. *Radial distribution of liquid saturation in 1D model.*

3.3.2 2D axi-symmetric Code_Bright model

Model description

The 2D model includes the bentonite as well as a cylinder of rock which is represented as intact rock intersected by a fracture. The bentonite was modeled as a filling in a 3 m deep borehole beneath a schematic representation of a tunnel. The geometry and the mesh are shown in Figure 3-21. The mesh consisted of 1 696 nodes and 1 597 elements.

The initial state was reached by keeping the liquid pressure at the rock wall in the tunnel and the bore hole at atmospheric pressure, and the outer boundary at 5 MPa during half a year, thereby reaching a steady flow through the rock. After that the installation was modeled through decreasing the liquid pressure in the bentonite material down to −99.9 MPa during a short period (approx. 8 hours). After this, the boundary conditions at the outer boundary and the rock wall of the tunnel were kept at 5 and 0.1 MPa, respectively (Figure 3-22).

The representation of the fracture was chosen in such a way that the inflow into the borehole would be 0.1 l/min at atmospheric pressure in the borehole and 5 MPa at the outer boundary. With a generic fracture material of a thickness of 0.1 m, this corresponds to an intrinsic permeability of 2.5×10^{-15} m^2 (see Figure 3-23).

For the intact rock, a hydraulic conductivity of 6×10^{-13} m/s was chosen. All other material parameters were chosen in accordance with the descriptions in the state-of-the-art sections above (see Table 3-3).

The temperature of the model was kept constant at 20 °C. No gravity was applied.

Table 3-3. Parameter values used for different materials.

Material	n (–)	P_0 (MPa)	λ (–)	k (m^2)	kr (–)
Bentonite	0.438	9.23	0.3	6.4×10^{-21}	S^3
Rock	0.003	1.74	0.6	6×10^{-20}	vG λ = 0.6
Fracture	0.003	1.74	0.6	2.5×10^{-15}	vG λ = 0.6

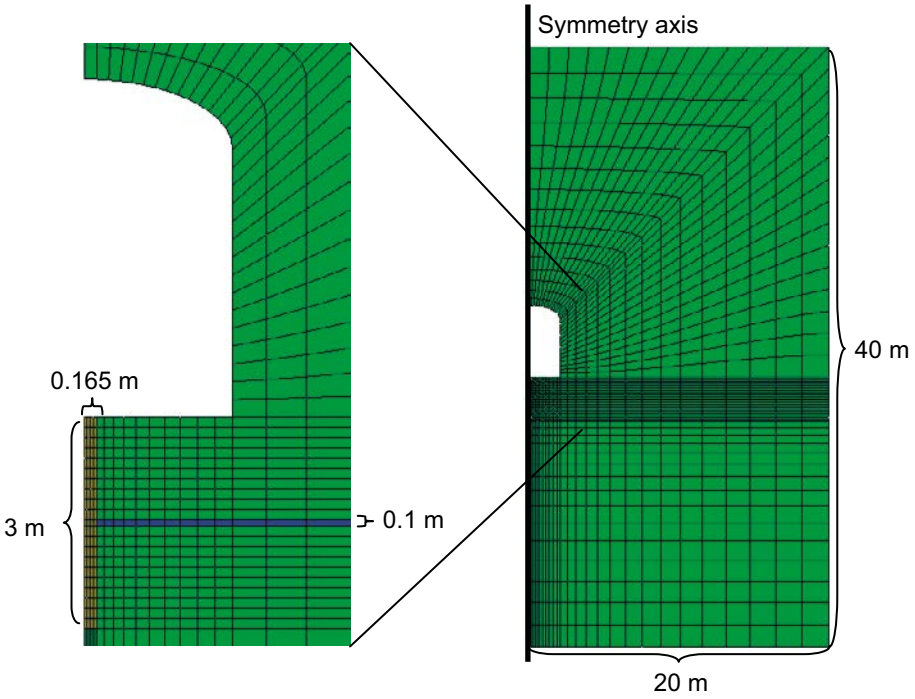

Figure 3-21. *Geometry and mesh of 2D axi-symmetric model.*

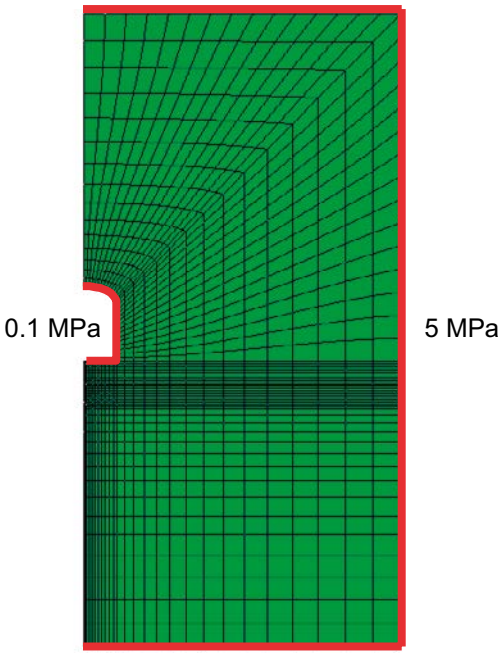

Figure 3-22. *Boundary conditions of 2D axi-symmetric model.*

Transmissivity:	$T := 2.5 \cdot 10^{-9}$	m^2/s
Head:	$\Delta h := 500$	m
Outer radius:	$r_o := 20$	m
Inner radius:	$r_i := 0.165$	m
Frac. model width:	$L := 0.1$	m
	$lpm := 1000\,60$	
Inflow:	$2 \cdot \pi \cdot T \cdot \frac{\Delta h}{\ln\left(\frac{r_o}{r_i}\right)} \cdot lpm = 0.098$	l/min
Permeability	$\frac{T}{L} \cdot 10^{-7} = 2.5 \times 10^{-15}$	m^2

Figure 3-23. *Adoption of fracture material permeability (excerpt from MathCad document).*

Model results

Contour plots of liquid pressure in the rock are shown in Figure 3-24. These plots show the initial drawdown around the tunnel, and that the fracture promotes a rapid advance of high pressures towards the borehole. A detail of the pressure distribution in and around the borehole is shown in Figure 3-25. This illustrates the high hydraulic gradients in the vicinity of the borehole which apparently can contribute to the bentonite hydration if the hydraulic conductivity of the intact rock is sufficiently high.

Axial and radial distributions of the saturation are shown in Figure 3-26. The radial propagation at the mouth of the fracture is similar to the results in the 1D model in Figure 3-20. The process is nevertheless faster in the 2D model, which probably is due to the higher boundary pressure used in this model. The axial propagation of the hydration of the bentonite is slower than the radial, as expected. Full saturation is reached after little more than two years. The hydration beneath the fracture is faster than above. The last point to be saturated is in the center of the bentonite at the tunnel floor level.

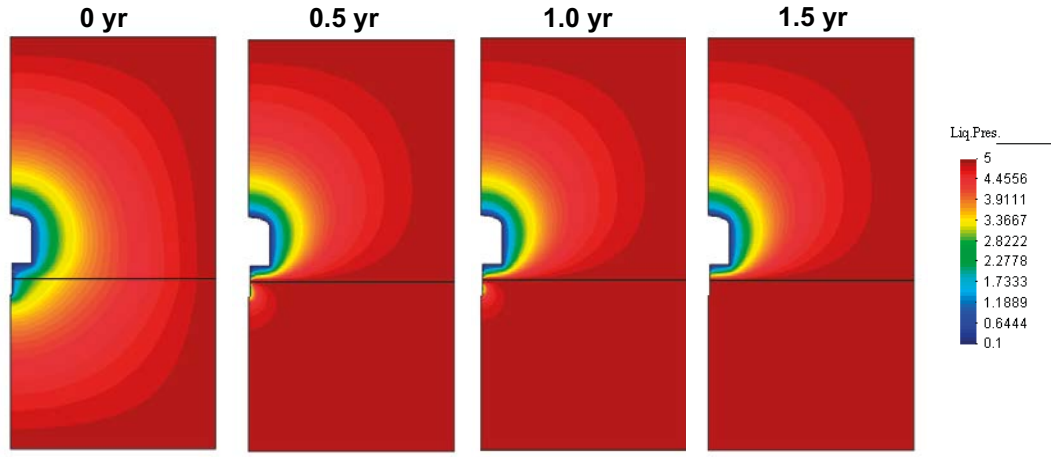

Figure 3-24. *Contour plots of liquid pressure in rock.*

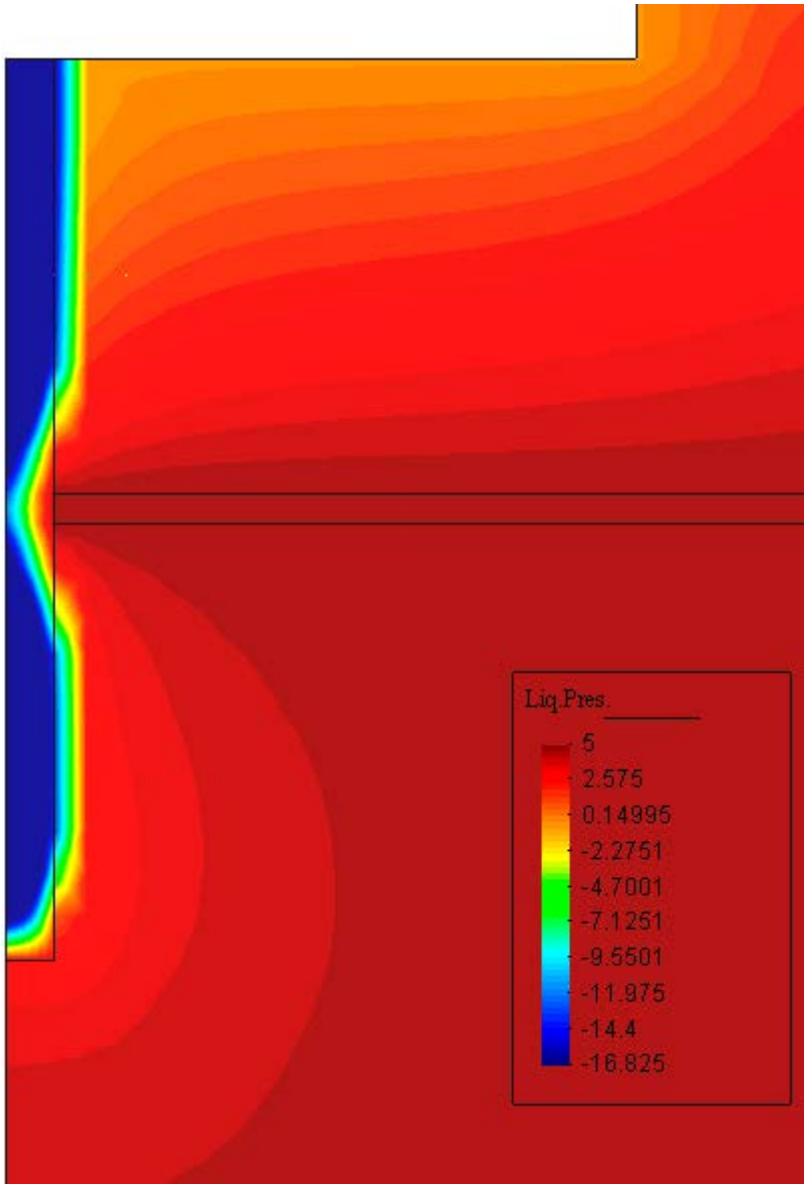

Figure 3-25. *Contour plots of liquid pressure in rock and bentonite after 0.5 years. The significant pressure gradients above and below the fracture can be noticed.*

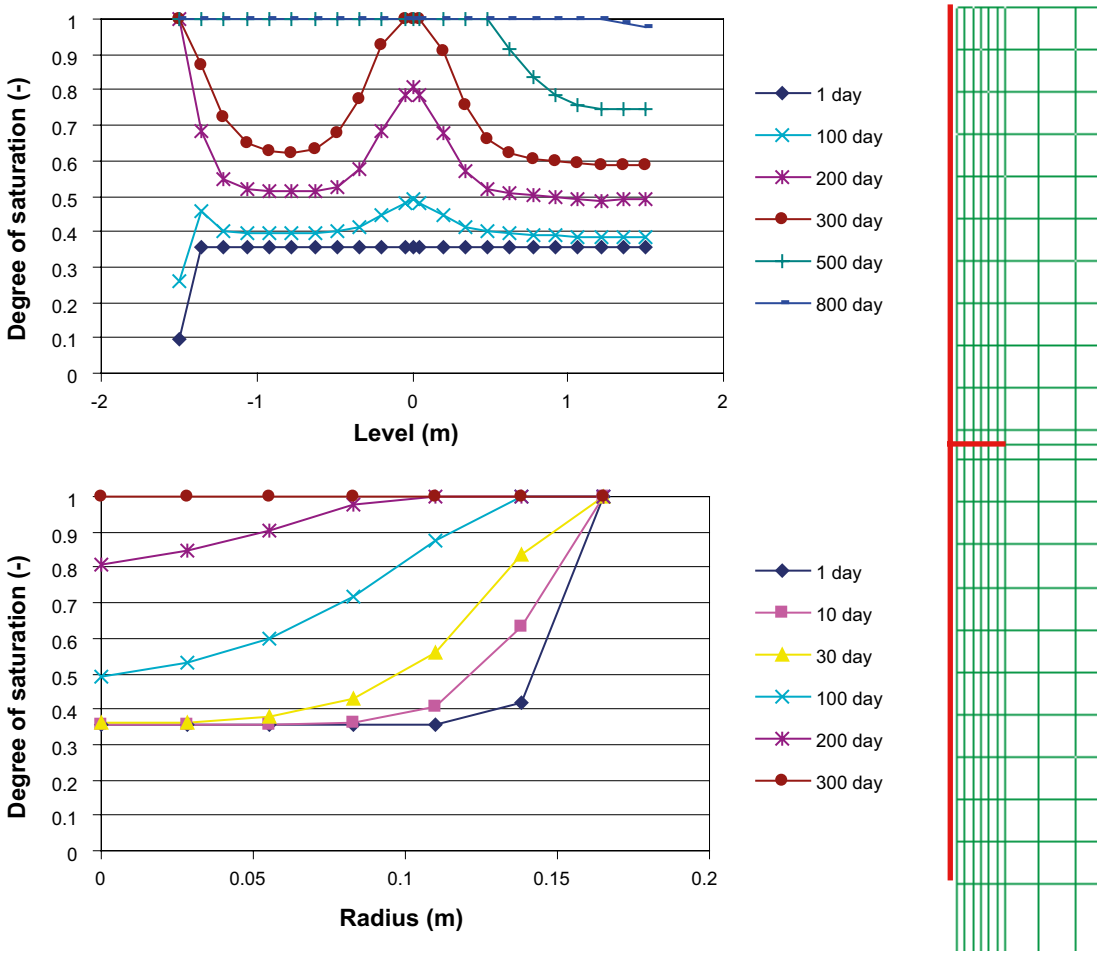

Figure 3-26. *Axial (upper) and radial (lower) distribution of liquid saturation in 2D model. Model mesh and position of axial and radial (in red) shown on right.*

3.3.3 Analytical solutions

The hydration of bentonite can to some extent be described as a diffusion process, and an early attempt to model water uptake used standard analytical solutions for diffusion (Börgesson 1985).

The moisture diffusivity can be evaluated from the quantities described in the state-of-the-art sections above according to the following expression:

$$D(S_l) = \frac{k \cdot k_r(S_l)}{n \cdot \mu} \cdot \frac{dP_l}{dS_l} \qquad (m^2/s) \qquad (3\text{-}16)$$

The diffusivity is a function of the degree of saturation, due to the saturation dependence of the retention curve and the relative permeability function. However, standard solutions of the diffusion partial differential equation are only valid for constant values of the diffusivity. A representative value therefore has to be chosen. An evaluation of this is shown in Figure 3-27, and a general value of 4×10^{-10} (m^2/s) has been adopted for the different solutions.

The radial uptake of water, corresponding to the 1D axi-symmetric model, was calculated with an analytical solution for diffusion in a cylinder (Crank 1975). The complete calculation is shown in Figure 3-28. The results from the numerical model are included for comparison, and it can be noted that the numerical calculation yields a slightly faster hydration. This is probably due to the difference between the constant diffusivity and the saturation dependent function in Figure 3-27.

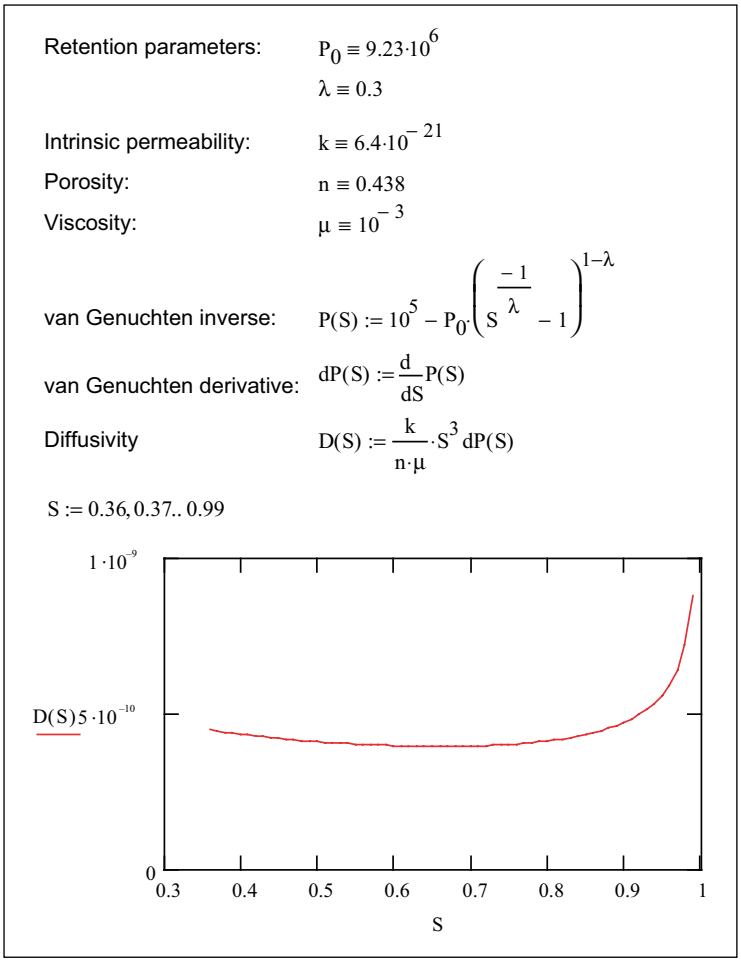

Figure 3-27. *Evaluation of moisture diffusivity (excerpt from MathCad document).*

The axial water uptake from the plane of the fracture, and with no contribution from the intact rock (Figure 3-29), can be calculated with a solution for diffusion in a plane (Crank 1975). It can be noted that the time scale for this process is much slower than the hydration in the 2D model (Figure 3-30). It can therefore be concluded that the intact rock can play a significant contribution to the hydration, even though the adopted hydraulic conductivity is as low as 6×10^{-13} m/s.

3.4 Combined tests with buffer and granitic rock: Isothermal test

The isothermal test was a full-scale test performed by Atomic Energy of Canada Limited (AECL) at 240 m depth in its Underground Research Laboratory during the 1990s. The test was carried out in a 5 m deep borehole with a diameter of 1.24 m (Figure 3-31). The lowermost two meters of the borehole were filled with in-situ compacted buffer material consisting of a 50-50 bentonite-sand mixture. The buffer material was sealed with a 1.25 m thick cap of high-performance concrete and was left undisturbed for 6.5 years.

The analyses performed on sampled material from the dismantling showed that the hydration of the buffer was far from complete at that time (Figure 3-31).

A more detailed description of this test can be found in Dixon et al. (2002). An attempt to model the test has been reported by Thomas et al. (2003). It can also be mentioned that the test has been one of the benchmarks in the EBS Taskforce.

$$\alpha := \left| \begin{array}{l} \text{for } n \in 1..nmax \\ \quad rg \leftarrow (n \cdot 3.137 - 0.847) \\ \quad \alpha_n \leftarrow \dfrac{root(J0(x), x, rg - 0.5, rg + 0.5)}{a} \\ \alpha \end{array} \right.$$

$nmax \equiv 30$

$a \equiv 0.165$

$D \equiv 4 \cdot 10^{-10}$

$day \equiv 3600 \cdot 24$

$S_{in} \equiv 0.36$

$$S(r,t) := S_{in} + (1 - S_{in}) \cdot \left[1 - \frac{2}{a} \cdot \sum_{j=1}^{nmax} \frac{\exp\left[-D \cdot (\alpha_j)^2 \cdot t\right] \cdot J0(r \cdot \alpha_j)}{\alpha_j \cdot J1(a \cdot \alpha_j)} \right]$$

$r := 0, 0.005 .. 0.165$

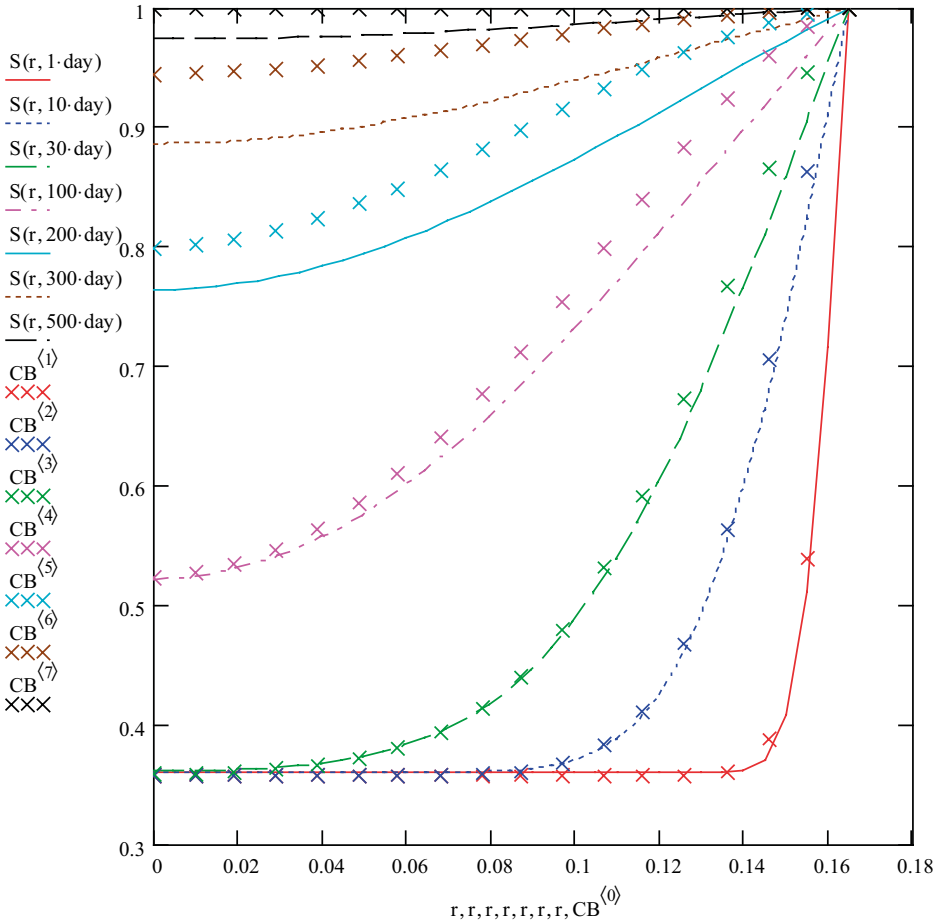

Figure 3-28. *Radial distribution of liquid saturation. Solid lines: analytical solution; crosses: numerical 1D model (excerpt from MathCad document).*

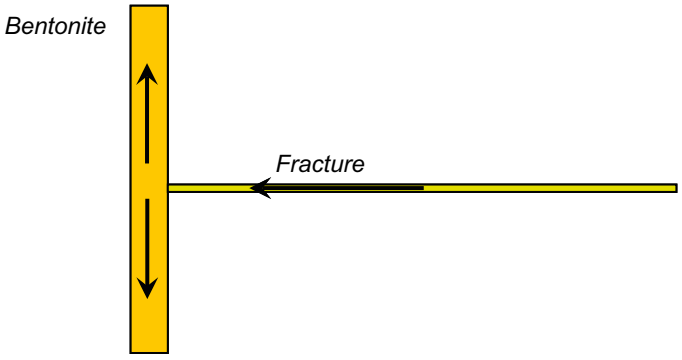

Figure 3-29. *Schematic illustration of axial water transport in bentonite without contribution from intact rock.*

$$S_{in} := 0.36 \qquad L := 1.5 \qquad D := 4 \cdot 10^{-10} \qquad nmax := 200 \qquad yr := 365 \cdot 24 \cdot 3600$$

$$S(x,t) := S_{in} + \left(1 - S_{in}\right) \cdot \left[1 - \frac{4}{\pi} \cdot \sum_{n=0}^{nmax} \left[\left[\frac{(-1)^n}{2 \cdot n + 1} \cdot \exp\left[-D \cdot (2 \cdot n + 1)^2 \cdot \frac{\pi^2 \cdot t}{L^2 \cdot 4}\right]\right] \cdot \cos\left[\frac{(2 \cdot n + 1) \cdot \pi \cdot x}{2 \cdot L}\right]\right]\right]$$

$$x := 0, 0.01 .. 1.5$$

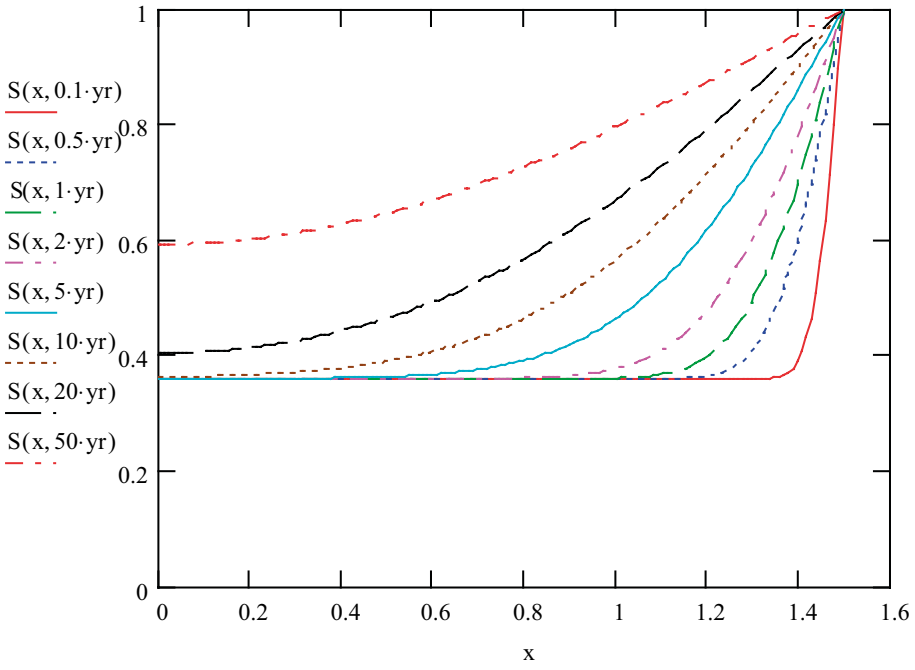

Figure 3-30. *Axial distribution of liquid saturation in a case with axial water transport. Analytical solution (excerpt from MathCad document).*

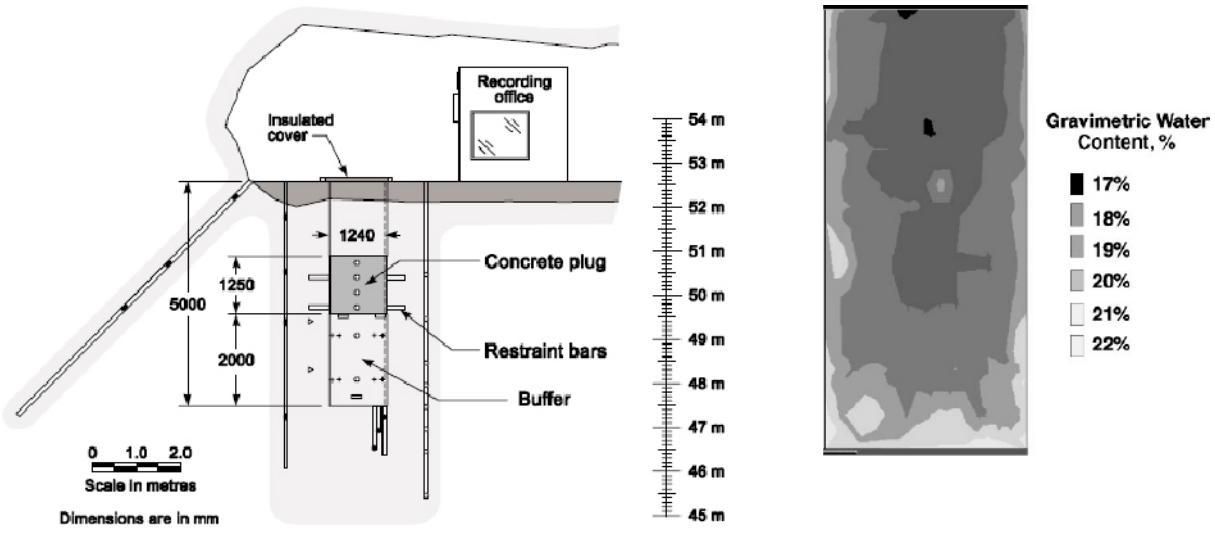

Figure 3-31. *Isothermal test. Section drawing of design (left); final distribution of water content (right). From Dixon et al. (2002).*

4 Task 8a Initial – Scoping Calculation

4.1 Introduction

It has been decided that Task 8 within the Äspö Task Force on Groundwater Flow and Transport among other issues will address the canister near-field, and especially the complicated issues surrounding the bedrock/bentonite interface. The problem of groundwater flow in bentonite has primarily been addressed by the bentonite research community and typically the bedrock is over-simplified.

This short note intends to give the necessary guidelines for set-up of scoping calculations of the bedrock bentonite problem.

The idea is to give the modellers a first insight in the problem concerning the unsaturated conditions in bentonite and how to address such conditions in a typical bedrock groundwater code for saturated flow conditions. This is done by simulations of two generic set-ups based on the overall design of the deposition hole and the engineered barrier.

The hydraulic conductivity value for the bentonite has previously been specified to be 2.4×10^{-13} m/s. The proper value should, however, be 6.4×10^{-14} m/s according to the parameter value adoption from the section on MX-80 hydraulic conductivity. This new value is used from now on. The value for the bentonite porosity has also been given one more significant digit, from 0.44 to 0.438. Also the transport aperture has been modified from 1×10^{-6} to 1×10^{-4} in order to match the conceptual fracture thickness and porosity for a porous media model.

4.2 Scope and objectives

The overall aim of Task 8 is to improve the knowledge of the bedrock-bentonite interface with regard to groundwater flow. It is not intended to be a coupled model exercise that fully incorporates mechanical, unsaturated, and saturated processes. Neither is it the intention to address the thermal nor the chemical aspects of bentonite. However, the proposed problem can be addressed by using any suitable type of code, including codes that incorporate unsaturated conditions, chemistry, and mechanics.

The scope of this initial scoping calculation exercise is contained within the simulation of two simplified and generic two-dimensional groundwater flow specifications presented below.

The main objectives of this initial phase are:

- To determine means of incorporating bentonite in numerical groundwater flow models. The importance of the bentonite should possibly be evaluated in order to discuss issues like: Good or bad methodologies to incorporate the bentonite and its impact on flow and pressure responses.
- To evaluate effects of different implementations of the bedrock-bentonite interface in groundwater flow models.
- To supply guidance to the field experiment on importance of bedrock fractures.

The simple models outlined here do not address all aspects of the near-field around the deposition hole, including:

- EDZ in the access drift and around the deposition hole;
- Pellets-filled slot between buffer and rock wall.

These and other process-related aspects may be addressed more fully in other tasks within Task 8.

Based on these simplified exercises and hopefully future availability and understanding of real data, each modelling group should be able to address their need and use of data in the successively added simulations of Task 8. During the Task 8 exercises a need to address questions like the ones given below is foreseen:

How much data are needed? What are the requirements for the coverage of data? Are all necessary data already available and if not can they be collected and delivered for the modellers within the necessary time frame? Which data/data type should be used for calibration and/or validation?

4.3 Case specifications

The Case 1 concerns a two-dimensional axi-symmetric set-up of intact rock (indicated by green colour), bentonite (indicated by blue colour), and a tunnel cross-section (Figure 4-1). For this case, the rock fracture (indicated by purple colour) should be ignored and replaced with intact rock.

The Case 2 concerns a two-dimensional axi-symmetric set-up of intact rock, one rock fracture (indicated by purple colour), bentonite, and a tunnel cross-section.

The boundary conditions are illustrated in Figure 4-2. The initial condition for the rock can be obtained as a resulting pressure field from a steady-state simulation based on the set-up but with bedrock bentonite-interface simulated as a constant atmospheric pressure boundary. The initial degree of saturation for the bentonite is 0.36 which corresponds to an initial suction value of 100 MPa with the retention curve defined below. The initial porosity is 0.438 and the corresponding dry density is 1 560 kg/m^3.

Specified hydraulic material properties are given in Table 4-1.

The following relationships are proposed to be used for the relative permeability:

$$k_r = \begin{cases} S^3 & (bentonite) \\ \sqrt{S}\left(1-\left(1-S^{1/\lambda}\right)^{\lambda}\right)^2 & (rock) \end{cases} \quad (4\text{-}1)$$

where S is the degree of saturation (volume of water over total volume of pores).

In addition, the following expression is proposed for the water retention curve:

$$S = \left[1+\left(\frac{P_g - P_l}{P_0}\right)^{\frac{1}{1-\lambda}}\right]^{-\lambda} \quad (4\text{-}2)$$

where P_g is the gas pressure (can be assumed to be atmospheric 0.1 MPa), P_l is the water pressure, and P_0 and λ are empirical constants (Table 4-2).

Table 4-1. Material specifications.

Material	Properties*	Value
Intact rock	Hydraulic conductivity	1×10^{-12} m/s
	Porosity	1×10^{-5}
	Specific Storage	1×10^{-10} m^{-1}
Rock fracture	Transmissivity	5×10^{-10} m^2/s
	Porosity for porous media	1×10^{-3}
	Transport aperture for DFN	1×10^{-4} m
	Storativity	1×10^{-9}
Bentonite	Hydraulic conductivity	6.4×10^{-14} m/s
	Porosity	0.438
	Specific Storage (suggested value)	1×10^{-11} m^{-1}

Definitions and explanations for used properties are found in the state-of-the-art chapter above.

* The reader is advised to use the parameter values noted here with care and to recognise the site dependent properties as being so-called apparent properties. Physically more relevant values are given in Chapter 7.

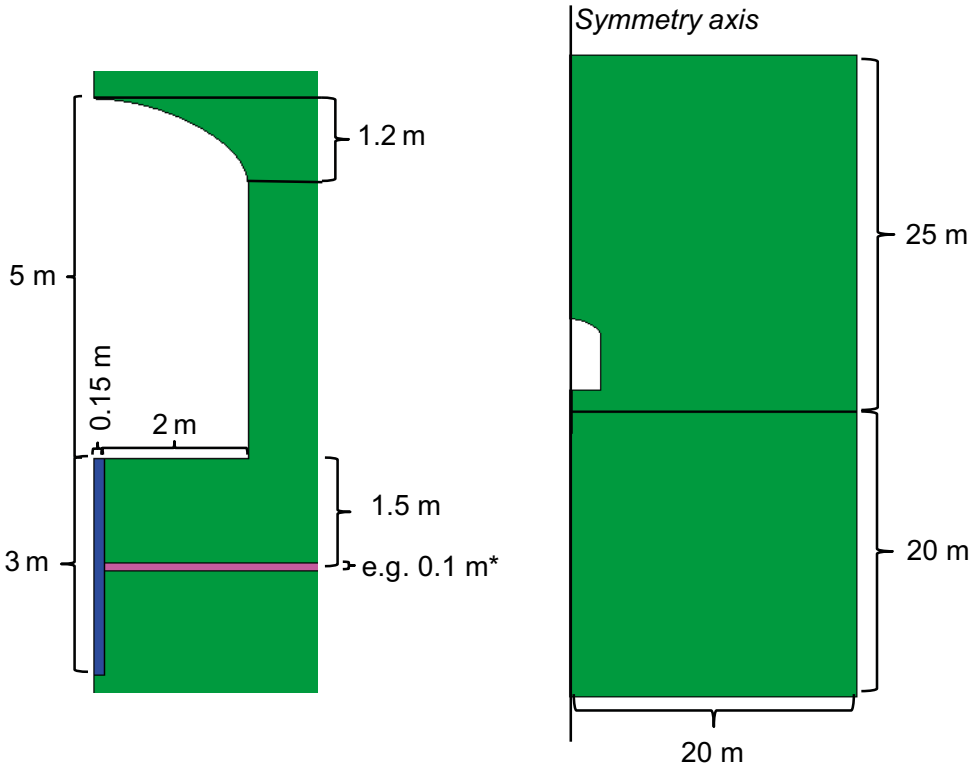

Figure 4-1. *Geometrical set up (relevant for porous media descriptions).*

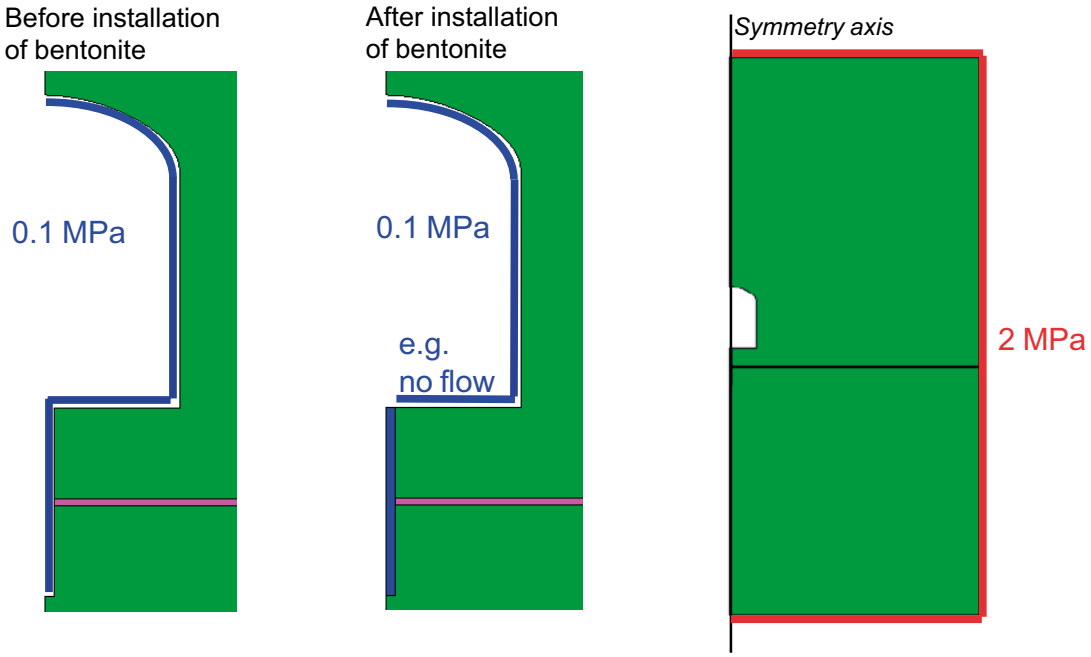

Figure 4-2. *Boundary conditions.*

Table 4-2. Parameter values used for water retention curves.

Material	P_0 (MPa)	λ (–)
Bentonite	9.23	0.3
Rock	1.74	0.6

4.4 Expected outcome

Contour plots of the deposition hole near-field pressures and degree of saturation[1] in bentonite as well as the bedrock for time steps at 0, 0.1, 0.5, 1.0, 10, 100 years. The contour plots should present the geometric situation of the deposition hole in detail (tunnel floor and 5 metres down * symmetry axis and 5 metres to the side) along this a second set of contour plots of the entire model set-up. The colour scale of the contour plots should be: 1.5, 1, 0.5, 0.2, 0.1, 0, −0.1, −0.2, −0.5, −1, −5, −10, −20, −50 MPa.

Graphs illustrating the pressure evolution with time within the bentonite at a position 0.01, 0.05, 0.1, 0.15 metres from the deposition hole wall. Three graphs should be provided, at 1.5 metres depth (in-front of the rock fracture), one at 0.75 metres down the hole, and one at 2.25 metres down the hole.

Graphs illustrating the pressure evolution with time within the bedrock at a position 0.01, 0.05, 0.1, 0.15, 1, 10 metres from the deposition hole wall. These graphs should be provided at the same depth positions as described above.

4.5 Sensitivity analysis for EBS-TF

At the EBS-TF meeting in May 2010 it was decided that the EBS-TF would focus on the generic axisymmetric geometry of Task 8a, rather than the 3D scoping calculations of Task 8b. Moreover, the sensitivity analysis encouraged for Task 8b should be addressed in Task 8a more specifically. This chapter therefore outlines a specification for such a sensitivity analysis. The set of parameter values defined previously is regarded as the base case (#1) and is compiled in Table 4-3.

The first variation addresses the influence of the hydraulic properties of the rock (i.e. hydraulic conductivity of the intact rock, and the fracture transmissivity). A compilation of fifteen additional cases (#2 to #16) is given in Table 4-4. This exercise is highly related to the main topic of the project, and addresses the issue of a localized water entry through a fracture into the bentonite-filled borehole, and whether this can imply a heterogeneous hydration of bentonite. The goal of the matrix of cases is to investigate the heterogeneity of the hydration for different combinations of the hydraulic properties, and also to identify the bounds for which the hydration is limited by either the bentonite or the rock. Three additional intact rock conductivities (10^{-14}, 10^{-13} and 10^{-11} m/s) are therefore considered. Two additional fracture transmissivities (10^{-12} and 10^{-8} m^2/s) are also considered, as well as modelling cases without fractures. It is expected that the boundary pressure (2 MPa) will prevail along the fracture if the transmissivity is sufficiently high, and that an increase beyond this will not influence the saturation process. The high transmissivity value was chosen for this reason. The matrix of cases is quite extensive, and the different cases have therefore been given three different priorities.

The second variation concerns the influence of the bentonite hydraulic conductivity. Two additional cases (#17 and #18) are given in Table 4-5. These values represent a span between a reduction of 40 % and an increase of 100 %. This was suggested in the section MX-80 hydraulic conductivity.

The third variation addresses the influence of the retention curves. For the bentonite (#19), an alternative curve is derived through a more rigorous adherence to the model by Dueck (2004). To do this, the so-called extended van Genuchten expression was employed. The difference between this and the original curve is quite small (see Figure 3-7 and Figure 4-3), but the influence of this is still regarded to be relevant to investigate. For the rock fracture (#20), an alternative curve is derived in accordance with the model by Jarsjö (2009). A detailed description of this derivation is given below (see Figure 4-4 and Figure 4-5), and this fracture retention curve is illustrated together with the base case curve in Figure 4-6. In an attempt to promote extensive desaturation of the rock, and to check how this will influence the hydration of the bentonite, a hypothetical high retention curve is adopted for both the intact rock and the fracture (#21).

Finally, the influence of the porosity of the rock is investigated for a case with 0.3 % porosity in both intact rock and in the material used to represent the fracture (#22). The chosen value has been determined for the total porosity in the Laxemar area (see section on porosity above).

[1] Or alternative equivalent measure of change in the bentonite due to inflow of water from the bedrock.

4.5.1 Requested results

The results outlined earlier in the task definition prescribe the delivery of 12 contour plots and 30 graphs. It is suggested that these sets of results are delivered only for the base case (#1).

In order to simplify the evaluation of this sensitivity analysis it is suggested that results for all 22 cases are presented and delivered in the form of history plots of the degree of saturation at two points only:

- At the central axis in the borehole at 1.5 m depth (the same depth as the fracture).
- At the central axis in the borehole at 2.25 m depth (half-way between the fracture and the bottom of the bore hole).

Illustrative compilations of these results are encouraged.

In addition, it is also of interest to illustrate the bentonite hydration as plots of the total amount of water (in litres) entering the bentonite versus time.

4.5.2 Additional remarks

In the geometrical set-up of the general definition of Task 8a it was indicated that the representation of the fracture could be modeled as a special material with the thickness of 0.1 m. Modelers should not be restricted by this, and can very well choose thinner representations of the fracture, as long as the transmissivity is given by the product of the hydraulic conductivity and the thickness of the fracture material. Modelers are encouraged to investigate the effects and relevance of this type of representations.

The hydraulic boundary condition toward the tunnel will require some considerations. The simplest option would be to apply a pressure BC with an atmospheric pressure. It should be observed, however, that this type of BC can supply water to the bentonite, and that an alternative therefore should be sought. A no-flow BC along the entire tunnel envelope should on the other hand imply that the pressure in the entire rock eventually will reach the same level as the outer boundary. Modelers are therefore encouraged to develop strategies for handling this complication. A no-flow BC along the tunnel floor only could, for instance, be a relevant compromise (see the general definition of Task 8a).

If some modelers intend to include mechanical processes as well, it should be observed that the goal is to prevent the bentonite from heaving through the use of a concrete plug fixed to the rock. The axial displacement at the plug can therefore be assumed to be zero.

The bentonite will be compacted as blocks, which will be installed into the borehole. The initial stresses in the bentonite can therefore be regarded to be very low. The slot between the blocks and the borehole should be as small as possible, and the goal is to make it approximately 1 mm. This would mean that the diameter of the blocks will be 298 mm. Finally, it should be mentioned that the slot may be artificially filled with water immediately after the installation of the bentonite.

Table 4-3. Base case parameter values (#1).

Material	Hydraulic conductivity K (m/s)	Transmissivity* T (m^2/s)	Relative permeability $k_r(S)$	Retention van Genuchten P_0 (MPa); λ (–)	Porosity n (–)
Intact rock	1×10^{-12}	–	$\sqrt{S}\left(1-\left(1-S^{1/\lambda}\right)^{\lambda}\right)^2$	1.74; 0.6	1×10^{-5}**
Rock fracture	–	5×10^{-10}	$\sqrt{S}\left(1-\left(1-S^{1/\lambda}\right)^{\lambda}\right)^2$	1.74; 0.6	1×10^{-3}**
Bentonite	6.4×10^{-14}	–	S^3	9.23; 0.3	0.438

* The transmissivity is given by the product of the hydraulic conductivity and the thickness of the fracture material.

** The reader is advised to use the parameter value noted here with care and to recognise the site dependent properties as being so-called apparent properties and in this case relates to a kinematic porosity. Physically more relevant value for intact rock is given in Chapter 7.

Table 4-4. Influence of rock hydraulic properties (#2 to #16).

Hydraulic conductivity of intact rock (m/s)	Fracture transmissivity (m^2/s) No fracture	1×10^{-12}	5×10^{-10}	1×10^{-8}
1×10^{-14}	#9	#5	#2	#13
1×10^{-13}	#10	#6	#3	#14
1×10^{-12}	#11	#7	Base case, #1	#15
1×10^{-11}	#12	#8	#4	#16

Note: #8 and #12 will coincide if the fracture is represented with a 0.1 m thick plate.
Three priorities: 1st (black); 2nd (red); and 3rd (green).

Table 4-5. Influence of bentonite hydraulic conductivity (#17 and #18).

Bentonite hydraulic conductivity (m/s)	
#17 – 40 % reduction	#18–100 % increase
3.8×10^{-14}	1.3×10^{-13}

Influence of bentonite retention curve #19:

$$S = \left(1 + \left(\frac{P_g - P_l}{P_0}\right)^{\frac{1}{1-\lambda}}\right)^{-\lambda} \left(1 - \frac{P_g - P_l}{P_1}\right)^{\lambda_1} \tag{4-3}$$

$P_0 = 6.258$ MPa; $\lambda = 0.21$; $P_l = 400$ MPa; $\lambda_l = 1$

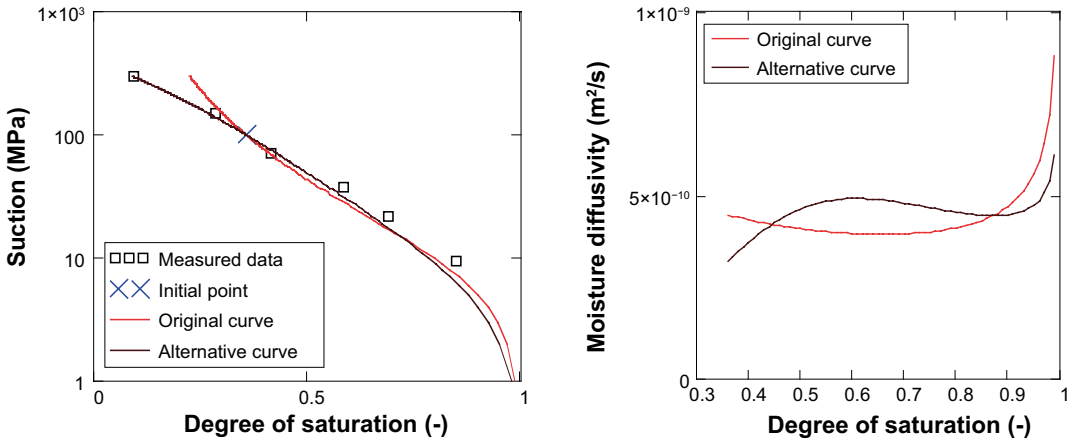

Figure 4-3. *Retention curves of bentonite (left), and corresponding moisture diffusivity (right).*

Influence of fracture retention curve, #20

Constants:

Viscosity (Pa*s): $\mu \equiv 0.001$

Unit weight of water (Pa/m): $\rho g \equiv 9810$

Mean/hydraulic aperture ratio: $C \equiv 1.7$

Aperture standard deviation: $\sigma \equiv 0.8$

Fracture transmissivity (m^2/s) $T \equiv 5 \cdot 10^{-10}$

Hydraulic aperture (m): $a_h := \sqrt[3]{\frac{T \cdot 12 \cdot \mu}{\rho g}}$ $a_h = 8.488 \times 10^{-6}$

Mean aperture (mm): $a_{max} := a_h \cdot C \cdot 1000$ $a_{max} = 0.014$

Mean of ln(a): $\mu_{lna} := \ln(a_{max}) - \frac{\sigma^2}{2}$ $\mu_{lna} = -4.558$

---

van Genuchten parameters derived from diagrams and μ_{lna} -value: $\delta \equiv 1.8$

$n \equiv 2.26$

Alternative forms of van Genuchten parameters:

$\lambda := 1 - \frac{1}{n}$ $\lambda = 0.558$

$P_0 := \frac{\rho g}{\delta}$ $P_0 = 5.45 \times 10^3$ (Pa)

Figure 4-4. *Evaluation of water retention curve parameters for fractures (excerpt from MathCad document).*

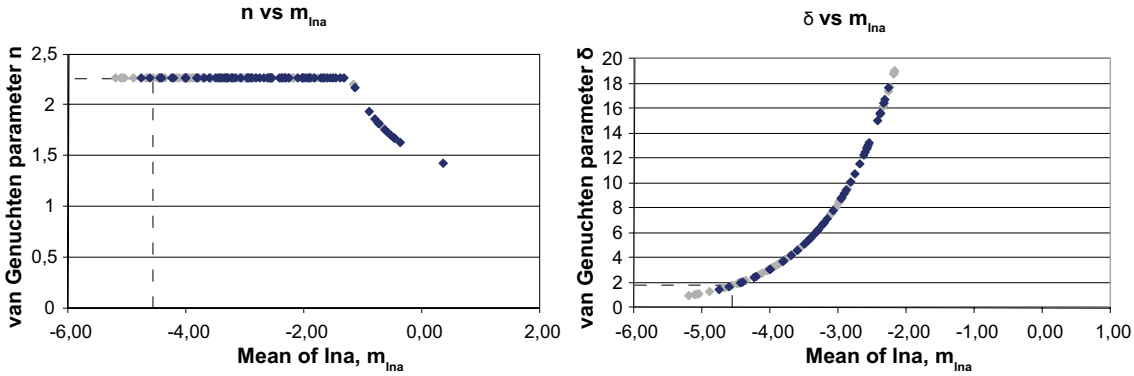

Figure 4-5. *Water retention curve parameters for fractures (according to model by Jarsjö 2009).*

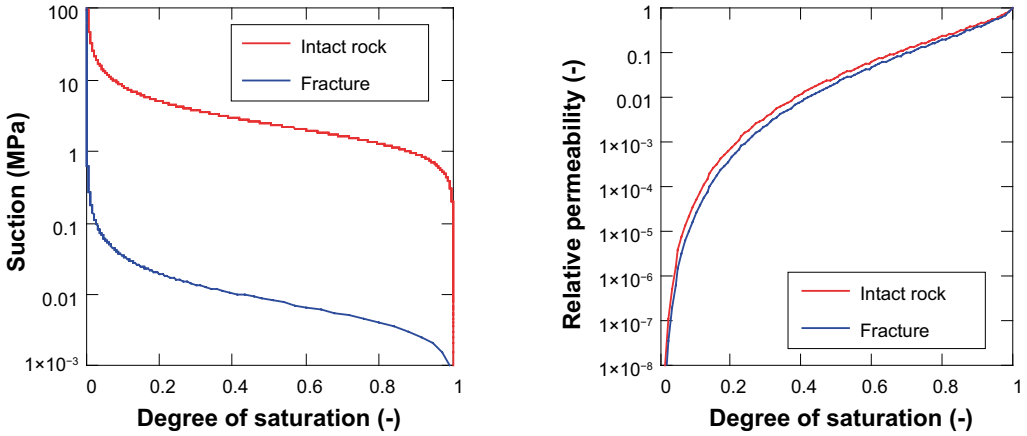

Figure 4-6. *Retention curves of intact rock and fractures (left), and corresponding relative permeability relations (right).*

Influence of rock retention, #21

Hypothetical rock and fracture retention parameters: P_0: 80 MPa; λ: 0.45. (It should be noted that the intention with this retention curve is only to check the influence of an extensive dehydration of the rock. It is not regarded to be relevant for the problem as such.)

Influence of rock porosity, #22

Rock and fracture porosity: 0.003.

5 Task 8b TASO – Scoping Calculation

5.1 Introduction

This note intends to give the necessary guidelines for set-up of scoping calculations of a simplified sub-local Äspö HRL site specific problem.

The idea is to give the modellers a first insight in the site while at the same time address the unsaturated conditions in bentonite and how conditions in a typical bedrock groundwater set-up for a deposition tunnel scale affects the results.

This is done by means of importing boundary conditions from a regional scale hydrogeological model which assesses the same geometrical framework that is supplied in this specification. Geometrical specifications along with a simplified site specific geological structure model are given as CAD data.

The hydraulic conductivity value for the bentonite has previously been specified to be 2.4×10^{-13} m/s on different occasions. The proper value should, however, be 6.4×10^{-14} m/s according to the parameter value adoption from the section MX-80: Hydraulic conductivity. This new value is used from now on.

Observe that Task 8b is only addressing one borehole filled with bentonite, much in the same manner as Task 8a. The other three deposition holes existing in the model domain are all open to atmospheric conditions. When we ask for expected outcomes from the additional borehole wall as well as from the wall of the deposition hole in the TASO tunnel, only the additional borehole will be filled with bentonite and the deposition hole is left open. The asked-for outcome is hopefully useful in showing the interaction that occurs between a bentonite filled borehole and a nearby existing open deposition hole.

5.2 Scope and objectives

One sub-aim of Task 8 is generally speaking to improve the knowledge of the bedrock bentonite interface with regard to groundwater flow. It is not intended to be a coupled model exercise that fully incorporates mechanical, unsaturated, and saturated processes. Neither is it the intention to address the thermal nor the chemical aspects of bentonite. However, it is free to address the proposed problem with all type of codes intended for groundwater problems. That is also codes incorporating unsaturated conditions, chemistry, and mechanics are encouraged.

The scope of this initial scoping calculation exercise is contained within the simulation of a simplified and sub-local site-specific three-dimensional groundwater flow specifications presented below.

The main objectives with this initial scoping exercise are:

- To determine means of incorporating unsaturated rock. Examine effects of different concepts and properties (K, K_{rel}, retention curves).
- To evaluate effects of different implementations of the rock as being fracture and matrix. Examine effects due to contrasts between matrix and fracture properties. Examine bounds for contrasts in order to reveal the significance of fractures.
- To evaluate effects of the fracture location along the deposition hole on the resulting wetting of the bentonite.
- To evaluate effects of different implementations of different boundary conditions. Examine whether the deposition tunnel is best described as a specified pressure boundary, no-flow boundary, or as a general head/flux boundary.
- To supply guidance to the field experiment on importance of bedrock fractures and matrix and where to place measurement instrumentation.

The simple model outlined here do not address all aspects of the near-field around the deposition hole, including:

- EDZ in the access drift and around the deposition hole;
- Pellets-filled slot between buffer and rock wall.

These and other process-related aspects may be addressed more fully within the later tasks of Task 8.

Based on these exercises and hopefully future availability and understanding of more real data each modelling group should be able to address their need and use of data in the successively added simulations of future tasks within Task 8.

5.3 Case specifications

5.3.1 Geometrical set-up

The coordinate system applied within Task 8 is the Swedish RT90 system. The suggested model domain is approximately $(40)^3$ m^3 bounded by the set of coordinates given in Table 5-1 (see Figure 5-1). As the BRIE experiment has been given the TASO tunnel as its primary investigation area the specifications given are based on the sub-local scale of the TASO tunnel area at the Äspö HRL. More detailed information will emerge as the BRIE experiment progresses.

Table 5-1. Coordinates for suggested model domain.

x	Y	z
1551603	6367769	−396
1551629	6367799	−396
1551600	6367826	−396
1551573	6367796	−396
1551603	6367769	−436
1551629	6367799	−436
1551600	6367826	−436
1551573	6367796	−436

The Äspö HRL geometrical framework is specified as CAD layers; along with the geometrical framework of the geological structure model is given as CAD layers in the file: TASO_v1.dxf (see Figure 5-2). It should be noted that the structures *should* connect to the boundaries; slight discrepancies may be found between the suggested model domain coordinates above and the modelled structures.

The additional borehole is given by the starting coordinate of its axis at the tunnel floor. The borehole should be modelled as 3 metres deep and with a diameter of 30 centimetres. The starting coordinates are x = 1551588, y = 6367795, z = −416.7.

A hypothetical single rock fracture is assigned as a circular (or equivalent) feature of a diameter of 10 metres with its centre along the centre axis of the additional borehole (above). As a reference case the single rock fracture should be horizontal and intersect the borehole described above at a depth of 1.5 metres below the tunnel floor.

5.3.2 Boundary condition

From a specified sub-grid of a DarcyTools v3.3 simulation of the full regional Äspö HRL model (Äspömodel05), pressure[2], salinity, and velocities along the x, y, and z coordinates are given over an approximately $(100)^3$ m^3 volume incorporating the suggested model domain just inside of the boundaries of the specified model domain (Figure 5-3). Data is found in the file: TASO_pressure_salinity_velocities.xls (Figure 5-4).

[2] Pressure given are dynamic pressure; absolute pressure could be calculated using $\rho_0 \times g \times z$, with reference altitude at present day shore line (0 altitude).

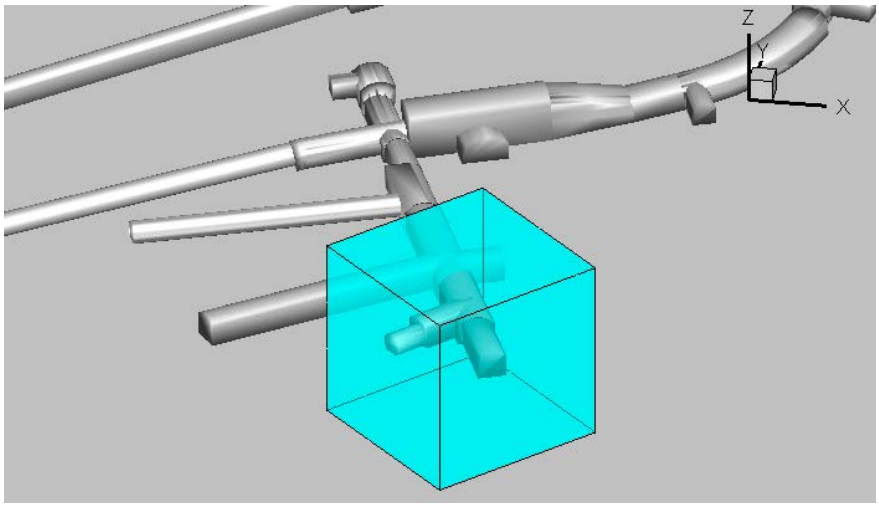

Figure 5-1. *Illustration of the suggested model domain in the vicinity of the assembly hall at the Äspö HRL.*

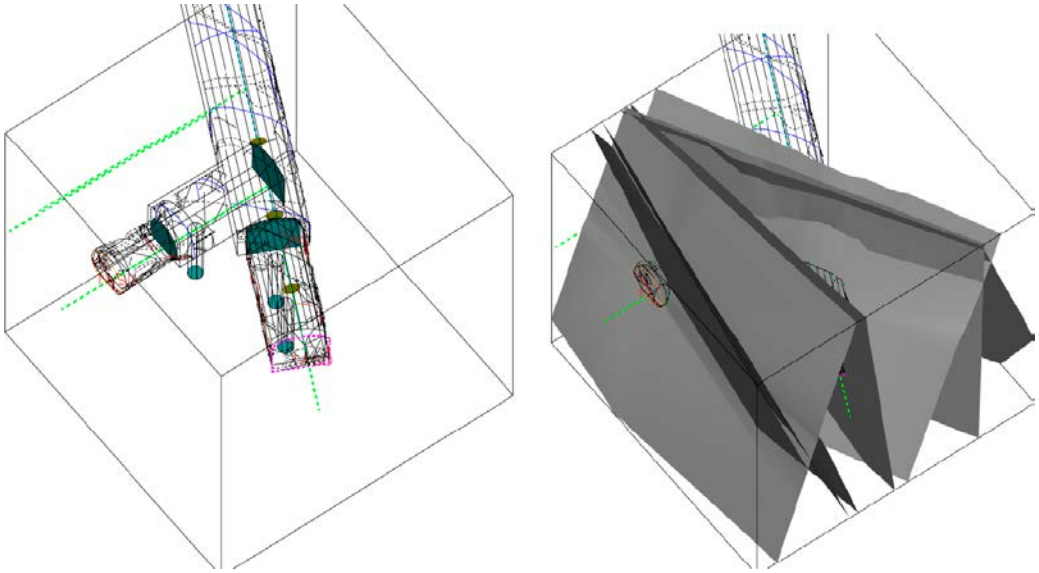

Figure 5-2. *Illustration of the CAD contained data along with the suggested model domain.*

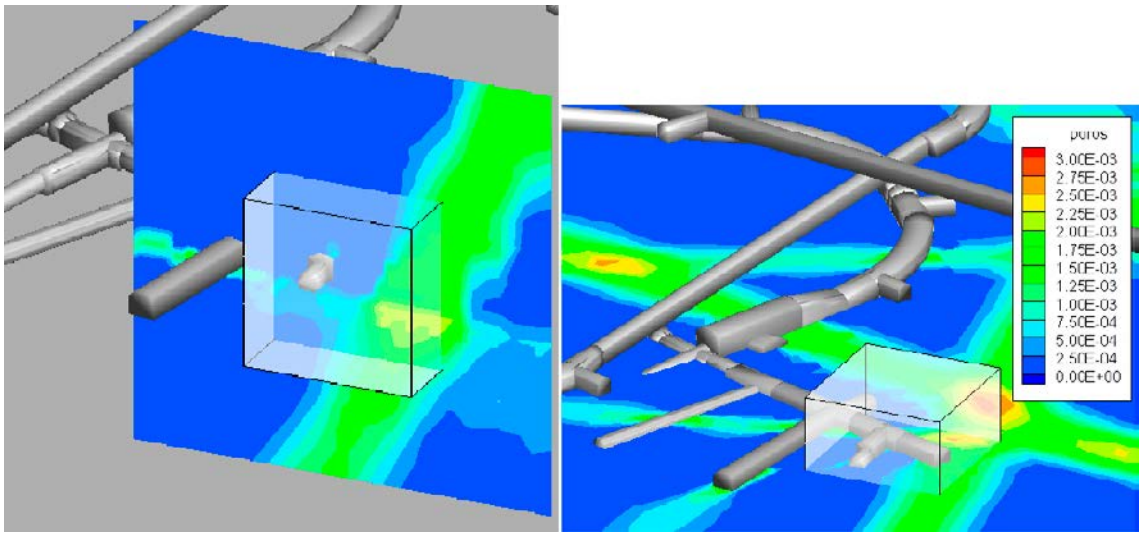

Figure 5-3. *Illustration of the larger scale setting of the suggested model domain. The DarcyTools set-up incorporates structures on a larger scale. Observe how one of the bounding sides is following a larger structure.*

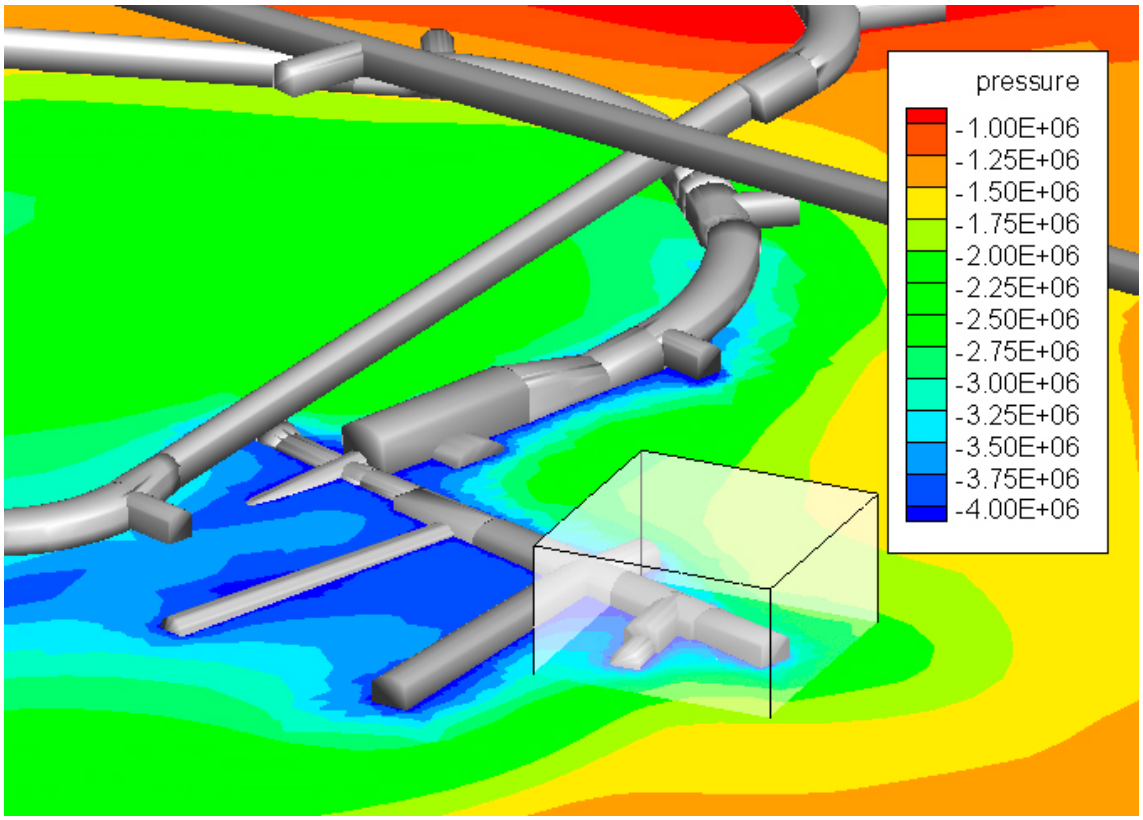

Figure 5-4. *Illustration of the pressure field (Pa), reference elevation is present day shore line (0 altitude).*

Modeled equation for salinity-density dependence is: $1\,000(1 + 0.0078 \times S)$ kg/m^3, where S is given in weight percent.

As a reference case the assigned boundary conditions in tunnels should be at atmospheric conditions.

5.3.3 Initial conditions

The initial conditions are the same as used in task 8a.

Rock:

Resulting pressure field of steady-state conditions simulated based on the set-up but with bedrock-bentonite interface at a constant atmospheric pressure.

Bentonite:

The initial degree of saturation is 0.36 which corresponds to an initial suction value of 100 MPa with the retention curve defined below.

5.3.4 Material specifications

As references case the same data as in Task 8a should be assessed: Specified hydraulic material properties are given in Table 5-2.

Table 5-2. Material specifications.

Material	Properties*	Value
Intact rock (matrix)	Hydraulic conductivity	1×10^{-12} m/s
	Porosity	1×10^{-5}
	Specific Storage	1×10^{-10} m^{-1}
Geological structure model fractures	Transmissivity	5×10^{-8} m^2/s
	Porosity for porous media descriptions	1×10^{-3}
	Transport aperture for DFN descriptions	1×10^{-5} m
	Storativity	1×10^{-8}
Single rock fracture	Transmissivity	5×10^{-10} m^2/s
(assigned by modelling groups)	Porosity for porous media descriptions	1×10^{-3}
	Transport aperture for DFN descriptions	1×10^{-6} m
	Storativity	1×10^{-9}
Bentonite:	Hydraulic conductivity	6.4×10^{-14} m/s
	Porosity	0.44
	Specific Storage (suggested value)	1×10^{-11} m^{-1}

* The reader is advised to use the parameter values noted here with care and to recognise the site dependent properties as being so-called apparent properties. Physically more relevant values are given in Chapter 7.

5.3.5 Proposed relationships

As of matrix and bentonite and as a reference case the proposed relationships are the same as in Task 8a.

The following relationships are proposed to be used for the relative permeability:

$$k_r = \begin{cases} S^3 & (bentonite) \\ \sqrt{S}\left(1-\left(1-S^{1/\lambda}\right)^{\lambda}\right)^2 & (rock) \end{cases} \qquad (5\text{-}1)$$

where S is the degree of saturation (volume of water over total volume of pores).

In addition, the following expression is proposed for the water retention curve:

$$S = \left[1+\left(\frac{P_g - P_l}{P_0}\right)^{\frac{1}{1-\lambda}}\right]^{-\lambda} \qquad (5\text{-}2)$$

where P_g is the gas pressure (can be assumed to be atmospheric 0.1 MPa), P_l is the water pressure, and P_0 and λ are empirical constants (Table 5-3).

Table 5-3. Parameter values used for water retention curves.

Material	P_0 (MPa)	λ (–)
Bentonite	9.23	0.3
Rock/matrix	1.74	0.6

For the rock fractures the following relationship should be used (in principal the same as above but in an alternative form; where $\delta = \rho \times g/P_0$ and $n = 1/(1-\lambda)$).

$$K(h) = K_s \frac{\left(1-\left(\delta|h|\right)^{n-1}\left(1+\left(\delta|h|\right)^n\right)^{-(1-1/n)}\right)^2}{\left(1+\left(\delta|h|\right)^n\right)^{m(1-1/n)}} \qquad \text{for } h<0 \qquad (5\text{-}3)$$

$$K(h) = K_s \qquad \text{for } h \geq 0$$

Suggested variation of the parameters is found in Figure 5-5 where the aperture is given in mm. As a reference case, δ and *n* should be assigned according to the cubic law hydraulic aperture based on the transmissivity values and m = 0.5. An explanation for how to derive van Genuchten parameters (δ and n, or λ and P_0) from a transmissivity value is given in Figure 4-4 and Figure 4-5.

5.4 Expected outcome

The expected outcome as presented below needs to be multiplied (produced in the same amount as variations simulated by the modelling group) in a realistic manner in order to illustrate the answers to the questions stated as objectives.

Contour plots of the deposition hole near-field pressures and saturation[3] in bentonite as well as the bedrock for time steps at 0, 0.1, 0.5, 1.0, 10, 100 years on one vertical cross-section incorporating both deposition hole and parallel with the TASO tunnel central line and one horizontal incorporating both deposition hole and cutting through at the depth of 1.5 metres.

The contour plots should present the geometric situation of the deposition holes in detail (tunnel floor and 5 metres down). The colour scale of the contour plots should be: 1.5, 1, 0.5, 0.2, 0.1, 0, −0.1, −0.2, −0.5, −1, −5, −10, −20, −50 MPa. Graphs illustration the pressure increase within the bentonite at a position 0.01, 0.05, 0.1, 0.15 metres from the different deposition holes walls. These graphs should come as six: one for each deposition hole at 1.5 metres depth, at 0.75 metres down the hole, and at 2.25 metres down the hole.

Graphs illustration the pressure change within the bedrock at a position 0.01, 0.05, 0.1, 0.15, 1, 5 metres from the deposition holes wall in the direction towards the other deposition hole. These graphs should also come as three for the same depth positions as described above.

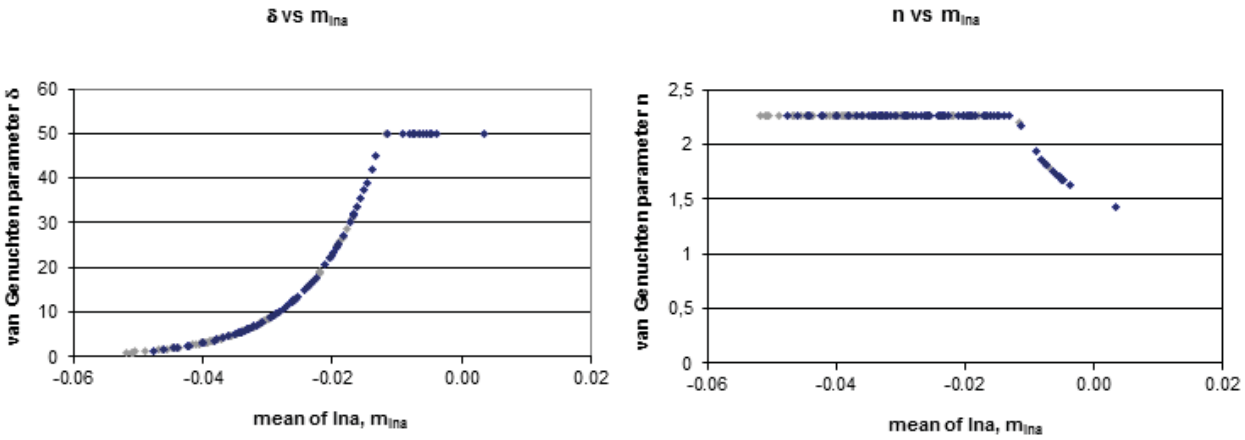

Figure 5-5. *Graphs derived with theory presented by Jarsjö (2009).*

[3] Or alternative equivalent measure of change in the bentonite due to inflow of water from the bedrock.

6 Task 8c BRIE – Prediction for central deposition hole

6.1 Introduction

This note intends to give the necessary guidelines for a set-up for calculations concerning predictions of inflow to the planned central boreholes in the TASO tunnel at a sub-local Äspö HRL site model domain.

The idea is to give the modellers a conceptual basis for the site, while at the same time address the saturated conditions around the TASO tunnel. The results is intended to work both as a model frame for future Task 8 simulations as well as being a guide for the management of the BRIE experiment.

This is done by means of importing boundary conditions from a regional scale hydrogeological model which in parts assess the same geometrical framework, however on a grander scale, that is supplied in this specification. Geometrical specifications, along with a site specific geological structure model are given as CAD data. Site specific stochastic fracture statistics are given as intensity, size and orientation data and serve as the basis for the hydraulic properties.

The task description of Task 8c is updated with the following information as of January 2012:

- The assessed values on storage especially for rock mass but also for rock fractures and bentonite is given based on large-scale values derived from different kinds of hydraulic tests. Little is known on the real values, but theoretical values indicate different values from the ones herein suggested. Modelling teams that assess the storage values in their models are encouraged to test the sensitivity of the simulation results to storage.
- The emplacement of the buffer in the deposition hole will be done with help of a metal construction that contains a steel plate at the bottom (Figure 6-1). This means that in the experiment the groundwater will not have direct access to the bentonite from the bottom of the deposition hole. Modelling teams are encouraged to investigate the influence of such an impermeable plate between the bentonite and the rock beneath.
- It has been decided that an interim report should be delivered. The time and content of this interim reporting is found under the expected outcome section at the end of the Task 8c part of this task description.

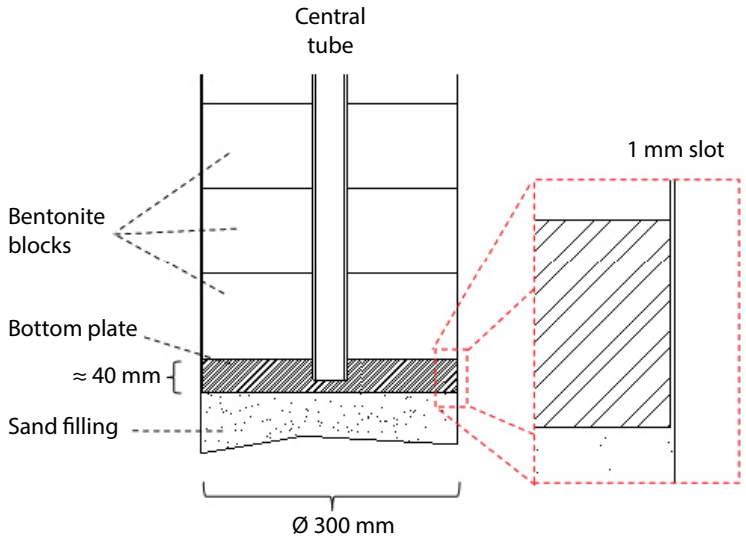

Figure 6-1. *Preliminary outline of the bottom part of the BRIE installations.*

6.2 Scope and objectives

One sub-aim of Task 8 is to improve the knowledge of the bedrock-bentonite interface with regard to groundwater flow. It is not intended to be a coupled model exercise; fully incorporating mechanical, unsaturated, and saturated properties. Neither is the intention to address the thermal nor the chemical aspects of bentonite. However, it is free to address the proposed problem with all type of suitable codes intended for groundwater and similar problems. Also, the use of codes incorporating unsaturated conditions, chemistry, and mechanics is encouraged.

Recently, Task 8c has been divided into two parts, i.e. Task 8c1 and Task 8c2. Incorporation of bentonite is not considered in the Task 8c1 exercise. Instead the inflow to open boreholes is addressed with a focus on being a guide to the management of the BRIE experiment but also to test the modelling tools' ability to predict inflow to deposition holes based on limited information. Task 8c2 addresses the wetting of bentonite based on the flow field and flow distribution established in Task 8c1.

The scope of this calculation exercise is contained within the simulation of a sub-local site-specific three-dimensional groundwater flow specifications presented below. The model should preferably be constructed so that it is easy to change surrounding boundary conditions when updates become available.

The main objectives with this exercise are:

Task 8c1
- To predict inflows and inflow characteristics to deposition holes
- To set up the main features of the TASO site
- To test the adopted boundary conditions in relation to the site-specific deformation zones (wfracture_01,wfracture_02 and NNW4).
- To supply guidance to the field experiment on importance of bedrock fractures and matrix and where to place measurement instrumentation.

Task 8c2
- To evaluate effects of the fracture locations along the deposition hole on the resulting wetting of the bentonite.
- To serve as a base case for comparison with later results based on more elaborated hydrogeological models.

Site-specific geological influences such as the EDZ, stress-induced changes, chemistry-induced changes (e.g. calcite precipitation) are not presently quantified. Modellers are welcome to address these issues as one mean of adjusting their models. All incorporated issues, however, need to be readily explained. These and other process-related aspects may be addressed more fully within the later parts of Task 8.

As one of the objectives is to illustrate and give numbers on inflow and inflow distributions within a deposition hole, the assessed models need to consider a cell/grid resolution that is able to capture details on a wall of a deposition hole of a size of 0.3 m in diameter and 3 m in depth.

Based on preliminary results of these exercises adoptions of alternative boundary conditions and geometrical frameworks may be addressed in the future.

6.3 Case specifications

6.3.1 Geometrical set-up

The coordinate system applied within Task 8 is the Swedish RT90 system. The suggested model domain is approximately $(40)^3$ m^3 bounded by the following set of coordinates given in Table 6-1 (see Figure 6-2).

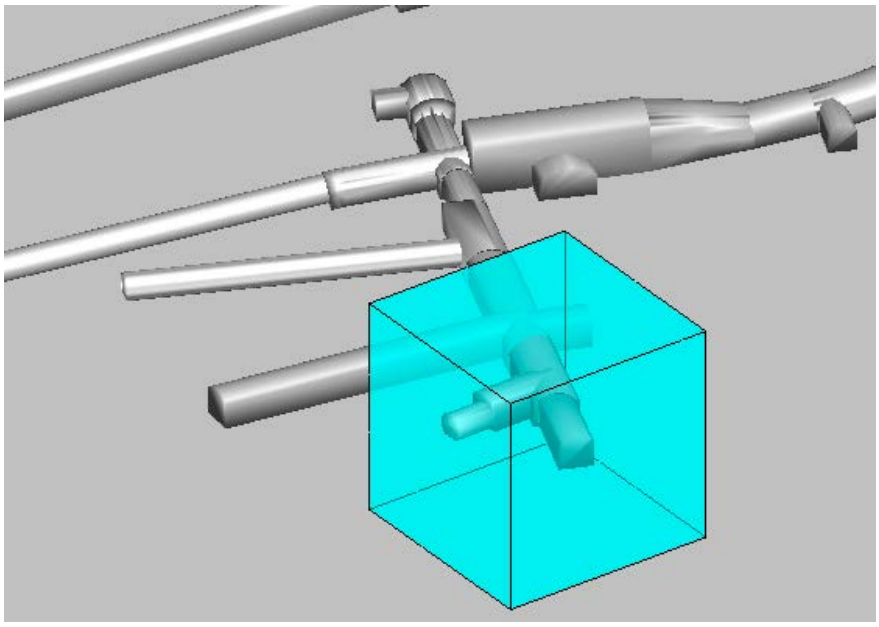

Figure 6-2. *Illustration of the suggested model domain in the vicinity of the assembly hall at the Äspö HRL. The size of the model domain that e.g. includes the TASO tunnel is 40 by 40 by 40 m^3.*

As the BRIE experiment has been given the TASO tunnel as its primary investigation area the specifications given are based on the sub-local scale of the TASO tunnel area at the Äspö HRL. More detailed information will emerge as the BRIE experiment progresses.

Table 6-1. Coordinates for suggested model domain.

x	Y	z
1551603	6367769	−396
1551629	6367799	−396
1551600	6367826	−396
1551573	6367796	−396
1551603	6367769	−436
1551629	6367799	−436
1551600	6367826	−436
1551573	6367796	−436

The Äspö HRL geometrical framework along with the geometrical framework of the geological structure model (see Figure 6-3 and Figure 6-4) is given as CAD layers in the files:

TASO_V0.1_TG.dxf..dxf and TASO_V0.1_DET.dxf..dxf respectively. It should be noted that the structures *should* connect to the boundaries of the assessed model domain.

The five probing borehole (Figure 6-6) so far established in the BRIE experiment are given in the CAD file TASO_V0.1_TG.dxf.

As a simplification the entire set of information is available in TASO_V1.1_ALL.dxf. The latter file also contains information on the principal stress orientation, etc.

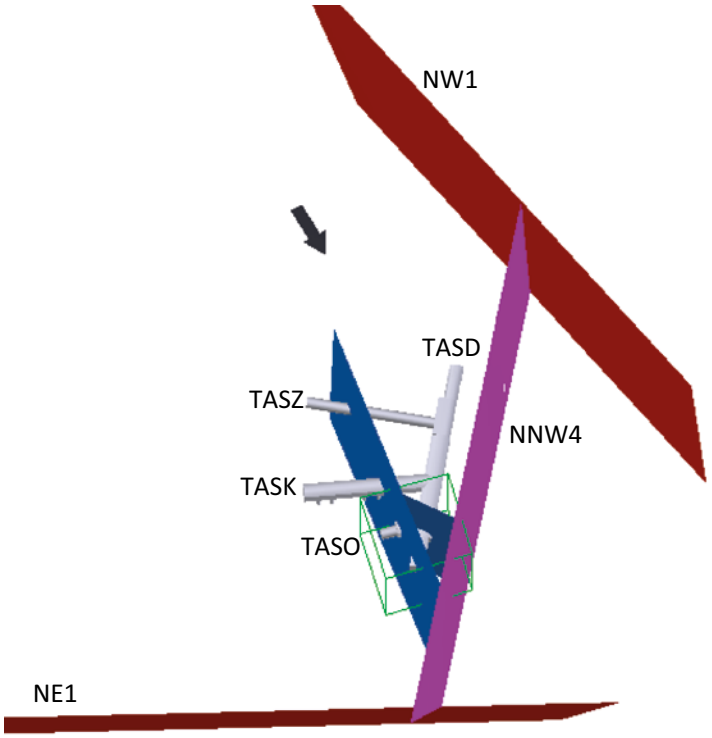

Figure 6-3. *Illustration of the CAD contained data along with the suggested model domain. The large structures are named according to the Äspö HRL model. The tunnel names are given for orientation. The thick black arrow indicates the major principal stress orientation.*

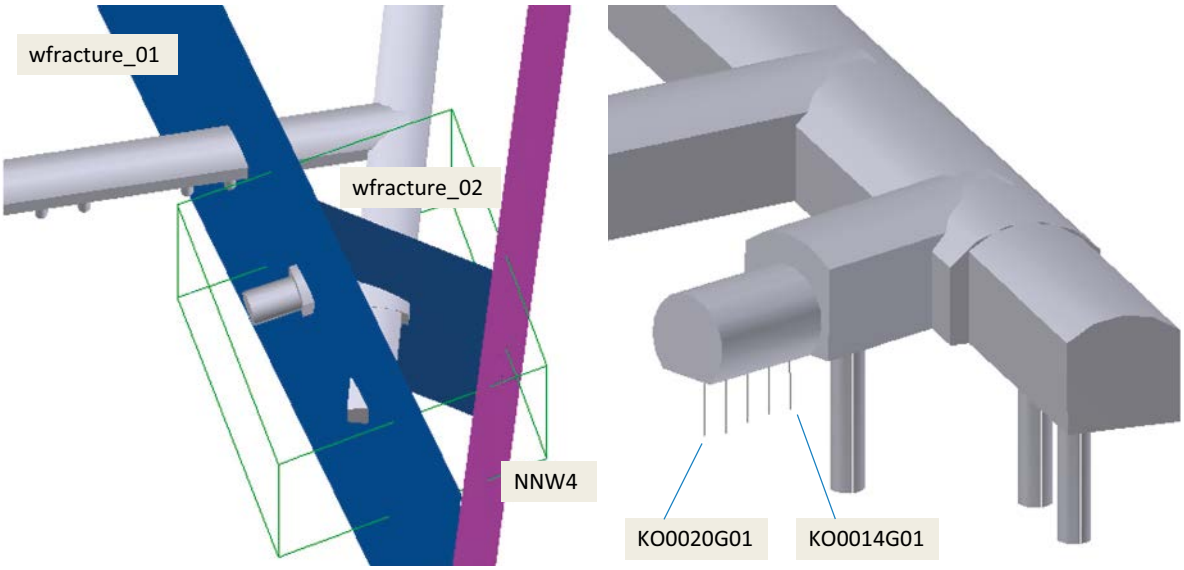

Figure 6-4. *Details closer to the TASO tunnel, naming the three deterministic structures that are contained within the suggested model domain. The five probing boreholes are illustrated on the right. The figure includes an indication of the naming of the boreholes by giving the outer boreholes name. See Figure 6-6 for the naming of boreholes in between.*

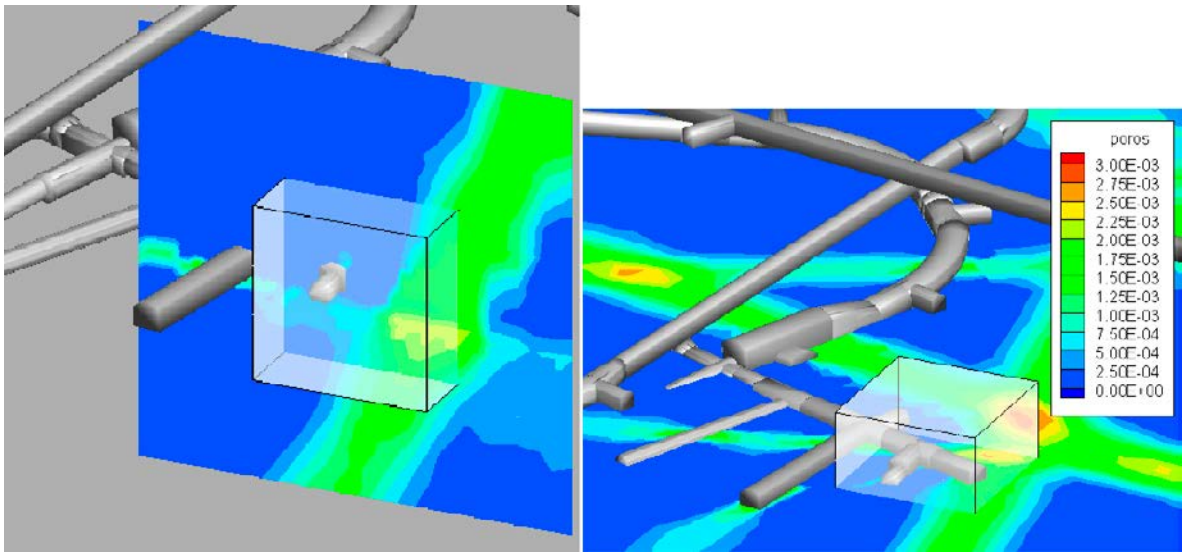

Figure 6-5. *Illustration of the larger scale setting of the suggested model domain. The DarcyTools set-up incorporates structures on a larger scale. Observe how one of the bounding sides is following a larger structure that actually represents the NE1 structure on a larger scale model.*

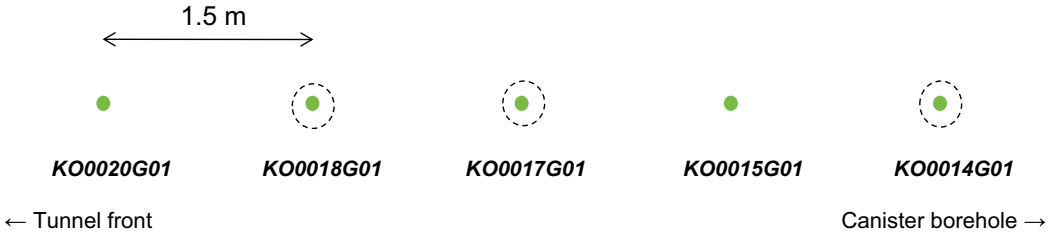

Figure 6-6. *Illustration of probing borehole spacing and naming. Dashed rings denote candidates of central boreholes.*

6.3.2 Background fracture statistics

Based on the collected and thereafter compiled data from TASO, TASD, TASK, and two deposition holes in close vicinity of the BRIE experimental site, three fracture sets have been defined primarily by visual inspection. Table 6-2 presents the suggested statistics for the TASO tunnel; however it should be noted that all modeling groups are welcome to address the available data (Fractures_TASK8C_filtered.xls) on their own as the relative small sample of data allows for alternative interpretations. As two examples one may note that the fractures smaller than 1 metre seem to follow a slightly different statistics and also that of the analysed data only the inner part of TASD and the entire TASO (our tunnel) share the same rock type.

The assessed length interval of fractures is also left for the modellers to choose. This may be constrained by individual codes. However, it should be noted that on the larger side no fractures have been found that actually cut the entire tunnel periphery except for the fractures that are modelled deterministically.

Table 6-2. Suggested fracture statistics to be used for the TASO tunnel.

Set	Orientation			Size		Spatial	Intensity
	Trend	Plunge	Fisher konc.	r_0	k_r	Distribution	P_{32} (r_0,∞)
Set 1	280	20	10	0.25	2.6	Poisonian	1.1
Set 2	20	10	15	0.25	2.6	Poisonian	2
Set 3	120	50	10	0.25	2.6	Poisonian	0.75

An excel sheet file is associated to help with rescaling the intensity due to different choice of fracture sizes. The file is named P32_interval_brie.xls. The power-law distribution can be scaled according to the following equation:

$$P_{32,r_a-r_b} = P_{32,r_1-r_2} \cdot \frac{r_a^{2-k_r} - r_b^{2-k_r}}{r_1^{2-k_r} - r_2^{2-k_r}} \tag{6-1}$$

Noticing that the terms r^{2-k} becomes zero if r equals infinity makes it possible for the modellers to scale the provided size-intensity relationship to cover fracture sizes of interesting ranges.

The amount (N) of fractures in a volume (V) within a certain size and intensity interval can be calculated using:

$$N = \frac{k_r - 2}{k_r} \cdot \frac{P_{32,r_1-r_2}}{\pi} \cdot \frac{\left(r_2^{-k_r} - r_1^{-k_r}\right)}{\left(r_2^{2-k_r} - r_1^{2-k_r}\right)} \cdot V \tag{6-2}$$

A documentation of the process conducted in establishing the information of Table 6-2 follows below.

Introduction

A Discrete Fracture Network, DFN, model is developed for the BRIE, Bentonite Rock Interaction Experiment, to be used as input to the hydrogeological work.

Development of DFN Model

The data used for developing the DFN is of lower quality and hence subjectivity has to be put into the evaluation of the data. A key point is to keep the model as simple as possible and expert judgement is used to fill the lack of high quality data to make sure that the end result makes sense. Below follow a short description of data used and how they are interpreted.

Input data

Some reflections of the input data are:

- Highly uncertain orientation in deposition holes.
- BRIE experiment is in TASO, unfortunately small data sample.
- TASK furthest away and situated in different rock type.
- TASD in conjunction to TASO and relatively large amount of data.

These constraints gives the result that the data from TASO, when existing, is ranked highest, then that from TASD and the data from TASK and the two deposition holes are used in a more cautious way.

Orientation distribution

A first compilation of the trace data from the two deposition holes, DD0086G01 and DD0092G01, and the three tunnels, TASD, TASK and TASO was done along with a desktop study of two virtual scanlines in the floor of the tunnels TASD and TASK, see Figure 6-7.

The data does not show any obvious divisions into sets, partly depending on multiple poles plotting on top of each other at even 5° locations, but also because of large uncertainty in the orientation data, especially for the two deposition holes. To be able to see data points that in the original data set plot on top of each other a small uniformly distributed random value, ±2°, is added for both strike and dip. The result is shown in Figure 6-8. By visual inspection 2 sets appear with fracture pole trend/plunge approximately around 280°/20° and 20°/10°.

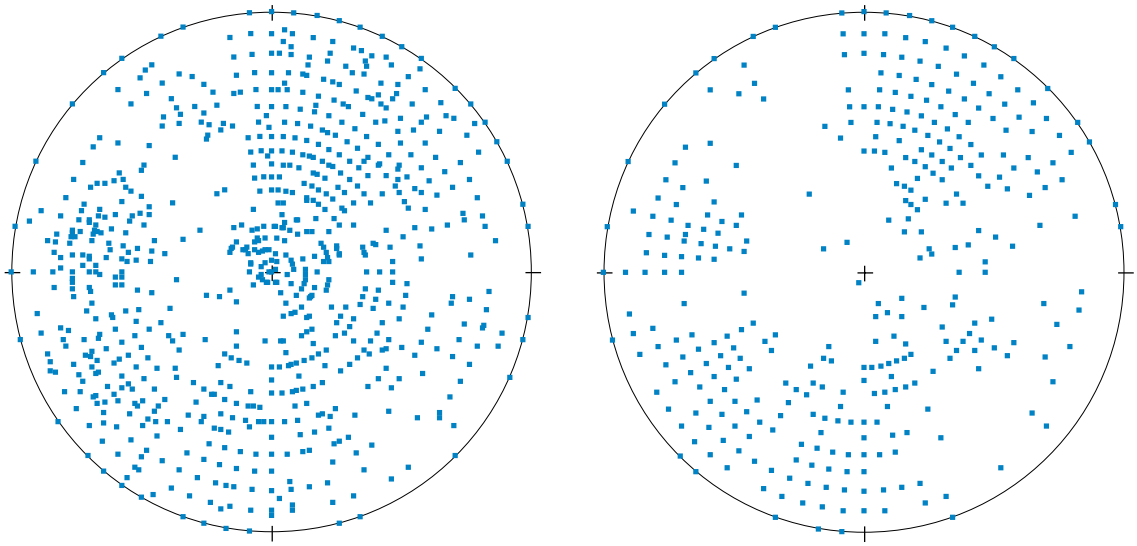

Figure 6-7. *Fracture poles. Left: Orientation of all, 1 772, fractures from the two deposition holes and the three tunnels. Right: Orientation of the 762 fractures mapped at the floor in the TASD and TASK.*

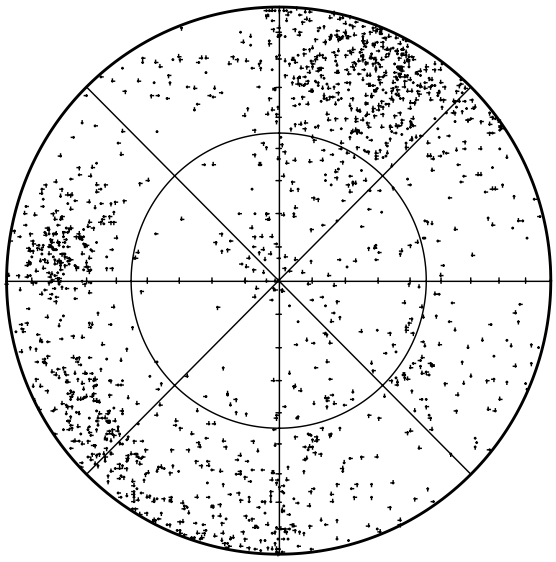

Figure 6-8. *Fracture poles when a uniformly random value is added.*

A division of the data into the tunnels TASD, TASK and TASO is shown in Figure 6-9. The figures shows an indication of a gently dipping set with pole trend about 120° and plunge about 50°.

Therefore a simple 3 set model is developed by visual inspection rather than running the data through any set identification software. It is assumed that the orientation distributions will follow a Fisher distribution. The Fisher concentration, κ, is estimated to 10, 15 and 10 respectively for the three sets.

A picture of the assignment of the poles to the sets are shown in Figure 6-10. Using the set assignment the relative intensity between the set are 0.29/0.52/0.20.

Spatial distribution

The data are presumed to scale in a Euclidian way, i.e. the fractures are randomly distributed in space without any correlation.

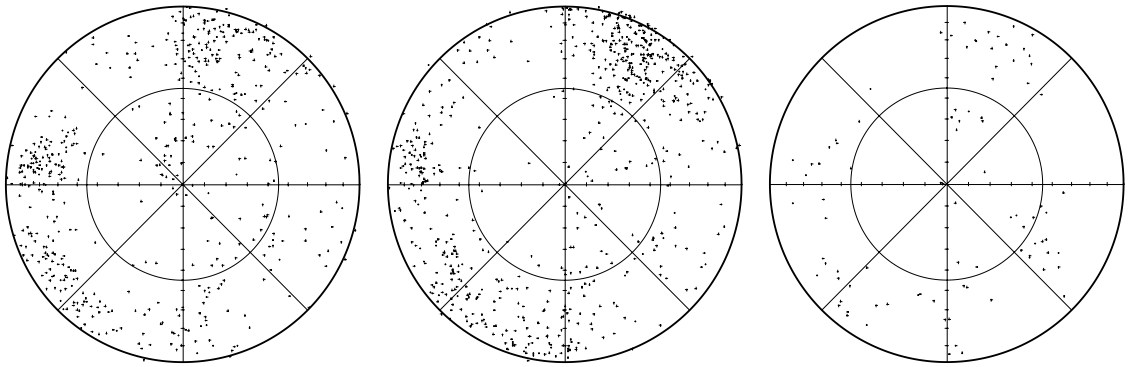

Figure 6-9. *Fracture poles from left: TASD, middle: TASK and right TASO.*

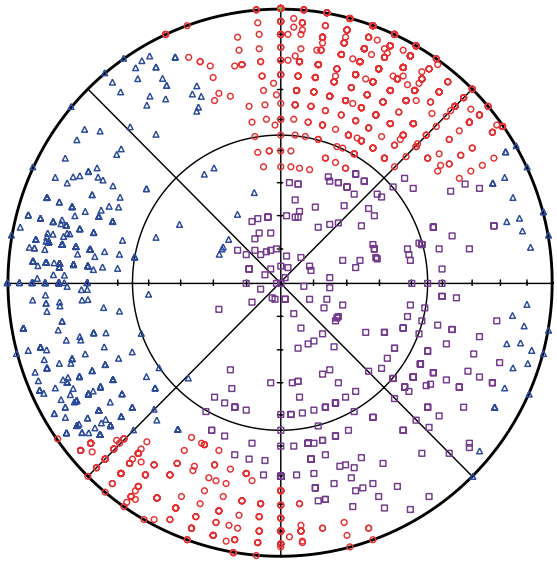

Figure 6-10. *Fracture poles assigned to the three sets. Set1: Blue triangles, set 2: red circles and set 3: purple squares.*

Size distribution

The slope of the size distribution is calculated from the fracture traces mapped on the tunnel walls, roofs and floors together with the traces in the two deposition holes. Unfortunately the cut-off value, as well as the censoring, is different for the different tunnels and holes. In DD0086G01 it is 0.3 m, in DD0092G01 0.2 m, TASK and TASD 0.4 m and TASO 1.0 m. However it does only affect the interval where the data are not affected by truncation (lower bound) or censoring (upper bound) and the location of the curve in a CCDF (complementary Cumulative Density Function) plot. The slope of the curve is not affected. The distributions of trace lengths are shown in Figure 6-11. The slope of the distribution is, by visual inspection, estimated to be −1.6, which corresponds to the Power law exponent, k_r, equal to 2.6 of the parent size distribution. The slope seems to fit all the 5 locations to a reasonable level. However, the CCDF curve of TASK does not seem to have any straight part where the slope can be evaluated.

The location parameter, r_0, i.e. the smallest regarded fracture cannot be evaluated by use of the trace length distributions only, since it is closely related to the intensity for a Power law function. Hence the location parameter is discussed in the next section.

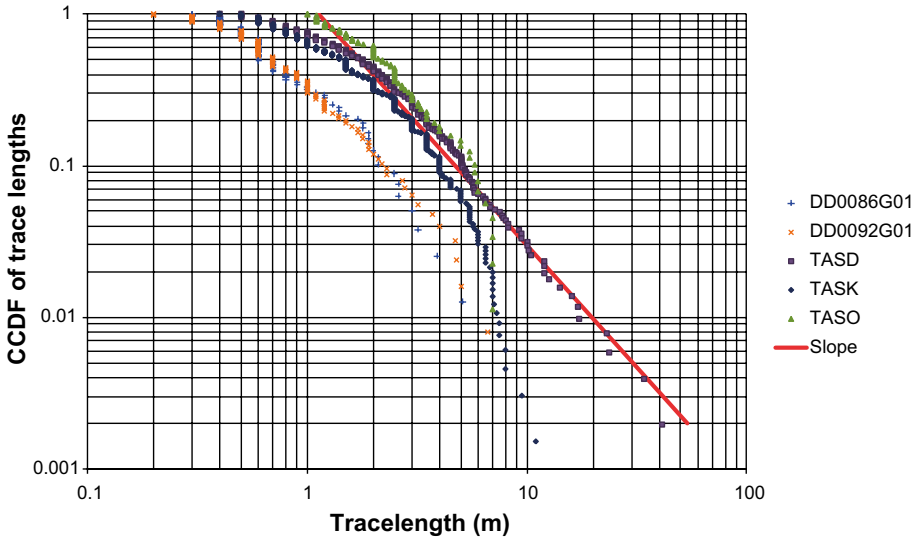

Figure 6-11. *The distribution of trace lengths in the different mapped locations.*

Intensity

The intensity, P_{32}, can be estimated by correcting the number of fractures intersecting a scanline with the Terzaghi correction. This measure is independent of the parent size distribution and hence some modelling has to be carried out to estimate the size-intensity relation. According to Äspö HRL geologists the shortest trace of the scanlines in the tunnels TASD and TASK is 0.5 m and therefore the related P_{32} calculated to the location parameter, r_0, was chosen equal to 0.25 m.

A virtual scan line from the TASD tunnel floor is used while TASK data is ignored for various reasons. Unfortunately the TASD scanline is short, only 16.5 m and 23 intersections which make the intensity estimation highly uncertain.

The relation between P_{32} And r_0 is evaluated using 3 scanlines, 16.5 m long in 10 models which adds to 30 scanlines. The results from the realisations are shown in Figure 6-12. There is a large difference between the different realisations but the cumulative average starts to get reasonable stable after about 20 realisations. With the underlying orientation model together with the assumed relationship between the different fracture sets it is impossible to replicate the data measured in the TASD tunnel. A compromise has been made where the model underestimates the given intensity P_{32} by about 10 % and over-estimates P_{10} by about 25 %. The intensities for the different sets $P_{32, r>0.25}$ are 1.1, 2.0 and 0.75 m^2/m^3 respectively.

Uncertainty

The data provided is limited and in some cases of less quality. Therefore there are large uncertainties in the DFN model developed for the modellers and hence they should feel free to re-evaluate the data or do sensitivity analysis of the models. The uncertainties are estimated to be in the range:

Mean pole 15° (dihedral angle)

$k_r \pm 0.15$

$P_{32} \pm 25$ %

Orientation

A comparison between the 762 poles in tunnel TASK and TASD and the model is shown in Figure 6-13. By visual inspection it is seen that the model produces slightly too many gently dipping fractures striking SW and too few gently to steeply dipping fractures striking NW.

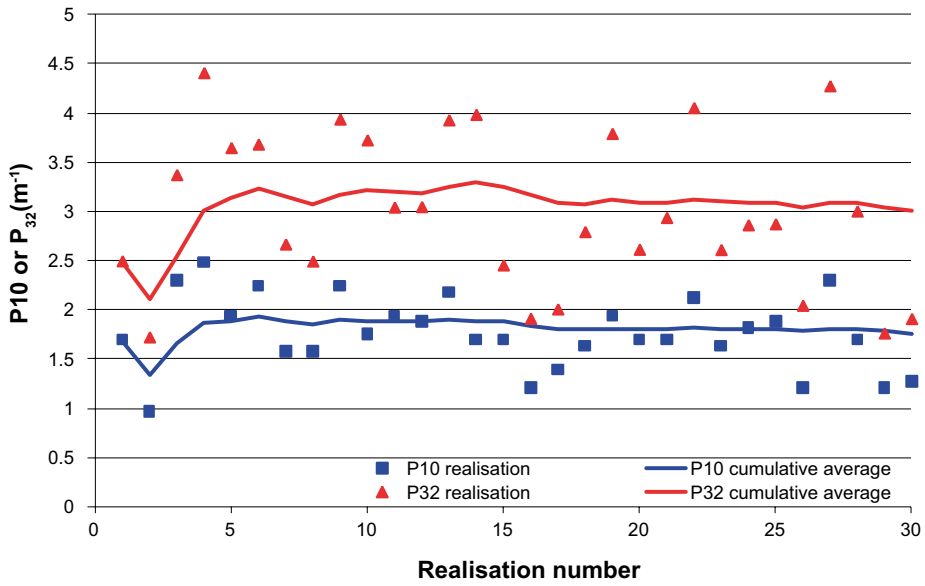

Figure 6-12. *Results from the 30 modelled scanlines.*

When comparing the model to the data measured in the TASO tunnel the steeply dipping Northwest striking fractures are somewhat underestimated otherwise it looks reasonable, see Figure 6-14.

Size

The length distribution of the traces intersecting the modelled scanlines should have a slope that equals $-(k_r - 2)$, i.e a slope of -0.6. Figure 6-15 shows the slopes of the two modelled scanlines in the TASD and TASK tunnels. The slope -0.6 is drawn for comparison and one can see on the curvature that the model suffer from edge effects, truncation and that only fractures with $r < 25$ m are modelled. However, it seems to be a reasonable approximation omitting fractures larger than 10 m.

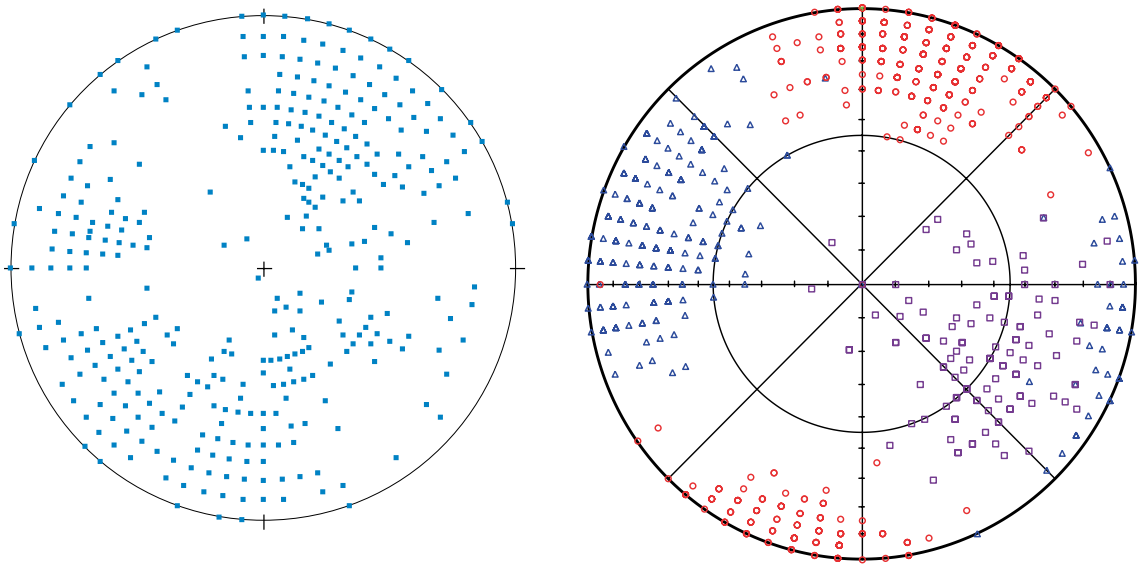

Figure 6-13. *Fracture poles mapped on the floor in the TASK and TASD tunnels to the left and sampled fracture poles along the scanlines in the model to the right. Observe that the simulated fractures have been rounded to the nearest 5° to reflect the measurement.*

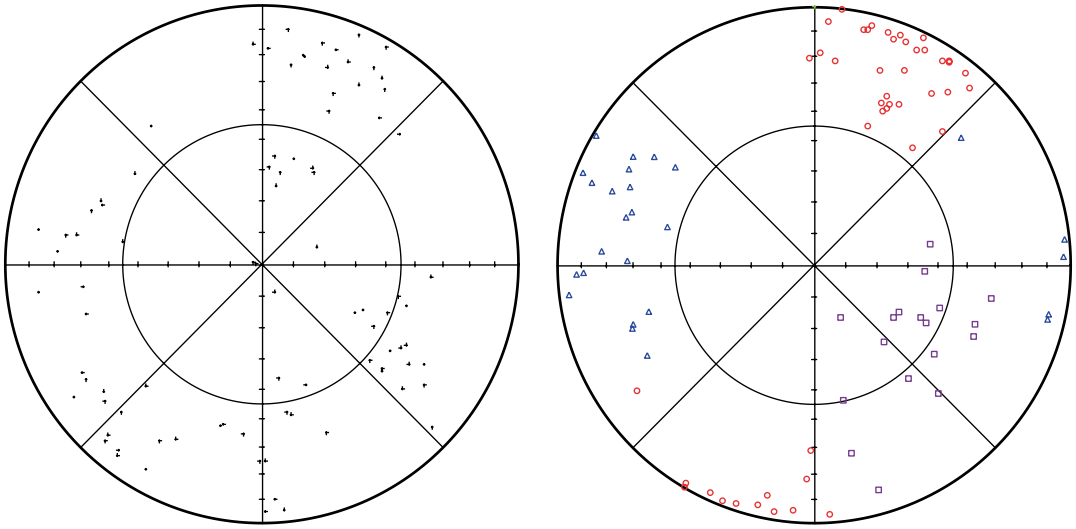

Figure 6-14. Fracture poles of the mapped fractures in the TASO tunnel to the left and modelled poles to the right.

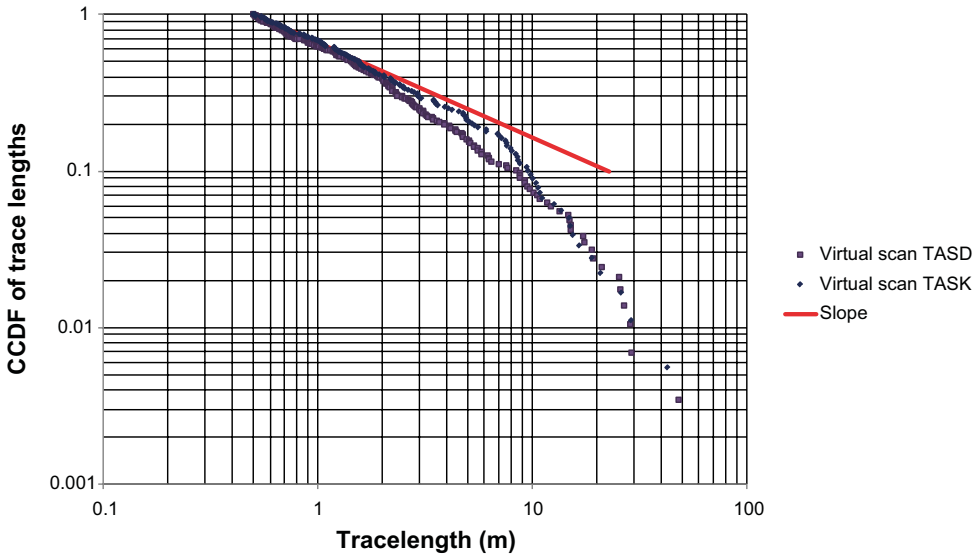

Figure 6-15. Distribution of fracture trace lengths intersecting the modelled scanlines. The red curve corresponds to a slope of –0.6, i.e. corresponds to a slope of the parent distribution, kr, of 2.6.

Intensity

The Fracture model produces 19 FPI, Full tunnel Perimeter Intersections, per 100m tunnel which is in good agreement with the measured values of the TBM tunnel that have 17 FPI/100 m tunnel. Therefore the size-intensity model seems to be in the range.

Optional: Generated fracture set

For those who do not have the ability to generate fractures within their assessed codes a delivery of one generated set of fractures are available in the file: Fractures_generated_and_crossing_boreholes.xls.

The fractures in the file are a sub-set of the entire population and represent only the single features that actually are in contact with one borehole, mostly very small fractures. The modelers that choose to use this set may choose different conceptual models to feed water into the fractures. One possible alternative is to extend the fractures out to a uniform and more conductive rock matrix at some distance from the boreholes.

6.3.3 Boundary condition[4]

From a specified sub-grid of a DarcyTools v3.3 simulation of the full regional Äspö HRL model (Äspömodel05) pressure[5], salinity, velocities along the x, y, and z coordinates are given over an approximately $(100)^3$ m^3 volume incorporating the suggested model domain just inside of the boundaries of the specified model domain (Figure 6-5). Data are found in the file: TASO_pressure_salinity_velocities_rev20101123.xls (Figure 6-16).

Modeled equation for salinity-density dependence is: $1\,000(1 + 0.0078 \times S)$ kg/m^3, where S is given in weight percent.

As a reference case the assigned boundary conditions in tunnels should be at atmospheric conditions.

The associated uncertainty within the boundary conditions is suggested to be treated with one or many sensitivity cases. It is recommended that one alternative boundary condition is tried as an isotropic and homogenous value of −50 metres of fresh water head on all boundary cells/nodes with no contact to the tunnel. For cells/nodes in contact with the tunnel the associated pressure should be addressed as atmospheric.

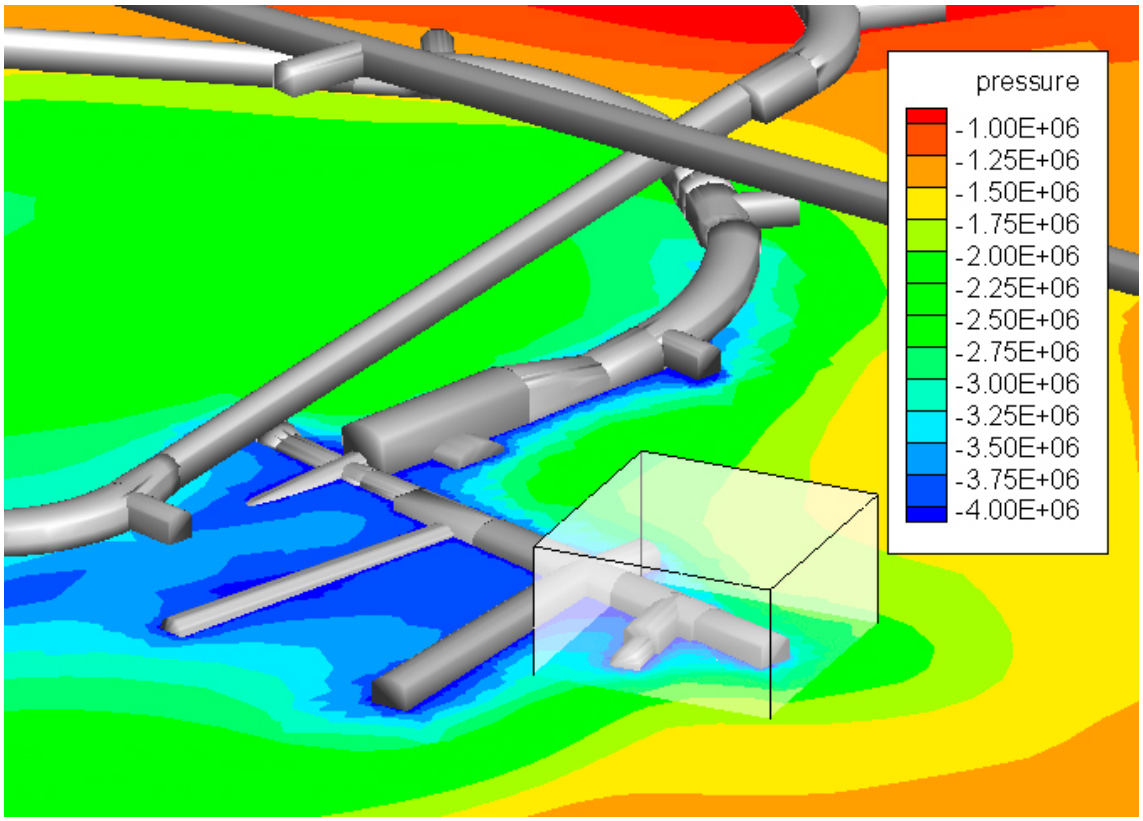

Figure 6-16. *Illustration of the pressure field (Pa), reference elevation is present day shore line (0 altitude).*

[4] The boundary conditions are established from the present official hydro-model of Äspö HRL. The model is (among others) based on the SDM site Laxemar deformation zone model and does, due to scale issues, contain known location errors. The model may develop during the planned Task 8.

[5] Pressures given are dynamic pressure; absolute pressure could be calculated using $\rho_0 \times g \times z$, with reference altitude at present day shore line (0 altitude).

Initial conditions

The initial conditions for the inflow predictions (Task 8c1) should be based on the "natural" conditions where all probing boreholes are packed off, assuming the packer to seal the upper 1 m of the borehole. For the Task 8c2 initial conditions are the results from Task 8c1. With the following deposition hole near-field clarifications:

Rock:

Resulting pressure field of steady-state conditions simulated based on the set-up but with bedrock-bentonite interface at a constant atmospheric pressure.

Bentonite:

The initial degree of saturation is 0.36 which corresponds to an initial suction value of 100 MPa with the retention curve defined below.

6.3.4 Material specifications

It should be noted that the suggested values below (Table 6-3) are based on expert judgment and/or theoretical approximations. Modelers are free to adjust parameters within their conceptual model.

Table 6-3. Material specifications.

Material	Properties	Value
Intact rock (fracture free, matrix)	Hydraulic conductivity	1×10^{-14} m/s
	Kinematic porosity[3)]	1×10^{-5}
	Specific Storage[3)]	1×10^{-11} m^{-1}
Geological structure model fractures[1)]:	Geological width[2)]	1 m
wfracture_01	Transmissivity	2×10^{-8} m^2/s
	Porosity for porous media descriptions	1×10^{-3}
	Transport aperture for DFN descriptions	1×10^{-5} m
	Storativity	1×10^{-8}
wfracture_02:	Single plan, geological width	0.001 m
	Transmissivity	2×10^{-9} m^2/s
	Porosity for porous media descriptions	1×10^{-3}
	Transport aperture for DFN descriptions	1×10^{-5} m
	Storativity	1×10^{-8}
NNW4:	Geological width	10 m
	Transmissivity	6.5×10^{-7} m^2/s
	Porosity for porous media descriptions	1×10^{-3}
	Transport aperture for DFN descriptions	1×10^{-5} m
	Storativity	1×10^{-7}
Bentonite:	Hydraulic conductivity	6.4×10^{-14} m/s
	Porosity	0.44
	Specific Storage (suggested value)	1×10^{-6} m^{-1}

[1)] All properties assigned are based on expert judgement. Presently no site specific information available.

[2)] The deformation zone named wfracture_01 is primary located to the west of the defined plane at the crossing of TASO.

[3)] The reader is advised to use the parameter values noted here with care and to recognise the site dependent properties as being so-called apparent properties. Physically more relevant values are given in Chapter 7.

6.3.5 Proposed relationships

For the matrix and bentonite and as a reference case the proposed relationships are the same as in Task 8a.

The following relationships are proposed to be used for the relative permeability:

$$k_r = \begin{cases} S^3 & (bentonite) \\ \sqrt{S}\left(1-\left(1-S^{1/\lambda}\right)^{\lambda}\right)^2 & (rock) \end{cases} \quad (6\text{-}3)$$

where S is the degree of saturation (volume of water over total volume of pores).

In addition, the following expression is proposed for the water retention curve:

$$S = \left[1+\left(\frac{P_g - P_l}{P_0}\right)^{\frac{1}{1-\lambda}}\right]^{-\lambda} \quad (6\text{-}4)$$

where P_g is the gas pressure (can be assumed to be atmospheric 0.1 MPa), P_l is the water pressure, and P_0 and λ are empirical constants (Table 6-4).

Table 6-4. Parameter values used for water retention curves.

Material	P_0 (MPa)	λ (–)
Bentonite	9.23	0.3
Rock/matrix	1.74	0.6

As of the rock fractures the following relationship should be used (in principal the same as above but in an alternative form; where $\delta = \rho \times g/P_0$ and $n = 1/(1-\lambda)$).

$$K(h) = K_s \frac{\left(1-\left(\delta|h|\right)^{n-1}\left(1+\left(\delta|h|\right)^n\right)^{-(1-1/n)}\right)^2}{\left(1+\left(\delta|h|\right)^n\right)^{m(1-1/n)}} \quad \text{for } h<0 \quad (6\text{-}5)$$

$K(h)=K_s$ for $h\geq 0$

Suggested variation of the parameters is found in Figure 6-17 where the aperture is given in mm. As a reference case, δ and n should be assigned according to the cubic law hydraulic aperture based on the transmissivity values and m = 0.5. An explanation for how to derive van Genuchten parameters (δ and n, or λ and P_0) from a transmissivity value is given in Figure 4-4 and Figure 4-5.

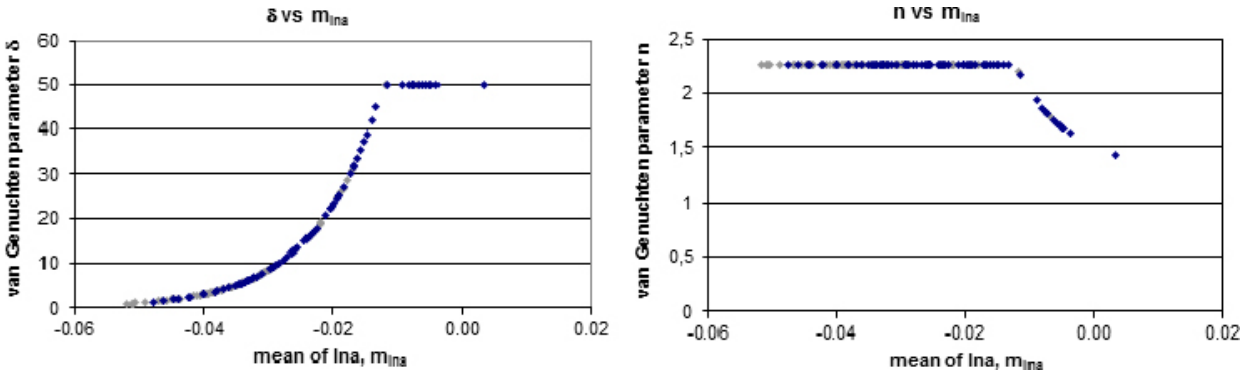

Figure 6-17. *Graphs derived with theory presented by Jarsjö (2009).*

6.3.6 Calibration targets

The calibration targets available for Task 8c are primarily simple inflow/outflow measurements to the individual probing boreholes. All boreholes were packed off; the packer should be assumed to seal off the upper 1 m of the borehole. In the packed off borehole the build-up pressure (P) was measured. If no pressure is given in Table 6-5 below, this indicates that for the time the measurement occurred no inflow large enough to fill up the borehole was measured.

Thereafter, one borehole at a time was opened and the outflow was measured, i.e. yielding the inflow for atmospheric pressure at the borehole top.

Table 6-5. Results of the initial pressure build-up in closed (packed off) boreholes and outflow measurements conducted in one borehole at a time thereafter. The second row indicates flow during injection test. That is the no flow results in KO0018G01 and KO0015G01 in the first test may be due to measurement limitations and or "leakage" in the upper parts of the boreholes. The symbol √ indicates where flow was identified.

	KO0020G01	KO0018G01	KO0017G01	KO0015G01	KO0014G01
Flow	(√)	"no"	√ Q ≈ 0.5 ml / min p ≈ 6 bar ≈ 2 − 3 m	"no"	√ Q ≈ 1 ml / min p ≈ 3 bar ≈ 0.5 − 1 m
Injection	√	√ above 1 m "no" below 1 m (then revised to 1 − 1.5 m)	√	√	√

Flow and pressure data during injection tests in KO0014G01 and KO0017G01 are available in a couple of associated files under the directories ID9_KO0014G01_Injtest_2 and ID5_KO0017G01_ Injtest in the zipped directory Task_8c_second_data_delivery.zip.

The pressure development in the five boreholes is illustrated in Figure 6-18 and Figure 6-19.

Additional to the simple pressure and flow data, some early geology data is available in a couple of associated files under the directories: Borehole fractures, Borehole fracture frequency, Borehole rock type, and BIPS (pdf) in the zipped directory Task_8c_second_data_delivery.zip.

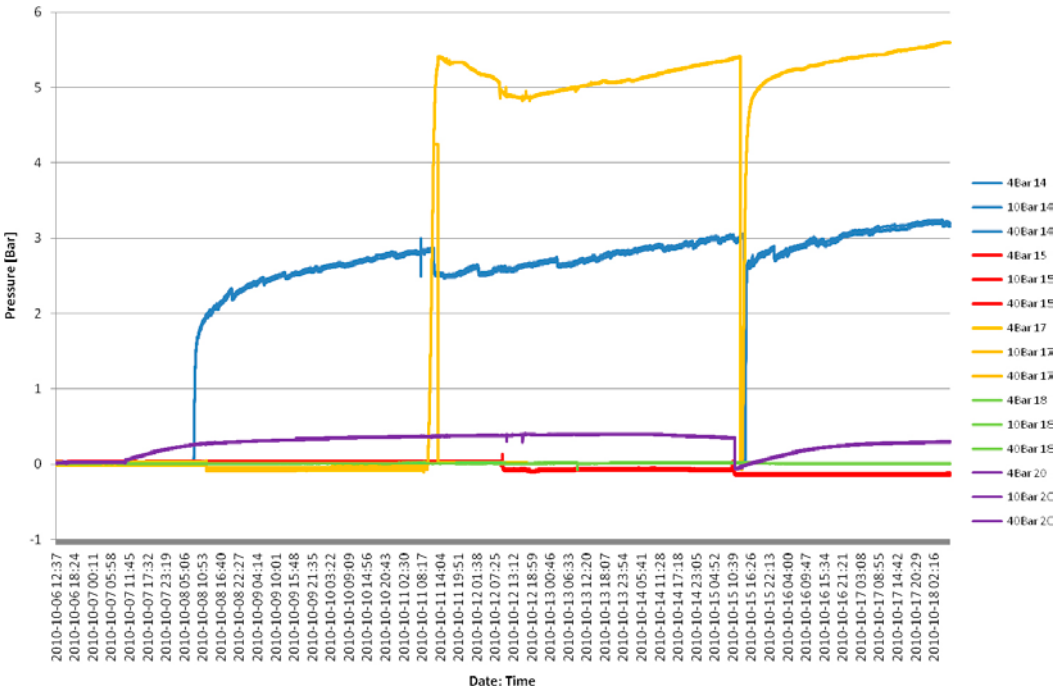

Figure 6-18. *Pressure development in borehole KO0014G01–KO0020G01 at the early times, just after drilling.*

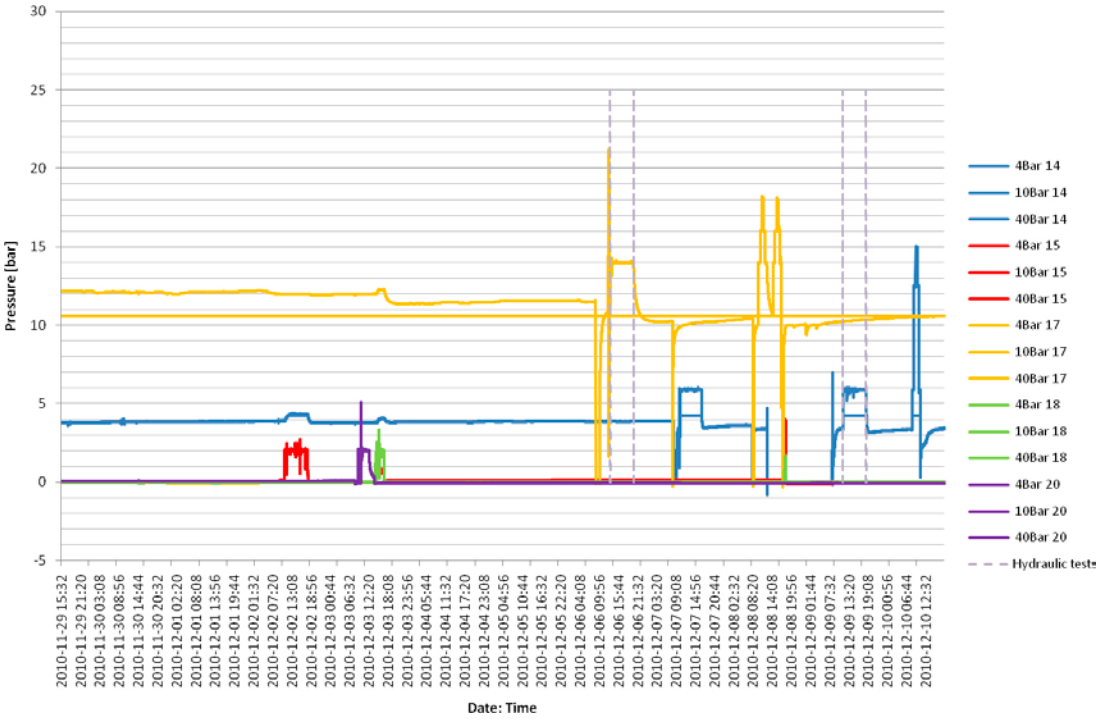

Figure 6-19. *Pressure development in borehole KO0014G01–KO0020G01 after steady conditions have started to prevail. At the second half of the diagram dashed lines indicate time periods for hydraulic tests.*

6.4 Modelling tasks

The modelling task is divided into three major parts:

1. Establishing the model of the site. Using the five probing boreholes information on inflow and built-up pressures, given above. During the simulations all boreholes should be assumed completely packed-off except for the time of an inflow/outflow measurement when one borehole is opened for a time. The packer should be assumed to seal off the upper 1 metre of the borehole.
2. With initial conditions from the results of the first part, the second part contains the expansion of boreholes KO0017G01 and KO0018G01 to a diameter of 0.3 m. The amount and location of inflow to the "deposition boreholes" should be predicted.
3. With initial conditions from the second part, this, the third part, contains the wetting of bentonite placed within the expanded boreholes, KO0017G01 and KO0018G01. The wetting of bentonite, as of wetting patterns and times, along with associated pressure development within the bentonite and the near-field bedrock should be predicted.

6.5 Expected outcome

The expected outcome as presented below needs to be multiplied (produced in the same amount as realisations simulated by the modelling group) in a realistic manner in order to answer up to the objectives.

Results for Task 8c1:

Contour plots of the deposition hole near-field, permeability structure (in m^2), pressures (in Pa) and Darcy fluxes (in m/s) on one vertical cross-section incorporating all five probing boreholes starting at the TASO tunnel entrance and ending at the TASO tunnel front and on one horizontal cross-section incorporating all five probing boreholes starting at the TASO tunnel entrance and ending at the TASO tunnel front and cutting through at the depth of 2.0 metres. The horizontal cross-section should capture the entire tunnel width and reach out at least 2 metres at each side; the vertical cross-section should capture the rock from the tunnel floor and at least 6 metres downward.

Contour plots of the inflows (in m/s) presented as folded up illustrations of the walls of the "deposition boreholes" KO0018G01 and KO0017G01.

Numbers of inflow (in m^3/s) to the entire part of the "deposition boreholes" KO0018G01 and KO0017G01.

Results are expected for steady-state conditions.

Results for Task 8c2:

Contour plots of the deposition hole near-field pressures and saturation[6] in bentonite as well as the bedrock for time steps at 0, 0.1, 0.5, 1.0, 10, 100 years on one vertical cross-section incorporating both deposition holes and parallel with the TASO tunnel central line and one horizontal cross-section incorporating both deposition holes and cutting through at the depth of 1.5 metres.

The contour plots should present the geometric situation of the deposition holes in detail (tunnel floor and 5 metres down). The colour scale of the contour plots should be: 1.5, 1, 0.5, 0.2, 0.1, 0, −0.1, −0.2, −0.5, −1, −5, −10, −20, −50 MPa. Graphs showing illustrations of the pressure increase within the bentonite at a position 0.01, 0.05, 0.1, 0.15 metres from the different deposition holes walls. These graphs should come as six: one for each of the deposition holes (KO0018G01 and KO0017G01) at 1.5 metres depth, at 0.75 metres down the hole, and at 2.25 metres down the hole.

Graphs illustrating the pressure change within the bedrock at a position 0.01, 0.05, 0.1, 0.15, 1, 5 metres from the deposition hole walls in the direction towards the other deposition hole are requested. These graphs should also come as three for the same depth positions as described above.

[6] Or alternative equivalent measure of change in the bentonite due to inflow of water from the bedrock.

7 Task 8d BRIE – Prediction of inflow and wetting of KO0017G01 and KO0018G01 based on detailed characterisation data

7.1 Introduction

This gives the necessary guidelines for setting up calculations concerning predictions of inflow to the two 30 cm diameter boreholes and the wetting of the emplaced bentonite in the TASO tunnel within a sub-local Äspö HRL site model domain.

The model results are primarily intended to provide predictions of the wetting that will be measured in the parallel on-going BRIE experiment.

Hydraulic boundary conditions are provided from a regional scale hydrogeological model which in part uses the same geometrical framework (as supplied in this specification), albeit at a larger scale. Geometrical specifications, along with a site-specific geological structure model are given as CAD data. Site specific stochastic fracture statistics are given as intensity, size and orientation data and serve as the basis for the hydraulic properties.

Some details of the structural model have been established that result in changes to the above mentioned input data. This includes data such as the local geometrical setting of the deformation zone wfracture_01 at the TASO tunnel, and fracture locations within the expanded boreholes KO0017G01 and KO0018G01.

7.2 Scope and objectives

One sub-aim of Task 8 is to improve the knowledge of the bedrock-bentonite interface with regard to groundwater flow. It is not intended to be a coupled model exercise; fully incorporating mechanical, unsaturated, and saturated properties. Neither is the intention to address the thermal or the chemical aspects of bentonite. However, it is free to address the proposed problem with any type of suitable code intended for groundwater flow or similar problems. Also, the use of codes incorporating unsaturated flow, chemistry, and mechanics is encouraged.

Task 8d has been divided into two parts, i.e. Task 8d1 and Task 8d2. Incorporation of bentonite is not considered in the Task 8d1 exercise. Instead the inflow to the open 30 cm boreholes is addressed and is intended to be compared with field data from the BRIE experiment but also to test the modelling tools' ability to predict inflow to deposition holes based on more detailed information. Task 8d2 addresses the wetting of the bentonite based on the flow model established in Task 8d1. The wetting results are planned to be used as predictions of the field results of the on-going field experiment of BRIE.

The scope of this calculation exercise is contained within the simulation of a sub-local site-specific three-dimensional groundwater flow specifications presented below, similar to Task 8c however now with additional detailed hydraulic data.

The main objectives with this exercise are:

Task 8d1

- To calculate inflows and inflow characteristics to two 76 mm diameter probing boreholes.
- To calculate inflows and inflow characteristics to two 30 cm diameter open boreholes.
- To compare inflows calculated for probing boreholes with inflows calculated for enlarged 30 cm boreholes.
- To supply boundary conditions and initial conditions to the field experiment on the emplaced bentonite packs within the two 30 cm boreholes.

Task 8d2

- To evaluate the resulting wetting of the bentonite installed in the borehole characteristics established in Task 8d1.
- To evaluate effects of heterogeneous fracture flow on the wetting.
- To evaluate effects of heterogeneous matrix properties on the wetting.
- To serve as a base case for comparison with earlier results based on less elaborated hydrogeological models.

Site-specific geological influences such as the chemistry-induced changes (e.g. calcite precipitation) are not presently quantified. Modellers are welcome to address these issues as one mean of adjusting their models. All incorporated issues, however, need to be readily explained.

As one of the objectives is to illustrate and give numbers on inflow and inflow distributions within a deposition hole, the assessed models need to consider a cell/grid resolution that is able to capture details on a wall of a deposition hole of a size of 0.3 m in diameter and 3 m in depth.

7.3 Case specifications

7.3.1 Geometrical set-up

All content and referred files in this section is the same as for Task 8c.

The coordinate system applied within Task 8 is the Swedish RT90 system. The suggested model domain is approximately $(40)^3$ m^3 bounded by the following set of coordinates given in Table 7-1 (see Figure 7-1).

As the BRIE experiment has been given the TASO tunnel as its primary investigation area the specifications given are based on the sub-local scale of the TASO tunnel area at the Äspö HRL.

Table 7-1. Coordinates for suggested model domain.

x	Y	z
1551603	6367769	−396
1551629	6367799	−396
1551600	6367826	−396
1551573	6367796	−396
1551603	6367769	−436
1551629	6367799	−436
1551600	6367826	−436
1551573	6367796	−436

The Äspö HRL geometrical framework (see Figure 7-2, Figure 7-3 and Table 7-2) along with the geometrical framework of the geological structure model is given as CAD layers in the files: TASO_V0.1_TG.dxf. and TASO_V0.1_DET.dxf respectively. It should be noted that the structures *should* connect to the boundaries of the assessed model domain.

The five probing borehole (Figure 7-5) established in the BRIE experiment derived before task 8c are given in the CAD file TASO_V0.1_TG.dxf.

As a simplification the entire set of information is available in TASO_V1.1_ALL.dxf. The latter file also contains information on the principal stress orientation, etc.

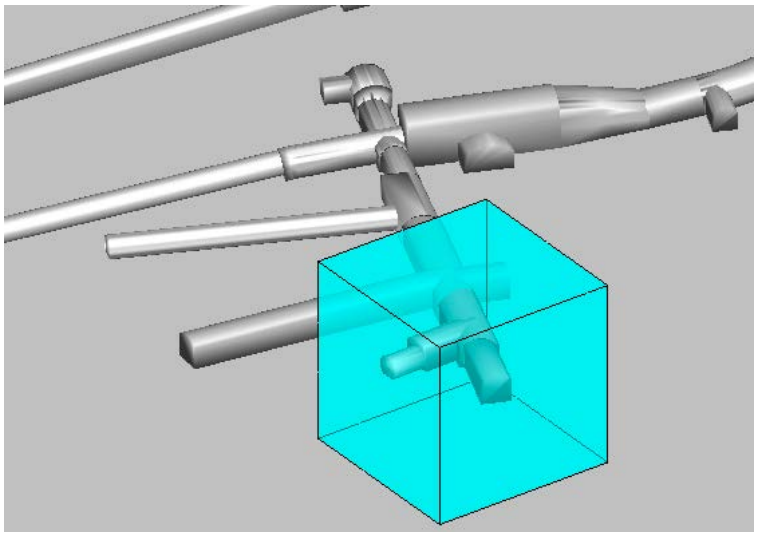

Figure 7-1. *Illustration of the suggested model domain in the vicinity of the assembly hall at the Äspö HRL. The size of the model domain that e.g. includes the TASO tunnel is 40 by 40 by 40 m^3.*

Table 7-2. Summary of files presented in this section.

CAD file	Content	Comment
TASO_V0.1_TG.dxf	Äspö HRL geometrical framework.	
TASO_V0.1_DET.dxf	Geological structure model.	Structures *should* connect to the boundaries of the assessed model domain.
TASO_V0.1_TG.dxf	Five probing boreholes prior to enlargement.	
TASO_V1.1_ALL.dxf	Simplified entire set of information.	Also contains information on the principal stress orientation.

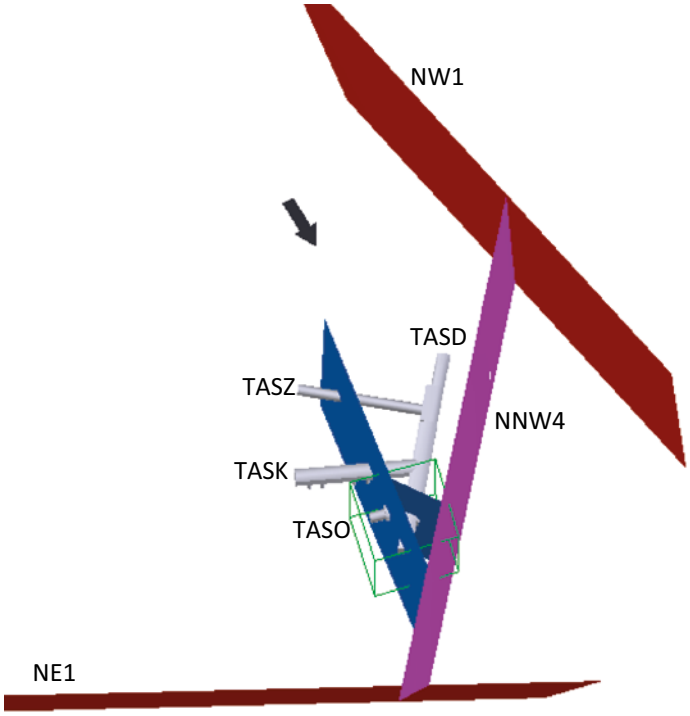

Figure 7-2. *Illustration of the CAD contained data along with the suggested model domain. The large structures are named according to the Äspö HRL model. The tunnel names are given for orientation. The thick black arrow indicates the major principal stress orientation.*

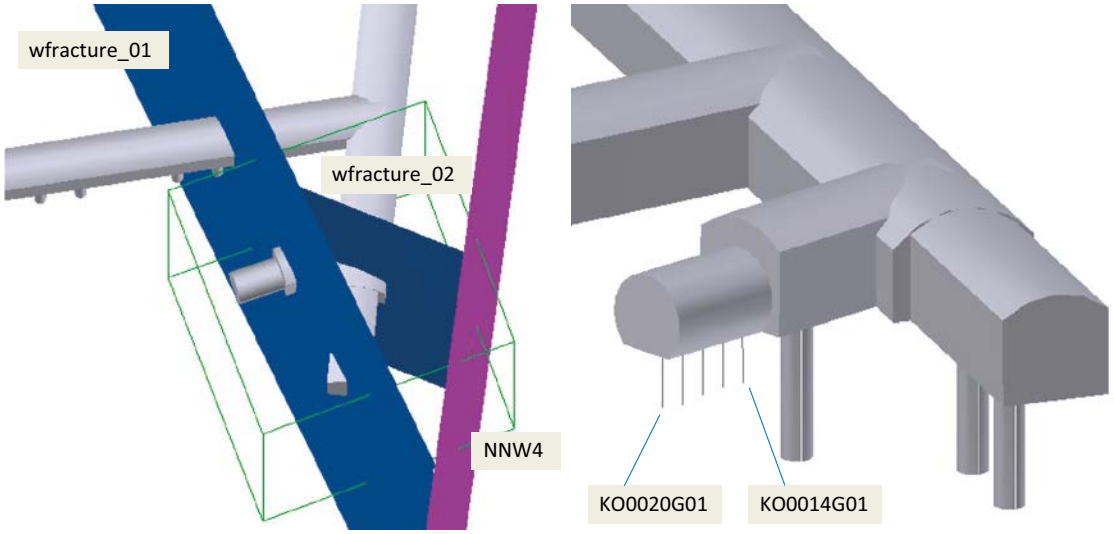

Figure 7-3. *Details closer to the TASO tunnel, naming the three deterministic structures that are contained within the suggested model domain. The five probing boreholes are illustrated on the right. The figure includes an indication of the naming of the boreholes by giving the outer boreholes name. See Figure 7-5 for the naming of boreholes in between.*

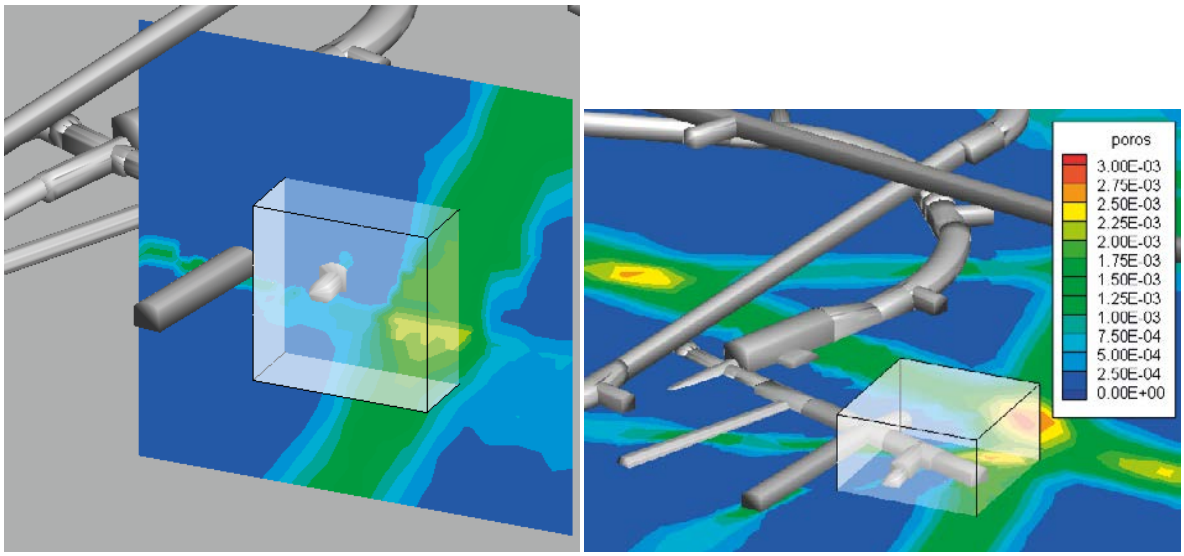

Figure 7-4. *Illustration of the larger scale setting of the suggested model domain. The DarcyTools set-up incorporates structures on a larger scale. Observe how one of the bounding sides is following a larger structure that actually represents the NE1 structure on a larger scale model.*

Figure 7-5. *Illustration of probing borehole spacing and naming.*

7.3.2 New geometric information

Additional fourteen boreholes have been drilled in the floor around the probing boreholes KO0014G01, KO0017G01, KO0018G01, and KO0020G01 (Figure 7-6). Four boreholes have been drilled in the TASO tunnel walls (Figure 7-7). One measurement weir is established in the entrance of the TASO tunnel at a distance of 765 mm in-front of borehole KO0013G01. Further the KO0017G01 and KO0018G01 has been expanded to a diameter of 30 cm. All coordinates given in the files referred to below is in RT90 (see Table 7-3).

Starting and ending positions for the fourteen new boreholes established in the floor are found in the file: borehole_coordinates_20121002.xls

Starting and ending positions for the four boreholes established in the walls are also found in the file: borehole_coordinates_20121002.xls

Table 7-3. Specification of new file presented in this section.

File	Content	Comment
borehole_coordinates_20121002.xls	Start, end coordinates of 14 floor boreholes. Start, end coordinates of 4 side-wall boreholes.	

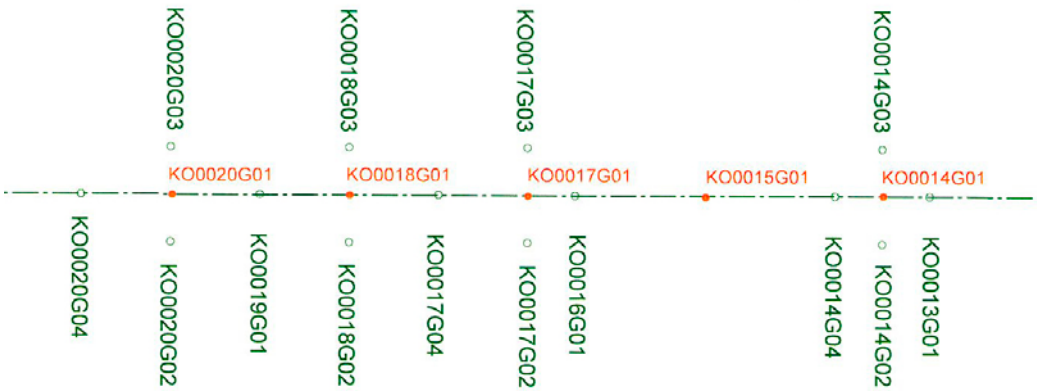

Figure 7-6. Boreholes in tunnel floor.

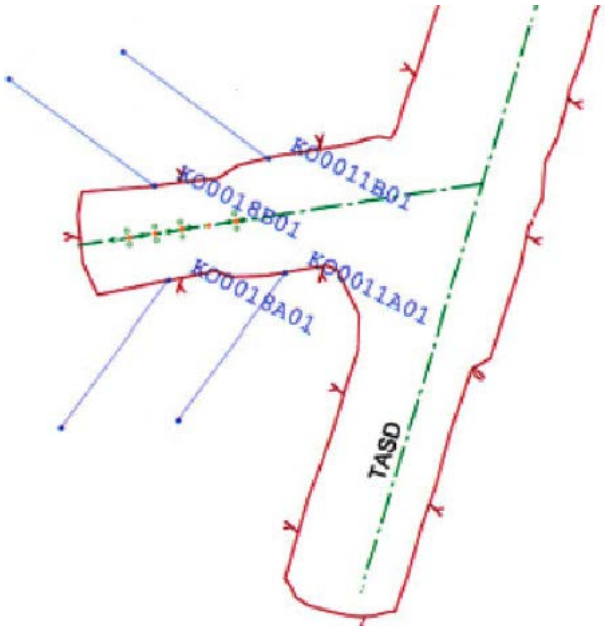

Figure 7-7. Boreholes in tunnel wall.

7.3.3 Design of bentonite installation

The bentonite was installed as cylindrical blocks threaded on a central tube. These blocks were compacted, drilled and subsequently machined in order to get well-defined properties and dimensions. The blocks had a dry density value slightly higher than the target dry density value, since the blocks would swell and fill the outer slot between the blocks and the borehole wall. The blocks were confined with plates in the bottom and at the top, and these plates were welded to the central tube (see Table 7-4 below and Figure 7-8).

The bore holes were filled with sand (actually macadam 2−4 mm) in the bottom. The reason for this was: i) to provide a means to fill the outer slot with water; ii) to level the uneven bottom of the bore holes; and iii) to adjust the level of the bentonite parcel above. The first reason was facilitated with a thin tube, located within the central tube, which was attached to a hole through the centre of the bottom plate.

Each bentonite parcel was instrumented at two sections (Hole 17 at 2.3 and 2.6 m; Hole 18 at 2.3 and 2.7 m). These sections denote specified levels, each with two instrumented blocks immediately above and beneath these levels. The blocks above contain RH-sensors, whereas the blocks beneath contain pressure sensors (see Figure 7-10). A general scheme with sensor positions internally specified for each section was adopted. These sections were oriented in the plane so that the pore pressure sensor came as close as possible to the fracture of interest in each bore hole. All cabling from the sensors was made through the central tubes. After the installation, the tubes leading to the sand fillings at the bottom of the bore holes were connected to pore pressure sensors located in the TASO tunnel. The coordinate of all sensors are shown in Table 7-5. The positions of the RH-sensors and the pore pressure sensors are illustrated in Figure 7-9.

The installations took place at the following times (see Figure 7-11):

Installation Hole 18: 2012-09-13 17:12

Installation Hole 17: 2012-09-14 10:19

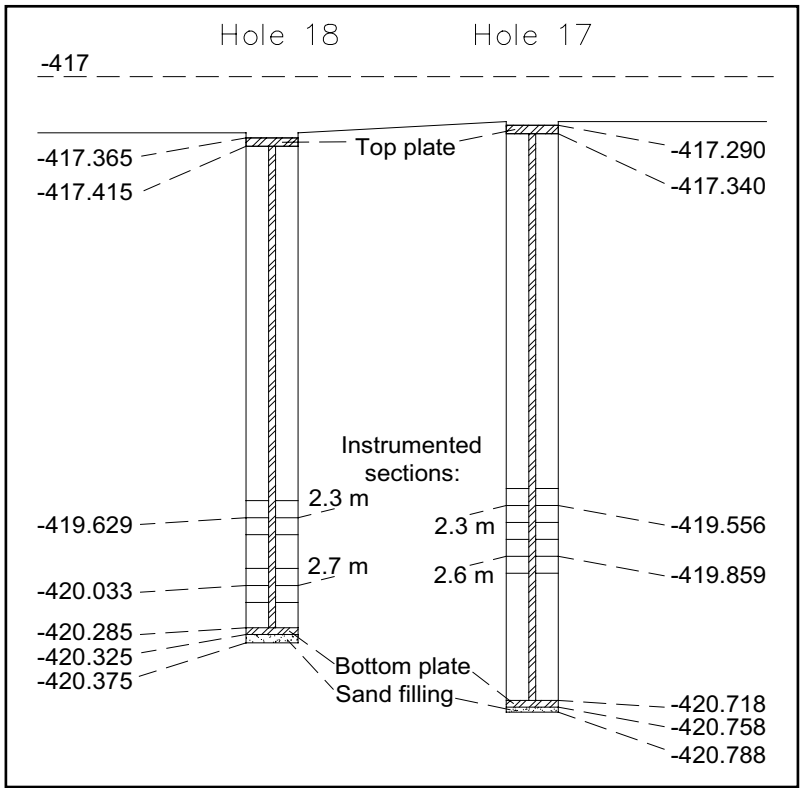

Figure 7-8. *Outline and final dimensions of the bentonite parcels.*

Table 7-4. Heights of components in bentonite parcels.

Component	Height (mm) Hole 18	Hole 17	Comment
Top plate	50	50	Ø298 mm, welded to central tube (Ø40 mm)
Bentonite	2870	3378	Initial outer diameter: 298 mm; inner diameter: 40 mm
Bottom plate	40	40	Ø298 mm, welded to central tube (Ø40 mm)
Sand filling	50	30	Macadam 2−4 mm

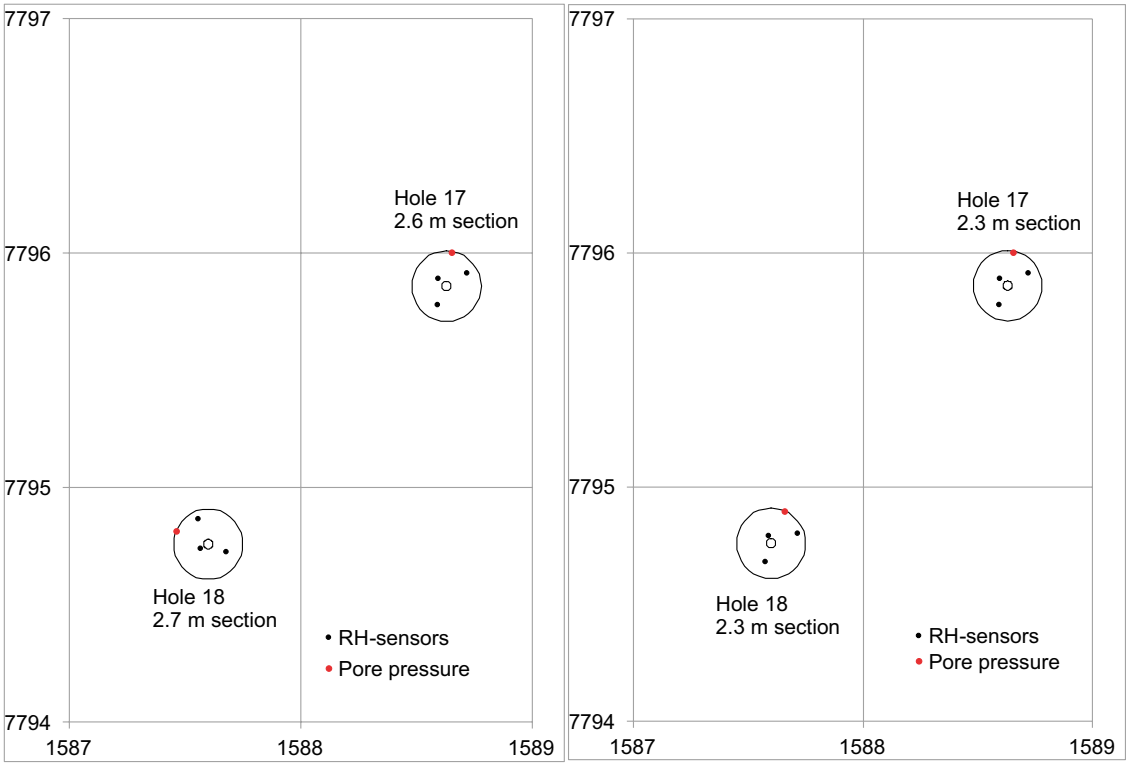

Figure 7-9. *Illustration of sensor positions in borehole KO0017G01 and KO0018G01. Coordinates correspond to RT90 with the first three figures omitted.*

Figure 7-10. *Instrumentation of blocks; left: block with pressures sensors; right: block with RH sensors.*

Figure 7-11. *Installation of bentonite parcel in Hole 17.*

7.3.4 Filling of the outer slot

An amount of 3.1 litre of formation water was poured into the outer slot of borehole KO0018G01 from above (i.e. at the slot between the bore hole and the top-plate) at 17:45 (2012-09-13). The outer slot appeared to be water-filled since water started to accumulate at the top-plate.

Table 7-5. Sensor locations for borehole KO0017G01 and KO0018G01.

Sensor type	Sensor	x	Y	z	Hole	Section	Comment
Total pressure	PBR0001	1551588.67	6367795.81	−419.867	17	2.6	Axial
	PBR0002	1551588.51	6367795.85	−419.897	17	2.6	Radial
	PBR0003	1551588.67	6367795.81	−419.564	17	2.3	Axial
	PBR0004	1551588.51	6367795.85	−419.594	17	2.3	Radial
	PBR0005	1551587.66	6367794.70	−419.637	18	2.3	Axial
	PBR0006	1551587.50	6367794.76	−419.667	18	2.3	Radial
	PBR0007	1551587.66	6367794.82	−420.041	18	2.7	Axial
	PBR0008	1551587.60	6367794.66	−420.071	18	2.7	Radial
Pore pressure	UBR0001	1551588.65	6367796.00	−419.871	17	2.6	
	UBR0002	1551588.65	6367796.00	−419.568	17	2.3	
	UBR0003	1551587.66	6367794.90	−419.641	18	2.3	
	UBR0004	1551587.46	6367794.82	−420.045	18	2.7	
	UBR0005	1551588.61	6367795.86	−420.758	17	3.5	In sand
	UBR0006	1551587.60	6367794.76	−420.325	18	3.1	In sand
Relative humidity	WBR0001	1551588.59	6367795.89	−419.846	17	2.6	
	WBR0002	1551588.59	6367795.78	−419.846	17	2.6	
	WBR0003	1551588.71	6367795.92	−419.846	17	2.6	
	WBR0004	1551588.59	6367795.89	−419.543	17	2.3	
	WBR0005	1551588.59	6367795.78	−419.543	17	2.3	
	WBR0006	1551588.71	6367795.92	−419.543	17	2.3	
	WBR0007	1551587.58	6367794.80	−419.616	18	2.3	
	WBR0008	1551587.57	6367794.69	−419.616	18	2.3	
	WBR0009	1551587.71	6367794.81	−419.616	18	2.3	
	WBR0010	1551587.56	6367794.74	−420.020	18	2.7	
	WBR0011	1551587.67	6367794.73	−420.020	18	2.7	
	WBR0012	1551587.55	6367794.87	−420.020	18	2.7	

An amount of 6.85 litre of formation water was poured through the sand filling of borehole KO0017G01 during 10:21 to 10:30 (2012-09-14). 1.05 litre was poured into the outer slot of from above immediately afterwards. Later on, it was noticed that water has entered the central tube of borehole KO0017G01, and this tube was therefore emptied of 2.2 litres on 2012-09-17 at approximately 10 am.

The total volumes that have been poured into the systems, can be compared with different estimated (easily accessible) pore volumes, ie. the outer slot, the sand filling and the central tube (found in hole 17 only), see Table 7-6. For Hole 17 there is a minor excess of water which could be accounted for by slots and cavities between the bentonite blocks. For Hole 18, the difference between the added volume and the estimated pore volume can be explained by the inflowing water from upper parts of the hole during the time period when the hole was open.

Table 7-6. Simple water balance for the filling of the outer-slot.

	Hole 17	Hole 18
Total added water volume	7.9 liter	3.1 liter
Outer slot	3.5 m á 0.1 liter/dm	3.1 m á 0.1 liter/dm
	3.5 liter	3.1 liter
Sand-filling with estimated porosity of 40 %	40 % of 4 liter	40 % of 5 liter
	1.6 liter	2 liter
Water in central tube	2.2 liter	–
Total	7.3 liter	5.1 liter
Excess	0.6 liter	−2 liter
	Possibly due to slots and cavities between blocks.	Due to inflowing water from the upper parts while the hole was open

7.3.5 Background fracture statistics

It should be noted that these statistics are the same as those for Task 8c.

Based on the collected and thereafter compiled data from TASO TASD, TASK, and two deposition holes in close vicinity of the BRIE experimental site, three fracture sets have been defined primarily by visual inspection. Table 7-7 presents the suggested statistics for the TASO tunnel; however it should be noted that all modeling groups are welcome to address the available data (Fractures_TASK8C_filtered.xls) on their own as the relative small sample of data allows for alternative interpretations. As two examples one may note that the fractures smaller than 1 metre seem to follow a slightly different statistics and also that of the analysed data only the inner part of TASD and the entire TASO (our tunnel) share the same rock type.

The assessed length interval of fractures is also left for the modellers to choose. This may be constrained by individual codes. However, it should be noted that on the larger side no fractures have been found that actually cut the entire tunnel periphery except for the fractures that are modelled deterministically.

Table 7-7. Suggested fracture statistics to be used for the TASO tunnel.

Set	Orientation trend	plunge	Fisher konc.	Size r_0	k_r	Spatial Distribution	Intensity P_{32} (r_0,∞)
Set 1	280	20	10	0.25	2.6	Poisonian	1.1
Set 2	20	10	15	0.25	2.6	Poisonian	2
Set 3	120	50	10	0.25	2.6	Poisonian	0.75

An excel sheet file is associated to help with rescaling the intensity due to different choice of fracture sizes. The file is named P32_interval_brie:xls. The power-law distribution can be scaled according to the following equation:

$$P_{32,r_a-r_b} = P_{32,r_1-r_2} \cdot \frac{r_a^{2-k_r} - r_b^{2-k_r}}{r_1^{2-k_r} - r_2^{2-k_r}} \quad (7\text{-}1)$$

Noticing that the terms r^{2-k} becomes zero if r equals infinity makes it possible for the modellers to scale the provided size-intensity relationship to cover fracture sizes of interesting ranges. The amount (N) of fractures in a volume (V) within a certain size and intensity interval can be calculated using:

$$N = \frac{k_r - 2}{k_r} \cdot \frac{P_{32,r_1-r_2}}{\pi} \cdot \frac{\left(r_2^{-k_r} - r_1^{-k_r}\right)}{\left(r_2^{2-k_r} - r_1^{2-k_r}\right)} \cdot V \quad (7\text{-}2)$$

A documentation of the process conducted in establishing the information of Table 7-7 follows below.

Introduction

A Discrete Fracture Network, DFN, model is developed for the BRIE, Bentonite Rock Interaction Experiment, to be used as input to the hydrogeological work.

Development of DFN Model

The data used for developing the DFN is of lower quality and hence subjectivity has to be put into the evaluation of the data. A key point is to keep the model as simple as possible and expert judgement is used to fill the lack of high quality data to make sure that the end result makes sense. A short description of data used and how they are interpreted follows below.

Input data

Some reflections of the input data are:

- Highly uncertain orientation in deposition holes.
- BRIE experiment is in TASO, unfortunately small data sample.
- TASK furthest away and situated in different rock type.
- TASD in conjunction to TASO and relatively large amount of data.

These constraints gives the result that data from TASO, when existing, is ranked highest, then that from TASD and the data from TASK and the two deposition holes are used in a more cautious way.

Orientation distribution

A first compilation of the trace data from the two deposition holes, DD0086G01 and DD0092G01, and the three tunnels, TASD, TASK and TASO was done along with a desktop study of two virtual scanlines in the floor of the tunnels TASD and TASK, see Figure 7-12.

The data does not show any obvious divisions into sets, partly depending on multiple poles plotting on top of each other at even 5° locations, but also because of large uncertainty in the orientation data, especially for the two deposition holes. To be able to see data points that in the original data set plot on top of each other a small uniformly distributed random value, ±2°, is added for both strike and dip. The result is shown in Figure 7-13. By visual inspection 2 sets appear with fracture pole trend/plunge approximately around 280°/20° and 20°/10°.

A division of the data into the tunnels TASD, TASK and TASO is shown in Figure 7-14. The figures shows an indication of a gently dipping set with pole trend about 120 and plunge about 50.

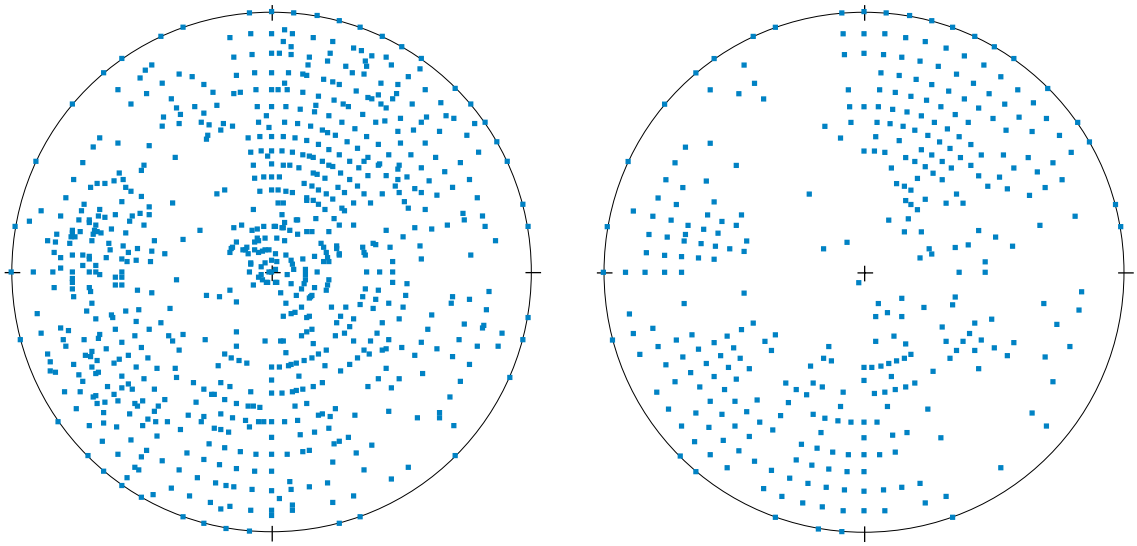

Figure 7-12. *Fracture poles. Left: Orientation of all, 1 772, fractures from the two deposition holes and the three tunnels. Right: Orientation of the 762 fractures mapped at the floor in the TASD and TASK.*

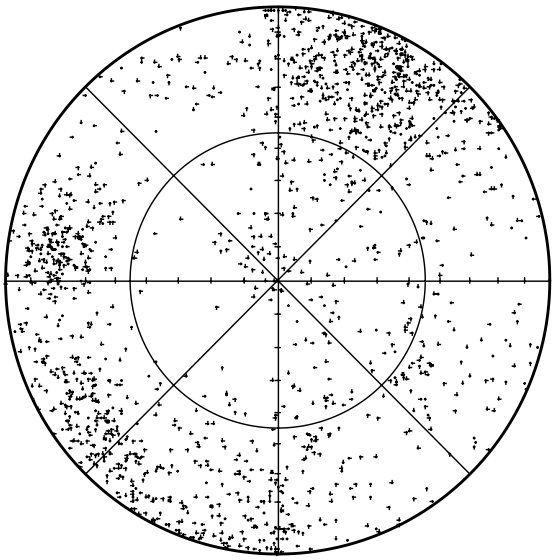

Figure 7-13. *Fracture poles when a uniformly random value is added.*

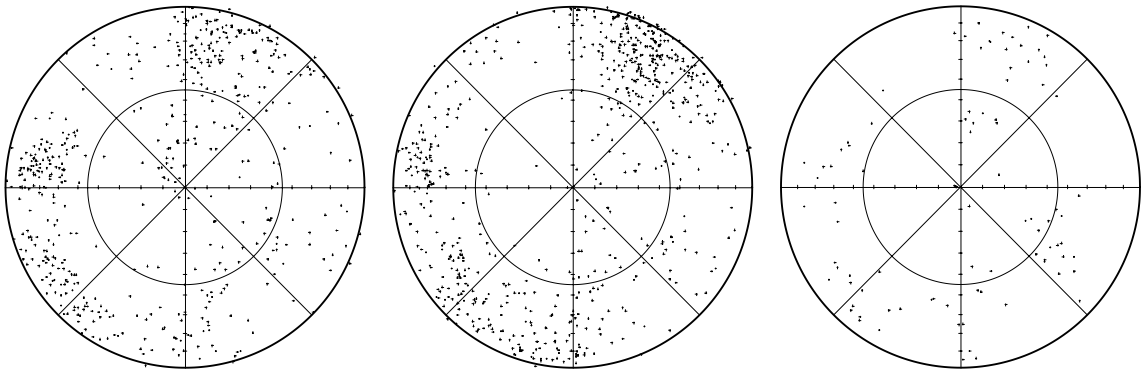

Figure 7-14. *Fracture poles from left: TASD, middle: TASK and right TASO.*

Therefore a simple 3 set model is developed by visual inspection rather than running the data through any set identification software. It is assumed that the orientation distributions will follow a Fisher distribution. The Fisher concentration, κ, is estimated to 10, 15 and 10 respectively for the three sets.

A picture of the assignment of the poles to the sets are shown in Figure 7-15. Using the set assignment the relative intensity between the set are 0.29/0.52/0.20.

Spatial distribution

The data are presumed to scale in a Euclidian way, i.e. the fractures are randomly distributed in space without any correlation.

Size distribution

The slope of the size distribution is calculated from the fracture traces mapped on the tunnel walls, roofs and floors together with the traces in the two deposition holes. Unfortunately the cut-off value, as well as the censoring, is different for the different tunnels and holes. In DD0086G01 it is 0.3 m, in DD0092G01 0.2 m, TASK and TASD 0.4 m and TASO 1.0 m. However it does only affect the interval where the data are not affected by truncation (lower bound) or censoring (upper bound) and the location of the curve in a CCDF (complementary Cumulative Density Function) plot. The slope of the curve is not affected. The distributions of trace lengths are shown in Figure 7-16. The slope of the distribution is, by visual inspection, estimated to be −1.6, which corresponds to the Power law exponent, k_r , equal to 2.6 of the parent size distribution. The slope seems to fit all the 5 locations to a reasonable level. However, the CCDF curve of TASK does not seem to have any straight part where the slope can be evaluated.

The location parameter, r_0, i.e. the smallest regarded fracture cannot be evaluated by use of the trace length distributions only, since it is closely related to the intensity for a Power law function. Hence the location parameter is discussed in the next section.

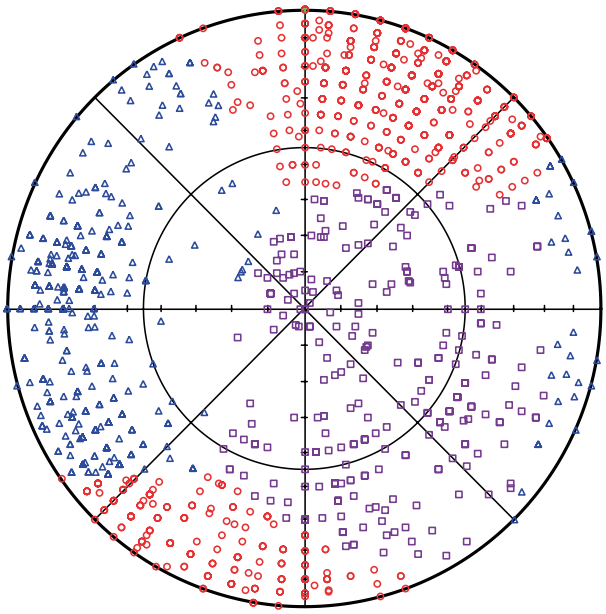

Figure 7-15. *Fracture poles assigned to the three sets. Set1: Blue triangles, set 2: red circles and set 3: purple squares*

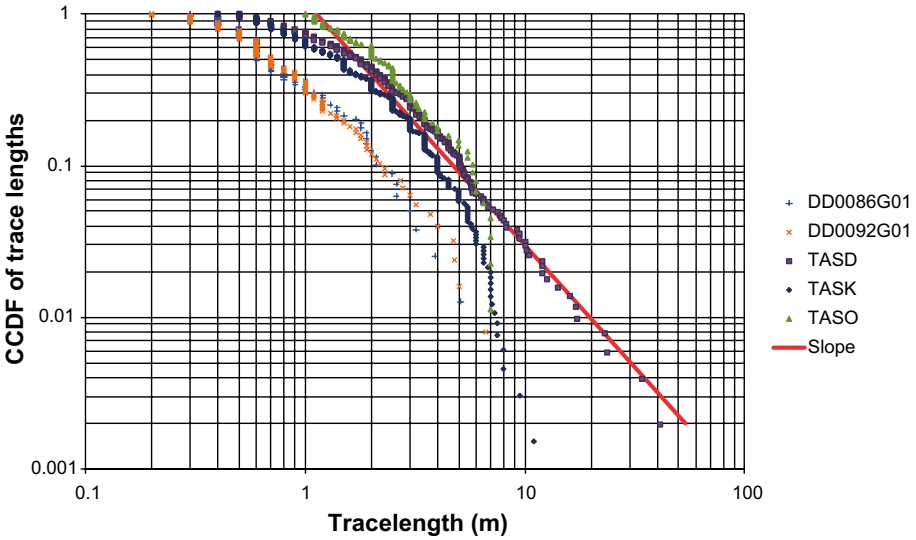

Figure 7-16. *The distribution of trace lengths in the different mapped locations.*

Intensity

The intensity, P_{32}, can be estimated by correcting the number of fractures intersecting a scanline with the Terzaghi correction. This measure is independent of the parent size distribution and hence some modelling has to be carried out to estimate the size-intensity relation. According to Äspö HRL geologists the shortest trace of the scanlines in the tunnels TASD and TASK is 0.5 m and therefore the related P_{32} calculated to the location parameter, r_0, was chosen equal to 0.25 m.

A virtual scan line from the TASD tunnel floor is used while TASK data is ignored for various reasons. Unfortunately the TASD scanline is short, only 16.5 m and 23 intersections which make the intensity estimation highly uncertain.

The relation between P_{32} and r_0 is evaluated using 3 scanlines, 16.5 m long in 10 models which adds to 30 scanlines. The results from the realisations are shown in Figure 7-17. There is a large difference between the different realisations but the cumulative average starts to get reasonably stable after about 20 realisations. With the underlying orientation model together with the assumed relationship between the different fracture sets it is impossible to replicate the data measured in the TASD tunnel. A compromise has been made where the model underestimates the given intensity P_{32} by about 10 % and overestimates P_{10} by about 25 %. The intensities for the different sets $P_{32,\, r>0.25}$ are 1.1, 2.0 and 0.75 m^2/m^3 respectively.

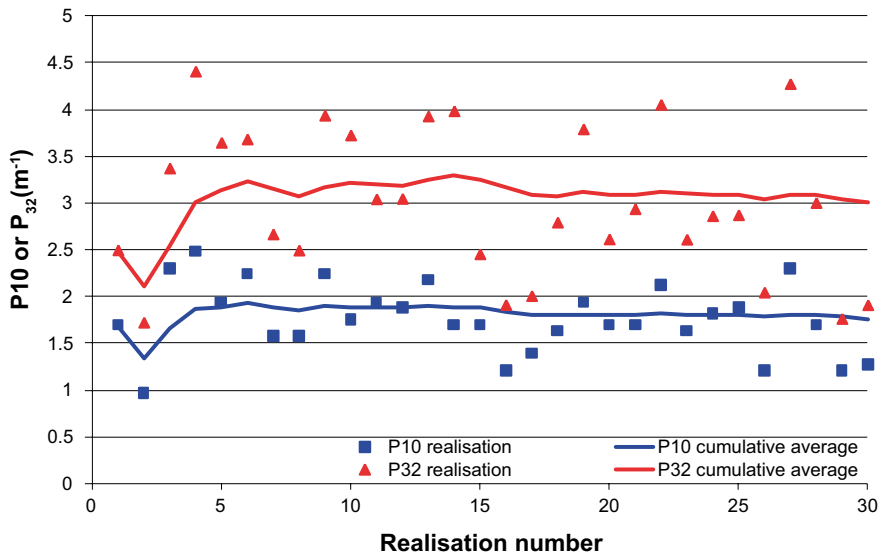

Figure 7-17. *Results from the 30 modelled scanlines.*

Uncertainty

The data provided is limited and in some cases of less quality. Therefore there are large uncertainties in the DFN model developed for the modellers and hence they should feel free to re-evaluate the data or do sensitivity analysis of the models. The uncertainties are estimated to be in the range:

Mean pole 15° (dihedral angle)

$k_r \pm 0.15$

$P_{32} \pm 25$ %

Orientation

A comparison between the 762 poles in tunnel TASK and TASD and the model is shown in Figure 7-18. By visual inspection it is seen that the model produces slightly too many gently dipping fractures striking SW and too few gently to steeply dipping fractures striking NW.

When comparing the model to the data measured in the TASO tunnel the steeply dipping Northwest striking fractures are somewhat underestimated otherwise it looks reasonable, see Figure 7-19.

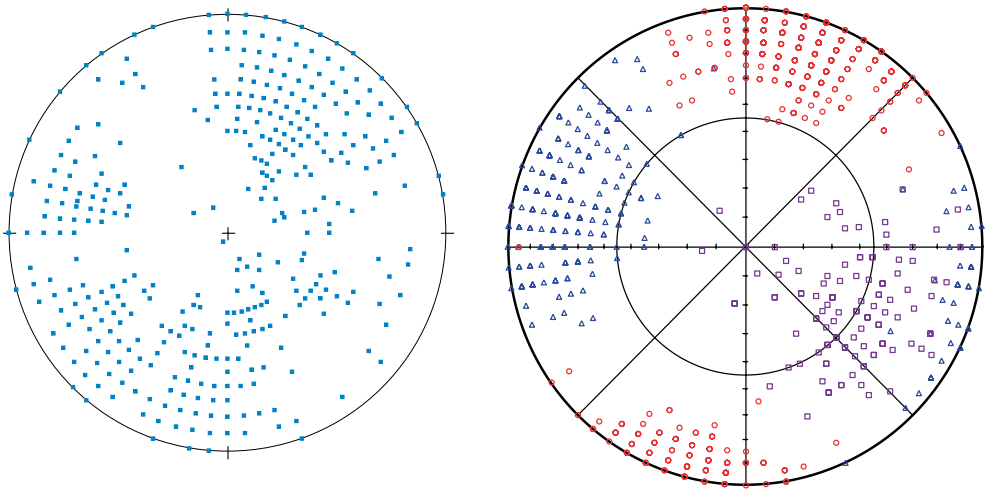

Figure 7-18. *Fracture poles mapped on the floor in the TASK and TASD tunnels to the left and sampled fracture poles along the scanlines in the model. Observe that the simulated fractures have been rounded to the nearest 5° to reflect the measurement.*

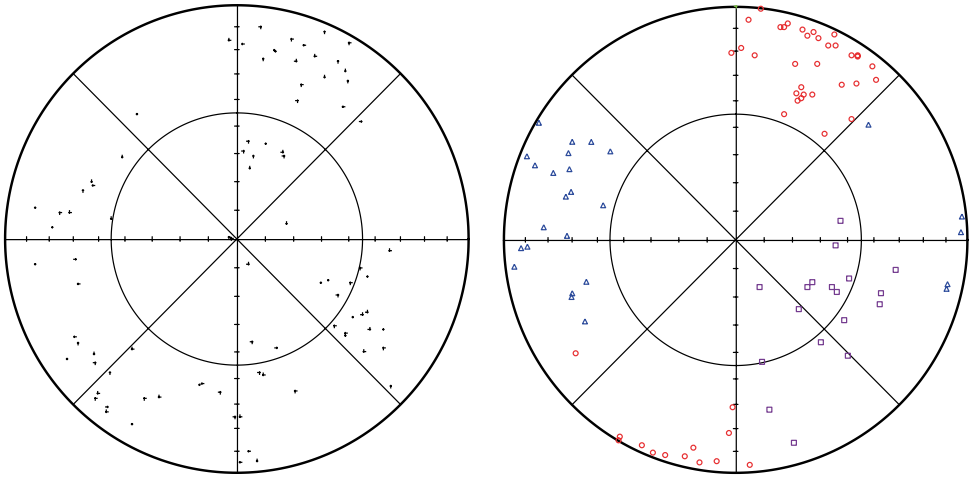

Figure 7-19. *Fracture poles of the mapped fractures in the TASO tunnel to the left and modelled poles to the right.*

Size

The length distribution of the traces intersecting the modelled scanlines should have a slope that equals $-(k_r - 2)$, i.e a slope of −0.6. Figure 7-20 shows the slopes of the two modelled scanlines in the TASD and TASK tunnels. The slope −0.6 is drawn for comparison and one can see on the curvature that the model suffer from edge effects, truncation and that only fractures with r < 25 m.

Intensity

The Fracture model produces 19 FPI, Full tunnel Perimeter Intersections, per 100m tunnel which is in good agreement with the measured values of the TBM tunnel that have 17 FPI/100m tunnel. Therefore the size-intensity model seems to be in the range.

Optional: Generated fracture set

For those whom not have the ability to generate fractures within their assessed codes a delivery of one generated set of fractures are available in the file: Fractures_generated_and_crossing_boreholes.xls.

The fractures in the file are a sub-set of the entire population and represent only the single features that actually are in contact with one borehole, mostly very small fractures. The modelers that choose to use this set may choose different conceptual models to feed water into the fractures. One possible alternative is to extend the fractures out to a uniform and more conductive rock matrix at some distance from the boreholes.

7.3.6 Deterministic fracture information

The setting of the deformation zone wfracture_01 is locally for TASO redefined in the files: TASO_V1-c120914_only_1_fracture.dxf. For visuals and ascii text see the associated .pdf and .xml files respectively. The modeler needs to adjust the large scale wfracture_01 from TASO_V0.1.dxf so that the larger scale structure connects with the local TASO information. The overlapping from the larger scale structure should be removed.

The defined flowing structures in KO0017G001 and KO0018G01 are given in Table 7-8. The Adjusted z-elevation refers to the depth at which estimated fracture plane cross the center axis of the borehole. The extension of the fractures is largely unknown.

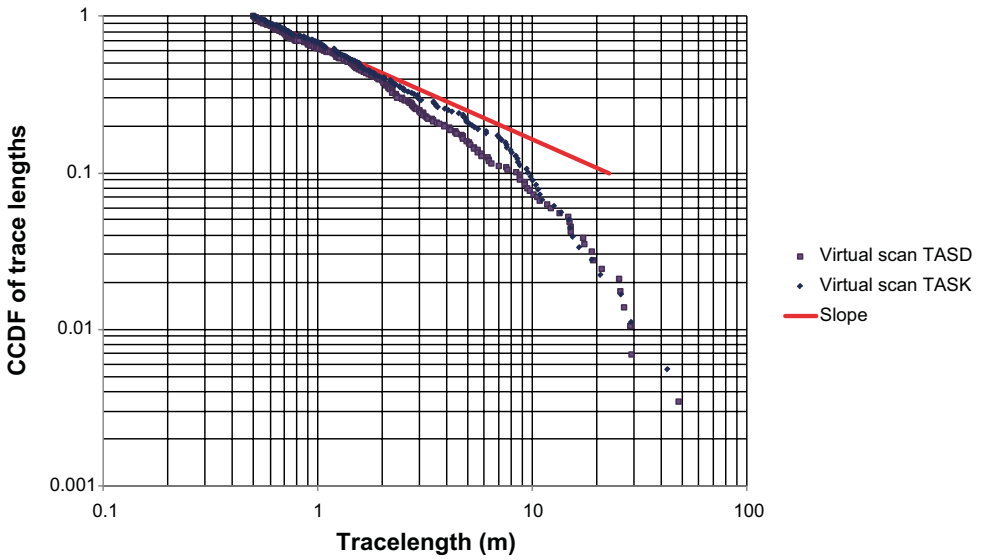

Figure 7-20. *Distribution of fracture trace lengths intersecting the modelled scanlines. The red curve corresponds to a slope of –0.6, i.e. corresponds to a slope of the parent distribution, kr, of 2.6 are modelled. However, it seems to be a reasonable approximation omitting fractures larger than 10 m.*

The fracture in KO0017G01 is not found in the tunnel floor mapping however it is clear from hydraulic responses that the fracture has a good connection with the deformation zone, denoted wfracture_01, however not likely a direct connection.

The fracture in KO0018G01 has not been found to have any good connection with any other observations. The fracture did not supply any water for the first couple of months.

The surface characteristics of the fracture found in KO0017G01 and the fracture found in KO0018G01, respectively are illustrated in Figure 7-21 and Figure 7-22, respectively. For information concerning fracture roughness etc. the modelers are asked to establish a wish-list containing requested data and format. The wish-list will be submitted to the company that has produced the scans.

Table 7-8. Fracture locations in boreholes KO0017G01 and KO0018G01.

Borehole	Diameter (mm)	Adjusted z-elevation (m)	Strike (deg) RT90	Dip (deg) RT90
KO0017G01	300	−420.07	139.5	62.8
KO0018G01	300	−419.58	214.7	54.1

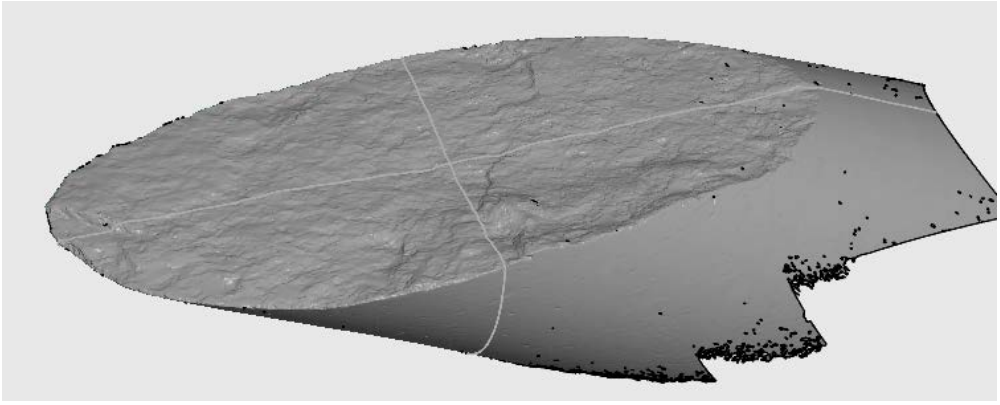

Figure 7-21. *Scanning (optical measurement) of fracture at 2.9 m, 76 mm core, KO0017G01. Fracture described as planar and rough.*

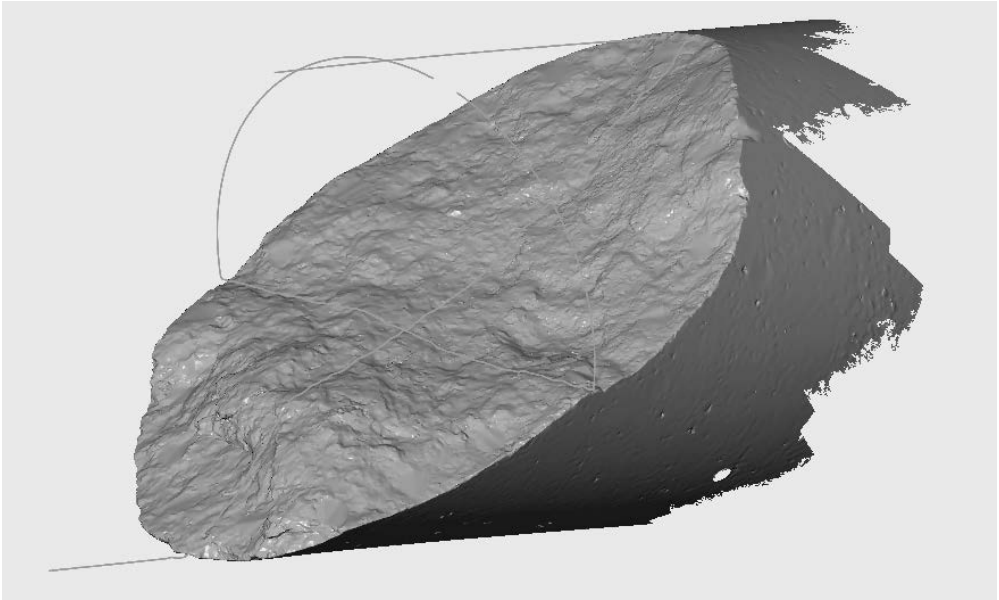

Figure 7-22. *Scanning (optical measurement) of fracture at 2.3 m, 76 mm core, KO0018G01. Fracture described as undulating and rough.*

7.3.7 Rock stresses

In-situ stresses from the near TASQ tunnel are described in Table 7-9. (Andersson 2007):

Table 7-9. In situ stresses from near TASQ tunnel.

	σ_1	σ_2	σ_3
Magnitude (MPa)	30	15	10
Trend (RT 90)	298	–	208
Plunge (from horizontal)	0	90	0

7.3.8 Boundary condition[7]

Pressure[8], salinity and velocities along the x, y, and z coordinates from a specified sub-grid of a DarcyTools v3.3 simulation of the full regional Äspö HRL model (Äspömodel05) are given over an approximate $(100)^3$ m^3 volume incorporating the suggested model domain (Figure 7-4). Data are found in the file: TASO_pressure_salinity_velocities_rev20101123.xls (Figure 7-23).

Modeled equation for salinity-density dependence is: $1\,000(1 + 0.0078 \times S)$.

As a reference case the assigned boundary conditions in tunnels should be at atmospheric conditions.

The associated uncertainty within the boundary conditions is suggested to be treated with one or many sensitivity cases. A recommended alternative boundary condition is an isotropic and homogenous value of −50 metres of fresh water head on all boundary cells/nodes with no contact to the tunnel. For cells/nodes in contact with the tunnel the associated pressure should be addressed as atmospheric.

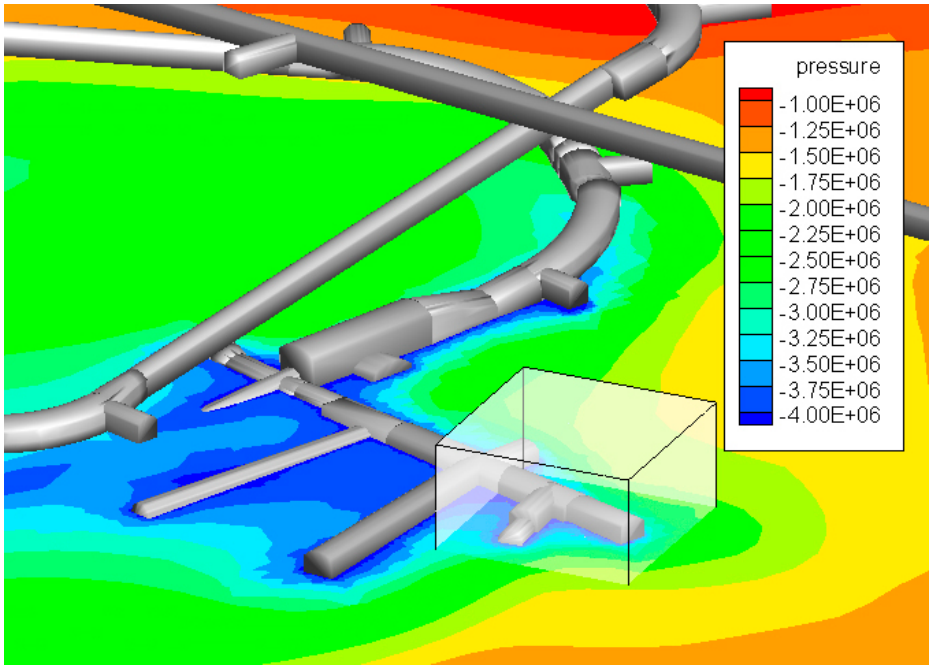

Figure 7-23. *Illustration of the pressure field (Pa), reference elevation is present day shore line (0 altitude).*

[7] The boundary conditions are established from the present official hydro-model of Äspö HRL. The model is (among others) based on the SDM site Laxemar deformation zone model and does due to scale issues contain known location errors. The model may develop during the planned Task 8.

[8] Pressures given are dynamic pressure; absolute pressure could be calculated using $\rho_0 \times g \times z$, with reference altitude at present day shore line (0 altitude).

7.3.9 Initial conditions

The initial conditions for the inflow predictions (Task 8d1) should be based on the "natural" conditions where all probing boreholes are packed off, assuming the packer to seal the upper 1 m of the borehole. For Task 8d2 initial conditions are the results from Task 8d1. With the following near-field clarifications:

Rock:

Resulting pressure field of steady-state conditions simulated based on the set-up but with bedrock-bentonite interface at a constant atmospheric pressure.

Bentonite:

The initial water content of 11.6 % corresponds to an initial degree of saturation of 0.413 for the target void ratio of 0.78 (i.e. after swelling into the outer slot). This saturation degree corresponds to an initial suction value of 70 MPa with the proposed retention curve (P0 = 9.23 MPa, $\lambda = 0.3$).

7.3.10 Material specifications

Rock matrix

Hydraulic conductivity

Laboratory tests on de-stressed matrix core samples (see Figure 7-24) are summariesed in Table 7-10.

Table 7-10. Hydraulic conductivity values from core samples.

Bore hole	Samples	Hydraulic conductivity (m/s)
KO0017G01	Diorite-Pegmatite 1	7.5×10^{-13}
	Diorite-Pegmatite 3	9.0×10^{-13}
	Diorite-Pegmatite 4	5.5×10^{-12}
KO0018G01	Diorite 1	6.0×10^{-14}
	Diorite 3	1.5×10^{-13}
	Diorite 4	1.5×10^{-13}
	Diorite 5	2.5×10^{-13}
	Diorite 7	3.3×10^{-13}

Figure 7-24. *Photo: Diorite-pegmatite (upper core, KO0017G01) and diorite (lower core, KO0018G01).*

Porosity

Laboratory tests indicate that the matrix rock porosity should be between 0.5–1 %. These values compare well with other laboratory tests conducted at Äspö type rock; these earlier tests indicate porosity values close to 0.5 %.

Specific Storage

The specific storage of the matrix is in general unknown. The field tests conducted at Äspö indicate a range between 1E−9 and 1E−6. Typically theoretical values for Äspö type rock points toward approximate 1E−7.

Water retention

Relative humidity RH and associated volumetric water content has been measured for two representative rock matrix core samples. The results are given in Table 7-11 below.

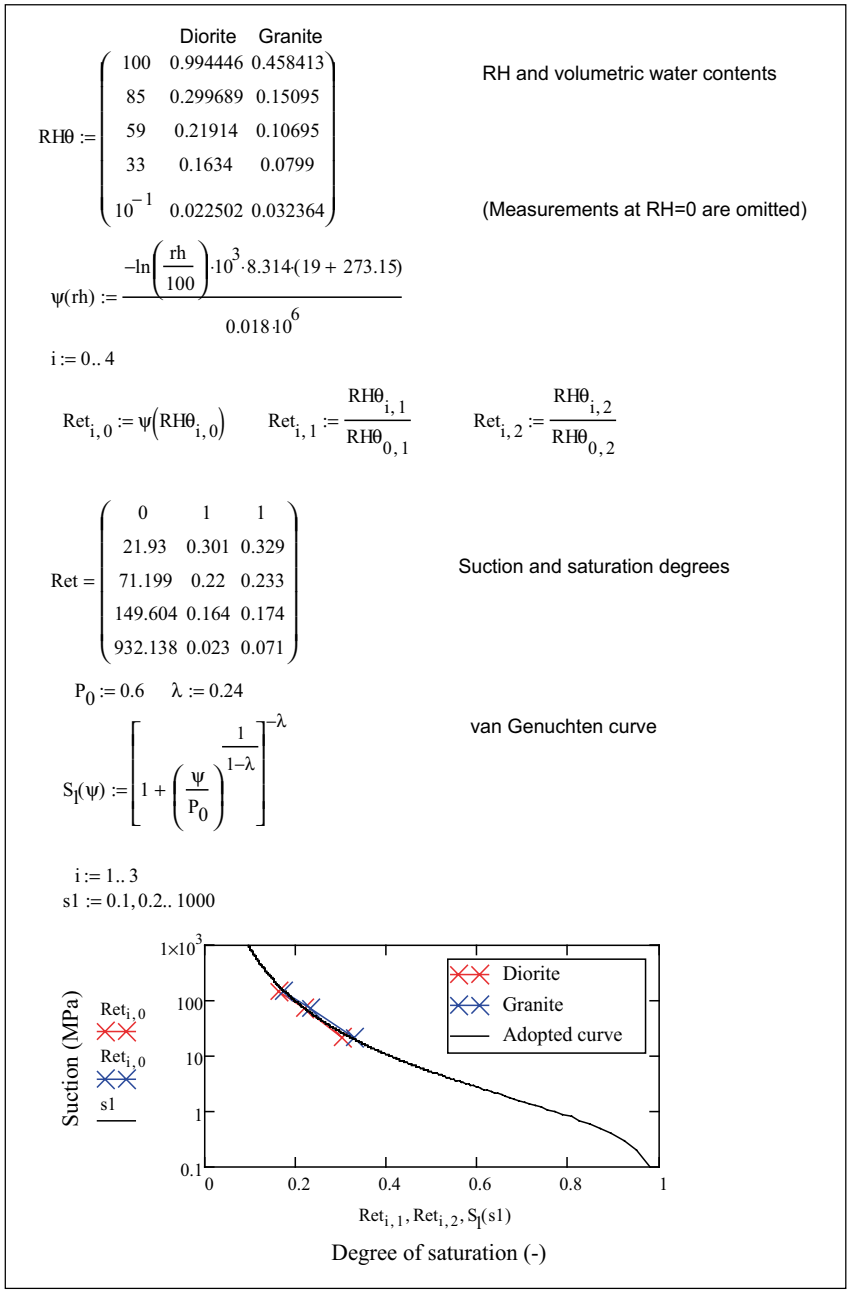

Figure 7-25. *Adoption of water retention curves for matrix core samples.*

These values have been adopted and parameter fitted to a van Genuchten curve (Figure 7-25). The RH values used provide data at relatively low saturations which may not be relevant to the saturation state of the granite close to the bentonite in the models. Therefore although the data is specific to the matrix at BRIE some caution should be used in applying the fitted model parameters to high water saturations. It is suggested that the modellers may wish to use a range of matrix properties incorporating previous literature values and the new site-specific data.

Table 7-11. Results from water retention measurements performed on core samples.

RH (%)	Water content (%)	
	Diorite A1	Granite B1
100 (saturated porosity)	0.99	0.46
85	0.30	0.15
59	0.22	0.11
33	0.16	0.08

Rock fractures

In the two enlarged boreholes only one flowing structure has been identified with certainty in each borehole. The hydraulic characterisation of these fractures gives:

Transmissivity of fracture found in borehole KO0017G01: 5E−11 m^2/s

Specific capacity of fracture found in KO0018G01:

Q (ml/min)	Section (m)	Pressure (bar)	Q/dh (m^2/s)
0.01–0.03	2.1–3.1	10 to 17	1E−12 to 5E−12

The locations of these fractures are given in Table 7-8. No geometric information of the extension of these structures is established.

Deformation zones

Hydraulic tests for transmissivity of the deformation zone denoted wfracture_01 done in borehole, KO0011A01 has been evaluated to 4E−9 m^2/s. A compilation of material properties for three deformation zones is given in Table 7-12.

Table 7-12. Material specifications.

Material	Properties	Value
wfracture_01:	Single plan, geological width*	0.001 m
	Transmissivity	4×10^{-9} m^2/s
	Porosity for porous media descriptions	1×10^{-3}
	Transport aperture for DFN descriptions	1×10^{-5} m
	Storativity	1×10^{-8}
wfracture_02:	Single plan, geological width	0.001 m
	Transmissivity	2×10^{-9} m^2/s
	Porosity for porous media descriptions	1×10^{-3}
	Transport aperture for DFN descriptions	1×10^{-5} m
	Storativity	1×10^{-8}
NNW4:	Geological width	10 m
	Transmissivity	6.5×10^{-7} m^2/s
	Porosity for porous media descriptions	1×10^{-3}
	Transport aperture for DFN descriptions	1×10^{-5} m
	Storativity	1×10^{-7}

* The deformation zone named wfracture_01 is primary located to the west of the defined larger plane at the crossing of TASO. An update for local geometry is distributed as a dxf file within the Task 8d task definition.

“EDZ / shallow fractures”

For KO0017G01 the evaluated fracture transmissivity is similar to the specific capacity based on an injection test. For KO0018G01 the specific capacity tested between the depth 2.1–3.1 m, in the 300 mm borehole is significantly lower (several orders of magnitude) compared to the full length test.

The table over specific capacities can be assessed as a basis when describing the upper part of the borehole (EDZ / shallow fractures / deformation zone).

Borehole specific capacity (injection test) results are given in Table 7-13.

Bentonite

Suggested properties for Bentonite are given in Table 7-14.

Table 7-13. Results from hydraulic tests.

Borehole	Section (m)	Q/dh (m^2/s)
KO0014G01	0.5–3.0	6E−10
KO0015G01	0.75–3.03	1.7E−7
KO0017G01	0.5–2.97	8E−11
KO0018G01	0.55–3.06	4.5E−7
KO0020G01	0.82–3.1	4.2E−10

Table 7-14. Material specifications for bentonite.

Properties	Value
Hydraulic conductivity	6.4×10^{-14} m/s
Porosity	0.44
Specific Storage	2×10^{-6} m^{-1}

7.3.11 Proposed relationships

The proposed relationship for rock/matrix is changed below; for fractures and bentonite the relationships are the same as in Task 8c.

The following relationships are proposed to be used for the relative permeability:

$$k_r = \begin{cases} S^3 & (bentonite) \\ \sqrt{S}\left(1-\left(1-S^{1/\lambda}\right)^{\lambda}\right)^2 & (rock) \end{cases} \quad (7\text{-}3)$$

where S is the degree of saturation (volume of water over total volume of pores).

In addition, the following expression is proposed for the water retention curve:

$$S = \left[1+\left(\frac{P_g - P_l}{P_0}\right)^{\frac{1}{1-\lambda}}\right]^{-\lambda} \quad (7\text{-}4)$$

where P_g is the gas pressure (can be assumed to be atmospheric 0.1 MPa), P_l is the water pressure, and P_0 and λ are empirical constants (Table 7-15).

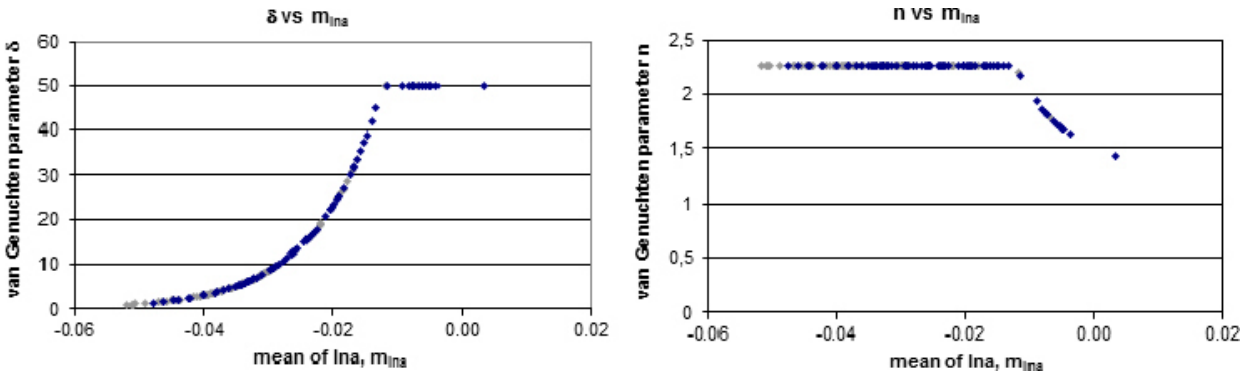

Figure 7-26. *Graphs derived with theory presented by Jarsjö (2009).*

Table 7-15. Parameter values used for water retention curves.

Material	P_0 (MPa)	λ (–)
Bentonite	9.23	0.3
Rock/matrix*	0.6	0.24

* Note that laboratory measurement is presented under properties. The proposed relationship for Task 8a–8c is more related to the Finsterle and Pruess (1995) data while the fitted laboratory measurement is more similar to the Thomas et al. (2003) relationship. Modellers are asked to treat the uncertainty of this new data set in a relevant manner as well as the uncertainty imposed by the different suggested relationships.

For the rock fractures the following relationship should be used (in principal the same as above but in an alternative form; where $\delta = \rho \times g/P_0$ and $n = 1/(1 - \lambda)$).

$$K(h) = K_s \frac{\left(1 - \left(\delta|h|\right)^{n-1}\left(1 + \left(\delta|h|\right)^{n}\right)^{-(1-1/n)}\right)^2}{\left(1 + \left(\delta|h|\right)^{n}\right)^{m(1-1/n)}} \quad \text{for } h<0 \qquad (7\text{-}5)$$

$$K(h)=K_s \quad \text{for } h\geq 0$$

Suggested variation of the parameters is found in Figure 7-26 where the aperture a is given in mm. As a reference case, δ and n should be assigned according to the cubic law hydraulic aperture based on the transmissivity values and $m = 0.5$. An explanation for how to derive van Genuchten parameters (δ and n, or λ and P_0) from a transmissivity value is given in Figure 4-4 and Figure 4-5.

7.4 Calibration targets

7.4.1 Ambient pressure

The z-level for pressure sensors: approx. −415 m.

Compilations of pressures measured in the investigation boreholes are given in Table 7-16 to Table 7-18.

Higher pressure in the lower part of the boreholes (see KO0017G01 below). While drilling, pressure decreases due to the increased hydraulic conductivity (Borehole Damaged Zone, BDZ). Use primarily KO0017G01 and boreholes in wall (11A01, 11B01, 18A01, 18B01).

Table 7-16. Phase 1 of the BRIE experiment, Floor, 2010-12.

Borehole	Section (m)	Pressure (bar)
KO0017G01	0.5–2.97	9–10
KO0017G01	2.0–2.97	17

Table 7-17. Phase 2 of the BRIE experiment, Floor, (lower part of boreholes), 2011-09.

Borehole	Section (m)	Pressure (bar)
KO0015G01	2.1–3.03	5
KO0017G01	2.11–2.97	5
KO0018G01	1.42–3.06	4
KO0020G04	2.0–3.5	10.5
KO0020G03	2.0–3.5	9

Table 7-18. Phase 2 of the BRIE experiment, Wall, 2011-09.

Borehole	Section (m)	Pressure (bar)
KO0011A01	1.01^{-10}	27
KO0011B01	1.24^{-10}	3
KO0018A01	1.11^{-10}	26
KO0018B01	1.28^{-10}	21

The pressure in KO0011A01 is slowly declining as of present it reads 25 bars.

7.4.2 Inflow to TASO

Scoping calculation of inflow based on pressure-distance data indicate the inflow to the TASO tunnel to 0.5 l/min.

Based on a water collection test (sorbing mats, see Figure 7-27) the inflow was estimated to 0.1 L/min. Table 7-19 and Figure 7-27 give an idea about the distribution of inflows (first column data located primarily by the deformation zone). The sorbing mats were placed by visual inspection where inflow occurred, i.e. no sorbing mats means no inflow.

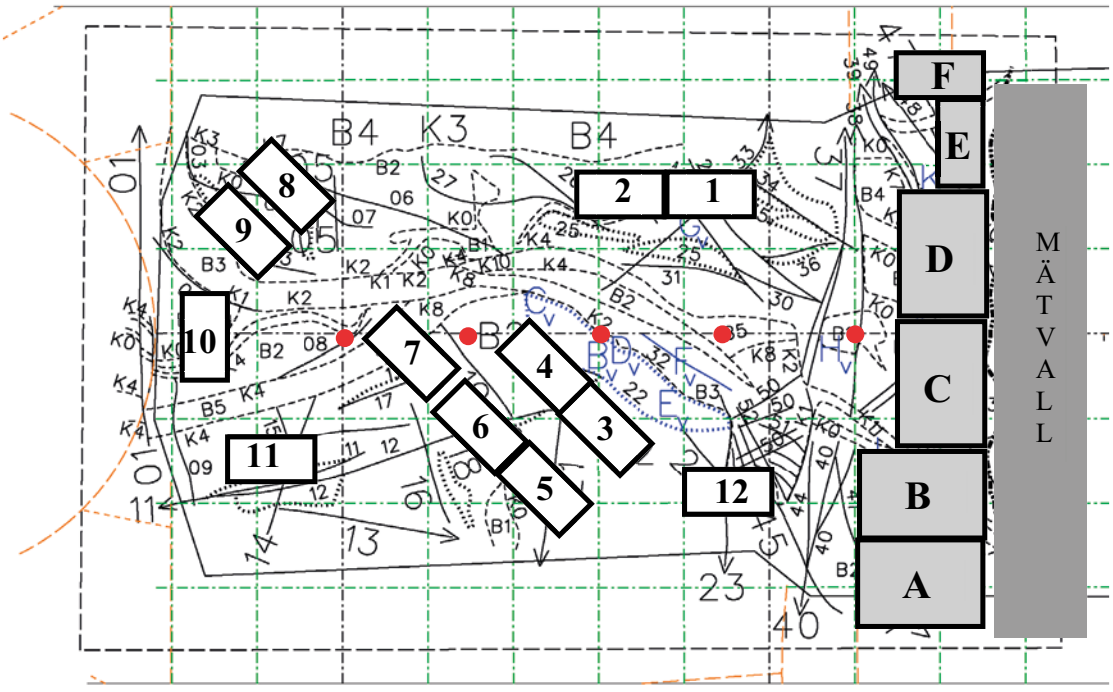

Figure 7-27. *Approximate location of sorbing mats. MÄTVALL = measurement weir.*

Table 7-19. Distribution of inflows using sorbing mats.

Mat no. (Def. zone)	Q (ml/min)	Mat no. (HRD)	Q (ml/min)
A	128	3	8
B	7	4	< 1
C	57	5	1
D	3	6	8
E	< 1	7	1
F	< 1	8	< 1
		9	< 1
12	1	10	2
1	1	11	1
2	2		

7.4.3 Inflow boreholes

Inflows from short duration tests differ from the long duration (see e.g. for KO0017G01 in Table 7-20 and in Figure 7-29). Table 7-20 presents inflows at approximately 15 minutes following opening of the boreholes.

Table 7-20. Phase 2, Floor, ID9 (duration approximately 15 min), 2011-09.

Borehole	Sec up (m)	Sec low (m)	Section length (m)	Q (ml/min)
KO0014G01	1.33	3.0	1.67	0.1
KO0015G01	2.1	3.03	0.93	0.6
KO0017G01	2.11	2.97	0.86	1
KO0018G01	1.42	3.06	1.64	0
KO0020G01	1	3.1	2.1	0.01

7.4.4 Pressure responses and flow

Constant pressure tests (flow and recovery) were performed in e.g. KO0017G01 (floor, 76 mm) and KO0011AO1 (left wall, intersecting deformation zone, 76 mm, see Figure 7-7). Flow and pressure response data for KO0017G01 and KO0011A01 are found in Figure 7-28 to Figure 7-31 and files: Phase 1 ID11 KO0017G01 flow_during_test_org_121003.xls, Phase 1 ID11 KO0017G01_105079_ ID11_ Inflödestest_121003.xls, Phase 2 ID05 KO0011A01_inflow_to_tunnel_121003.xls and Phase 2 ID05 KO0011A01_Pressure_Wall_121003.xls (see Table 7-21).

Table 7-21. Summary of files referred to in this section.

Excel file	Content
Phase 1 ID11 KO0017G01 flow_during_test_org_121003.xls	Flow
Phase 1 ID11 KO0017G01_105079_ID11_ Inflödestest_121003.xls	Pressure
Phase 2 ID05 KO0011A01_inflow_to_tunnel_121003.xls	Flow
Phase 2 ID05 KO0011A01_Pressure_Wall_121003.xls	Pressure

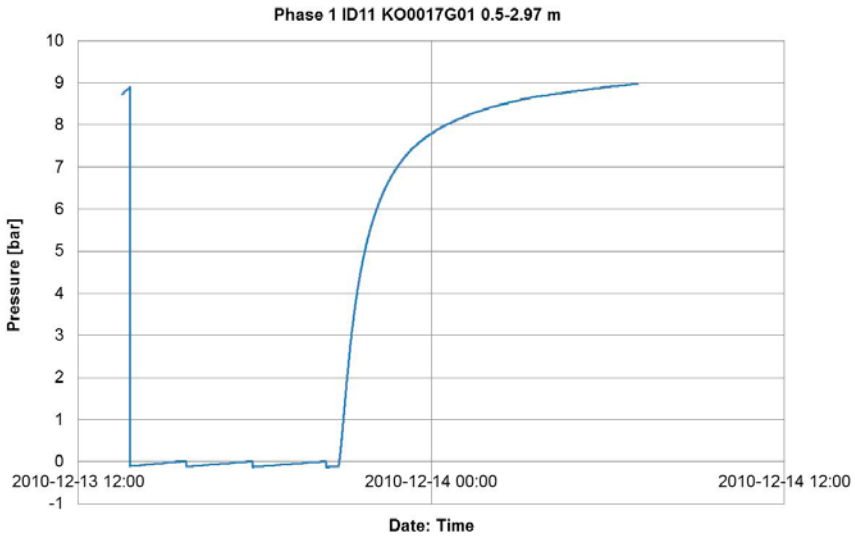

Figure 7-28. *Pressure, KO0017A01 0.5–2.97 m, 76 mm, 2010-12.*

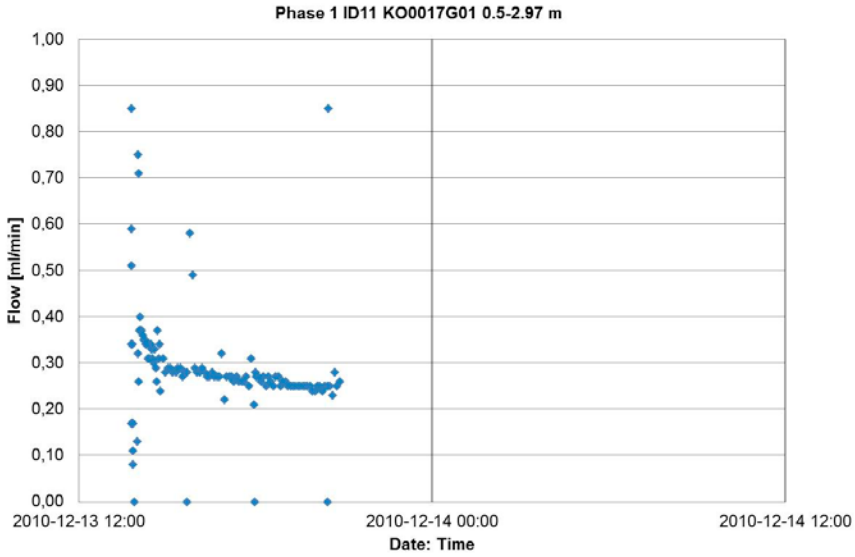

Figure 7-29. *Flow, KO0017G01 0.5–2.97 m, 76 mm, 2010-12. Flow in ml/min.*

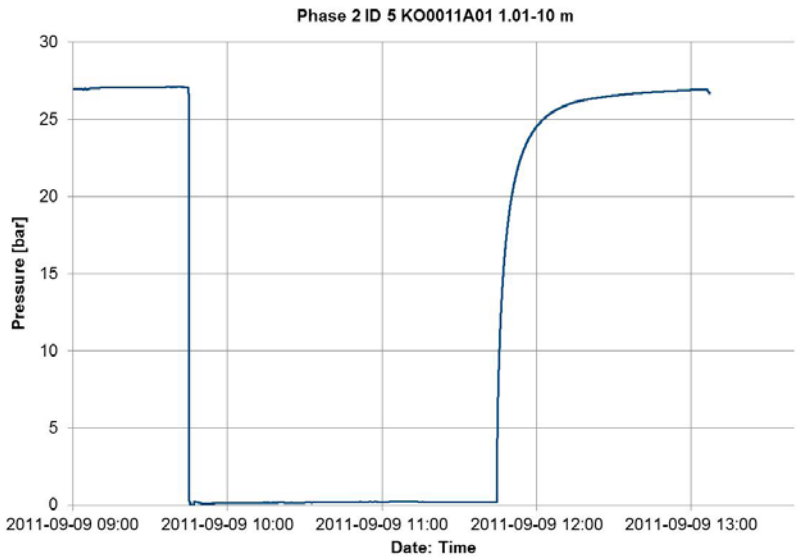

Figure 7-30. *Pressure, KO0011A01 1.01–10 m, intersecting deformation zone, 2011-09.*

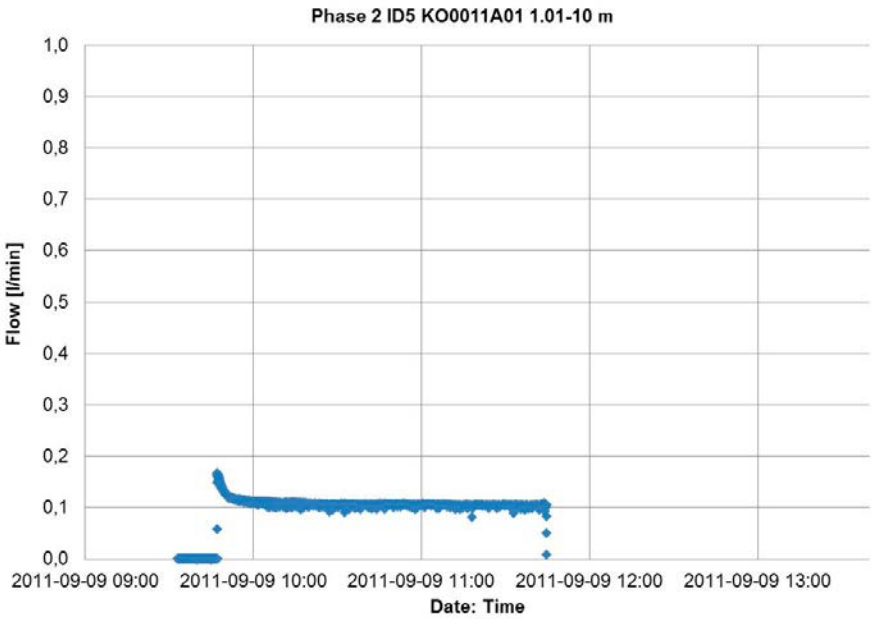

Figure 7-31. *Flow, KO0011A01 1.01–10 m, 2011-09, intersecting deformation zone. Flow in l/min.*

7.4.5 Inflow to 30 cm boreholes

Amount

Table 7-22 presents inflow data for KO0017G01 (76 mm, PFL, 300 mm and nappy test) and KO0018G01 (only 300 mm, observations indicate hydro-mechanically induced changes).

Table 7-22. Flow data for KO0017G01 (76 mm, PFL, 300 mm and nappy test) and KO0018G01.

Measurement	KO0017G01	KO0018G01
Flow (76 mm) borehole	0.25 ml/min (0.5–2.97 m, ~ 400 min) Phase 1 (see Figure 7-29 above)	–
Flow PFL	~ 0.5 ml/min (< 30 ml/h or 0.5 ml/min, uncertain)	–
Flow (300 mm) borehole	0.12 to 0.25 ml/min (2.1–3.5 m, ~400 min) Phase 3	0.01–0.03 ml/min (2.1–3.1 m, ~ 400 min) Phase 3
Flow “nappy test”	~ 0.1 ml/min Possibly water is entering in the lower part of the borehole (along pegmatite vein, see Table 7-23).	–

Pattern

An inflow characteristic test, a nappy test, was conducted on the walls of the extended KO0017G01. Figure 7-32 shows inflow for individual “nappies” in ml/min (total number of nappies: 5 rows, 2.25–3.25 m, and 15 columns,$0.3 \times \pi$ m). An approximate background value based on the first row data (2.25–2.45 m, dry section) is subtracted. Main inflows are found at approximately 2.45–2.65 m and N to NE (see photo, Figure 7-33, and BIPS-image, Figure 7-34). Inflows are also identified in the lower section of the borehole (3.25 m to 3.5 m), see a possible compilation of data from different tests in Table 7-23.

The following features of KO0017G01 may need to be considered:

- Fracture at 2.9 m (wet part in figure).
- Pegmatite vein (seen in figure, also wet) may be the reason for high pressures at the bottom of borehole KO0017G01. No detailed information on this feature is available at present.

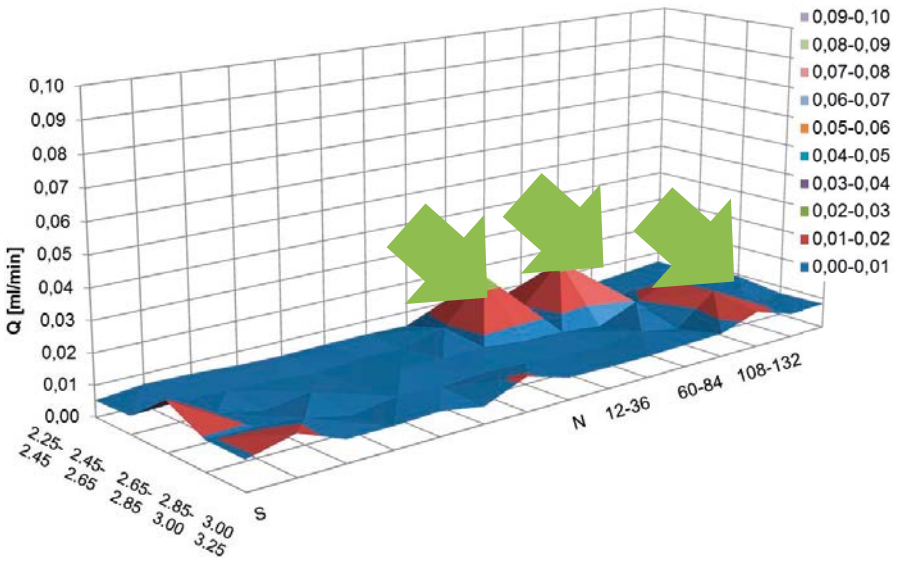

Figure 7-32. *Inflow for individual "nappies" in ml/min (total number of nappies: 5 rows, 2.25–3.25 m, and 15 columns, 0.3 × π m). Main inflows at approx. 2.45–2.65 m and N to NE (see photo and BIPS-image).*

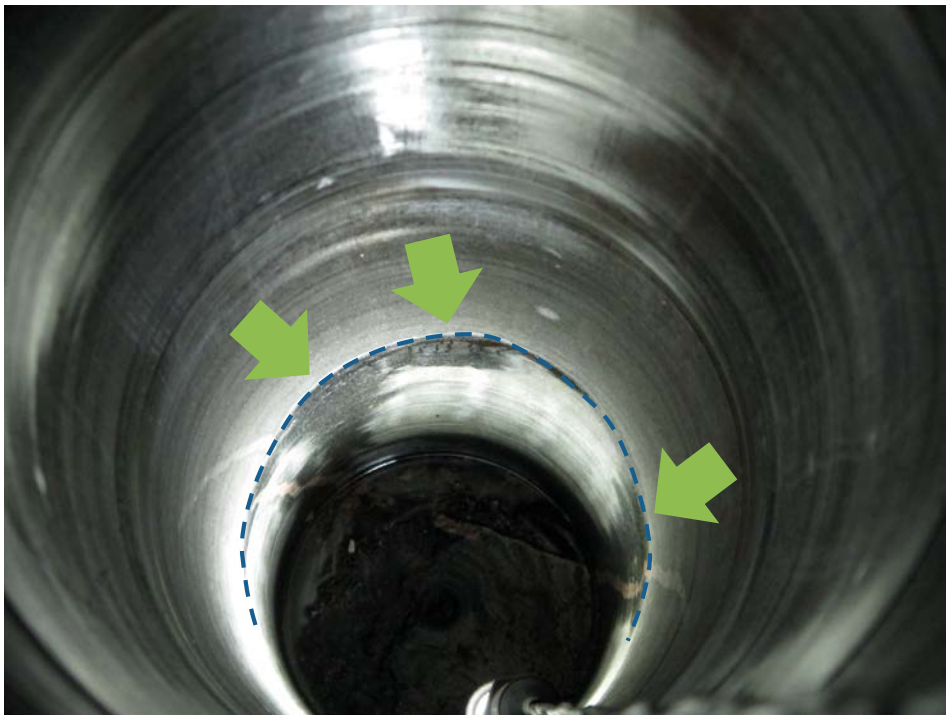

Figure 7-33. *Location of inflows along fracture at 2.9 m in KO0017G01. See also the pegmatite vein that may conduct water.*

A suggested distribution of inflow below 2.1 meter is shown in Table 7-23. Green (major inflows identified in photo) and yellow (uncertain) represents results from nappy test (higher value in italics includes back-ground value). Right hand side of figure shows results from section hydraulic tests (to identify flow in lower part of the borehole). In the middle, an approximate distribution if compiling information is presented.

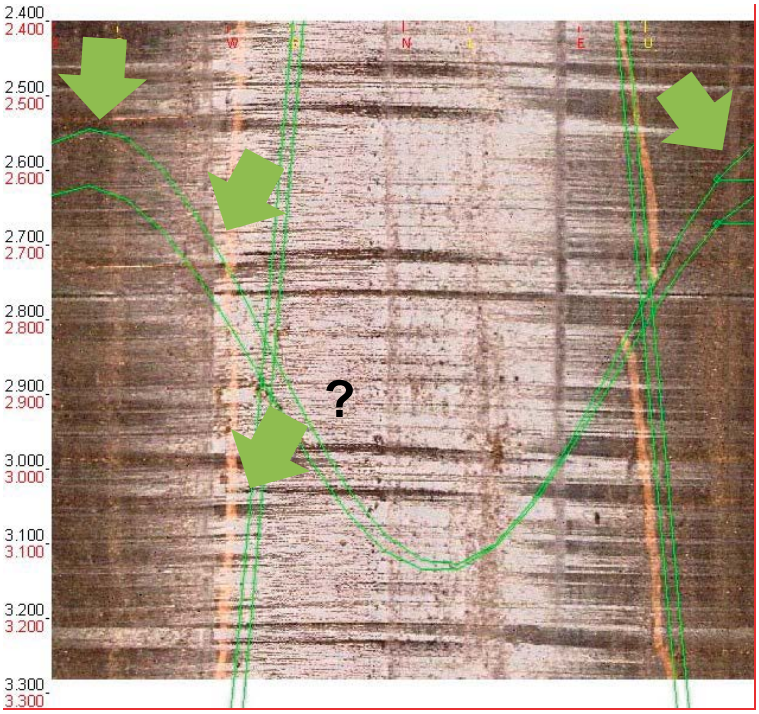

Figure 7-34. *BIPS-image from KO0017G01. Main inflows at approximately 2.45–2.65 m. Possibly flow along the pegmatite vein.*

Table 7-23. A suggested distribution of inflow below 2.1 meter in KO0017G01, 300 mm, based on nappy test and inflow tests.

Depth [m]	Nappy [ml/min]		Possible distribution		Inflow sections [ml/min]		
2.1							
2.15				0	**0.12**		
2.2				**0.05**	**0.25**		
2.25							
2.3							
2.35	0	0					
2.4	*0*	*0*					
2.45							
2.5							
2.55	0.018	0.017	0.05				
2.6	*0.024*	*0.023*					
2.65							
2.7							
2.75	0.009	0.01					
2.8	*0.014*	*0.016*					
2.85							
2.9							
2.95	0.009						
3	*0.015*			0.05		**0.13**	
3.05				**0.13**		**0.2**	
3.1							
3.15	0.006	0.014	0.05				
3.2	*0.012*	*0.024*					
3.25							
3.3							
3.35			0.05				
3.4							
3.45							
3.5			0.05	**0.07**			**0.06-0.08**

7.5 Modelling tasks

The modelling task is divided into four major parts:

- Develop a revised model of the site. Using the new borehole information on inflow and build-up pressures, given above, and the inflow measurement within probing boreholes as well as the two 30 cm boreholes. The calculated inflow to the 76 mm borehole should be compared with the calculated inflow to the 30 cm borehole. Differences should be discussed and explained and the results should be compared with the field data given above. During the simulations all boreholes should be assumed completely packed-off except for the time of an inflow/outflow measurement when only one borehole is opened for a time. The packer should be assumed to seal off the upper 1 metre of the borehole.
- Conditioned from the results of the first part, the second part contains the expansion of boreholes KO0017G01 and KO0018G01 to a diameter of 30 cm. The amount and location of inflow to the "two 30 cm boreholes" should be predicted.
- With initial conditions from the second part, this, the third part, contains the wetting of bentonite placed within the 30 cm boreholes, KO0017G01 and KO0018G01. The wetting of the bentonite (wetting pattern/saturation distribution with time) along with associated pressure development within the bentonite and the near-field bedrock should be predicted.
- The results of the wetting, time development and spatial pattern should be compared to the results derived in task 8c, details are specified below.

7.6 Expected outcome

The expected outcome as described below should be provided for each model realisation or variant in order to meet to the objectives.

Results for Task 8d1:

Contour plots of the borehole near-field, permeability structure (in m^2), pressures (in Pa) and Darcy fluxes (in m/s) on one vertical cross-section incorporating all five original probing borehole starting at the TASO tunnel entrance and ending at the TASO tunnel front and on one horizontal cross-section incorporating all five probing borehole starting at the TASO tunnel entrance and ending at the TASO tunnel front and cutting through at the depth of 1.5 metres. The horizontal cross-section should capture the entire tunnel width and reach out at least 2 metres at each side; the vertical cross-section should capture the rock from the tunnel floor and at least 6 metres downward. Plots should be comparable to those produced in Task 8c.

Contour plots of the inflows (in m^3/s over a defined unit area, eg. cell size etc.) presented as folded up illustrations of the walls of the "30 cm boreholes" KO0017G01 and KO0018G01. Plots should be comparable to those produced in Task 8c.

Numbers of inflow (in m^3/s) to the entire part of first the 76 mm boreholes and then the "30 cm boreholes" KO0017G01 and KO0018G01. Again plots to be comparable to those from Task 8c.

Results are expected for steady-state conditions.

Results for Task 8d2:

Contour plots of the deposition hole near-field pressures and saturation[9] in bentonite as well as the bedrock for time steps at 0, 0.1, 0.5, 1.0, 10, 100 years on one vertical cross-section incorporating both deposition holes and parallel with the TASO tunnel central line and one horizontal cross-section incorporating both deposition holes and cutting through at the depth of 1.5 metres. Plots should be comparable to those produced in Task 8c.

[9] Or alternative equivalent measure of change in the bentonite due to inflow of water from the bedrock, eg. RH or suction.

The contour plots should present the geometric situation of the deposition holes in detail (tunnel floor and 5 metres down). The colour scale of the contour plots should be: 1.5, 1, 0.5, 0.2, 0.1, 0, −0.1, −0.2, −0.5, −1, −5, −10, −20, −50 MPa. Graphs showing illustrations of the pressure increase within the bentonite at a position 0.01, 0.05, 0.1, 0.15 metres from the different deposition holes walls. These graphs should come as six: one for each of the deposition holes (KO0017G01 and KO0018G01) at 1.5 metres depth, at 0.75 metres down the hole, and at 2.25 metres down the hole. Plots should be comparable to those produced in Task 8c.

Graphs illustrating the pressure change within the bedrock at a position 0.01, 0.05, 0.1, 0.15, 1, 5 metres from the two 30 cm borehole walls in the direction towards the other deposition hole are requested. These graphs should also come as three for the same depth positions as described above. Assess these requested plots same as in Task 8c.

Evolution of RH and pore pressure at sensor positions (see Table 7-5) for the period of 0 to 250 days counting from installation.

Horizontal saturation contour plots for the specified depths given in Table 7-24 below (corresponding to instrumented bentonite blocks) for times: 100, 150, 175, 200, 225 and 250 days. These plots may be used to support decisions on the optimal dismantling time for BRIE.

Table 7-24. Depths for requested saturation contour plots.

Hole 17	Hole 18
−419.506	−419.579
−419.606	−419.679
−419.809	−419.983
−419.909	−420.083
−420.618	

Reporting

It is likely that Task8d is the final part of Task 8 to directly address the BRIE experiment. Task 8e will probably focus on larger scale aspects of bentonite buffer saturation. It is therefore intended that the reporting from 8d should contain a summary of all tasks 8a–8d and should document the role numerical modelling plays (a) to improve our understanding of the interaction between engineered and natural barriers, (b) to support the design and analysis of the BRIE experiment, and (c) as a screening tool to evaluate the performance of deposition holes.

The report should provide some background; briefly discuss objectives, scope, overall approach, model setup, simulation results, interpretation, conclusions and recommendations. Details about the specific analyses can be included in appendices to the main report.

While the content of the report should be flexibly adapted to match the actual analyses performed, the following specific questions should be addressed:

Quantitative results:

(1) What is the range of predicted inflows into an open deposition hole?

(2) What is the range of predicted times needed to rewet the bentonite to a saturation of 95 %?

Qualitative discussion:

(3) What are the key features and properties of the natural and engineered systems that need to be known for deposition hole screening?

(4) What information and data from the BRIE experiment are most valuable for (a) overall system understanding, and (b) model development?

(5) How does the conceptualization of the natural and engineered systems influence (a) quantitative model predictions, and (b) interpretation of the expected system behaviour?

8 Water uptake test

8.1 Introduction

The Bentonite Rock Interaction Experiment (BRIE) is a field experiment which addresses the hydraulic interaction between the system components of compacted bentonite and the near-field host rock. This experiment is a joint modeling task (Task 8) of the SKB Task forces on Engineered Barrier Systems (EBS) and on Groundwater Flow and Transport of Solutes (GWFTS). The BRIE water-uptake test was a laboratory test with the objective to provide data from an experiment with radial water-uptake, which would give a clear-cut description of the hydraulic processes in the bentonite in the BRIE field experiment. In addition, it would also be a contribution to the validation of the material model. These tests have previously been described in detail by Fransson et al. (2017). This report presents: i) a hydraulic evaluation of the water-uptake tests; and ii) a task description of the water-uptake tests intended to be included as a modeling task within Task 8.

The hydraulic evaluation consists of: i) the optimization of two saturation dependent moisture diffusivity functions, which were either based on the water-uptake data (i.e. inflows) or on the water saturation data (measured after dismantling); ii) the adoption of two in-situ retention curves (van Genuchten and square law type), which were based on initial and final data from RH sensors and measured degrees of saturation; and iii) the evaluation of saturation-dependent permeability functions from the diffusivity functions and retention curves. Results from 1D axisymmetric Code_ Bright models (four cases with different parameter value combinations) are finally presented and compared with experimental data, and one of these cases is described as a task for Task 8.

8.2 Hydraulic evaluation of BRIE water-uptake test

8.2.1 Water balance

A water balance of the water-uptake tests (Test 1 and Test 2) is illustrated in Figure 8-1. The lower bars represent water masses determined from data on water content, density, and volumes; the mean initial mass as well as the final masses for Test 2 and Test 1, respectively. The upper bars represent the total water-uptake in Test 2 and Test 1, respectively. The water-uptake masses are added to the initial mass, except for the filter volume which was subtracted. Some fraction of the filter water may have been absorbed by the bentonite during the dismantling and should therefore not be subtracted. This was however neglected, since the calculated final masses were based on the confining volume of the equipment (cylinder and lids), which implies a minor underestimation of the final masses.

A comparison of the right ends of the bars shows the largest discrepancy for water mass in T2 (0.12 kg). One explanation for this could be an elastic expansion during the dismantling of the tests, which would imply that the measured dry density values, and therefore also the evaluated saturation degree values were slightly underestimated. Another explanation for the discrepancy may be that water was lost from the water supply reservoirs during the test period. The evaporated mass was however measured with a reference reservoir, and was found to be ~ 0.03 kg and therefore neglected from the water balance. Still, the observed discrepancy illustrates that different experimental data sets can imply different values of the water transport coefficients.

8.2.2 Tool for water-uptake calculations in terms of moisture diffusivity

In order to have an efficient and transparent tool for evaluating the water-uptake a MathCad algorithm has been prepared, in which the water transport is described by a saturation-dependent moisture diffusivity function D(S), and in which the diffusion equation is solved with an explicit finite-difference method.

The 1D radial geometry of the water-uptake tests are discretized in n elements according to Figure 8-2 (left). The index *i*, with values between 0 and n-1, denote the element. The radial width of each element is $\Delta r = (R_{out} - R_{in})/(n-1)$, except for the inner and outer elements which have half this width. The numerical scheme used to calculate the saturation profile for a point in time, with index *j*, is illustrated in Figure 8-2 (right). The time step between two successive point in time is denoted Δt.

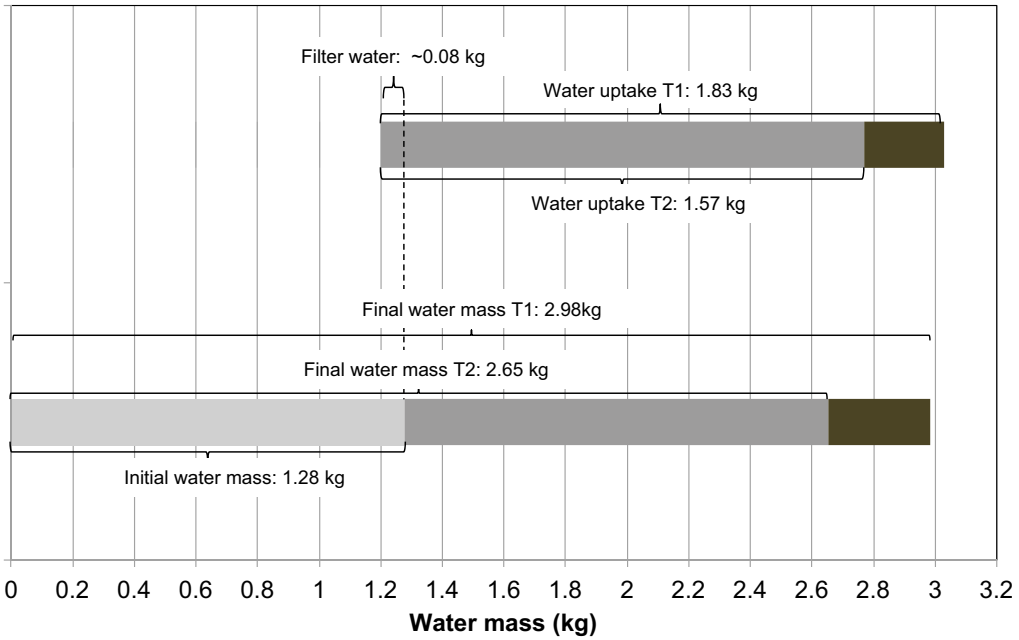

Figure 8-1. *Water balance for Test 1 and Test 2. Upper bar based on inflow data. Lower bar based on data on water content, density and volumes.*

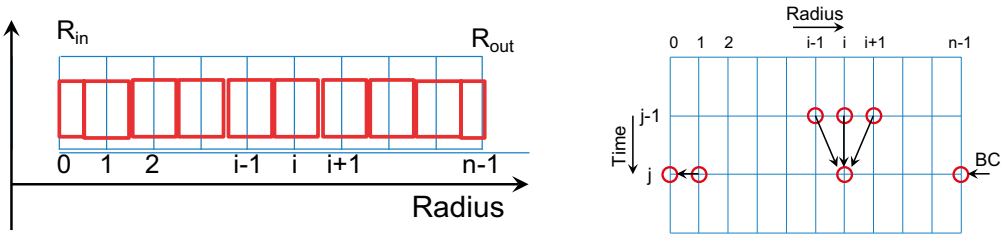

Figure 8-2. *Discretization of geometry in n elements with index i, shown as red boxes (left). Numerical scheme used to update the saturation profile (right). Points in time are denoted with index j.*

The diffusion equation for radial diffusion can be developed in the following four terms:

$$\frac{\partial S}{\partial t} = \frac{1}{r}\cdot\frac{\partial}{\partial r}\left(rD\frac{\partial S}{\partial r}\right) = D\frac{\partial^2 S}{\partial r^2} + \frac{D}{r}\cdot\frac{\partial S}{\partial r} + \frac{\partial D}{\partial r}\cdot\frac{\partial S}{\partial r} \tag{8-1}$$

These terms with partial derivatives are estimated with the following corresponding finite differences:

$$\begin{cases} \dfrac{\partial S}{\partial t} & \approx & \dfrac{S_{j,i} - S_{j-1,i}}{\Delta t} \\ D\dfrac{\partial^2 S}{\partial r^2} & \approx & D(S_{j-1,i})\cdot\dfrac{S_{j-1,i+1} - 2S_{j-1,i} + S_{j-1,i-1}}{\Delta r^2} \\ \dfrac{D}{r}\cdot\dfrac{\partial S}{\partial r} & \approx & \dfrac{D(S_{j-1,i})}{R_{in} + i\cdot\Delta r}\cdot\dfrac{S_{j-1,i+1} - S_{j-1,i-1}}{2\cdot\Delta r} \\ \dfrac{\partial D}{\partial r}\cdot\dfrac{\partial S}{\partial r} & \approx & \dfrac{D(S_{j-1,i+1}) - D(S_{j-1,i-1})}{2\cdot\Delta r}\cdot\dfrac{S_{j-1,i+1} - S_{j-1,i-1}}{2\cdot\Delta r} \end{cases} \tag{8-2}$$

Note that the radius of element *i* is expressed as $R_{in}+i\times\Delta r$. For convenience, the following constant is defined:

$$R = \frac{\Delta t}{\Delta r^2} \tag{8-3}$$

Based on Equations (8-1) to (8-3), the following expressions can be derived for the saturation degree in all elements, except for the inner and outer elements:

$$\begin{aligned} S_{j,i} = \; & S_{j-1,i} + R \cdot D(S_{j-1,i}) \cdot \left[S_{j-1,i+1} - 2S_{j-1,i} + S_{j-1,i-1}\right] \\ & + \frac{\Delta t}{2\Delta r} \frac{D(S_{j-1,i})}{R_{in} + i \cdot \Delta r} \cdot \left[S_{j-1,i+1} - S_{j-1,i-1}\right] \\ & + \frac{R}{4}\left[D(S_{j-1,i+1}) - D(S_{j-1,i-1})\right] \cdot \left[S_{j-1,i+1} - S_{j-1,i-1}\right] \end{aligned} \tag{8-4}$$

The saturation degree of the inner element is the same as for the adjacent element ($S_{j,0} = S_{j,1}$), and for the outer element this is given as a boundary condition, which is full saturation ($S_{j,n-1} = 1$).

A function describing the moisture diffusivity was defined with two parameters: D_0, which describes the level of the diffusivity half way between initial and final saturation value (S_{mid}), and k, which describes the influence of the saturation (Figure 8-3):

$$D(S) = D_0 \cdot \left(\frac{S}{S_{mid}}\right)^k \tag{8-5}$$

These two parameters are defined as input to the algorithm for the water-uptake calculations. The output from the same algorithm is the saturation profiles and the water-uptake.

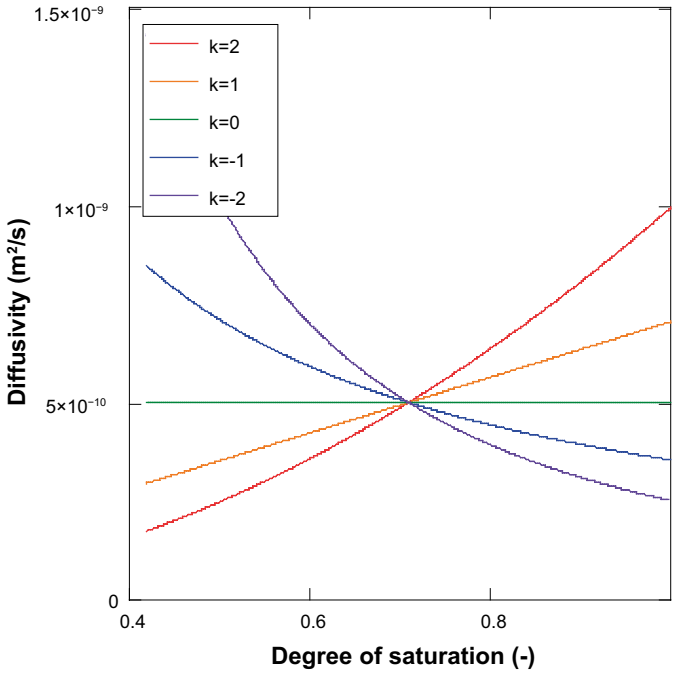

Figure 8-3. *Moisture diffusivity function. Influence of the parameter k.*

The following parameters and geometries have been defined for the water-uptake tests:

- Inner radius: 0.02 m.
- Outer radius 0.15 m; i.e. a homogenized description of the bentonite.
- Height: 0.1 m.
- Porosity: 0.44; based on a block dry density of 1 587 kg/m^3 and a radial swelling from 0.149 to 0.15 m.
- Initial saturation: 0.42; based on a water content of 11.75 %.
- Number of element: 14; If the outer element is kept saturated from the start, this implies that the initially added volume of water in the model corresponds to the volume of the slot immediately filled at the start, i.e. 0.20–0.08 (in filter) = 0.12 liter.
- Number of time steps: 10 000.

The MathCad algorithm for the water-uptake and the corresponding result may be seen in Figure 8-13 and Figure 8-14 at the end of this chapter.

8.2.3 Optimization of moisture diffusivity functions

The moisture diffusivity function was optimized through: i) calculating the error between the model results and the experimental data for a specific set of parameters D_0 and k; and ii) by performing a parameter analysis of the influence of parameters D_0 and k. A parameter set which yields a minimum error was considered to be optimized. Due to the discrepancy of the water balance as noted in section 0, this analysis was performed in two different ways.

In the first analysis, the model was compared with water-uptake data. Cumulative volumes from Test 1 (V_{T1}) for 17 points in time (t_i) were compared with corresponding volumes from the model (V_{model}). The points in time when the test volume reached the values of 0.2, 0.3 … up to 1.8 liters were selected. The error was calculated with the following expression:

$$\log\left(\sum_{i=0}^{16}\left[V_{T1}(t_i)-V_{\text{model}}(t_i)\right]^2\right) \tag{8-6}$$

Note that the filter volume of 0.08 liters was added to the V_{model} values. The result from the parameter analysis of the error is shown in Figure 8-4 (left), and a minimum can be identified for the parameter set: $D_0 = 5.5 \times 10^{-10}$ m^2/s and k = 0.

In the second analysis, the model was compared with water saturation data. Measured saturation degree values from innermost sample positions in Test 2 and Test 1 (i.e. 68 and 91 % respectively), were compared with the corresponding saturation values in the inner element of the model (S_{model}) after 107 and 203 days, respectively. The error was calculated with the following expression:

$$\log\left(\left[S_{\text{model}}^{i=0}(t=107d)-0.68\right]^2+\left[S_{\text{model}}^{i=0}(t=203d)-0.91\right]^2\right) \tag{8-7}$$

The result from the parameter analysis of the error is shown in Figure 8-4 (right), and a minimum can be identified for the parameter set: $D_0 = 3.7 \times 10^{-10}$ m^2/s and k = 1.2.

Model results for the optimized parameter sets regarding: i) water-uptake and, ii) saturation profiles for day 107 and 203, are shown together with experimental results in Figure 8-5. As expected, the agreement with the water-uptake curve is best for the first parameters set, whereas for the saturation profiles the agreement is best for the second parameters set.

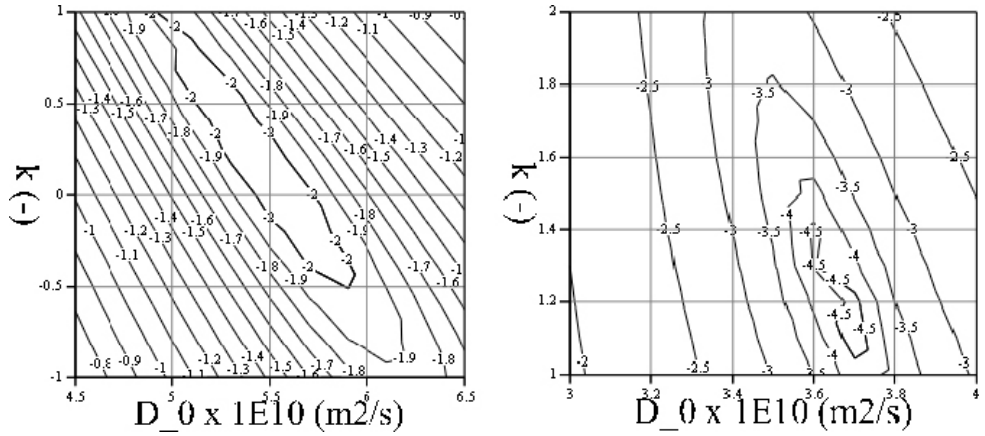

Figure 8-4. *Log sum of squared error as a function of the parameter D_0 and k. Left graph shows results for comparison with water-uptake curve. Right graph shows results for comparison with degree of satutation at inner points at day 107 and 203.*

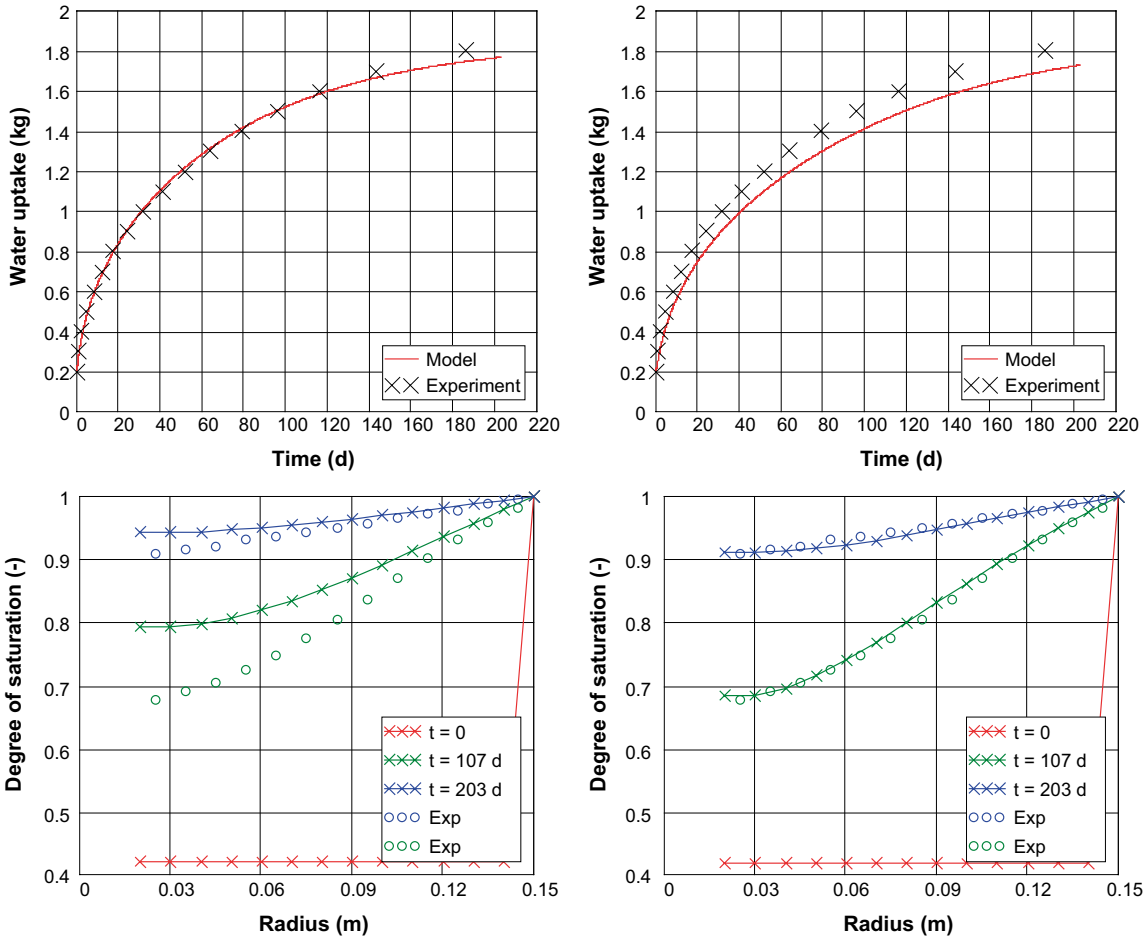

Figure 8-5. *Model results for optimized diffusivity function: $D_0 = 5.5105 \times 10^{-10}$; k = 0 (left graphs); $D_0 = 3.7 \times 10^{-10}$; k = 1.2 (right graphs).*

8.2.4 Parameter value adoption

An optimized moisture diffusivity function can, together with an in-situ retention curve, be used to adopt parameter values for the standard hydraulic model, i.e. the intrinsic permeability, the relative permeability relation and the retention curve.

The experimental data points, i.e. initial and final points for Test 1 and Test 2, are presented together with two adopted retention curves in Figure 8-6. Both curves were adopted so that the initial saturation degree of 42 % corresponds to a suction value of 90 MPa.

The first curve follows the van Genuchten expression with the parameter values P_0 = 10 MPa and λ = 0.28:

$$S_l(P_l) = \left(1 + \left(\frac{P_g - P_l}{P_0} \right)^{\frac{1}{1-\lambda}} \right)^{-\lambda} \tag{8-8}$$

The second curve follows the so-called square law (implemented in Code_Bright) with the parameter value P_0 = 19.3 MPa:

$$S_l(P_l) = \frac{1}{\sqrt{1 + \frac{P_g - P_l}{P_0}}} \tag{8-9}$$

The moisture diffusivity function $D(S_l)$ is related to the permeability function $k \times k_r(S_l)$, the derivative of the inverse retention curve dP_l/dS_l, the porosity n, and the water viscosity μ according to the following equation:

$$D(S_l) = \frac{k \cdot k_r(S_l)}{n \cdot \mu} \cdot \frac{dP_l}{dS_l} \qquad (m^2 / s) \tag{8-10}$$

The permeability function can be evaluated by rearranging this to:

$$k \cdot k_r(S_l) = \frac{n \cdot \mu \cdot D(S_l)}{\frac{dP_l}{dS_l}} \qquad (m^2) \tag{8-11}$$

This function has been evaluated for four different parameter combinations which are shown in Figure 8-7. Relations based on a moisture diffusivity function optimized from water-uptake data are marked with blue lines, whereas corresponding relation based on a diffusivity function optimized from saturation data are marked with red lines. Relations based on the van Genuchten type of retention curve are marked with solid coloured lines, whereas corresponding relations based on the square law type of retention curve are marked with dotted coloured lines. A standard permeability function, previously used in Task 8, i.e. $S_l^3 \times 6.4 \times 10^{-21}$ m^2, is shown for comparison with a solid black line. A modified relation in which the exponent in the relative permeability law is changed to 4 is shown with a dotted black line.

It can be noted that blue lines (optimized from water-uptake data) are very close to the standard Task 8 relation, whereas the red lines (optimized from saturation data) are very close to the relation with a fourth order power law. It can also be noted that van Genuchten based relations display a strong decreasing trend close to saturation, and therefore diverges from the standard permeability relations, whereas the square law based relations are very similar to the standard permeability relations.

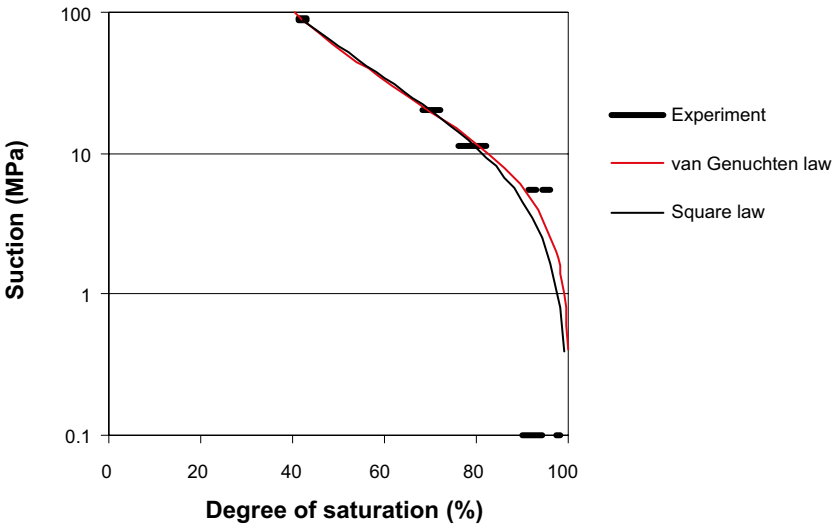

Figure 8-6. *In-situ retention curve. Experimental data points and adopted functions.*

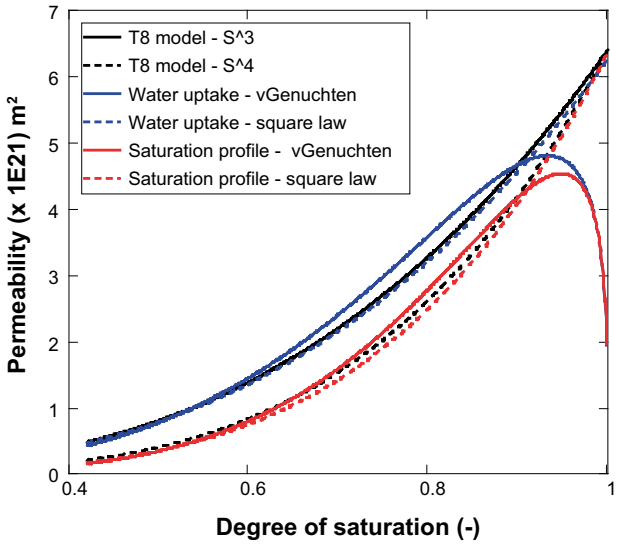

Figure 8-7. *Evaluated permeability functions.*

8.2.5 Code_Bright models of water-uptake tests

The water-uptake test was modelled with Code_Bright (v4) as a purely hydraulic problem with a 1D axisymmetric geometry, see Figure 8-8. The block was described as homogenized with a single constant porosity (44 %). The initial degree of saturation (42 %) was applied with an initial suction value of 90 MPa and the adopted retention curves. The initial water filling of the outer slot was taken into account by applying water saturated conditions from the start in the outer 5 mm of the bentonite (corresponding to an additional water volume of 0.12 liters for a height of 0.1 m). The liquid pressure at the outer boundary was kept constant at an atmospheric level (0.1 MPa) throughout the calculations. The used parameter values are shown in Table 8-1. The models were run for 203 days, at a constant gas pressure of 0.1 MPa, at a constant temperature of 20 °C (which implies a constant viscosity), and with no gravity. The geometry was discretized as an array of 130 elements. Four different model cases were analyzed according to Table 8-2.

The model results are shown in Figure 8-9 to Figure 8-11. The modelled evolution of RH at the radii 0.04, 0.08 and 0.12 m are shown together with data from the RH sensors in Test 1 in Figure 8-9. Modelled saturation profiles for day 0, 107 and 203 are shown in Figure 8-10 together with measured saturation profiles at the dismantling of Test 1 and 2. The modelled water-uptake is shown in Figure 8-11 together with the measured cumulative water-uptake in Test 1. The water-uptake was evaluated as the flow rate for the entire circumference, and adjusted for a block height of 0.1 m. Moreover, an initial inflow 0.2 litres was added to the water-uptake (0.08 litres representing the filter volume, and 0.12 litres volume of the outer slot, see above).

Table 8-1. Parameter values.

Parameter		Value		
Porosity	n (–)	0.44		
Intrinsic permeability	k (m^2)	6.4×10^{-21}		
Relative permeability	k_r (–)	S_l^3	or	S_l^4
Water retention curve		van Genuchten law: P_0: 10 MPa; λ: 0.28	or	Square law: P_0: 19.3 MPa
Water density	ρ_l (kg/m^3)	1 000		
Water viscosity	μ_l (Pa × s)	0.001		

Table 8-2. Model cases.

Model	Relative permeability	Water retention curve
BRIEVUF_6	S_l^3	van Genuchten law: P_0: 10 MPa; λ: 0.28
BRIEVUF_7	S_l^4	van Genuchten law: P_0: 10 MPa; λ: 0.28
BRIEVUF_8	S_l^3	Square law: P_0: 19.3 MPa
BRIEVUF_9	S_l^4	Square law: P_0: 19.3 MPa

It can be noted that the models with a cubic power law generally display a better agreement than the models with the fourth order power law concerning the experimental water-uptake data (Figure 8-11). In contrast, the models with the fourth order power law generally display a better agreement with the measured RH-evolution (Figure 8-9) and the measured saturation profiles (Figure 8-10). In addition, it can be noted that the models with the van Genuchten retention curve generally display a faster hydration than the models with the square law retention curve (e.g. see the red curves in Figure 8-10), and also faster than the diffusivity based model (cf. lower graphs in Figure 8-5).

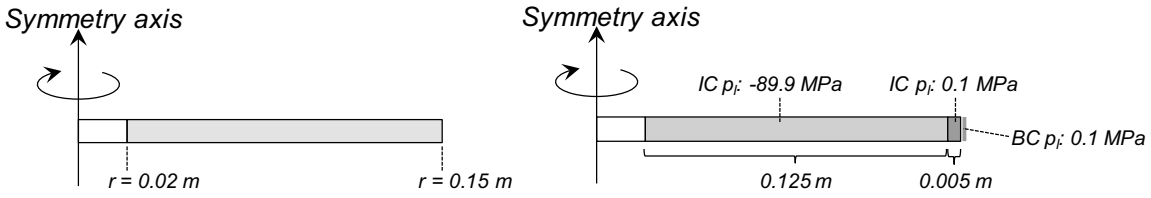

Figure 8-8. *Model geometry (left) and model initial and boundary conditions (right).*

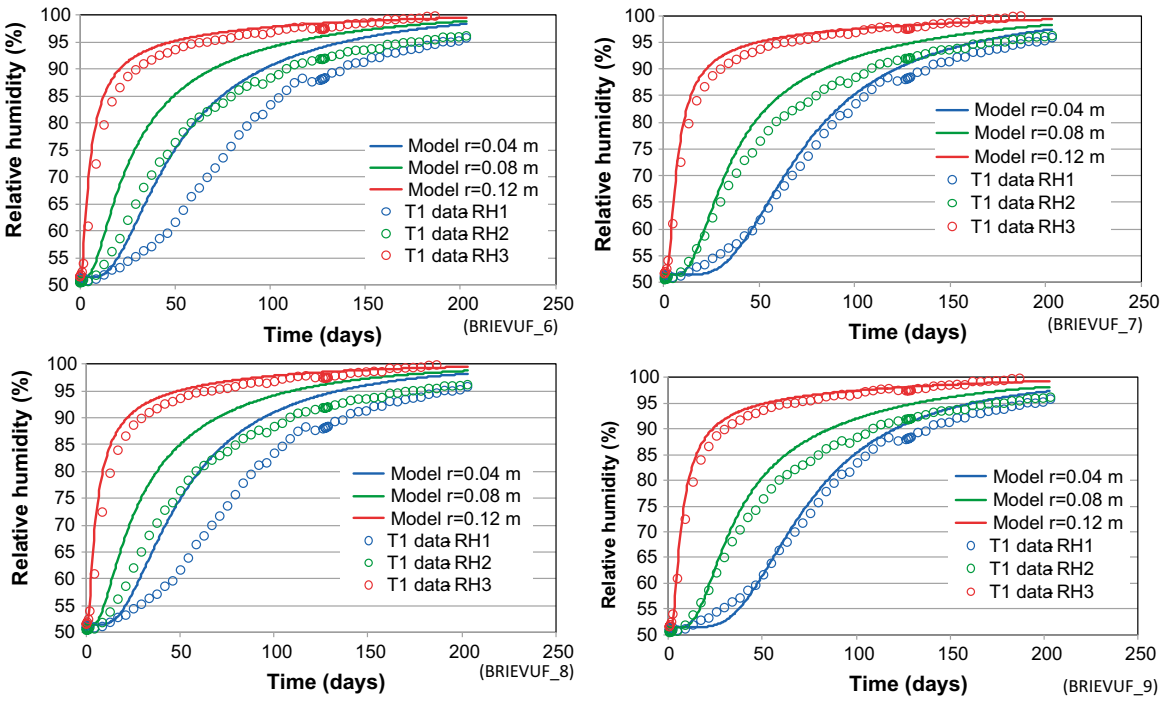

Figure 8-9. *Modelled evolution of RH at three radii and data from RH sensors in Test 1; van Genuchten retention curve (upper graphs); square law retention curve (lower graphs). $k_r(S_l) = S_l^3$ (left graphs); and $k_r(S_l) = S_l^4$ (right graphs).*

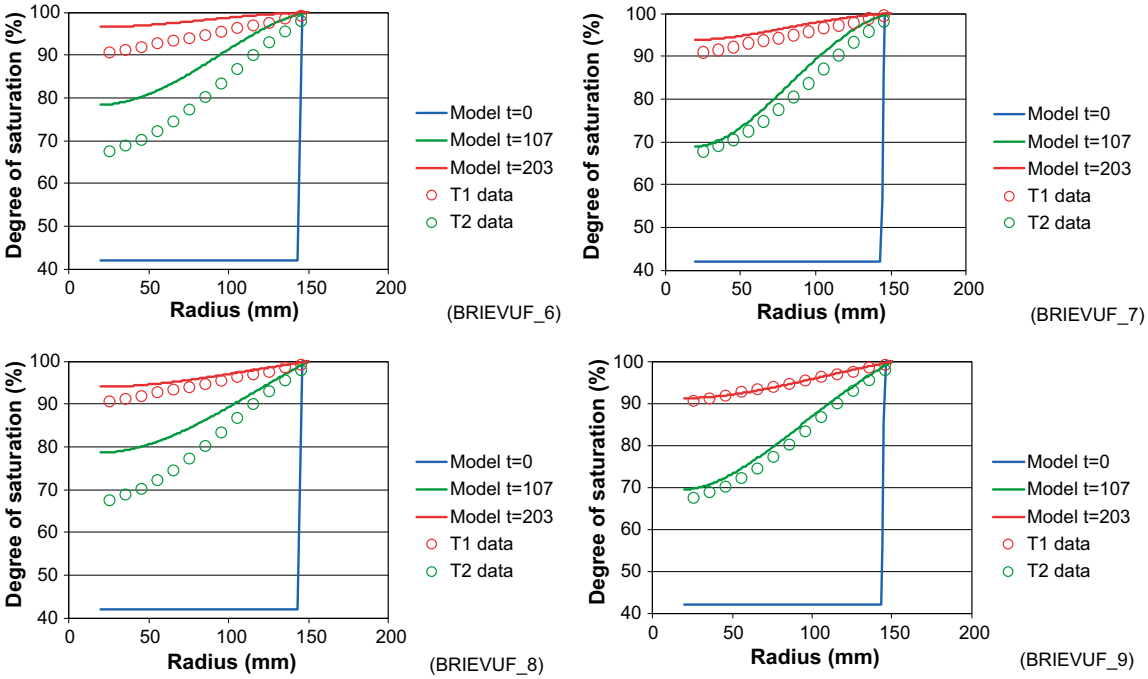

Figure 8-10. *Modelled saturation profiles at day 0, 107 and 203 and measured data from Test 1 and Test 2; van Genuchten retention curve (upper graphs); square law retention curve (lower graphs). $k_r(S_l) = S_l^3$ (left graphs); and $k_r(S_l) = S_l^4$ (right graphs).*

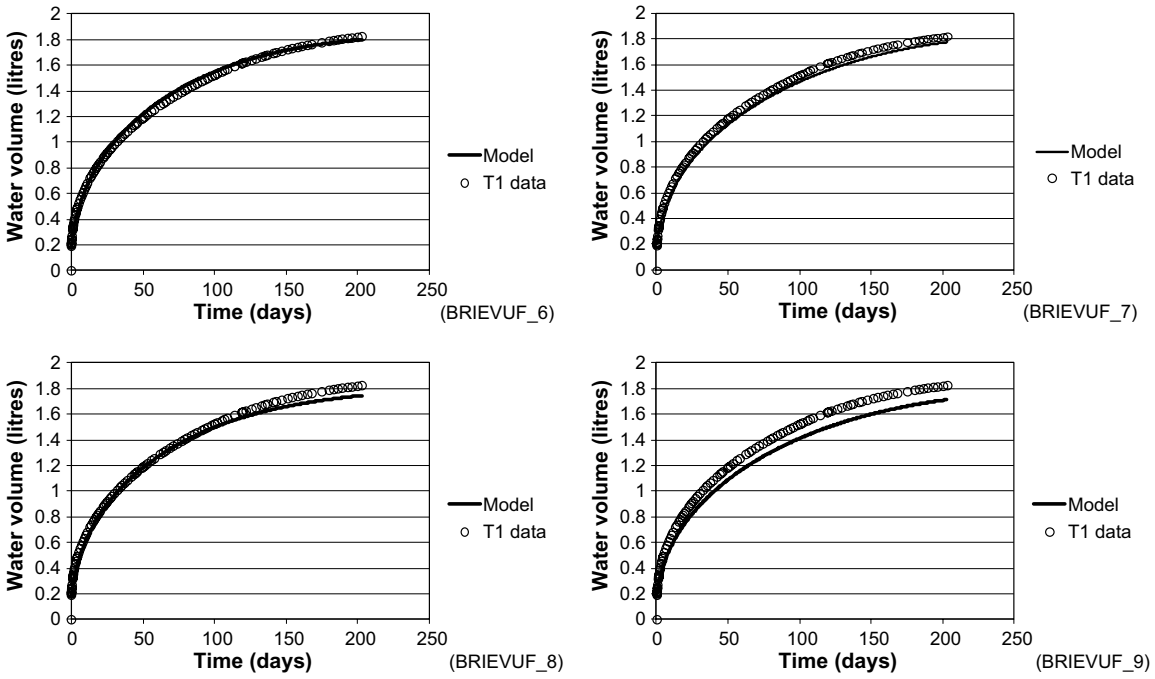

Figure 8-11. *Modelled cumulative water upt and measured data from Test 1; van Genuchten retention curve (upper graphs); square law retention curve (lower graphs). $k_r(S_l) = S_l^3$ (left graphs); and $k_r(S_l) = S_l^4$ (right graphs).*

8.2.6 Final remarks on hydraulic evaluation

The presented evaluation demonstrates how all hydraulic parameters can be quantified from one single experiment. The chosen approach to do this was to first evaluate a moisture diffusivity function, and secondly to evaluate a permeability function from the diffusivity and an in-situ retention curve. An alternative approach could be to adopt the retention curve to begin with, and then to make a parameter analysis of the intrinsic permeability and the exponent in the relative permeability law and make the parameter value adoption in this way.

One advantage of the chosen approach is however that the moisture diffusivity can be evaluated independently of any retention curve. And if the tests wouldn't be equipped with RH sensors, then it would still be possible to evaluate the moisture diffusivity without making any assumptions about the retention properties, which would be the case if the permeability parameters were evaluated.

It is also quite interesting to notice that one of the data sets (the water-uptake data) implies that the water-uptake can be described by one single parameter value (i.e. the D_0 value, see Figure 8-5, left). A constant diffusivity value implies that the cubic power law for the relative permeability is precisely associated with a square law for the retention curve, according to Eq (8-11).

Finally, it has been decided that the water-uptake tests should be included as a specific task in Task8, and that this task should follow a highly specified description, thereby enabling a comparison of codes. In addition to this, the modelers are free to use alternative parameter values and constitutive laws if they wish. Among the four cases presented above, the case with a fourth order power law for the relative permeability and a van Genuchten retention curve was selected as a task to be included in Task 8. The former relation was chosen due to the better agreement concerning the RH-evolution and the saturation profiles, whereas the latter curve was chosen for its widespread use and implementation.

A comparison of the parameter values defined in this task and in previous Task 8 definitions yields the following remarks:

- Hydraulic conductivity: 6.4×10^{-14} m/s (or intrinsic permeability 6.4×10^{-21} m^2) is exactly the same as previously.
- Relative permeability law: a fourth order power law (S_l^4) is defined instead of a cubic power law (S_l^3).
- van Genuchten retention curve parameters: P_0 = 10 MPa and λ = 0.28 are defined instead of P_0 = 9.23 MPa and λ = 0.3.

It can thus be noted that the differences between the two data sets are small.

8.3 Task description

The water-uptake test is to be modelled as a hydraulic problem with a 1D axisymmetric geometry, see Figure 8-12. The block is described as homogenized with a single constant porosity. The initial degree of saturation (42 %) is applied with an initial suction value of 90 MPa and the specified retention curve. The initial water filling of the outer slot is taken into account by applying water saturated conditions from the start in the outer 5 mm of the bentonite. The liquid pressure at the outer boundary is kept constant at 0.1 MPa throughout the calculations. The specified parameter values are shown in Table 8-3. The models should be run for 203 days, at a constant gas pressure of 0.1 MPa, at a constant temperature of 20 °C (which implies a constant viscosity), and with no gravity.

The following results are requested:

i. Cumulative water-uptake for the time period 0–203 days. This is evaluated as the flow rate for the entire circumference, and adjusted for a block height of 0.1 m. Moreover, an initial inflow of 0.2 litres is added to the water-uptake (corresponding to the volume in the filter and the outer slot).

ii. RH evolution at three radii: 0.04, 0.08 and 0.12 m; and for the time period: 0–203 days.

iii. Saturation profiles for two times: 107 and 203 days.

Table 8-3. Parameter values.

Parameter		Value
Porosity	n (–)	0.44
Intrinsic permeability	k (m^2)	6.4×10^{-21}
Relative permeability	k_r (–)	S_l^4
Water retention curve	P_0 (MPa)	10 MPa
(van Genuchten law)	λ (–)	0.28
Water density	ρ_l (kg/m^3)	1 000
Water viscosity	μ_l (Pa × s)	0.001

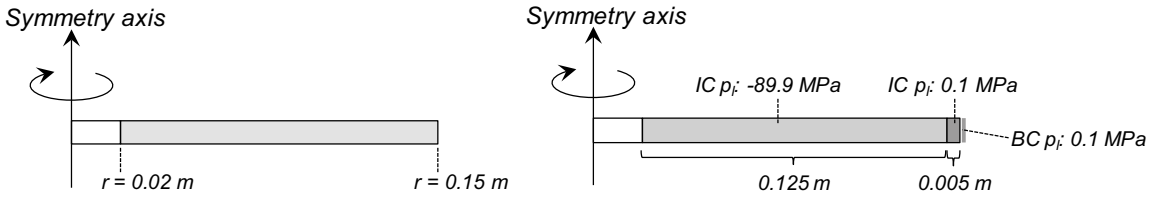

Figure 8-12. *Model geometry (left) and model initial and boundary conditions (right).*

8.4 MathCad algorithm for water-uptake calculation

Radii: $R_{in} \equiv 0.02 \quad R_{out} \equiv 0.15$

Duration: $T \equiv 203 \cdot days$

Number of elements: $n \equiv 14$

Number of time steps: $m \equiv 10000$

Radial element width: $\Delta r := \left(R_{out} - R_{in}\right) \cdot (n - 1)^{-1}$

Time step: $\Delta t := T \cdot (m - 1)^{-1}$

Constant: $R := \Delta t \cdot \Delta r^{-2}$

Seconds per day: $days \equiv 3600\,24$

Initial saturation: $S_{in} \equiv 0.42$

Porosity: $\phi \equiv 0.44$

Initial water volume: $V0 := \pi \cdot 0.1 \cdot \phi \cdot S_{in} \cdot \left(R_{out}^{\ 2} - R_{in}^{\ 2}\right)$

Moisture diffusivity function: $D\left(D_0, k, S\right) := D_0 \cdot 10^{-10} \cdot \left[\frac{S}{\left(S_{in} + 1\right) \cdot 0.5}\right]^k$

Pore volumes in element array:

$$\begin{aligned}
&PoreVolume := \\
&\quad PV_0 \leftarrow 0.1 \cdot \pi \cdot \phi \cdot \left[\left(R_{in} + 0.5 \cdot \Delta r\right)^2 - \left(R_{in}\right)^2\right] \\
&\quad \text{for } i \in 1..n-2 \\
&\qquad PV_i \leftarrow 0.1\pi \cdot \left[\left[R_{in} + \Delta r \cdot (i + 0.5)\right]^2 - \left[R_{in} + \Delta r \cdot (i - 0.5)\right]^2\right] \cdot \phi \\
&\quad PV_{n-1} \leftarrow 0.1\pi \cdot \left[\left[R_{in} + \Delta r \cdot (n - 1)\right]^2 - \left[R_{in} + \Delta r \cdot (n - 1.5)\right]^2\right] \cdot \phi \\
&\quad PV
\end{aligned}$$

$V_P := PoreVolume$

$$\begin{aligned}
&M\left(D_0, k1\right) := \\
&\quad \text{for } i \in 0..n-2 \\
&\qquad S_{0,i} \leftarrow S_{in} \\
&\quad S_{0,n-1} \leftarrow 1 \\
&\quad WU_0 \leftarrow \sum_{i=0}^{n-1} \left(S_{0,i} \cdot V_{P_i}\right) - V0 \\
&\quad \text{for } j \in 1..m-1 \\
&\qquad S_{j,n-1} \leftarrow 1 \\
&\qquad \text{for } i \in 1..n-2 \\
&\qquad\quad S_{j,i} \leftarrow S_{j-1,i} + R \cdot D\left(D_0, k1, S_{j-1,i}\right) \cdot \left(S_{j-1,i+1} - 2 \cdot S_{j-1,i} + S_{j-1,i-1}\right) \\
&\qquad\quad S_{j,i} \leftarrow S_{j,i} + \frac{\Delta t}{2 \cdot \Delta r} \cdot \frac{D\left(D_0, k1, S_{j-1,i}\right)}{R_{in} + i \cdot \Delta r} \cdot \left(S_{j-1,i+1} - S_{j-1,i-1}\right) \\
&\qquad\quad S_{j,i} \leftarrow S_{j,i} + \frac{R}{4} \cdot \left(D\left(D_0, k1, S_{j-1,i+1}\right) - D\left(D_0, k1, S_{j-1,i-1}\right)\right) \cdot \left[\left(S_{j-1,i+1}\right) - \left(S_{j-1,i-1}\right)\right] \\
&\qquad S_{j,0} \leftarrow S_{j,1} \\
&\qquad WU_j \leftarrow \sum_{i=0}^{n-1} \left(S_{j,i} \cdot V_{P_i}\right) - V0 \\
&\quad \left(S \quad WU\right)^T
\end{aligned}$$

Figure 8-13. *MathCad algorithm for water-uptake calculation.*

Model := M(5.5, 0)

(Diffusivity function optimized for water-uptake data)

M0 := Model$_0$ M2 := Model$_1$

i := 0.. n − 1j := 0.. m − 1

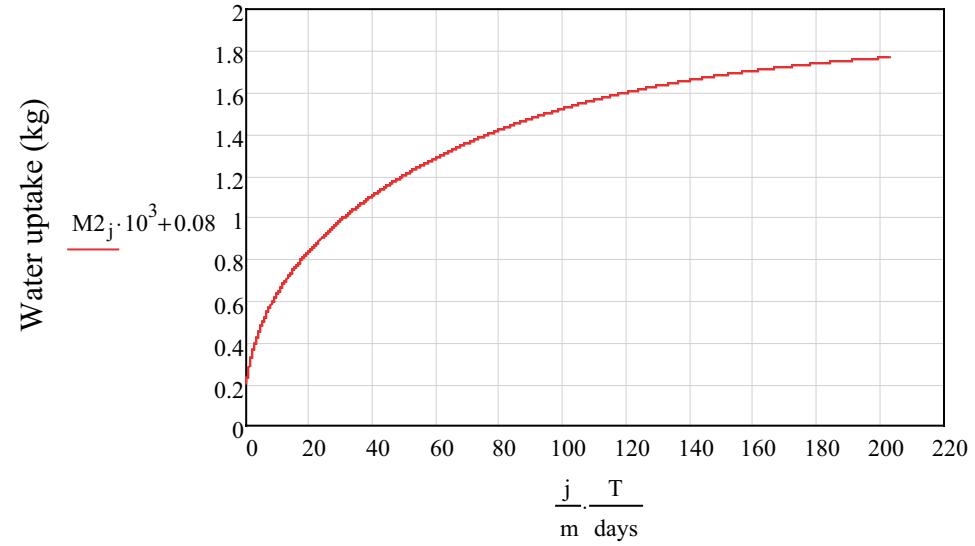

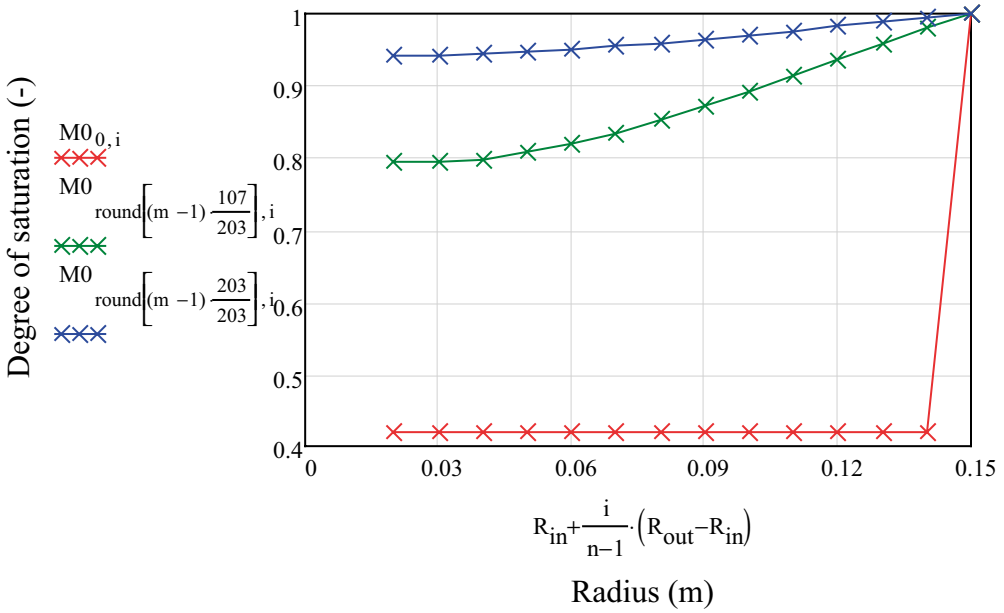

Figure 8-14. *Calculated water-uptake and the degree of saturation.*

9 Task 8e – The Prototype Repository

9.1 Introduction

This task definition gives the necessary guidelines for setting up calculations concerning predictions of deposition hole interactions as part of modelling the Prototype Repository experiment. The exercise is primarily intended to be a hydrogeological model with coupled heat transport along with the calculation of bentonite- and backfill saturation.

The modelling will in many aspects be similar to the task "The Prototype Repository" assessed within the EBS taskforce. As such it serves as a means of continued collaboration between the task forces and could further help clarify the importance of the bedrock

The model results are primarily intended to provide representations of the actual thermo-hydraulic situation surrounding the Prototype tunnel and could be based on pre-investigation data, on-going field measurement and for the parts of the Prototype experiment that have been excavated on post-mortem results. These data will be made available within this task description and associated compilations and reports.

Hydraulic boundary conditions are provided from a regional scale hydrogeological model which in part uses the same large scale geometrical framework (as supplied in this specification). Geometrical specifications, along with a site-specific geological structure model are given as CAD data. Stochastic fracture statistics are given as intensity, size and orientation data and serve as the basis for the hydraulic properties.

Some data, for instance matrix permeability and rock saturation information are based on results from the BRIE experiment. It is important to view Task 8e not as a new and stand-alone exercise but as a tool to test the lessons learned in the modelling of BRIE and to further test results and assumptions developed in BRIE and other relevant experiments.

9.2 The Prototype Repository

9.2.1 General

The Prototype Repository simulates a part of a KBS-3 nuclear waste repository. Within the Prototype Repository project the performance of such a repository on the tunnel scale during the first years after deposition is tested.

The aim of the Prototype Repository is to demonstrate the integrated function of the repository components and to provide a full-scale reference for comparison with models and assumptions. The aim is also to develop and test appropriate engineering standards, quality criteria and quality systems.

The Prototype Repository is designed, constructed and tested, to the extent possible, to simulate the real deep repository system regarding preparations, machinery for installation and deposition, geometry, materials, and rock environment.

The experiment is located at 450 m depth in the Äspö HRL.

The Prototype Repository drift, 65 m long and 5 m in diameter, was excavated using a Tunnel Boring Machine (TBM). Actually, two new tunnels were utilized for the project, TADSA (Prototype Repository Tunnel) and TASG (Data acquisition tunnel, indicated by the arrow naming the LOT project in Figure 9-1). The tunnels run sub-parallel to each other. Holes were drilled to lead cables for power and instruments between the tunnels, see Figure 9-2.

Six full-scale vertical deposition holes, 8.37 m deep and 1.75 m in diameter, were bored in the TADSA tunnel. A compilation of approximate geometric data of relevance for the experiment is provided in Table 9-1.

The Prototype Repository consists of two sections. The installation of section 1 of the Prototype Repository was made during summer and autumn 2001 and section 2 was installed in spring and summer 2003.

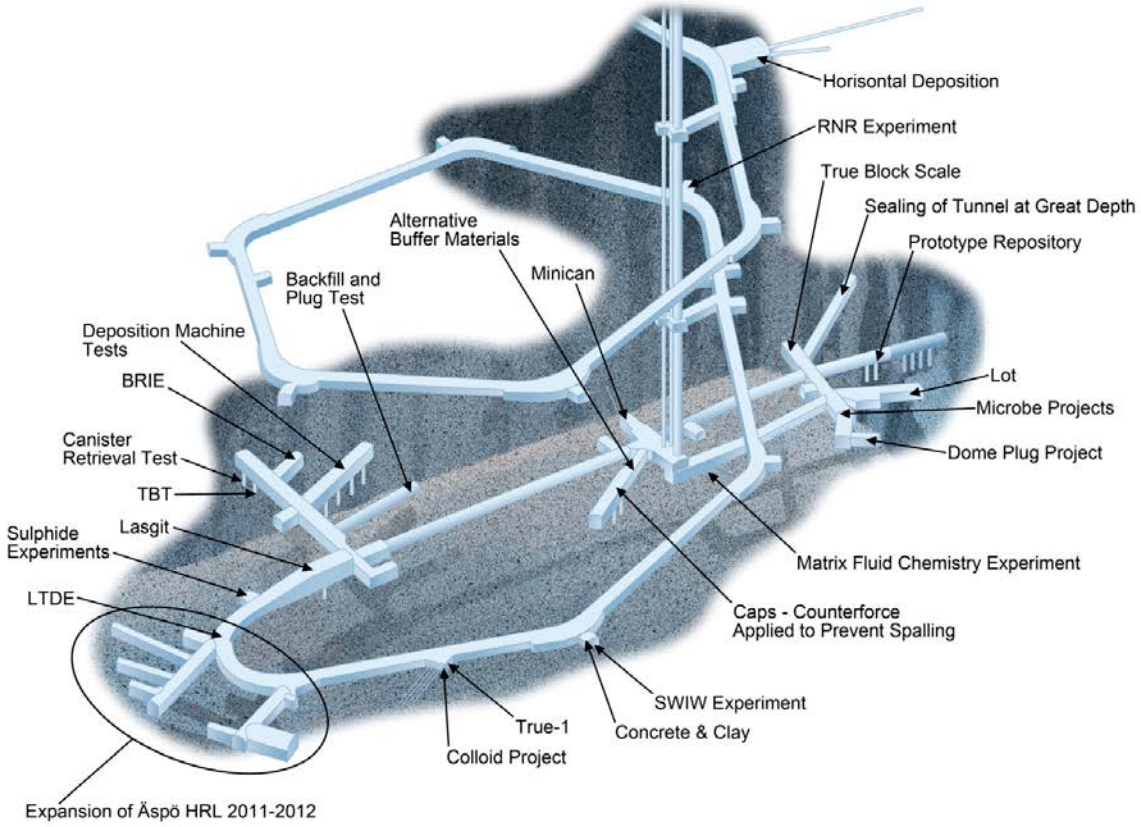

Figure 9-1. *Illustration of the Äspö HRL and some experimental sites on-going or finalized.*

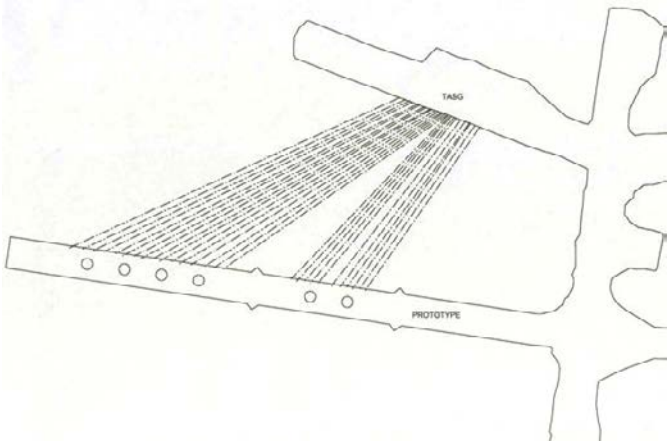

Figure 9-2. *Plan view of the prototype repository site.*

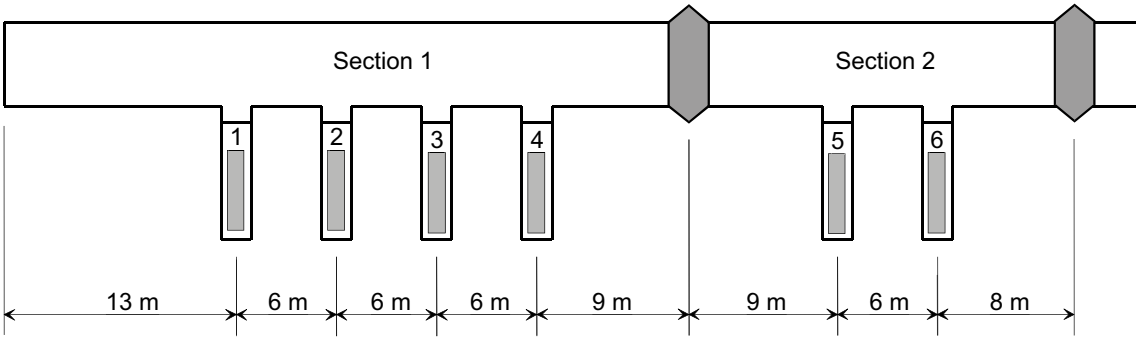

Figure 9-3. *Schematic view of the Prototype Repository.*

Section 1 consists of four full-scale deposition holes, copper canisters, bentonite blocks and a deposition tunnel backfilled with a mixture of bentonite and crushed rock and ends with a concrete plug as shown in Figure 9-3. The inner part of section 1 was mapped as wet, and in order to handle the water inflow a draining system (a sump inside of deposition hole 1 where water was drained from) was installed. Section 2 consists of two full-scale deposition holes with a backfilled tunnel section and ends also with a concrete plug. To simulate the thermal behaviour of the nuclear waste, heaters are installed in the canisters.

The bentonite buffer in deposition holes 1, 3, 5 and 6, the backfill and the surrounding rock are instrumented with gauges for measuring temperature, water pressure, total pressure, relative humidity, resistivity and canister displacement. The instruments are connected to data collection systems by cables protected by tubes, which are led through the rock in watertight lead-throughs. Instrumentation is used to monitor processes and properties in the canister, buffer material, backfill, and the near-field rock.

Table 9-1. Approximate geometric data relevant for the Prototype Repository.

Deposition hole depth	8 m
Deposition hole diameter	1.75 m
Canister height	~ 5 m
Canister diameter	1.05 m
Bentonite thickness below the canister	0.5 m
Bentonite thickness above the canister	1.5 m
Total tunnel length	63 m
Length of section I	40 m
Length of section II	23 m
Tunnel diameter	5 m

9.2.2 The tunnel backfill

The backfill material consists of a mixture of crushed rock with a maximum grain size of 20 mm (70 %) and a sodium converted bentonite from Greece, Milos (30 %). In Table 9-2 the properties of the Milos bentonite are listed. The backfill was mixed with water pumped out of the Äspö HRL to a water ratio of about 12 %. The mixing water had a salinity of about 0.6 %. The mixing was made in a mobile mixing station.

Table 9-2. Properties of the Milos bentonite after processing.

Quartz content	1.04 %
Sillica content	51.4 %
K_2O	0.85 %
N_2O	2.90 %
Sulphur content	0.318%
CaO	6.40 %

9.2.3 The bentonite buffer

The buffer around the six canisters in the Prototype Repository consists of highly compacted bentonite blocks. A schematic drawing of the buffer is shown in Figure 9-4. The blocks used for buffer material in the Prototype Repository were made of Na-bentonite MX-80 mixed with tap water and were compacted to two different shapes; ring shaped blocks, which are placed around the canister (see Figure 9-4 block R1–R10) and massive cylindrical blocks (C1–C4), which are placed above and under the canister. The blocks were uniaxially compacted in a rigid form to an outer diameter of about 1 650 mm and a height of about 500 mm. The inner diameter of the ring shaped blocks was about 1 070 mm. In order to have similar average density everywhere (including the slots), the two types of blocks were compacted to different densities.

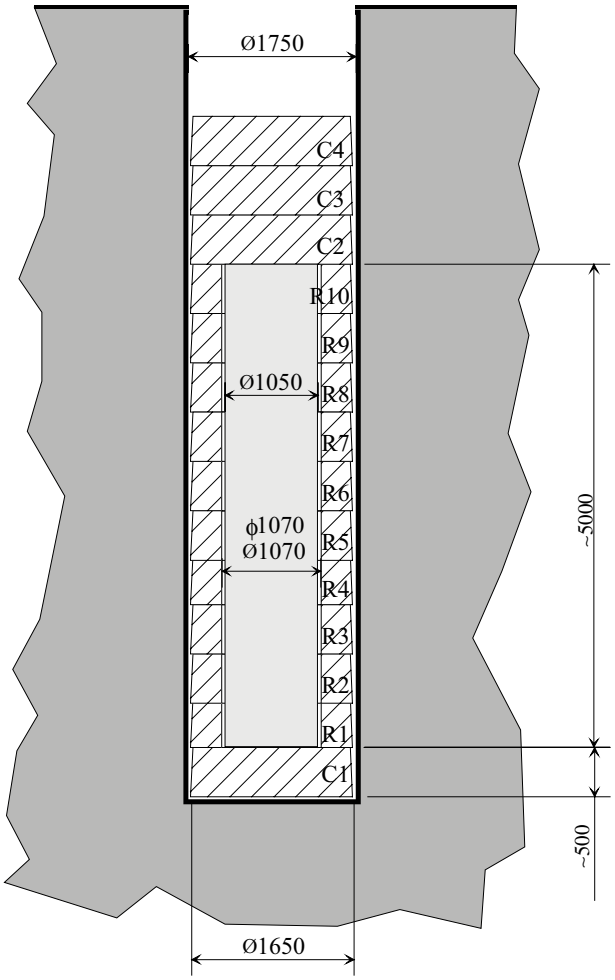

Figure 9-4. *Schematic drawing of a deposition hole with buffer and canister.*

Since the ten ring-shaped blocks placed around the canister had a total height larger than the canister, the volume between the lid of the canister and the upper surface of the tenth ring was filled with bricks of bentonite.

The approximately 50mm slot between the compacted bentonite and the rock surface of the deposition holes was filled with bentonite pellets in order to get a sufficient density of the buffer after saturation. The pellets had an initial water ratio of about 10 %.

9.3 Governing events in the Prototype Repository

Below key activities are listed for both sections (Table 9-3). The tables are obtained from the sensor data report IPR-09-17 where the activities are discussed.

Table 9-3. Main events during the opening and retrieval of the outer section.

2010115	20110211	Remove and sample outer plug.
20110214	20110311	Excavate and sample backfill up to dh6
20110314	20110610	Excavate and sample buffer in dh6
20110613	20110701	Continue backfill excavation, retrieve canister and excavate lower buffer in dh6.
20110808	20110812	Excavate backfill on top of dh5.
20110815	20111111	Excavate and sample buffer in dh5.
20111114	20111125	Retrieve canister and excavate lower buffer in dh5

Key activities for section 1	Key activities for section 2
Start backfilling 3/9 2001	Start backfilling 29/4 2003
Start heating canister 1 17/9 2001	Start heating canister 5 8/5 2003
Start heating canister 2 24/9 2001	Start heating canister 6 23/5 2003
Start heating canister 3 11/10 2001	Finished backfilling 25/6 2003
Start heating canister 4 22/10 2001	Plug casting 11/9 2003
Finish backfilling 20/11 2001	Decreased power (−30 W) 8/9 2004
Plug casting 14/12 2001	The power to all canisters was switched off
Decreased power (−20 W) 17/9 2002	The drainage of the tunnel was opened
Decreased power (−40 W) 5/9 2003	The power to the canisters was switched on
Decreased power (−30 W) 8/9 2004	The power to canister 6 was switched off
The drainage of tunnel was closed 1/10 2004	The power to canister 6 was switched on
The power to all canisters was switched off 2/12 2004	2/12 2004
The drainage of the tunnel was opened 6/12 2004	6/12 2004
The power to the canisters was switched on 15/12 2004	15/12 2004
Decreased power (−30 W) 2/12 2005	6/9 2005
A packer installed in the rock was broken 18/5 2006	2/11 2005
Decreased power (−30 W) 21/12 2006	Decreased power (−30 W) 2/12 2005
Decreased power (−30 W) 11/12 2007	Decreased power (−30 W) 21/12 2006
Decreased power (−30 W) 29/1 2009	Decreased power (−30 W) 11/12 2007
	The power to canister 6 was decreased with about 200 W due to problems with the heaters 8/4 2008
	The power to canister 6 was decreased with about 300 W due to problems with the heaters 5/6 2008
	Decreased power to canister 5 (−30 W) 29/1 2009

9.4 Scope and objectives

One aim of Task 8 is to improve the knowledge of the bedrock-bentonite interface with regard to groundwater flow. The main objectives with this exercise are to:

- Test the gained understanding of fractured bedrock control on bentonite wetting. Primarily intended to test the approaches, conceptual models, and numeric developed within Task 8a–8d.
- Scale up to a full-scale deposition hole scale as well as the deposition tunnel scale. Primarily intended to test the approaches, conceptual models, and numeric developed within Task 8a–8d.
- Test the thermal influences created by the waste (in the Prototype Repository project mimicked by heaters).
- Test interactions between deposition holes.
- Test effects on the wetting due to backfilling.
- Test effects on the wetting due to drainage effects.
- Serve as a blind prediction of the future state of the wetting in deposition holes 1–4.

Modellers are free to address the proposed objectives with any type of suitable code intended for groundwater flow or similar problems. The use of codes incorporating heat flow, unsaturated flow, chemistry, and mechanics is encouraged. However, Task 8e request results relevant to the thermal and hydraulic conditions. Therefore it may be necessary to address the questions asked in Task 8e with a thermo-hydraulic coupled methodology although this might be done with loosely coupled approaches.

In order to provide a realistic comparison with results from Task 8a–d and between different modelling groups a suggested approach for Task 8e has been divided into three parts, i.e. Task 8e1, Task 8e2, and Task 8e3.

Incorporation of bentonite is not considered in the Task 8e1 exercise. Instead the inflow to the open deposition holes is addressed and is intended to be compared with field data from the Prototype Experiment.

Task 8e2 addresses the wetting of the bentonite and backfilling based on the transient backfilling operations, the heating process and with initial conditions based on the flow and temperature model established in Task 8e1 but calibrated to the known information from field measurements and dismantling results, especially from the outer section (section 2). The final calculated wetting results for deposition holes 1–4 in the inner section (section 1) are to be reported as a blind predictions of the Prototype Repository.

Task 8e3 will be used to address the main objectives listed above that cannot be addressed within Task 8e1 and Task 8e2. As an example one could investigate alternative transient backfilling operations, such as what is the effect in deposition hole 2 when the tunnel and deposition holes 1 and 3 are left open?

The main scope of the exercise is:

Task 8e1

- To calculate inflows and inflow characteristics to six deposition holes.
- To supply boundary conditions and initial conditions to the buffer/backfill wetting simulations.
- Optional: to investigate effects of heterogeneous fracture flow on inflow.
- Optional: to investigate effects of heterogeneous matrix properties on inflow.

Task 8e2

- To evaluate the resulting wetting of the bentonite installed in the deposition holes in a calibrated model that explicitly resolves fractures and matrix properties.
- To investigate the effect of thermal processes on the wetting.
- To blind predict the wetting of the bentonite buffer in deposition holes 1–4.
- Optional: to investigate effects of heterogeneous fracture flow on the wetting.
- Optional: to investigate effects of heterogeneous matrix properties on the wetting.

Task 8e3

- To evaluate the resulting wetting of the bentonite installed in specific deposition holes in a predictive mode of the developed Task 8e2 model.
- To investigate effects of alternative backfilling operations.
- To provide indications of deposition hole interactions

Site-specific geological influences such as the chemistry-induced changes (e.g. calcite precipitation) are not presently quantified. Modellers are welcome to address these issues as one mean of adjusting their models. All incorporated issues, however, need to be readily explained.

As one of the objectives is to illustrate inflow and inflow characteristics within a deposition hole, the assessed continuum models need to consider a cell/grid resolution that is able to capture details on a wall of a deposition hole of a size of 1.75 m in diameter and approx. 8 m in depth.

9.4.1 Literature available

Report No	Title	Author/Authors	Author organization
IPR-00-33	Prototype Repository, Hydrogeology – Deposition – and lead – through boreholes: Inflow measurements, hydraulic responses and hydraulic tests.	Torbjörn Forsmark (1), Ingvar Rhén (1), Christer Andersson (2)	1) VBB VIAK 2) SKB
IPR-01-39	Prototype Repository, Hydraulic DFN model no:2.	Martin Stigsson, Nils Outters, Jan Hermansson	Golder Associates
IPR-01-65	Prototype Repository, Hydrogeology – Summary report of investigations before the operation phase.	Torbjörn Forsmark, Ingvar Rhén	VBB VIAK
IPR-02-23	Prototype Repository, Installation of buffer, canisters, backfill, plug and instruments in Section 1.	Lennart Börgesson, David Gunnarsson, Lars-Erik Johannesson, Torbjörn Sandén	Clay Technology
IPR-03-22	Äspö Hard Rock Laboratory. Prototype repository. Hydrogeological, hydrochemical, hydromechanical and temperature measurements in boreholes during the operation phase of the prototype repository tunnel section II.	Rhén, Ingvar; Forsmark, Torbjörn; Magnusson, Johan; Alm, Patrik	SWECO VIAK AB
IPR-04-13	Prototype Repository, Installation of buffer, canisters, backfill, plug and instruments in Section II.	Lars-Erik Johannesson, David Gunnarsson, Torbjörn Sandén, Lennart Börgesson	Clay Technology
IPR-04-22	Äspö Hard Rock Laboratory. Prototype repository. Hydromechanical behaviour of fractures due to excavation and thermal load.	Rhén, Ingvar; Alm, Patrik	SWECO VIAK AB
IPR-05-03	Prototype Repository, Hydrogeology – diaper measurements in DA3551G01 and DA3545G01, flow measurements in section II and tunnel G, past grouting activities.	Torbjörn Forsmark, Ingvar Rhén	VBB VIAK
IPR-05-04	Äspö Hard Rock Laboratory. Prototype Repository. Installations foe measurements of flow into tunnels, water pressure in rock and hydromechanical responses in boreholes during operation phase.	Alm, Patrik; Forsmark, Torbjörn; Rhén, Ingvar	SWECO VIAK AB
IPR-07-22	Prototype Repository – THM modeling of the bentonite buffer – Canister mid-hight 1D radial models, holes #1 and #3.	Ola Kristensson, Harald Hökmark	Clay Technology
IPR-10-04	Äspö Hard Rock Laboratory – Prototype Repository – Analyses of microorganisms, gases, and water chemistry in buffer and backfill.	Sara Lydmark	Microbial Analytics Sweden AB
IPR-10-17	Prototype repository – Tracer dilution tests during operation phase, test campaign 3.	Johan Harrström, Peter Andersson	Geosigma AB
IPR-99-16	Äspö Hard Rock laboratory. Prototype repository. Finite element analyses of mechanical consequences due to the rock excavation and thermal load.	Zeng, Lingfu; Dahlström, Lars-Olof	NCC AB
P-12-12	Prototype Repository. Sensor data report (Period 100917 – 11-01-01) Report No 24.	Reza Goudarzi	Clay Technology
Part 1 IPR-09-17 Part 2 IPR-09-17	Prototype Repository, Sensors data report (Period 010917 – 090601) Report No:21.	Reza Goudarzi, Lars-Erik Johannesson	Clay Technology

There are also a large number of reports that has been made available during this project. Examples are:

P-13-14	Prototype Repository. Measurements of water content and density of the excavated buffer material form deposition hole 5 and 6 and the backfill in the outer section of the Prototype Repository.	Johannesson L-E,	Clay Technology
P-13-15	Prototype Repository. Method for opening and retrieval of the outer section.	Johannesson L-E, Hagman P,	Clay Technology
P-13-31	Prototype Repository. Validation of retrieved sensors from the Prototype experiment at Äspö Hard Rock laboratory	Nilsson U	Clay Technology
P-13-39	Prototype Repository – Sensor data report (period 010917–130101). Report No 25.	Goudarzi R,	Clay Technology
R-12-12	Prototype Repository. Hydro-mechanical measurements during operation phase 2003-05-01 – 2010-02-01.	Rhén I, Forsmark T	Sweco Environment
TR-13-21	Prototype Repository. Hydromechanical, chemical and mineralogical characterization of the buffer and backfill material from the outer section of the Prototype Repository	Siv Olsson, Viktor Jensen, Lars-Erik Johannesson, Emelie Hansen, Ola Karnland, Sirpa Kumpulainen, Daniel Svensson, Staffan Hansen Johan Lindén J	Clay Technology B+Tech SKB LTH Åbo Akademi
TR-13-22	Prototype Repository. Opening and Retrieval of the outer section of Prototype Repository at Äspö Hard Rock Laboratory – Summary Report	Christer Svemar, Lars-Erik Johannesson, Pär Grahm, Daniel Svensson, Ola Kristensson, Margareta Lönnqvist, Ulf Nilsson	SKB Clay Technology
R-13-10	Thermal and thermo-mechanical evolution of the Äspö Prototype Repository rock mass. Modelling and assessment of sensors data undertaken in connection with the dismantling of the outer section.	Margareta Lönnqvist Harald Hökmark	Clay Technology

9.5 Case specifications

9.5.1 Geometrical set-up

The coordinate system applied within Task 8 is the Swedish RT90 system. The suggested model domain for which calculated boundary conditions will be available is approximately $(150 \times 150 \times 100)$ m^3 bounded by the following set of coordinates:

X min	X max	Y min	Y max	Z min	Z max
1551115	1551265	6367660	6367810	−500	−400

9.5.2 Tunnels and designed structures

The tunnels and designed structures are supplied as CAD objects.

9.5.3 Boreholes and packer locations

Boreholes and packer locations are supplied in excel files.

9.5.4 Deformation zones

Deformation zones are provided as CAD objects. Observe that not all of these deformation zones are hydraulically active. The hydraulic properties of hydraulic active deformation zones are found in referred literature.

9.5.5 The geology of the TBM tunnel

Geological mapping information is available in the referenced literature. Alternatively, the Task 8c and Task 8d fracture statistics can be used.

The reported and essential water bearing structures as mapped on the tunnel walls are supplied as CAD objects.

9.5.6 Rock stresses

In-situ stresses relevant for the Prototype Repository area are described in the referenced literature.

9.5.7 Boundary condition[10]

Pressure[11], temperature and velocities (Darcy flux) along the x, y, and z coordinates from a specified sub-grid of a DarcyTools v3.4 simulation of the full regional Äspö HRL model are given over a volume incorporating the suggested model domain (Figure 9-5). Data are found in file: BC_task8e.xls. As a reference case the assigned boundary conditions in tunnels should be at atmospheric conditions.

A first alternative set-up could be a specified pressure of 200 metres of water at the boundary and atmospheric conditions inside tunnels.

The associated uncertainty within the boundary conditions is suggested to be treated with one or more sensitivity cases. Data for alternative pressure situations can be found in the referenced literature.

9.5.8 Initial conditions

The initial conditions for the inflow predictions (Task 8e1) should be based on the "natural" conditions where all deposition holes are open.

The initial conditions for the wetting simulations (Tasks 8e2 and 3) should be based on the simulated results from Task 8e1.The models should then successively follow the backfilling operations.

Rock:

Resulting pressure field of conditions simulated based on the set-up of Task 8e1 but with bedrock-bentonite interface at a constant atmospheric pressure.

Resulting temperature field of conditions simulated based on the set-up of Task 8e1 but with bedrock-bentonite interface at a constant temperature of 12 °C.

Backfilling and Bentonite:

The initial state of these materials is given by the information found in the referred literature.

---

[10] The boundary conditions are established from the present official hydro-model of Äspö HRL. The model is (among others) based on the SDM site Laxemar deformation zone model and, due to scale issues, contains known location errors. The model may develop during the planned Task 8.

[11] Pressures given are dynamic pressure; absolute pressure could be calculated using $\rho_0 \times g \times z$, with reference altitude at present day shore line (0 altitude).

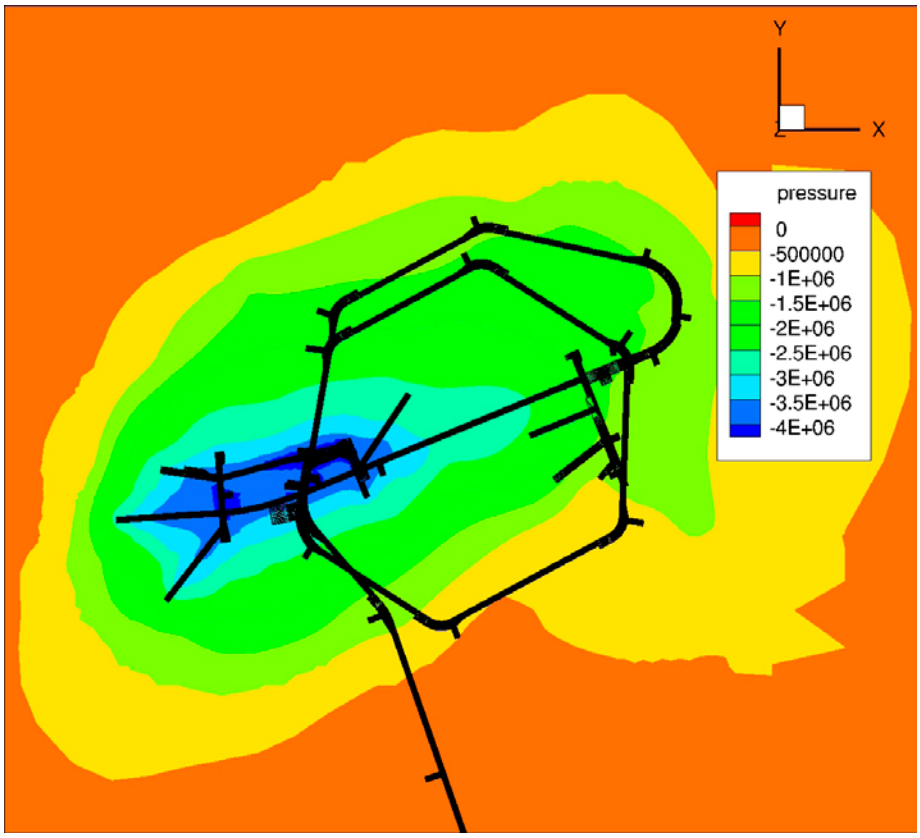

Figure 9-5. *Illustration of the pressure field (Pa) at the –455 m elevation, reference elevation is present day shore line (0 altitude). The pressure field includes the TASS tunnel.*

9.6 Material specifications

9.6.1 Rock matrix

Hydraulic conductivity

Laboratory tests on de-stressed matrix core samples from BRIE are summarized in Table 9-4 below.

Table 9-4. Hydraulic conductivity values from core samples.

Bore hole	Samples	Hydraulic conductivity (m/s)
KO0017G01	Diorite-Pegmatite 1	7.5×10^{-13}
	Diorite-Pegmatite 3	9.0×10^{-13}
	Diorite-Pegmatite 4	5.5×10^{-12}
KO0018G01	Diorite 1	6.0×10^{-14}
	Diorite 3	1.5×10^{-13}
	Diorite 4	1.5×10^{-13}
	Diorite 5	2.5×10^{-13}
	Diorite 7	3.3×10^{-13}

The data indicate a range of matrix hydraulic conductivity of about 2 orders of magnitude. In investigations on the effect due to this variability a relevant distribution could be used based on minimum, mean, and maximum values from the data presented above.

A sensitivity case testing the effect of an approximate one order of magnitude less permeable matrix hydraulic conductivity in stressed conditions could be addressed or if results from the Task 8a–d simulations indicate other matrix conductivity values could be assessed.

Porosity

Laboratory tests from BRIE indicate that the matrix rock porosity should be between 0.5–1 %. These values compare well with other laboratory tests conducted at Äspö type rock; these earlier tests indicate porosity values close to 0.5 %.

Specific Storage

The specific storage of the matrix is in general unknown. The field tests conducted at Äspö indicate a range between 1E−9 and 1E−6 (m^{-1}). Typically theoretical values for Äspö type rock points toward an approximate value of 1E−7 (m^{-1}).

Thermal conductivity

Values for thermal conductivity for the Prototype Repository area are found in the referred literature.

Heat capacity

Values for heat capacity for the Prototype Repository area are found in the referred literature.

Water retention

Relative humidity RH and associated volumetric water content has been measured for two representative rock matrix core samples from the BRIE site. The results are given in Table 9-5 below.

Table 9-5. Results from water retention measurements performed on core samples.

RH (%)	Water content (%)	
	Diorite A1	Granite B1
100 (saturated porosity)	0.99	0.46
85	0.30	0.15
59	0.22	0.11
33	0.16	0.08

These values have been adopted and parameters fitted to a van Genuchten curve. The RH values used provide data at relatively low saturations which may not be relevant to the saturation state of the granite close to the bentonite in the models. Therefore, although the data is specific to the matrix at BRIE, some caution should be used in applying the fitted model parameters to high water saturations. It is suggested that the modellers use a range of matrix properties incorporating previous literature values and the new site-specific data.

Fractured bedrock

The referenced literature provides the available data for the fractured bedrock.

Fracture specific treatment should be explained and assessed values motivated.

Tunnel backfill

The referenced literature provides the available data for the backfill material.

Bentonite

The referenced literature provides the available data for the buffer material.

9.6.2 Proposed relationships

The proposed relationship for rock/matrix is changed below; for fractures and bentonite the relationships are the same as in Task 8c.

The following relationships are proposed to be used for the relative permeability:

$$k_r = \begin{cases} S^3 & (bentonite) \\ \sqrt{S}\left(1-\left(1-S^{1/\lambda}\right)^{\lambda}\right)^2 & (rock) \end{cases} \quad (9\text{-}1)$$

where S is the degree of saturation (volume of water over total volume of pores).

In addition, the following expression is proposed for the water retention curve:

$$S = \left[1+\left(\frac{P_g - P_l}{P_0}\right)^{\frac{1}{1-\lambda}}\right]^{-\lambda} \quad (9\text{-}2)$$

where P_g is the gas pressure (can be assumed to be atmospheric 0.1 MPa), P_l is the water pressure, and P_0 and λ are empirical constants (Table 9-6).

Table 9-6. Parameter values used for water retention curves.

Material	P_0 (MPa)	λ (–)
Bentonite	9.23	0.3
Rock/matrix*	0.6	0.24

* Note that laboratory measurement is presented under properties. The proposed relationship for Task 8a–8c is more related to the Finsterle and Pruess (1995) data while the fitted laboratory measurement is more similar to the Thomas et al. (2003) relationship. Modellers are asked to treat the uncertainty of this new data set in a relevant manner as well of the uncertainty imposed by the different suggested relationships.

As of the rock fractures the following relationship should be used (in principal the same as above but in an alternative form; where $\delta = \rho \times g/P_0$ and $n = 1/(1-\lambda)$).

$$K(h) = K_s \frac{\left(1-\left(\delta|h|\right)^{n-1}\left(1+\left(\delta|h|\right)^n\right)^{-(1-1/n)}\right)^2}{\left(1+\left(\delta|h|\right)^n\right)^{m(1-1/n)}} \quad \text{for } h<0 \quad (9\text{-}3)$$

$$K(h)=K_s \quad \text{for } h\geq 0$$

Suggested variation of the parameters is found in Figure 9-6 where the aperture is given in mm. As a reference case, δ and n should be assigned according to the cubic law hydraulic aperture based on the transmissivity values and m = 0.5. An explanation for how to derive van Genuchten parameters (δ and n, or λ and P_0) from a transmissivity value is given in Figure 4-4 and Figure 4-5.

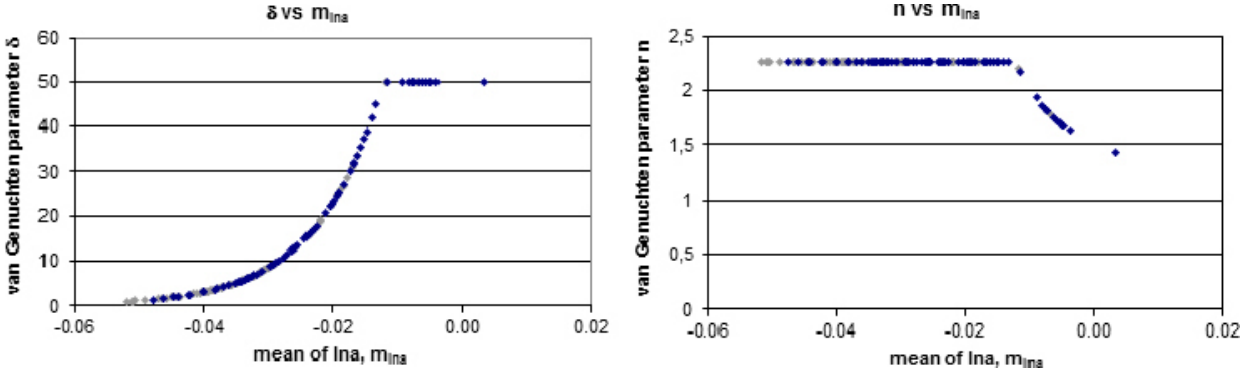

Figure 9-6. *Graphs derived with theory presented by Jarsjö (2009).*

9.7 Calibration targets

9.7.1 Ambient pressure

Ambient pressure data are found in the referred literature.

9.7.2 Ambient temperature development

Ambient temperature data are found in the referred literature.

9.7.3 Inflow tunnel

Tunnel inflow values are found in the referenced literature.

9.7.4 Inflow deposition holes

Inflow values to the deposition hole before bentonite installation are found in the referenced literature.

9.7.5 Pressure responses

Pressure responses in associated borehole sections are found in referred literature.

9.8 Modelling tasks

There are two main exercises within Task 8e that each may demand development of new methodologies or the use of those developed as part of Tasks 8a–d. These exercises are:

Characterization and assessment of the deposition holes (Task 8e1), and modelling and evaluation of wetting of the bentonite buffer (Task 8e2).

From the results of BRIE and Task 8 presented so far, the characterization of fractures and rock matrix, and their influence on inflow to the deposition holes and the bentonite wetting, will significantly affect the results. The modelling groups are requested to address the uncertainty in "natural" inflow and bentonite wetting imposed by the uncertainty in field and laboratory data along with the capability of codes assessed. By addressing these uncertainties it is believed that an improvement of the understanding of limitations in current understandings and technologies for prediction of deposition hole inflow and associated wetting could be gained.

For the Task 8e it is important to consider Task 8e1 with great care before continuing with Task 8e2.

9.9 Expected outcome

The expected outcome as described below should be provided for each model realisation or variant that is deemed necessary in order to meet to the objectives.

Results for Task 8e1:

Provide contour plots of the deposition holes near-field, permeability structure (in m^2), pressures (in Pa), temperatures (in °C), and Darcy fluxes (in m/s) on horizontal cross-sections incorporating all six deposition holes starting at the end of the Prototype tunnel and ending at the entrance to the tunnel. The cross-sections should be placed on the depth of 2, 4, and 6 metres below the top of the centre line of deposition hole 1. Additionally, provide the same information on one vertical cross-section incorporating all six deposition holes starting at the end of the Prototype tunnel and ending at the entrance to the tunnel. The horizontal cross-sections should capture the entire tunnel width and reach out at least 2 metres at each side; the vertical cross-section should capture the rock from the tunnel floor and at least 10 metres downward.

Provide contour plots of the permeability (m^2), inflows (in m^3/s over a defined unit area, eg. cell size) presented as folded up illustrations of the walls of the deposition holes.

Graphs or plots deemed necessary to illustrate the model performance compared to available data on the ambient pressure situation and section or deposition hole related inflows.

Results are expected for steady-state conditions.

Results for Task 8e2:

Provide contour plots of the deposition holes near-field pressures, temperatures, and saturation[12] in bentonite as well as the bedrock for time steps at 0, 0.1, 0.5, 1.0, 10, 100, 200, 1 000 years on one vertical cross-section incorporating all six deposition holes starting at the end of the Prototype tunnel and ending at the entrance to the tunnel are requested. The vertical cross-section should capture the rock from the tunnel floor and at least 10 metres downward.

Provide contour plots of the deposition holes near-field pressures, temperatures, and saturation in bentonite as well as the bedrock for time steps at 0, 0.1, 0.5, 1.0, 10, 100, 200, 1 000 years on horizontal cross-sections incorporating all six deposition holes starting at the end of the Prototype tunnel and ending at the entrance to the tunnel. The cross-sections should be placed on the depth of 2, 4, and 6 metres below the top of the centre line of deposition hole 1. The horizontal cross-sections should capture the entire tunnel width and reach out at least 2 metres at each side.

Contour plots of the deposition holes near-field pressures and saturation in bentonite as well as the bedrock for time steps at 0, 0.1, 0.5, 1.0, 10, 100, 200, 1 000 years presented as folded up illustrations of the walls of the deposition holes.

The colour scale of the contour plots should be: 1.5, 1, 0.5, 0.2, 0.1, 0, −0.1, −0.2, −0.5, −1, −5, −10, −20, −50 MPa.

Graphs showing illustrations of the pressure and temperature increase within the bentonite along two orthogonal lines (the diameter) for the six deposition holes at the depth of 2, 4, and 6 metres below the top of centre line of deposition hole 1. One of the chosen directions should coincide with the tunnel centre line (i.e. the vertical cross-section above)

Graphs illustrating the pressure and temperature change within the bedrock at a position 0.01, 0.05, 0.1, 0.15, 1, 5 metres from deposition hole walls in the direction towards the other deposition holes are requested. These graphs should also come for the same depth positions as described above.

Graphs or plots deemed necessary to illustrate the model performance compared to available data on the ambient pressure situation and section drainage values.

As for the prediction of wetting in Section 1 provide the above requested plots and graphs also for times 20 and 30 years after installation.

Results for Task 8e3:

The results asked for are similar to those from Task 8e2 in order to be fully comparable.

Provide contour plots of the deposition holes near-field pressures, temperatures, and saturation in bentonite as well as the bedrock for time steps at 0, 0.1, 0.5, 1.0, 10, 100, 200, 1 000 years on one vertical cross-section incorporating all six deposition holes starting at the end of the Prototype tunnel and ending at the entrance to the tunnel are requested . The vertical cross-section should capture the rock from the tunnel floor and at least 10 metres downward.

[12] Or alternative equivalent measure of change in the bentonite due to inflow of water from the bedrock, e.g. RH or suction.

Provide contour plots of the deposition holes near-field pressures, temperatures, and saturation in bentonite as well as the bedrock for time steps at 0, 0.1, 0.5, 1.0, 10, 100, 200, 1 000 years on horizontal cross-sections incorporating all six deposition holes starting at the end of the Prototype tunnel and ending at the entrance to the tunnel. The cross-sections should be placed on the depth of 2, 4, and 6 metres below the top of the centre line of deposition hole 1. The horizontal cross-sections should capture the entire tunnel width and reach out at least 2 metres at each side.

Provide contour plots of the deposition holes near-field pressures and saturation in bentonite as well as the bedrock for time steps at 0, 0.1, 0.5, 1.0, 10, 100, 200, 1 000 years presented as folded up illustrations of the walls of the deposition holes.

The colour scale of the contour plots should be: 1.5, 1, 0.5, 0.2, 0.1, 0, −0.1, −0.2, −0.5, −1, −5, −10, −20, −50 MPa.

Provide graphs showing illustrations of the pressure and temperature increase within the bentonite along two orthogonal lines (the diameter) for the six deposition holes at the depth of 2, 4, and 6 metres below the top of centre line of deposition hole 1. One of the chosen directions should coincide with the tunnel centre line (i.e. the vertical cross-section above)

Graphs illustrating the pressure and temperature change within the bedrock at a position 0.01, 0.05, 0.1, 0.15, 1, 5 metres from deposition hole walls in the direction towards the other deposition holes. These graphs should also come for the same depth positions as described above.

Reporting

It is likely that Task8e is the final part of Task 8 and is expected to be reported in a stand-alone report.

The report should provide some background and briefly discuss objectives, scope, overall approach, model setup, simulation results, interpretation, conclusions and recommendations. Details about the specific analyses can be included in appendices to the main report.

While the content of the report should be flexibly adapted to match the actual analyses performed, the following specific questions should be addressed:

Quantitative results:

(1) What is the range of predicted inflows into an open deposition hole?

(2) What is the range of predicted times needed to wet the entire bentonite package to a saturation of 95 %?

(3) What is the range of predicted times needed to wet the different parts of one individual bentonite package to a saturation of 95 %?

(4) What is the range of predicted times needed to wet the different parts at the rock bentonite interface of one individual bentonite package to a saturation of 95 %?

Qualitative discussion:

(5) What are the key features and properties of the natural and engineered systems that need to be known for deposition hole screening?

(6) What are the key features and properties of the natural and engineered systems that need to be known to reduce uncertainty in estimates of saturation time for the bentonite buffer and backfill?

(7) What information and data are most valuable for (a) overall system understanding, and (b) model development?

(8) How does the conceptualisation of the natural and engineered systems influence (a) quantitative model predictions, and (b) interpretation of the expected system behaviour?

10 Task 8F BRIE – The final Task 8 BRIE modelling

10.1 Introduction

This gives the tentatively necessary guidelines for adopting the previous calculations concerning predictions of inflow to the two 30 cm diameter boreholes and the wetting of the emplaced bentonite in the TASO tunnel within a sub-local Äspö HRL site model domain based on the results presented in the BRIE report (Fransson et al. 2017). A set of diagrams and photos from this report is reproduced in Figure 10-1 to Figure 10-7.

Task 8F provides the modellers with an opportunity to complete their studies of the BRIE experiment within Task 8. Previous subtasks have involved predictive modelling where results from bentonite wetting were not available to the modellers. Within Task 8F modellers may use the results documented in the BRIE report (Fransson et al. 2017) to:

- Discuss the predictive modelling and compare with results;
- perform back-analysis, inverse modelling;
- perform additional sensitivity studies.

Hydraulic boundary conditions, if needed, are provided from a regional scale hydrogeological model which in part uses the same geometrical framework (as supplied in this specification), albeit at a larger scale. Geometrical specifications, along with a site-specific geological structure model are given as CAD data in the Task 8d delivery. Site specific stochastic fracture statistics are given as intensity, size and orientation data and serve as the basis for the hydraulic properties.

10.2 Scope and objectives

One sub-aim of Task 8 is to improve the knowledge of the bedrock-bentonite interface with regard to groundwater flow.

Task 8f has not as Task 8c and 8d been divided into two parts; Task 8f only considers the bentonite wetting part.

The scope of this calculation exercise is contained within the simulation of a sub-local site-specific three-dimensional groundwater flow specifications presented below, similar to Task 8c and 8d however now with all available data along with the answer.

The main objective of Task 8f is to evaluate the resulting wetting of the bentonite installed in the two boreholes.

Task 8f also provides the modelling groups with an opportunity to re-evaluate their initial hypotheses and address sensitivities concerning conceptual issues addressed by each group, such as geometrical uncertainty, process dependence, and mathematical model, as we are approaching the end of the Task 8 BRIE modelling.

10.3 Case specifications

10.3.1 Geometrical set-up

All geometric descriptions are the same as for Task 8d. The details are found in the task description of Task 8d.

10.3.2 Design of bentonite installation

A description of the bentonite installation is found in the task description of Task 8d.

10.3.3 Background fracture statistics

It should be noted that these statistics are the same as those for Task 8c and 8d. The statistics are found in conjunction to these sections.

10.3.4 Deterministic fracture information

The specifications given in the task description of Task 8d is still valid and found under the Task 8d section.

Additional information can be found in figures in the BRIE report.

10.3.5 Rock stresses

All data on rock stresses are the same as in task descriptions of Task 8c and 8d.

10.3.6 Boundary condition[13]

All pressure[14] and salinity data are the same as given in the task description of Task 8c and 8d.

10.3.7 Initial conditions

The initial conditions for the inflow predictions (Task 8d1) should be based on the "natural" conditions where all probing boreholes are packed off, assuming the packer to seal the upper 1 m of the borehole. For Task 8f initial conditions are the results from Task 8d1.

All data and assessments should be as in Task 8d.

10.3.8 Material specifications

All material specifications are found in the task description of Task 8d with some relevant information that can be assessed for updates found in the BRIE report.

10.4 Calibration targets

10.4.1 Ambient pressure

All pressure data are found in the task description of Task 8d with some relevant information that can be assessed for updates found in the BRIE report.

10.4.2 Inflow to TASO

All inflow data relevant for the TASO tunnel are found in the task description of Task 8d with some relevant information that can be assessed for updates found in the BRIE report.

10.4.3 Inflow boreholes

All inflow data to boreholes are found in the task description of Task 8d with some relevant information that can be assessed for updates found in the BRIE report.

[13] The boundary conditions are established from the present official hydro-model of Äspö HRL. The model is (among others) based on the SDM site Laxemar deformation zone model and does due to scale issues contain known location errors.

[14] Pressures given are dynamic pressure; total pressure could be calculated using $\rho_0 \times g \times z$, with reference altitude at present day shore line (0 altitude).

10.4.4 Pressure responses and flow

All pressure and flow response data are found in the task description of Task 8d with some relevant information that can be assessed for updates found in the BRIE report.

10.4.5 Inflow to 30 cm boreholes

All inflow to the two extended boreholes is found in the task description of Task 8d with some relevant information that can be assessed for updates found in the BRIE report.

10.4.6 Wetting of the bentonite

All assessable wetting data are found in the BRIE report. Some relevant data from the BRIE report that are helpful for modelling are illustrated below.

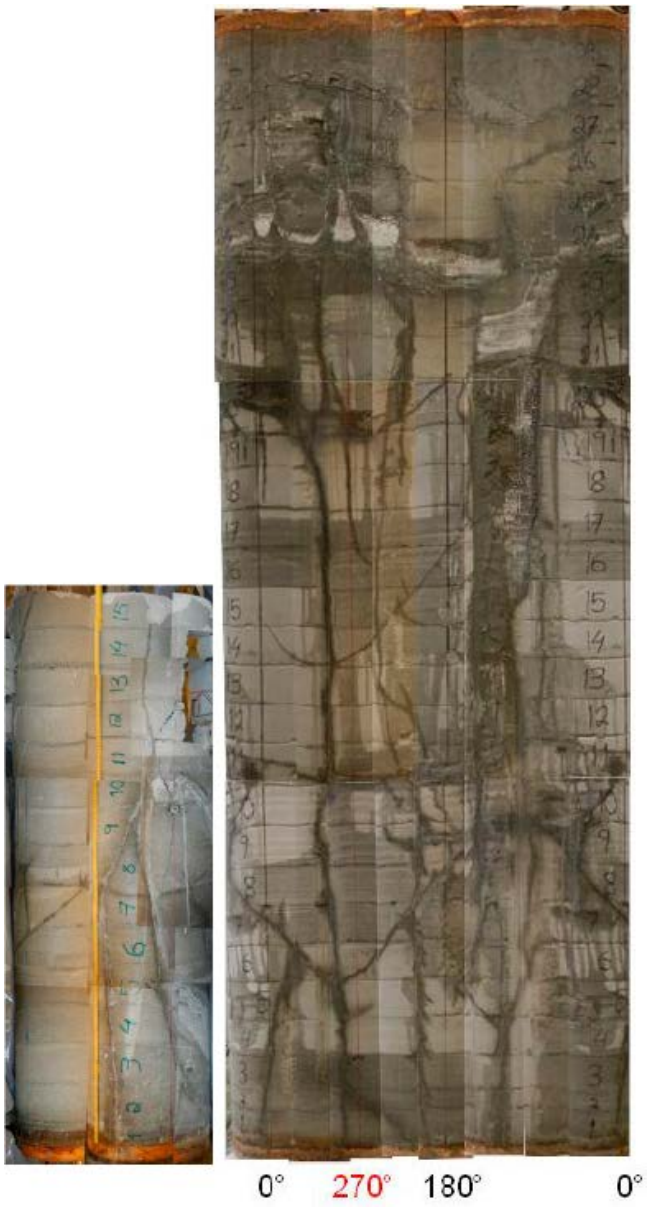

Figure 10-1. *Documentation of the 15 lower blocks from parcel in Hole 17, and all blocks from parcel in Hole 18. The latter image, on Hole 18, covers the complete circumference of the parcel and the marked angles correspond to the marked lines on the bentonite surface.*

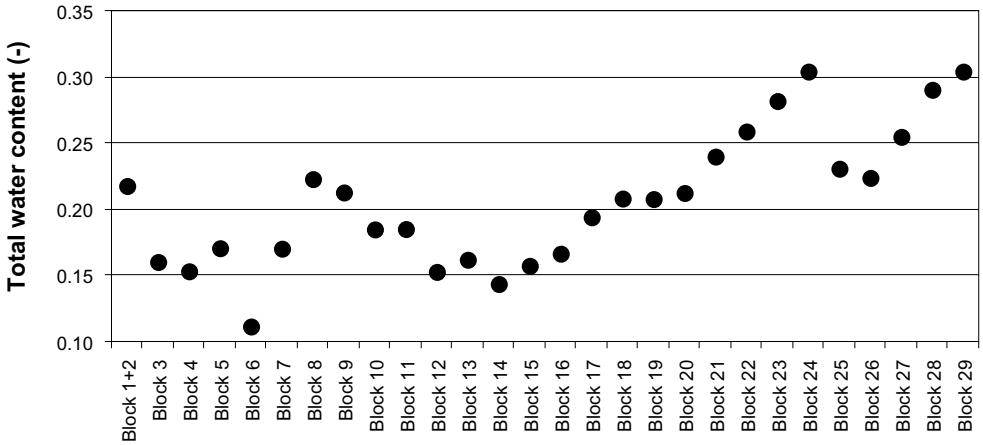

Figure 10-2. *Total water contents estimated from block masses for blocks in Hole 18. It should be noted that some blocks were broken in several pieces and thus constitute an uncertainty. Especially the water content value for Block 6 is considered to be non-relevant.*

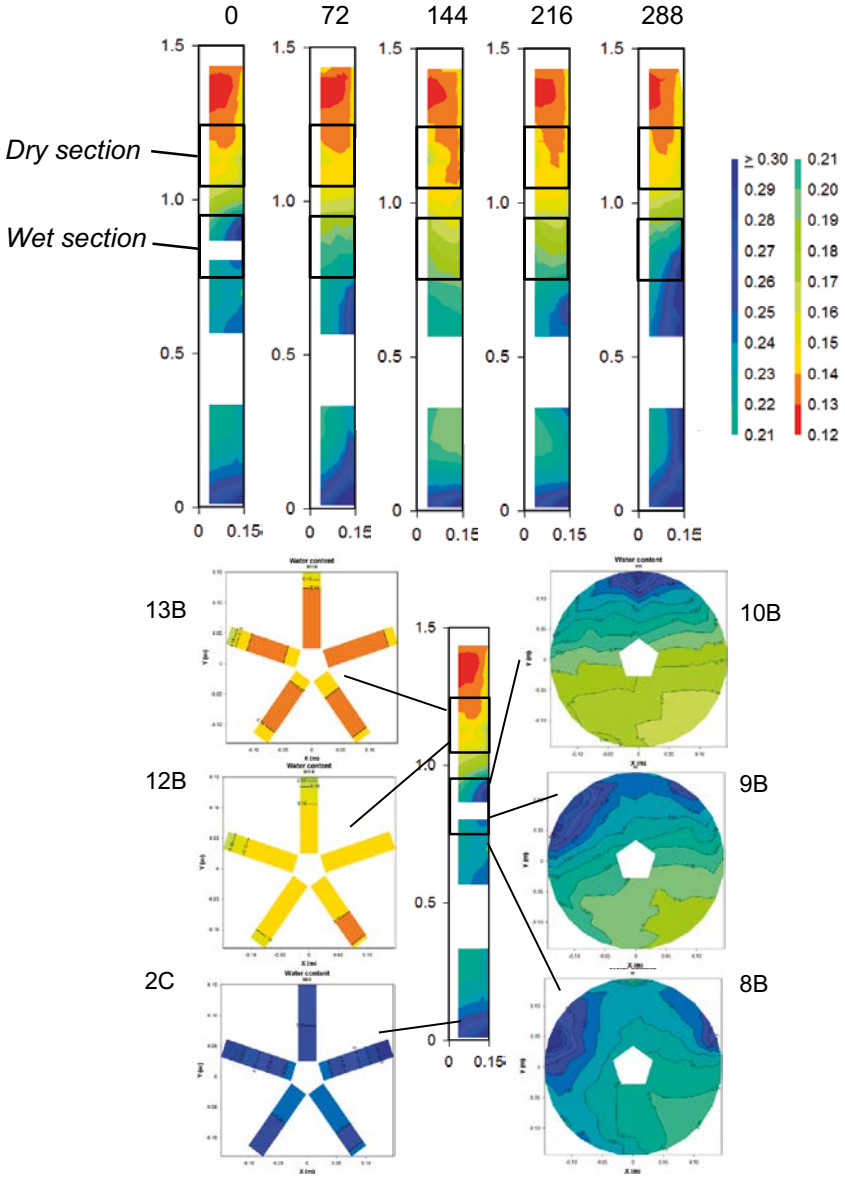

Figure 10-3. *Contour plots of water content in Hole 17.*

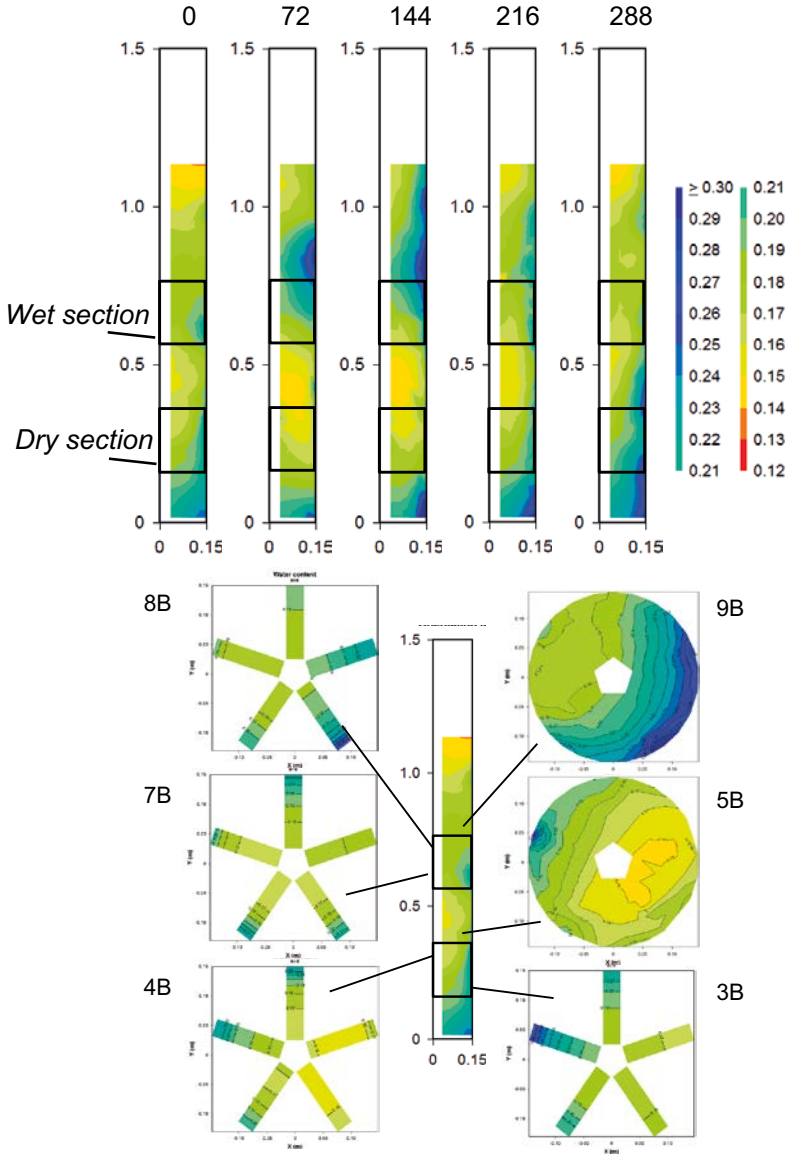

Figure 10-4. *Contour plots of water content in Hole 18.*

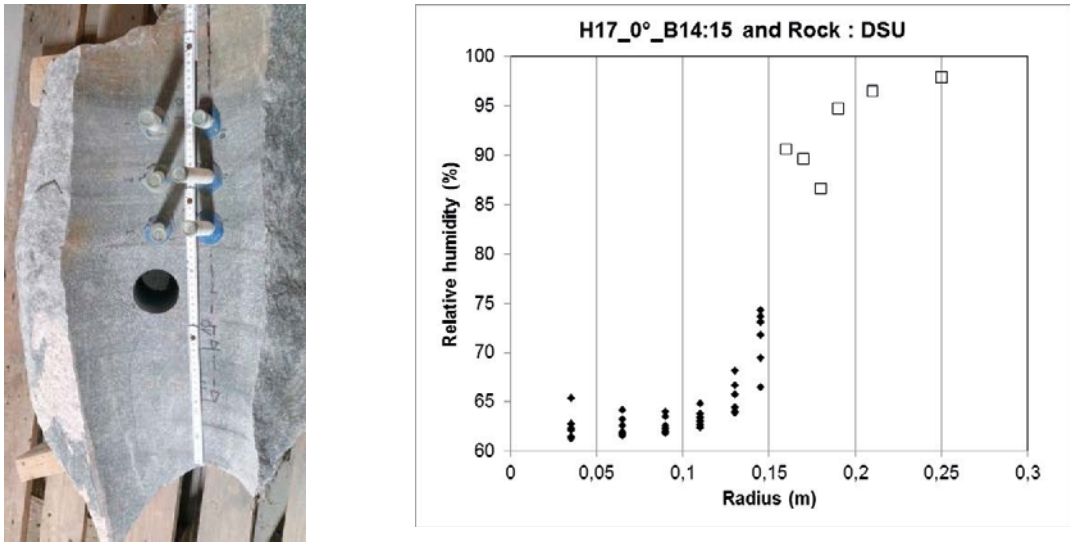

Figure 10-5. *Snap-shot of RH-profile in bentonite and rock (squares), 17G01 Dry Section Upper (DSU).*

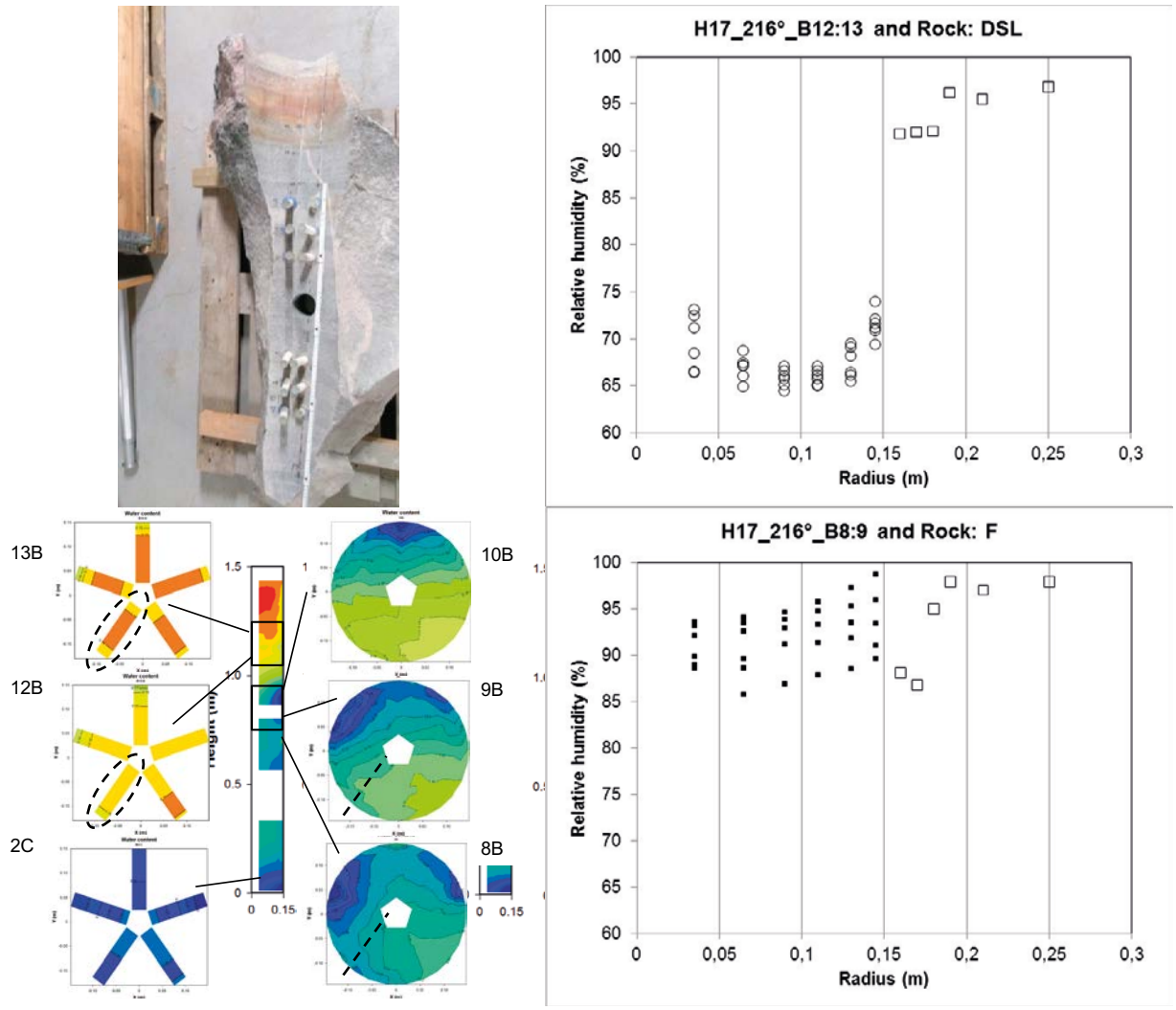

Figure 10-6. *Snap-shot of RH-profile in bentonite and rock, 17G01. Dry Section Lower (DSL) and close to fracture (F).*

10.5 Modelling tasks

The modelling task is divided into two parts:

- With initial conditions from a defensible description similar to the final results of Task 8d1, the wetting of bentonite placed within the 30 cm boreholes, KO0017G01 and KO0018G01 is calculated. The wetting of the bentonite (wetting pattern/saturation distribution with time) along with associated pressure development within the bentonite and the near-field bedrock should be assessed and compared with the results presented in the BRIE report.
- The results of the wetting, time development and spatial pattern should be compared to the results derived in Task 8d, details are specified below.

As mentioned above Task 8f provides the modelling groups with an opportunity to use additional back-analysis or inverse modelling approaches to the BRIE experiment. They may also wish to re-evaluate their initial hypotheses and address sensitivities concerning conceptual issues.

10.6 Expected outcome

The expected outcome as described below should be provided for each model realisation or variant in order to meet to the objectives.

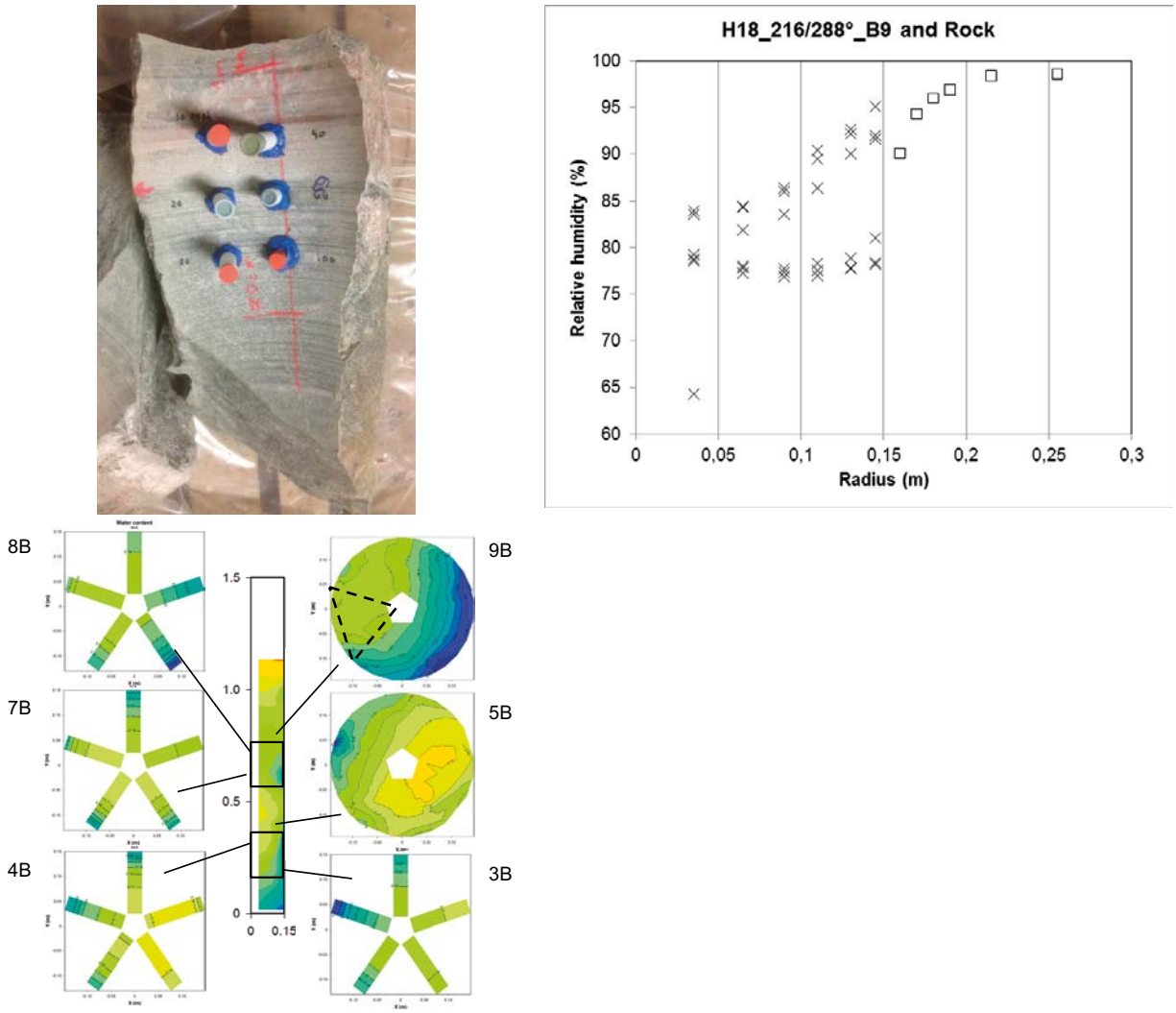

Figure 10-7. *Snap-shot of RH-profile in bentonite and rock, 18G01.*

Results for Task 8f:

Contour plots of the deposition hole near-field pressures and saturation[15] in bentonite as well as the bedrock for time steps at 0, 0.1, 0.5, 1.0, 10, 100 years on one vertical cross-section incorporating both deposition holes and parallel with the TASO tunnel central line and one horizontal cross-section incorporating both deposition holes and cutting through at the depth of 1.5 metres. Plots should be comparable to those produced in Task 8c and 8d.

The contour plots should present the geometric situation of the deposition holes in detail (tunnel floor and 5 metres down). The colour scale of the contour plots should be: 1.5, 1, 0.5, 0.2, 0.1, 0, −0.1, −0.2, −0.5, −1, −5, −10, −20, −50 MPa. Graphs showing illustrations of the pressure increase within the bentonite at a position 0.01, 0.05, 0.1, 0.15 metres from the different deposition holes walls. These graphs should come as six: one for each of the deposition holes (KO0017G01 and KO0018G01) at 1.5 metres depth, at 0.75 metres down the hole, and at 2.25 metres down the hole. Plots should be comparable to those produced in Task 8c and 8d.

Graphs illustrating the pressure change within the bedrock at a position 0.01, 0.05, 0.1, 0.15, 1, 5 metres from the two 30 cm borehole walls in the direction towards the other deposition hole are requested. These graphs should also come as three for the same depth positions as described above. Assess these requested plots same as in Task 8c and 8d.

[15] Or alternative equivalent measure of change in the bentonite due to inflow of water from the bedrock, eg. RH or suction.

Evolution of RH and pore pressure at sensor positions (see sections for task description of Task 8d for the period of 0 to 250 days counting from installation).

Horizontal saturation contour plots for the specified depths given in Table 10-1 below (corresponding to instrumented bentonite blocks) for times: 100, 150, 175, 200, 225 and 250 days.

Table 10-1. Depths for requested saturation contour plots.

Hole 17	Hole 18
−419.506	−419.579
−419.606	−419.679
−419.809	−419.983
−419.909	−420.083
−420.618	

Reporting

Task 8f is the final part of Task 8 to directly address the BRIE experiment. Each participating modelling group should include all new results in their main Task 8 report incorporating all BRIE tasks 8a–8d and Task 8f. The report should document the role numerical modelling plays (a) to improve our understanding of the interaction between engineered and natural barriers, (b) to support the design and analysis of the BRIE experiment, and (c) as a screening tool to evaluate the performance of deposition holes.

The report should provide some background; briefly discuss objectives, scope, overall approach, model setup, simulation results, interpretation, conclusions and recommendations. Details about the specific analyses can be included in appendices to the main report.

While the content of the report should be flexibly adapted to match the actual analyses performed, the following specific questions should be addressed:

Quantitative results:

(1) What is the range of predicted inflows into an open deposition hole?

(2) What is the range of predicted times needed to rewet the bentonite to a saturation of 95 %?

Qualitative discussion:

(3) What are the key features and properties of the natural and engineered systems that need to be known for deposition hole screening?

(4) What information and data from the BRIE experiment are most valuable for (a) overall system understanding, and (b) model development?

(5) How does the conceptualization of the natural and engineered systems influence (a) quantitative model predictions, and (b) interpretation of the expected system behaviour?

In the final Task 8 report modellers should address feedback provided by the Task 8 reviewer in specific comments to them and more generally in the Interim Evaluation Report. Most importantly modellers should analyse the simulation results with a perspective towards the overall project goal or by addressing some of the guiding questions suggested within the Interim Evaluation Report.

References

SKB's (Svensk Kärnbränslehantering AB) publications can be found at www.skb.com/publications.

Andersson J C, 2007. Äspö Hard Rock Laboratory. Äspö Pillar Stability Experiment, Final report. Rock mass response to coupled mechanical thermal loading. SKB TR-07-01, Svensk Kärnbränslehantering AB.

Andersson J C, Martin C D, 2009. The Äspö pillar stability experiment: Part I – Experiment design. International Journal of Rock Mechanics and Mining Sciences 46, 865–878.

Andersson J C, Martin C D, Stille H, 2009. The Äspö Pillar Stability Experiment: Part II – Rock mass response to coupled excavation-induced and thermal-induced stresses. International Journal of Rock Mechanics and Mining Sciences 46, 879–895.

Autio J, 1997. Characterization of the excavation disturbance caused by boring of the experimental full scale deposition holes in the Research Tunnel at Olkiluoto. SKB TR 97-24, Svensk Kärnbränslehantering AB.

Byegård J, Gustavsson E, Tullborg E-L, 2006. Bedrock transport properties. Data evaluation and retardation model. Preliminary site description. Laxemar subarea – version 1.2. SKB R-06-27, Svensk Kärnbränslehantering AB.

Börgesson L, 1985. Water flow and swelling pressure in non-saturated bentonite-based clay barriers. Engineering Geology 21, 229–237.

Börgesson L, Hernelind J, 1999. Coupled thermo-hydro-mechanical calculations of the water saturation phase of a KBS-3 deposition hole. Influence of hydraulic rock properties on the water saturation phase. SKB TR-99-41, Svensk Kärnbränslehantering AB.

Börgesson L, Johannesson L-E, Sandén T, Hernelind J, 1995. Modelling of the physical behaviour of water saturated clay barriers. Laboratory tests, material models and finite element application. SKB TR 95-20, Svensk Kärnbränslehantering AB.

Crank J, 1975. The mathematics of diffusion. 2nd ed. Oxford: Oxford University Press.

Dixon D, Chandler N, Stroes-Gascoyne S, Kozak E, 2001. The isothermal buffer-rock-concrete plug interaction test: final report. Report No: 06819-REP-01200-10056-R00. Atomic Energy of Canada.

Dixon D, Chandler N, Graham J, Gray M N, 2002. Two large-scale sealing tests conducted at Atomic Energy of Canada's underground research laboratory: the buffer–container experiment and the isothermal test. Canadian Geotechnical Journal 39, 503–518.

Dueck A, 2004. Hydro mechanical properties of a water unsaturated sodium bentonite, Laboratory study and theoretical interpretation. PhD thesis. Department of Building and Environmental Technology, Division of Soil Mechanics and Foundation Engineering, Lund University.

Dueck A, Nilsson U, 2010. Thermo-hydro-mechanical properties of MX-80. Results from advanced laboratory tests. SKB TR-10-55, Svensk Kärnbränslehantering AB.

Finsterle S, Pruess K, 1995. Solving the estimation-identification problem in two-phase flow modeling. Water Resources Research 31, 913–924.

Fransson Å, 2009. Literature survey: relations between stress change, deformation and transmissivity for fractures and deformation zones based on in situ investigations. SKB R-09-13, Svensk Kärnbränslehantering AB.

Fransson Å, Åkesson M, Andersson L, 2017. Bentonite Rock Interaction Experiment. Characterization of rock and installation hydration and dismantling of bentonite parcels. SKB R-14-11, Svensk Kärnbränslehantering AB.

Gudmundsson A, 2000. Fracture dimensions, displacements and fluid transport. Journal of Structural Geology 22, 1221–1231.

Gustafson G, Butrón C, Fransson Å, 2008. Characterisation of the hydraulic properties of fractured rock from grouting data. Proceedings of the 36th IAH Congress on Integrating Groundwater Science and Human Well-being, Toyama, Japan, 27–31 October 2008.

Gustafsson E, 2001. Äspö Hard Rock Laboratory. Matrix fluid chemistry experiment. Hydraulic character of the rock matrix. Äspö Hard Rock Laboratory. SKB ITD-01-07, Svensk Kärnbränslehantering AB.

Jarsjö J, 2009. Geological storage of CO_2 in deep aquifers: open research questions on how to minimize return flows to the atmosphere. Proceedings of the First International Conference on Applied Energy (ICAE'09), Hong Kong, 5–7 January 2009.

Jarsjö J G, Destouni G, Gale J, 2001. Groundwater degassing and two-phase flow in fractured rock. SKB TR-01-13, Svensk Kärnbränslehantering AB.

Munier R, 2006. Using observations in deposition tunnels to avoid intersections with critical fractures in deposition holes. SKB R-06-54, Svensk Kärnbränslehantering AB.

Olson J E, 2003. Sublinear scaling of fracture aperture versus length: An exception or the rule? Journal of Geophysical Research 108. doi:10.1029/2001JB000419

Pollard D D, Segall P, 1987. Theoretical displacements and stresses near fractures in rock: with applications to faults, joints, veins, dikes, and solution surfaces. In Atkinson B K (ed). Fracture mechanics of rock. London: Academic Press, 277–349.

Rhén I, Forsmark T, 2001. Äspö Hard Rock Laboratory. Prototype Repository. Hydrogeology. Summary report of investigations before the operation phase. SKB IPR-01-65, Svensk Kärnbränslehantering AB.

Rhén I (ed), Bäckblom G (ed), Gustafson G, Stanfors R, Wikberg P, 1997. Äspö HRL – Geoscientific evaluation 1997/5. Model based on site characterization 1986–1995. SKB TR 97-06, Svensk Kärnbränslehantering AB.

Rhén I, Forsmark T, Hartley L, Jackson C P, Roberts D, Swan D, Gylling B, 2008. Hydrogeological conceptualisation and parameterisation. Site descriptive modelling, SDM-Site Laxemar. SKB R-08-78, Svensk Kärnbränslehantering AB.

SKB, 2010a. Design, production and initial state of the buffer. SKB TR-10-15, Svensk Kärnbränslehantering AB.

SKB, 2010b. Design, construction and initial state of the underground openings. SKB TR-10-18, Svensk Kärnbränslehantering AB.

Snow D T, 1968. Rock fracture spacings, openings, and porosities. Journal of the Soil Mechanics and Foundations Division 94, 73–91.

Thomas H R, Cleall P J, Chandler N, Dixon D, Mitchell H P, 2003. Water infiltration into a large-scale in-situ experiment in an underground research laboratory. Geotechnique, 53, 207–224.

Vermilye J M, Scholz C H, 1995. Relation between vein length and aperture. Journal of Structural Geology 17, 423–434.

Vidstrand P, 1999. Hydrogeological scale effects in crystalline rocks, Comparison of field data from Äspö HRL with data from predictive upscaling methods. Lic. thesis. Chalmers University of Technology, Sweden.

Vilks P, Miller N H, 2007. Evaluation of experimental protocols for characterizing diffusion in sedimentary rocks. atomic energy of Canada limited. NWMO TR-2007-1, Nuclear Waste Management Organization, Canada.

Zimmerman R W, Bodvarsson G S, 1996. Hydraulic conductivity of rock fractures. Transport in Porous Media 23, 1–30.

Åkesson M, Börgesson L, Kristensson O, 2010. SR-Site Data report. THM modeling of buffer, backfill and other system components. SKB TR-10-44, Svensk Kärnbränslehantering AB.

Arkitektkopia AB, Bromma, 2017

SKB is responsible for managing spent nuclear fuel and radioactive waste produced by the Swedish nuclear power plants such that man and the environment are protected in the near and distant future.

skb.se